ANALYSIS AND MODELLING
OF
ARTERIAL BLOOD VELOCITY WAVEFORMS

A thesis submitted for
the Degree of Doctor of Philosophy
in the Faculty of Engineering
of the University of London

by

Habib Emile Talhami

January 1985

Engineering in Medicine Laboratory
Department of Electrical Engineering
Imperial College of Science and Technology
London SW7.

ABSTRACT

How can we characterise arterial stenosis using blood velocity measurements downstream of a stenosis? The question sums up the problem at hand and the thesis is an attempt to provide a simple answer although the fluid dynamics of such a physical system are complex.

The data i.e. the velocity signal is acquired from an in vivo experiment where an external constriction is imposed on the descending aorta. The percent stenoses (by area) considered are 0, 20, 40, 58, 74, and 88%. These form the database for subsequent signal processing and analysis.

Conventional techniques of signal analyis like ensemble averaging and Fourier spectral analysis are used to characterise the velocity waveforms and their limitations are noted. In comparison, autoregressive techniques are explored and are found to give better spectral estimates than conventional methods.

The disturbance velocity waveforms, which are derived from the velocity signal, are the focus of the last part of this thesis since they convey useful information related to the occlusion level. Two modelling techniques, which appear to give an insight into the disturbed flow field, are suggested. These are: (i) the adaptive autoregressive technique which tracks nonstationarities in the signal and provides time-variant spectra, and (ii) the impulsive noise model which suggests that the disturbance signal can be thought of as a narrow-band process or a wave packet driven by impulsive noise.

Eventually, the work is concluded with a summary of the analysis techniques used and certain clinical considerations in relation to the detection of atherosclerosis. The need for more experimental work is discussed as well as the necessity and importance of more sophisticated signal analysis techniques.

ACKNOWLEDGEMENTS

It is hard to acknowledge all those whose assistance has reduced the level of my ignorance. For, thanks to them I can state with confidence that today I know much more than three years ago yet today is just the beginning.

Since the acquisition of knowledge remains a costly privilege in a world of high technology and nuclear missiles especially to those Third World countries where food comes before knowledge, I acknowledge with gratitude the financial assistance of the Arab British Chamber of Commerce whose award allowed me to finish this work.

I owe my recently acquired addiction-research work addiction- to my supervisor and friend, Dr. Kitney, whose hard work and informal guidance have been an excellent driving force.

Much gratitude is also due to Prof.D.P.Giddens for supplying us with data and for his constructive advice on issues of great importance to this project.

I am also grateful to members of my section who helped to create a cheerful and encouraging atmosphere especially my friend, Dr. Zaid Chalabi, whose positive and broad-minded advice has been extremely conforting.

Finally, special thanks are due to my parents and also to my wife Beatriz for her patience, understanding and constant encouragement especially in the final and most demanding stages of study.

TABLE OF CONTENTS

TABLE OF ILLUSTRATIONS

Fig page

TABLES

CHAPTER 1

INTRODUCTION

Blood flow in the arteries is an area of research where challenges never end. Its natural diversity has aroused the interests of scientists from various fields. Biomedical engineers are no exception in that they try to reconcile the two worlds of Medicine and Engineering motivated by the need to understand the relationship between flow and arterial disease.

Among the most interesting blood flow phenomena are those which arise as a consequence of atherosclerosis. Atherosclerosis is a progressive disorder which begins with the deposition of lipid material in the intima which gradually increases in size and extent of involvement. In its earliest stages the arterial plaque does little to interfere with the delivery of blood but ultimately it reduces the arterial cross-sectional area and distorts the constituents of the vessel wall (Mitchell and Schwartz,1965).

The flow field resulting from this occlusive disease is complex and consequently its description taxes even the most sophisticated mathematical analysis. Yet, there is always a fruitful strategy that the engineer can employ, by developing and applying signal processing techniques to the analysis of blood flow, it is possible to simplify even a problem which involves an array of interrelated variables.

1.1 Arterial Stenosis: Basic Physiological Considerations

Arterial stenosis refers to a narrowing of an arterial segment.

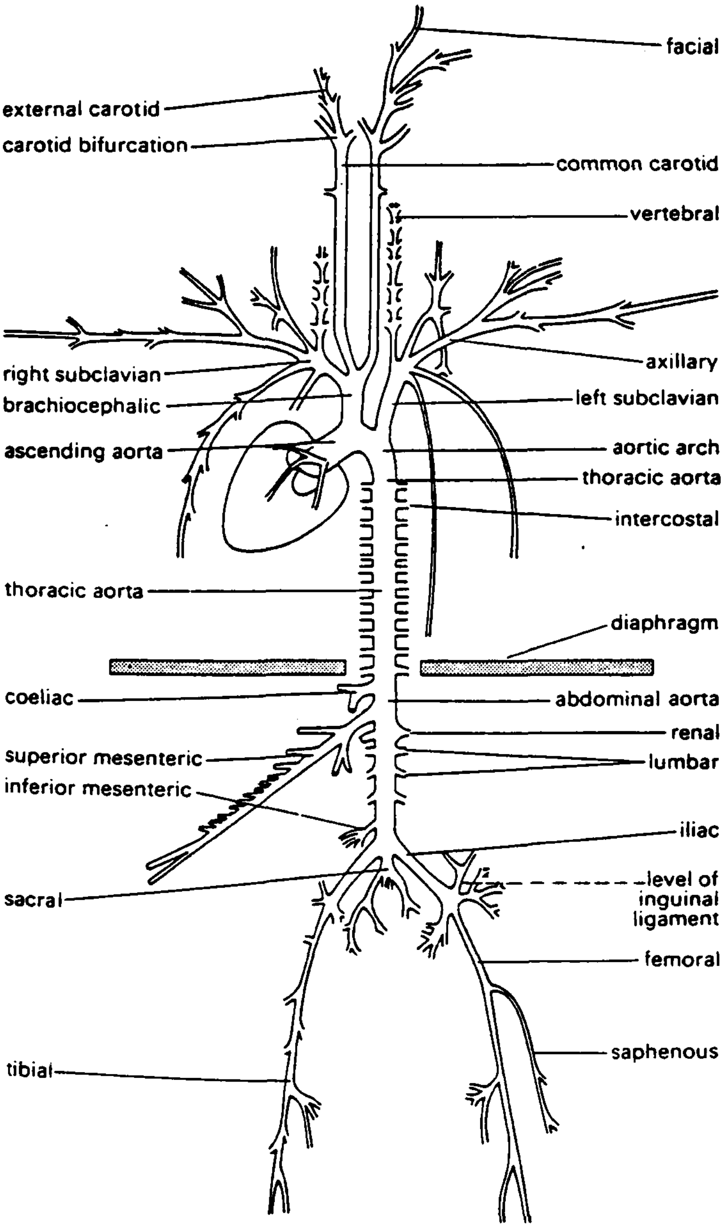

Fig.1.1 A diagramatic representation of the major branches of the canine arterial tree. (After McDonald,1974)

This is most frequently caused by intravascular atherosclerotic plaques which develop at the arterial walls. These fatty plaques are distributed preferentially at certain locations like,for example, the outer walls of arterial junctions, the inside walls of curves (e.g. the aortic arch), the carotid sinus and the abdominal aorta (Pedley,1980; see also Fig.1.1 for a description of the arterial tree). Hence the assumption that there are haemodynamic factors involved in the initiation of atherosclerosis cannot be disregarded. Therefore, the aim of this chapter is to emphasize both the importance and complexity of these factors without resorting to an exhaustive literature review.

1.1.1 The Properties of Blood

Blood consists of different biological structures: red blood cells, white blood cells, platelets etc... suspended in plasma. Although the plasma itself is Newtonian, blood is classified according to its shear rate (shear rate is defined as the gradient of the velocity (Caro,Pedley,Schroter and Seed, 1978). At low shear rates, blood exhibits non-Newtonian behaviour while at higher shear rates, which is the case in the larger arteries, blood is usually assumed to be Newtonian (Young 1979). The density of normal blood is approximately 1050 kg/m^3 and its apparent viscosity (measured at high shear rates above $100s^{-1}$ at 37^{o} C) is in the range 3 - $4.5x10^{-3}$ $N.s/m^2$ for dogs and humans.

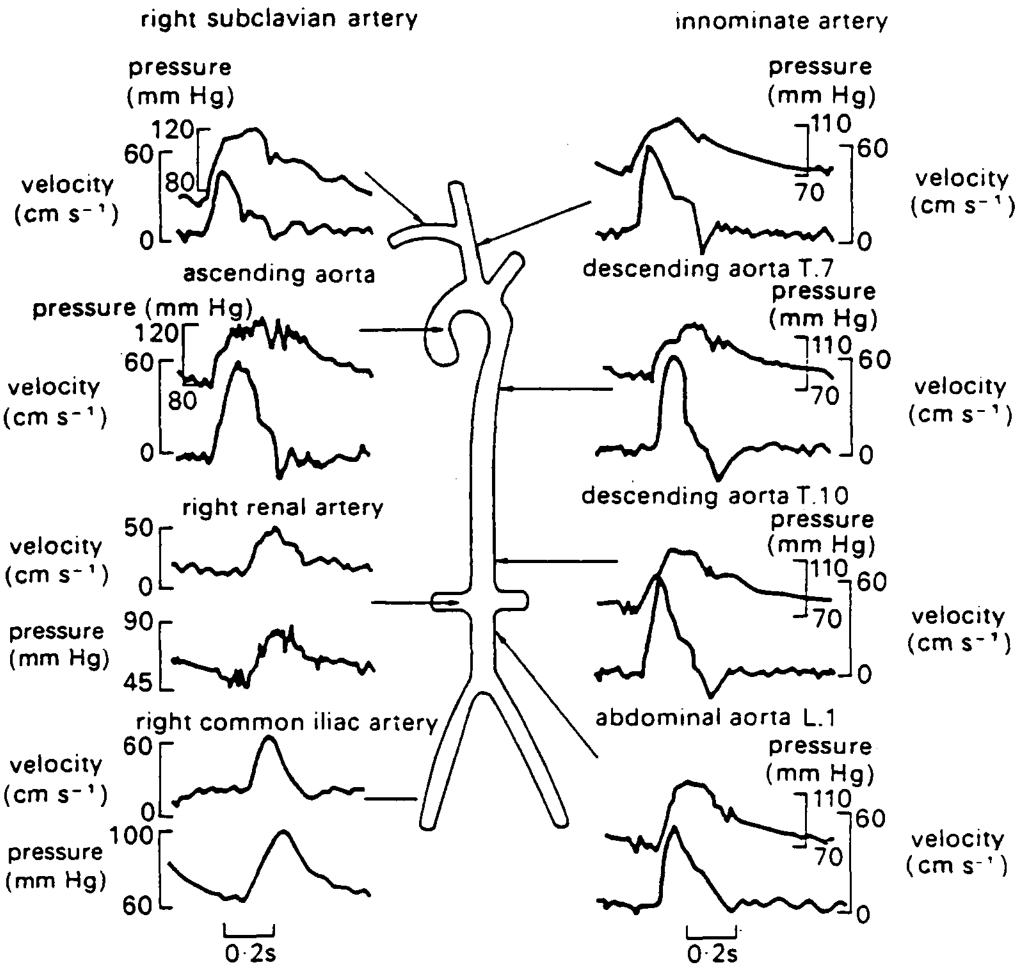

Fig.1.2 Simultaneous pressure and blood velocity waveforms at numerous points in the human arterial tree. (After Mills, Gabe, Gault, Ross, Braunwald & Shillingford, 1970)

1.1.2 Flow in the Arteries

Blood flow in the arteries is pulsatile and the velocity and pressure waveforms vary depending on the location in the arterial tree as shown in Fig.1.2. Three parameters are usually used to characterise these flow patterns: (i) the Reynolds number, (ii) the frequency parameter, α , and (iii) the Strouhal number.

(i) The Reynolds number is defined as:

$$Re = (D\ U)/\nu \tag{1.1}$$

where D is the lumen diameter, U some characteristic velocity and ν is the kinematic viscosity.

(ii) The frequency parameter " α " is as follows: (R=D/2)

$$\alpha = R \cdot \sqrt{w/\nu} \tag{1.2}$$

where w is the fundamental frequency of the pulsating flow.

(iii) The Strouhal number is defined as:

$$St = wD/U \tag{1.3}$$

Because of the variability of living systems it is hard to specify these parameters accurately for an individual. Examples of physiological variability are heart rate changes and respiratory effects (Kitney and Giddens,1982).

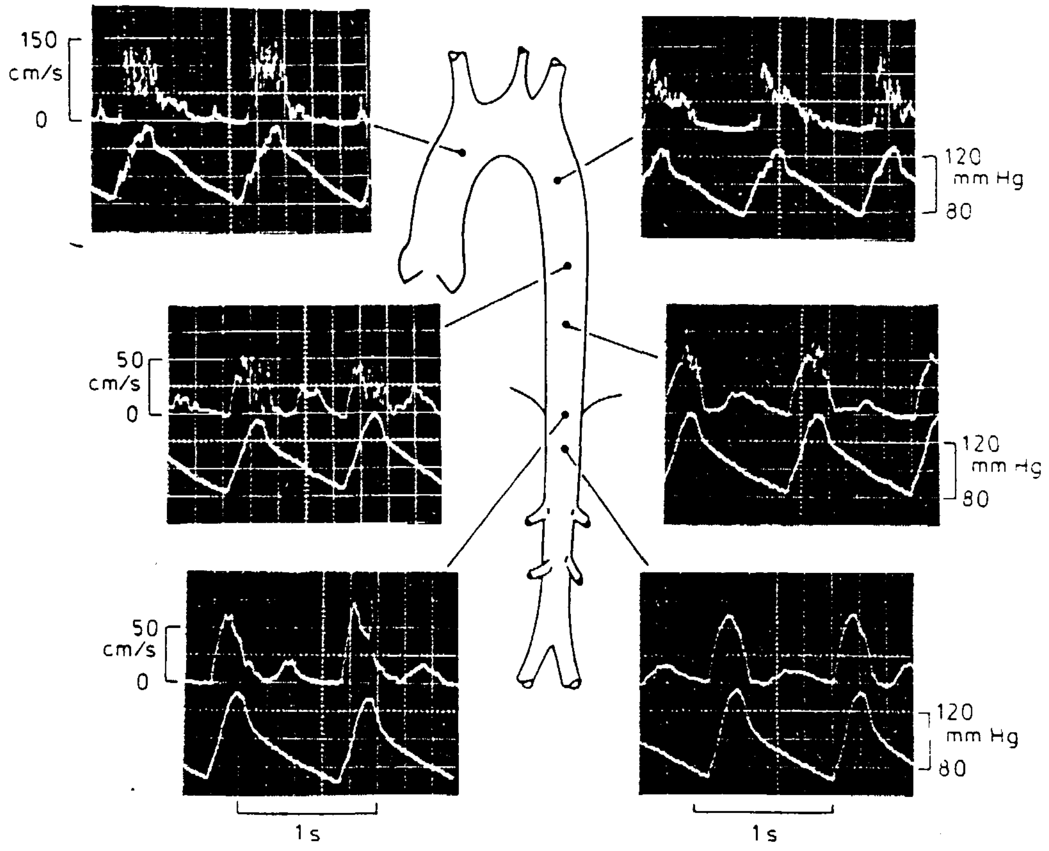

Fig.1.3 Simultaneous velocity and pressure measurements in the aorta of a patient with severe aortic stenosis using catheter-tip instruments. (After Clark,1980)

1.1.3 The Effect of Stenosis on Arterial Blood Flow

The presence of a stenosis in an artery causes a major disruption in the flow field. Stenotic blood disturbances have been described by many workers including Schultz, Tunsball-Pedoe,Lee,Gunning and Bellhouse(1969)(humans), Nerem and Seed (1972)(dogs), Clark and Schultz(1973)(dogs) and Giddens,Mabon and Cassanova(1976)(dogs). Measurement of these disturbances are strongly dependent on axial and radial positions of the probe as well as on the geometries of the artery and the stenosis (for example Fig.1.3 illustrates axial variations). Clark(1976) states that: given an instantaneous blood velocity, v, of 4 m/s in the stenosis the dynamic pressure ($= 1/2(\rho v^2)$, where ρ = fluid density) is 63mm Hg and, if it behaves like a steady flow, pressure in the ascending aorta may increase by more than 15mm Hg over a distance of a few cm.

Because the circulatory system is a complex, tapered, branching, network of distensible vessels, it is difficult to account for all these factors in experimental or analytical models. Rather, in attempting to model a stenotic flow field, it is common to consider the stenosis as a rigid-walled constriction in a rigid-walled tube. Such simplifications frequently resulted in models which have little or no relation to the living system. The stenosis is geometrically complex, yet the variable which is most commonly used to describe it is the ratio of the minimum cross-sectional area, A_1, to the unobstructed lumen area A_o. Thus the term 'percent stenosis',P_{st}, defined as:

$$P_{st} = (1 - \frac{A_1}{A_o}) \times 100 \qquad (1.4)$$

and this term will be used extensively in the following chapters.

1.2 The Fluid Mechanics of Arterial Stenosis

1.2.1 Pulsatile Blood Flow through a Distensible Vessel

In analysing pulsatile flow in a distensible vessel, difficulties arise in solving the equations that describe the flow and those that describe the movement of the vessel walls because of their interrelationship. If it is assumed that blood can be treated as an incompressible fluid and that the flow has cylindrical symmetry, then the basic flow equations can be defined as follows (Attinger,1981):

(a) The continuity equation:

$$\frac{\partial v_r}{\partial r} + \frac{v_r}{r} + \frac{\partial v_z}{\partial z} = 0 \qquad (1.5)$$

(b) The Navier Stokes equations for an incompressible Newtonian fluid:

$$\frac{\partial v_z}{\partial t} + v_r\frac{\partial v_z}{\partial r} + v_z\frac{\partial v_z}{\partial z} = F_z - \frac{1}{\rho}\frac{\partial p}{\partial z} + \nu\left(\frac{\partial^2 v_z}{\partial r^2} + \frac{1}{r}\frac{\partial v_z}{\partial r} + \frac{\partial^2 v_z}{\partial z^2}\right)$$

$$\frac{\partial v_r}{\partial t} + v_r\frac{\partial v_r}{\partial r} + v_z\frac{\partial v_r}{\partial z} = F_r - \frac{1}{\rho}\frac{\partial p}{\partial r} + \nu\left(\frac{\partial^2 v_r}{\partial r^2} + \frac{1}{r}\frac{\partial v_r}{\partial r} - \frac{v_r}{r^2} + \frac{\partial^2 v_r}{\partial z^2}\right)$$

$$(1.6)$$

where r is the radial coordinate, z is the longitudinal coordinate, t is the time, p is the pressure, r is the internal vessel radius, ρ is the density of blood and ν is the kinematic viscosity of blood where $\nu = \mu/\rho$, μ being the viscosity of blood, V_z is the instantaneous axial velocity, V_r is the instantaneous radial velocity, and F is the sum of external body forces. Equations (1.6) can alternatively be expressed as:

INERTIAL FORCES = BODY FORCES - PRESSURE GRADIENT FORCES
+ FRICTIONAL FORCES

The description of the vessel motion represents a much more difficult problem. Such descriptions can range from the simple assumption of rigid tube to elaborate formulations for a thick-walled tube, with non-uniform properties and geometrical tapering. For example, Lou(1975) assumes that the dynamic motion of the axisymmetric vessel can be represented by a radial oscillation of finite amplitude which decays exponentially along the axial direction, i.e.:

$$[\text{Total motion of vessel}]=[\text{Finite radial motion}] \times \text{Exp}(-jkx)] \quad (1.7)$$

After a lengthy derivation and some simplifications, Lou presents an expression for the radial motion which describes the total motion.

In general it is very difficult, if not practically impossible, to obtain solutions in closed form for such equations without first carrying out some form of linearisation and/or simplification. Also such equations have not been used successfully to describe disturbed flow such as that found downstream of a stenosis.

1.2.2 Flow through a Stenosis

As mentioned earlier, atherosclerosis has certain preferential sites in the human body, two main regions of plaque formation being

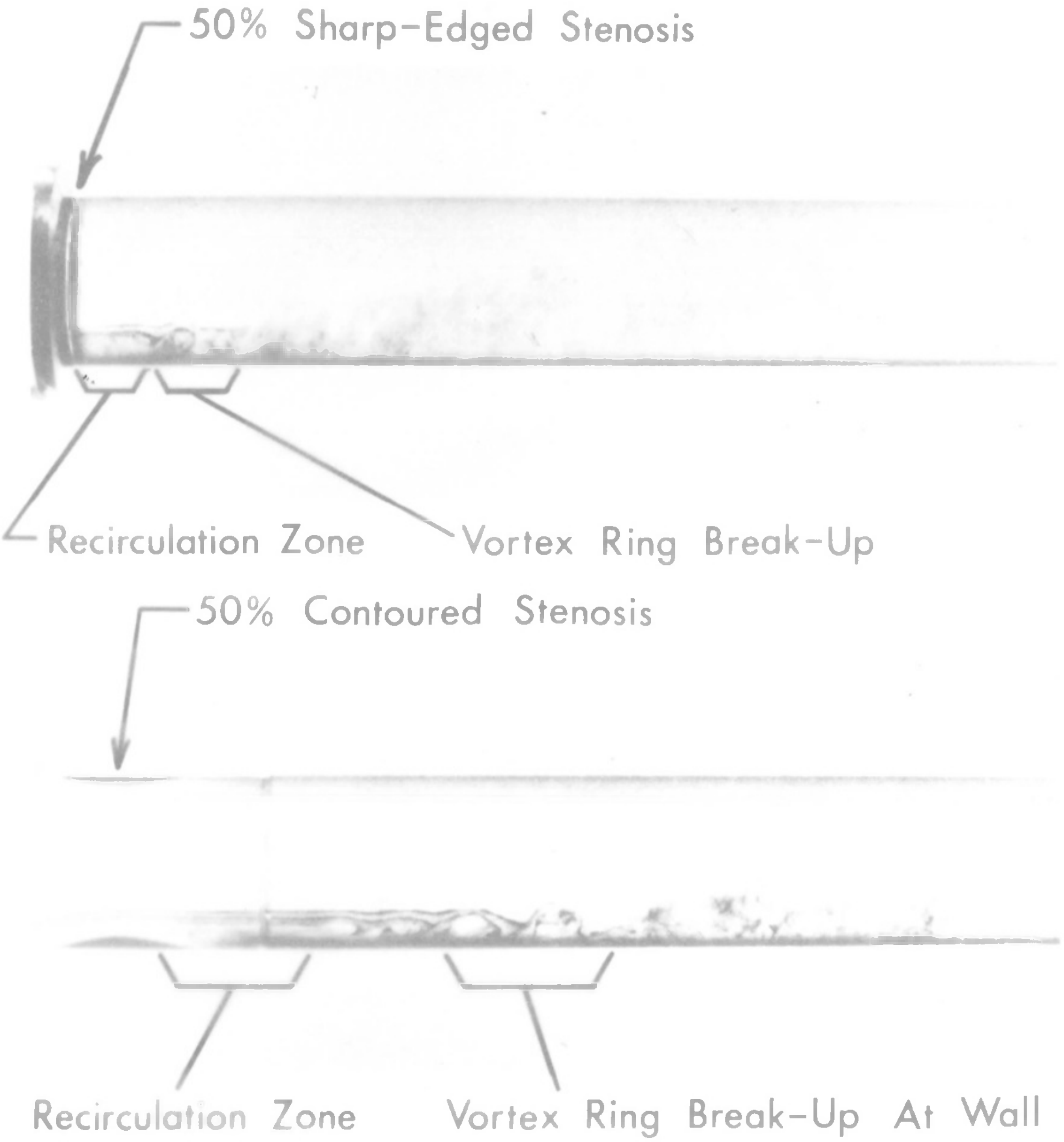

Fig.1.4(a) Flow patterns for the 50% stenoses in steady flow; $Re_D=2540$, $Re_d=3590$. (After Cassanova and Giddens, 1978)

NOMENCLATURE FOR FIGURES 1.4 AND 1.5

Re_d	Reynolds number based on constriction diameter and average velocity in the tube.
Re_D	Reynolds number based on tube diameter and average velocity in the tube.
Re_{Dp}	Reynolds number based on peak waveform velocity and tube diameter.

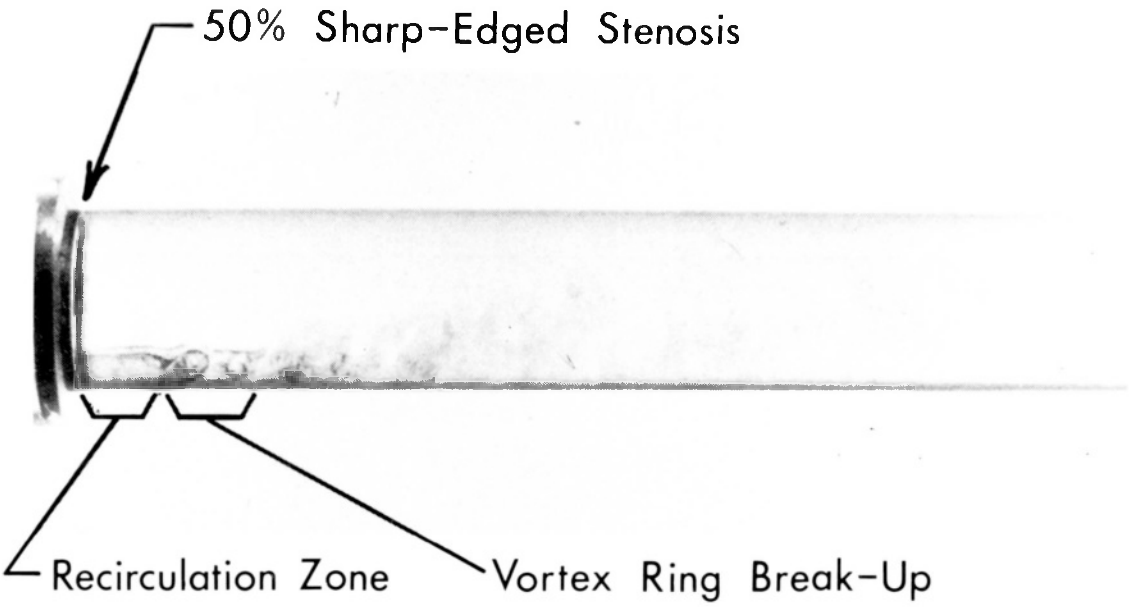
50% Sharp-Edged Stenosis
Recirculation Zone
Vortex Ring Break-Up

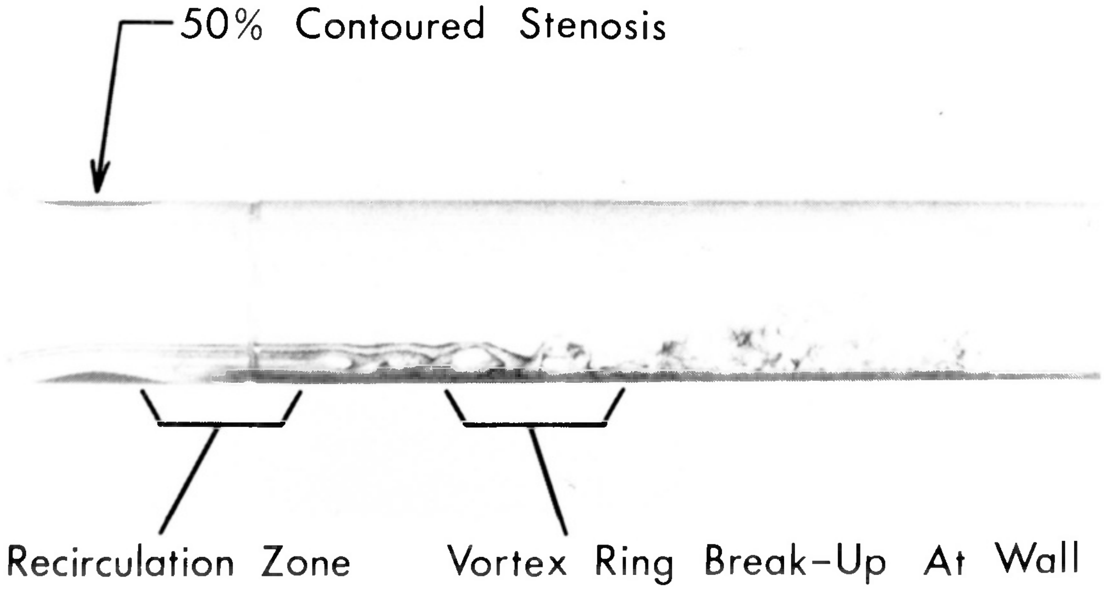
50% Contoured Stenosis
Recirculation Zone
Vortex Ring Break-Up At Wall

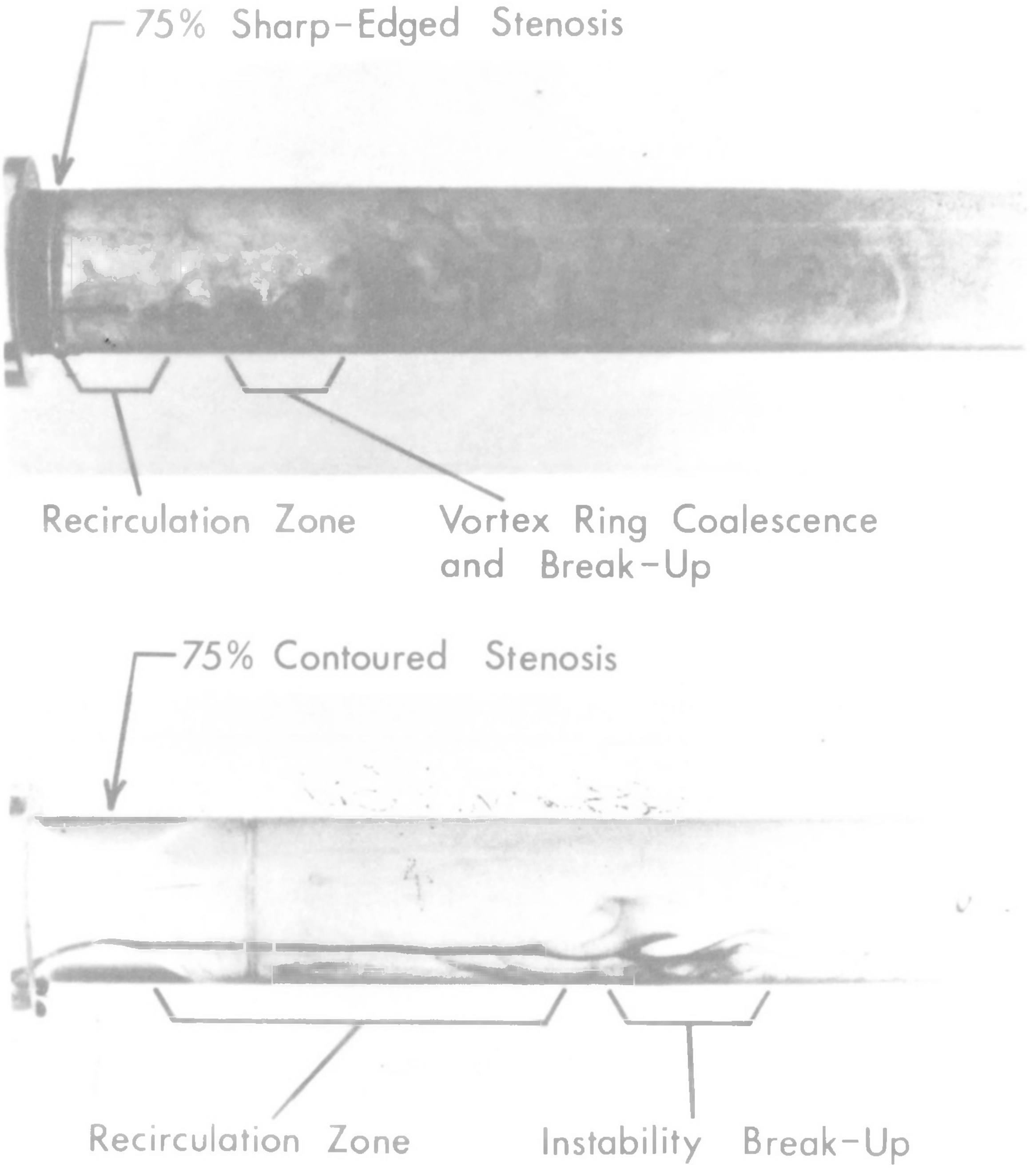

Fig.1.4(b) Flow patterns for the 75% stenoses in steady flow; $Re_D=635$, $Re_d=1270$. (After Cassanova and Giddens,1978)

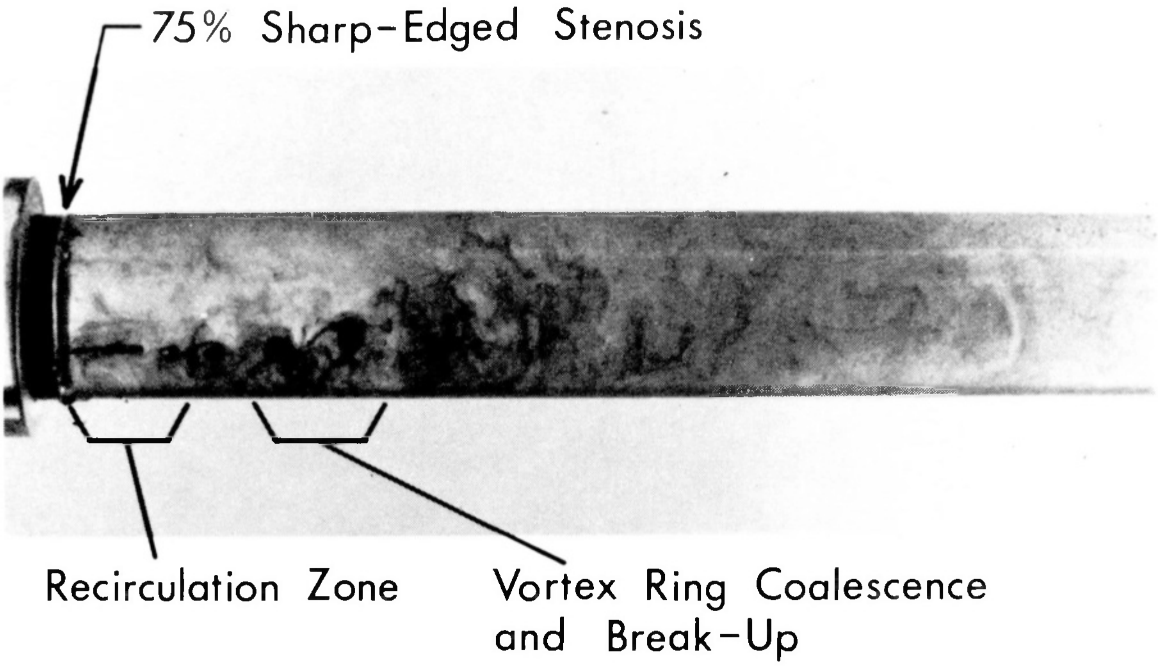
75% Sharp-Edged Stenosis
Recirculation Zone
Vortex Ring Coalescence and Break-Up

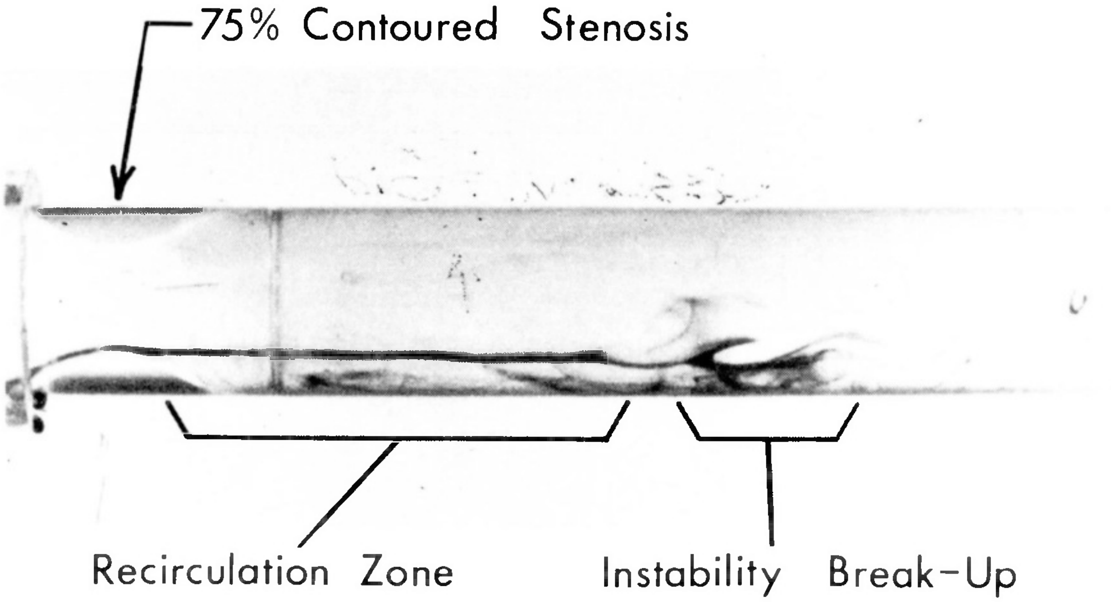
75% Contoured Stenosis
Recirculation Zone
Instability Break-Up

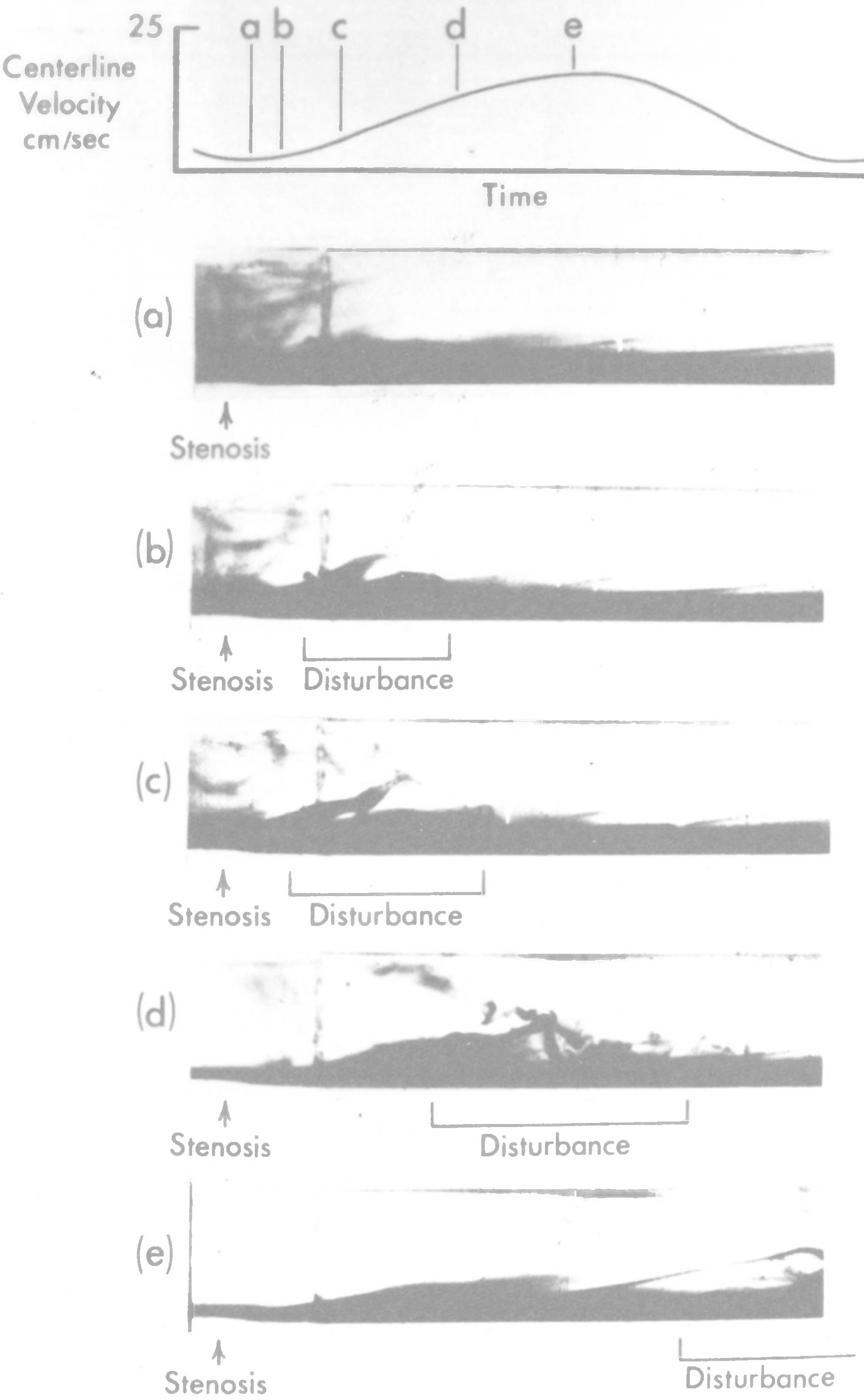

Fig.1.5 Development of flow disorder distal to the 25% contoured stenosis in pulsatile flow with Re_{Dp}=2540 and α=15(After Cassanova & Giddens,1978)

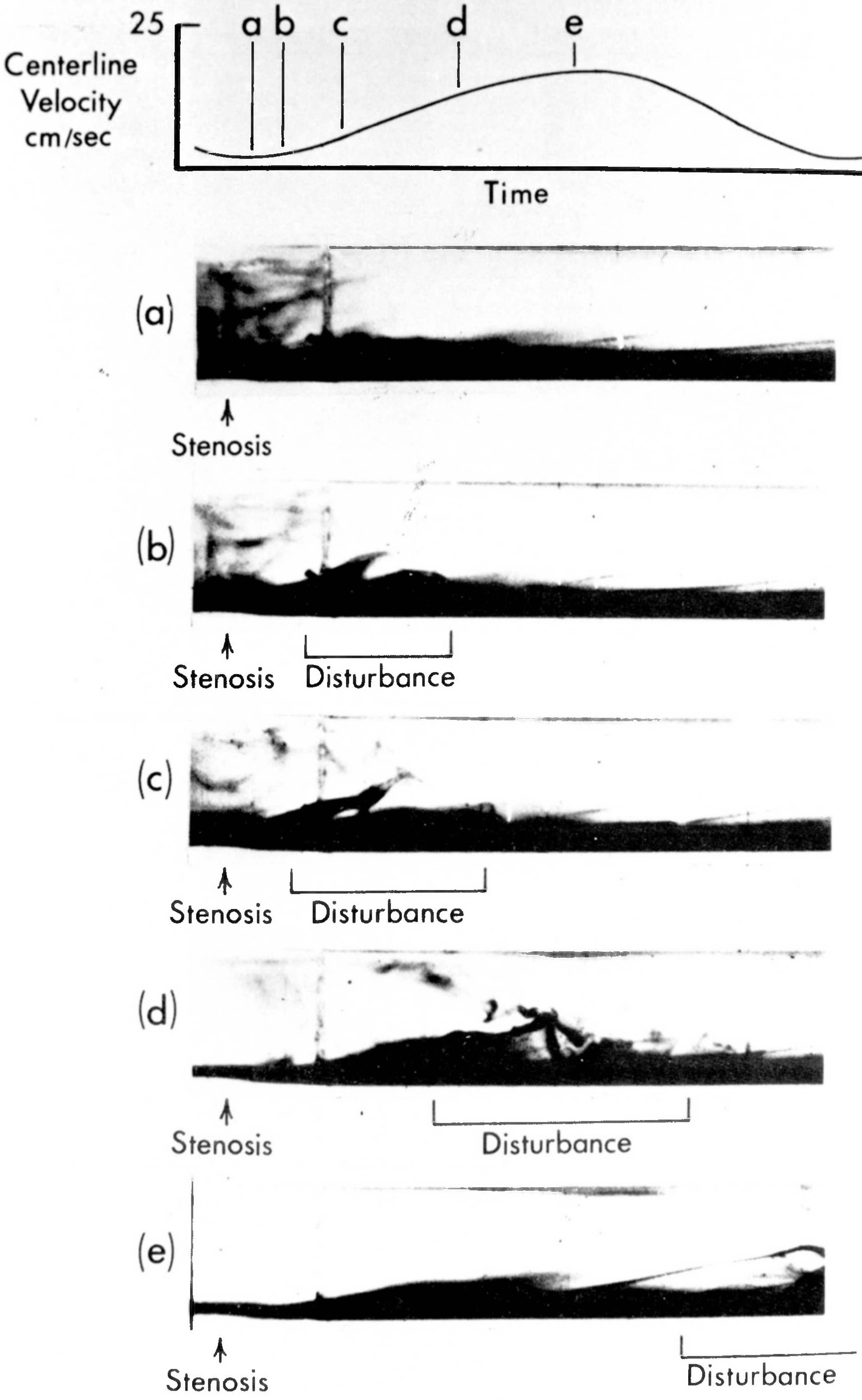
25
Centerline
Velocity
cm/sec
a
b
c
d
e
Time
(a)
Stenosis
(b)
Stenosis
Disturbance
(c)
Stenosis
Disturbance
(d)
Stenosis
Disturbance
(e)
Stenosis
Disturbance

the coronary arteries and the carotid bifurcation. The geometry of these locations make it difficult for any analytical, or even numerical, study to attempt to assess the flow field downstream of a stenosis. However, experimental investigations, though in some cases oversimplify the problem, tend to provide a basic description that can be common to both the model and the physical system. Cassanova and Giddens (1978) developed a rigid tube model of arterial stenosis using both contoured and sharp edged stenoses. Their results can be summarised as follows:

(i) The Steady Case

The results for 50 and 75% occlusion are shown in Fig.1.4(a) and (b). Referring to the figures it is important to note that in both types of stenoses there are three main zones: (1) the recirculation zone which is in the vicinity of the stenosis, mainly downstream but also upstream in the case of a very abrupt stenosis such as the orifice type, (2) a vortex ring break-up region, and (3) a more disturbed or turbulent region which is further downstream. Ahmed(1981) performed a similar experiment and used a laser Doppler velocimeter to measure the velocity. The two variables considered were the Reynolds number and the degree of constriction, as defined by area. Ahmed observed that the size of the separation zone increases with either an increase in Re or in the degree of constriction. He noted also a vortex ring structure near the tube walls which expanded while being shed and conveyed downstream, the strength and shedding frequency being proportional to Re and degree of constriction. The

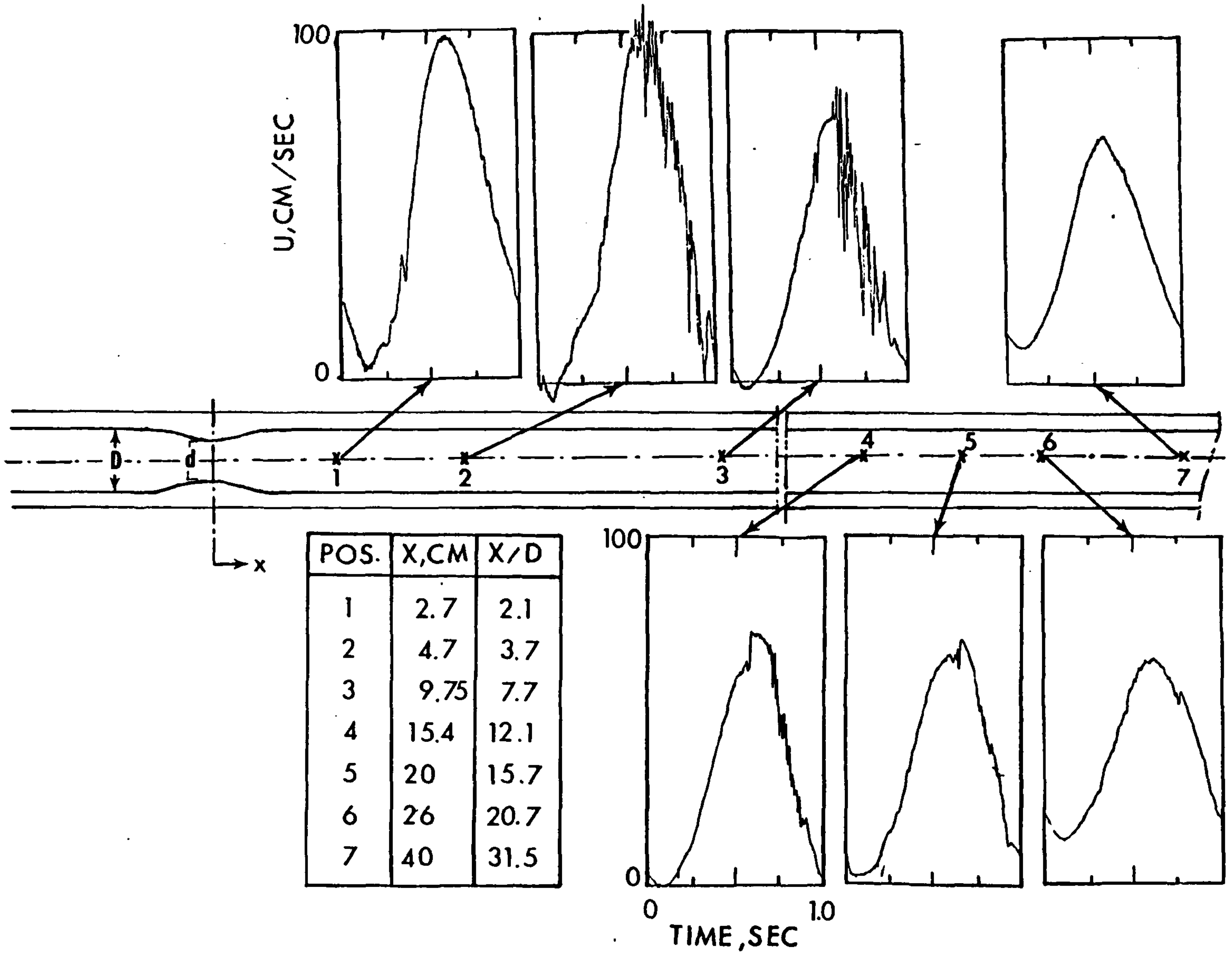

POS.	X,CM	X/D
1	2.7	2.1
2	4.7	3.7
3	9.75	7.7
4	15.4	12.1
5	20	15.7
6	26	20.7
7	40	31.5

Fig.1.6 Centerline velocity waveforms measured at seven axial positions downstream of a 50% axisymmetric stenosis.(After Khalifa and Giddens,1981)

vortex structures might break up into smaller irregular patterns or decay depending on specific parameter values.

(ii) The Pulsatile Case

Fig.1.5 shows the complexity of pulsatile flow through a constriction. The pulse shape used by Cassanova and Giddens(1978) was approximately sinusoidal (top diagram). Flow visualization for times (a), (b), (c), (d), and (e) are shown in the respective figures. There is separation near the wall at (a), flow disturbances form at (b) and are convected downstream at (c), (d) and (e). At (d) and (e) the region immediately downstream of the stenosis is completely relaminarised. Velocity waveforms for different axial positions are shown in Fig.1.6 for a modelled stenosis. Khalifa and Giddens(1981) state that the disturbances observed consist of: a start-up structure during the acceleration phase and subsequent quasi-periodic fluctuation during the decceleration phase, as well as turbulence. Ahmed(1981) noted a recirculation zone which expanded during the acceleration interval and contracted during the deceleration interval and vortex shedding. The activity in the separation region is dependent upon the frequency parameter, α. For an increase in α, Ahmed observed the formation of a relatively violent swirling vortex ring with the following properties: its decay was dependent upon conditions and area reduction, its strength increased with α or the degree of constriction, and its axial velocity was proportional to α.

It is important to note that Ahmed's results are for rigid tube models of stenoses. A literature search was unable to find any detailed experiments involving pulsatile flow in a flexible tube. Hence, there is a need for detailed experimental evidence concerning the differences, rather than the similarities, between human or dog data on the one hand and those obtained from rigid tube models on the other.

1.3 The Clinical Assessment of Arterial Stenosis

The diagnosis of stenotic obstructions is of particular concern to the clinician. The initiation of a stenosis is not completely understood although its presence can lead to serious circulatory disorders (e.g. Stein,Sabbah and Mandal,1976). A severe stenosis in one or more of the major vessels supplying the brain can lead to a 'stroke'. Alternatively, partial occlusion of the blood supply to a limb can cause severe pain and loss of motor function. Hence, the detection of disease at an early stage is of utmost importance to clinicians. The most common method for obtaining information about the presence (and size) of a stenosis is contrast arteriography (Strandness,1983; Young,1979). This invasive technique is only effective when the disease reaches an advanced stage and also involves some risk to the patient.

Breslau and Strandness(1983) separate techniques for the non-invasive diagnosis of carotid artery disease into direct and indirect methods. Direct methods according to their definition, provide anatomical and/or physiological information about the artery. Examples are: phonoangiography, ultrasonic Doppler imaging, B-mode imaging and Duplex scanning. Indirect techniques test for haemodynamic changes at some site removed from the stenosis. Supra-orbital directional Doppler examination, fluid-filled oculoplethysmography and air filled oculoplethsmography are defined as indirect methods. Examples of these methods will now be considered in greater detail.

1.3.1 Direct Methods

(a) Carotid Phonoaniography

Phonoangiography makes use of the vibrations induced by turbulence which appear at the skin surface as sound waves. These waves are detected by a hand held microphone which is placed over the carotid artery at the low, middle and high locations. A phonoangiographic display of bruits in relation to the first and second heart sounds is produced. The frequency spectrum of the bruits is analysed and a 'break frequency', f_o, estimated. The 'break frequency' is defined as the frequency beyond which the power of all higher frequencies sharply declines (Duncan ,Gruber,Dewey,Meyers and Lees, 1975). The realtionship between the residual lumen (dp) of the stenotic vessel and f_o is given by:

$$dp = U/f_o \tag{1.8}$$

where U is the peak systolic velocity in the unoccluded portion of the artery. The main disadvantage of this method is that neither mild nor very severe stenoses necessarily produce bruits.

(b) Ultrasonic Imaging Methods

Three of the most commonly used ultrasonic imaging methods are: (i) Doppler imaging, (ii) B-mode imaging and (iii) Duplex scanning. The last method can be considered as a combination of the first two methods and perhaps an improvement on both as we shall see in the following brief descriptions of these techniques.

(i) Doppler Imaging

Recently, it has been possible to use the Doppler effect to generate 'flow images' with the continuous-wave or pulsed ultrasonic systems. This is achieved when an ultrasonic beam is directed at a blood vessel and the flow is registered at points where the velocity of the red blood cells produces a frequency shift which is higher than the shift resulting from wall motion. If the system is pulsed, it is possible to sample the flow from any point along the path of the sound beam. A two-dimensional image of the flow field can be produced by the use of the position-sensing arm attached to the transducer.

This method has been developed for use in the carotid artery whereby a probe is moved over the skin of the neck and a picture is produced on the screen of a storage oscilloscope. However, the image can be obscured by the presence of calcific plaques which absorb ultrasonic waves. This constitutes a major disadvantage to the employment of this technique.

(ii) B-mode Imaging

While the Doppler ultrasound method records information related to the flow in the arteries, the B-mode technique on the other hand, registers echoes that are related to variations in the acoustical impedance of the tissues. The brightness on the screen of an oscilloscope is made to correspond to the amplitudes of the reflected echoes which in turn are tissue dependent. The scan across the vessel under investigation produces lines with varying intensities which are stored to produce a two-dimensional image of the vessel.

Nevertheless, this technique is not highly reliable in the detection of plaques which exhibit a variation in absorption characteristics that is dependent upon the material in the lesion. Soft, fatty plaques have an acoustic impedance similar to that of the blood while calcific plaques have a high reflectivity.

(iii) Duplex Scanning

Potentially, high resolution images and important haemodynamic information could be attained by combining a real-time B-scan instrument and a Doppler device. This is termed as 'Duplex Scanning'. In such a system, the B-mode image is used to identify the carotid arteries and visualise plaques. The picture is 'frozen' and a Doppler beam is directed towards a chosen blood sample volume. The angle between the beam and the vessel is measured. A Doppler angle of approximately 60 degrees provides a convenient orientation and a favourable return signal(Langlois, Roederer,Chan,Philips, Beach,Martin,Chikos and Strandness,1983). The output Doppler signal is sent to an on-line spectrum analyser where grey or colour scale images are produced. Although a Duplex scan can have a high sensitivity (ability to detect the presence of disease), its specificity (ability to recognize the absence of disease) can be very poor(Breslau and Strandness 1983).

1.3.2 Indirect Methods

(a) Supraorbital Doppler Examination

The supraorbital artery is a branch of the opthalmic artery, which is in turn a branch of the internal carotid artery. Normally, the ophthalmic artery supplies the forehead through its branches the supraorbital and medial frontal arteries. With complete or severe stenosis in the internal carotid, the external carotid becomes an important collateral source to the brain through the ophthalmic artery, thus reversing the flow in this artery. By compressing the branches of the external carotid artery, one can measure the re-reversal of flow in the ophthalmic using a Doppler ultrasound device. This will indicate the presence of a stenosis in the internal carotid. Yet, this method remains unsuitable for a mild degree of stenosis, since severe constrictions are required before opthalmic arterial flow reverses.

(b) Plethysmographic Systems

This method also relies on the fact that the ophthalmic artery is the first branch of the internal carotid artery. Two systems are available: the oculoplethysmograph combined with angiography, and the oculopneumoplethsmograph.

In oculoplethysmography, fluid-filled plastic cups are placed against the eyes and subjected to a negative pressure of 40mm Hg. A pulse wave representing the volume change of ocular filling is generated and recorded. A significant delay in pulse arrival time is the prime determinant of disease. Among the main disadvantages of this method is the fact that it cannot distinguish between a tight stenosis and total occlusion and that it is unable to detect small ulcerating plaques or mild disease.

In oculopneumoplethysmography, the negative pressure applied is much greater, namely 300mm Hg. The point at which pulses appear during the gradual reduction in the vacuum pressure accurately measures the pressure in the opthalmic artery, but the test cannot measure pressures above 110 mm Hg. Further, it is insensitive to lesions which do not produce pressure drop.

In summary, although significant advances in non-invasive detection of localised atherosclerotic plaques have been achieved in recent years, the recognition of early stages of the disease development remains difficult. For example, with regard to the carotid arteries it is usually possible to diagnose only the haemodynamically significant stenosis by methods of phonoangiography, oculoplethysmography, and directional Doppler ultrasound studies. Since most of the diagnostic techniques involve some aspects of haemodynamics, a detailed study of the flow field downstream of a stenosis could help in lowering the threshold of recognition of arterial disease; for, even a relatively mild stenosis (e.g. 20% by area) can produce the most interesting flow patterns as we shall see in the subsequent analysis.

CHAPTER 2

EXPERIMENT, INSTRUMENTATION, AND DATA PROCESSING

A good starting point when studying the fluid dynamics of arterial stenoses is to consider an arterial location whose geometry is relatively simple. The carotid bifurcation is geometrically complex and hence flow field analysis in this region is difficult. The work reported in this thesis is derived mainly from measurements in vivo of the velocity field created by subtotal, externally placed constriction imposed on the descending thoracic aorta of mongrel canines.

2.1 Basic Physiological Preparation

The animals used were mongrel dogs, weighing 18-25 kg. Each dog was anesthetized initially with 2.5% thiamylal sodium (Surital sodium)(10-20 ml,iv). This was followed immediately by injection of atropine sulfate (0.4 mg,iv) and later, sodium pentobarbital (150 mg). The dog was maintained in a satisfactory anesthetized state by administering sodium pentobarbital at a rate of 200 mg/hour.

The thoracic descending aorta was exposed for a distance of approximately 15 cm. An electromagnetic flowmeter was placed about the vessel at the most distal accessible position above the diaphragm. The hot-film anemometer probe was then inserted into the aorta and stationed in the midline (see Fig.2.1).

Several precisely measured, notched, plastic strips were placed at pre-determined locations around the aorta for the extravascular occlusions. These strips were then attached individually to a device specially fabricated to cause varying degrees of occlusion by use of a micrometer adjustment. This device gives a measurement of external occlusion diameter. The internal diameter is computed by increasing the constriction until flow is totally obstructed, noting the resultant external diameter, and then assuming that the vessel wall is deformed isovolumetrically at each stage of occlusion.

The local instantaneous velocity was obtained by a DISA Electronics model 55D01 anemometer and 55D10 linearizer. Each probe was calibrated with blood taken from the dog under study and the anemometer output was linearized in accordance with this calibration. Giddens ,Mabon and Cassanova(1976) describe the difficulties associated with in vivo hot film measurements. Reverse flows could not be determined accurately with the single sensor; and transverse velocities occurring in a turbulent flow will affect the anemometer output which was calibrated only for the axial flow. Although the conical probe tip tends to reduce this latter effect, it is nonetheless present and has an increasing effect as flow becomes more turbulent. The velocity signal and the ECG were both recorded on FM tape for further processing.

2.2 Hot Film versus Doppler Ultrasound

During much of the cardiac cycle the arterial flow is positive. The response of hot-film probes is considered to be good up to 1000 Hz (Giddens et al. 1976). In comparison, the laser Doppler velocimeter has a frequency response of 200 Hz when employed in a similar fluid dynamic situation. Thus the data obtained with the hot-film probes is

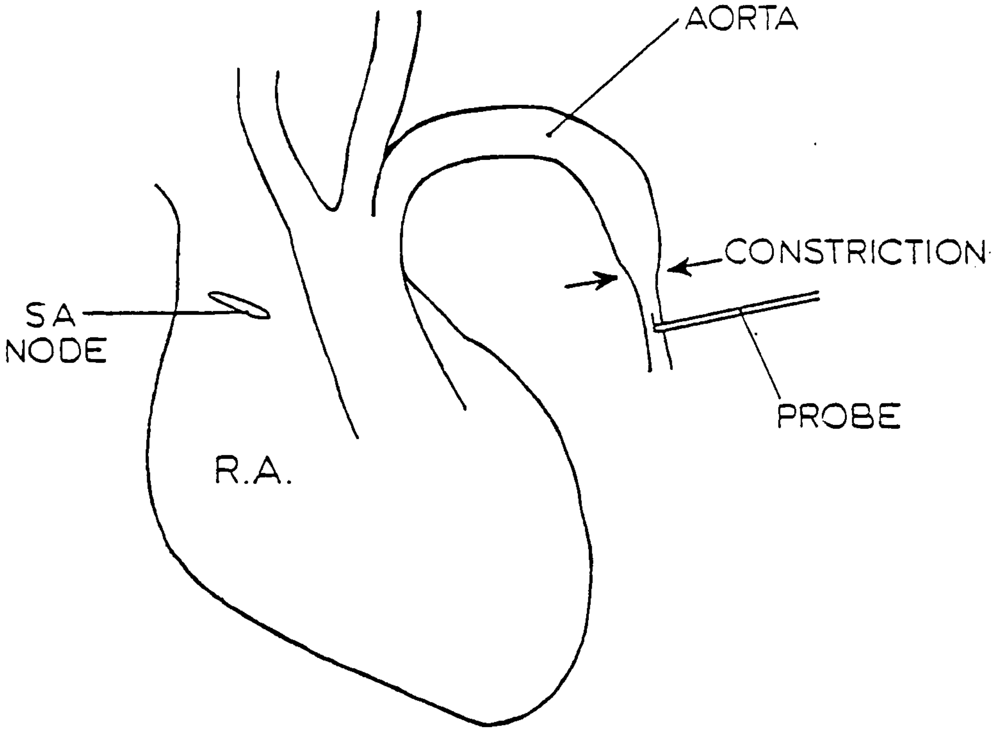

Fig. 2.1 A sketch of the physiological preparation showing hot-film probe and external constriction.

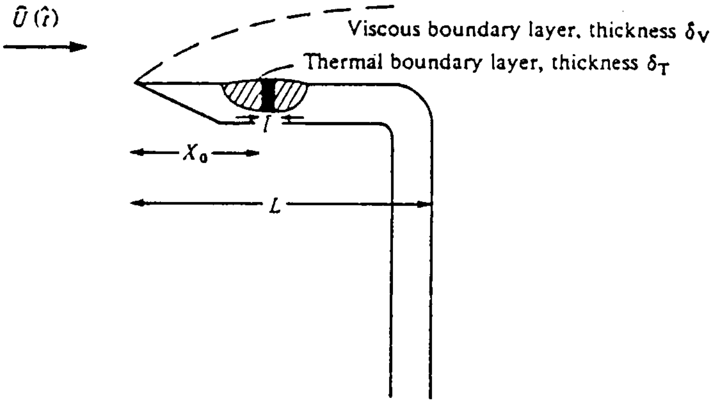

Fig. 2.2 A sketch of a hot-film anemometer probe. The dark rectangle represents the film; the shaded region around it represents the insulating substrate. (After Pedley,1976)

more useful in the understanding of blood flow disturbances caused by a stenosis especially if a bandwidth above 200 Hz is required. Inspite of the fact that the hot-film anemometer is believed to be superior to the Doppler ultrasound velocimeter for measuring disturbed flow with a bandwidth of about 500 Hz (Pedley,1980), the description of both techniques in more detail is essential in assessing the reliability of the measured data.

2.2.1 The Hot Film Anemometer

The hot film anemometer (HFA) measures the flow-related cooling of a heated probe by moving blood. A constant-temperature HFA consists of a thin metallic film mounted flush with the surface of an insulated solid probe as shown in Fig.2.2. The temperature of the film is kept at a fixed value slightly higher than the temperature of fluid which is assumed to be constant, by an electronic feedback circuit. The power required to maintain the probe at constant temperature is proportional to the rate at which heat is lost to the fluid. This in turn is related to the velocity of the fluid flowing past the probe. The conduction of heat to the blood from the hot-film is a very complex problem. An empirical equation governing the transfer of heat is given by Schultz ,Tunsball, Lee and Gunning(1969) as:

$$Nu = A\ (Pr)^{1/3}.(Re)^{1/2} + B\ (Pr)^{1/3} \qquad (2.1)$$

where Nu is the Nusselt number, Re is the Reynolds number, Pr is the Prandtl's number, and A and B are constants. Nu and Pr may be written as:

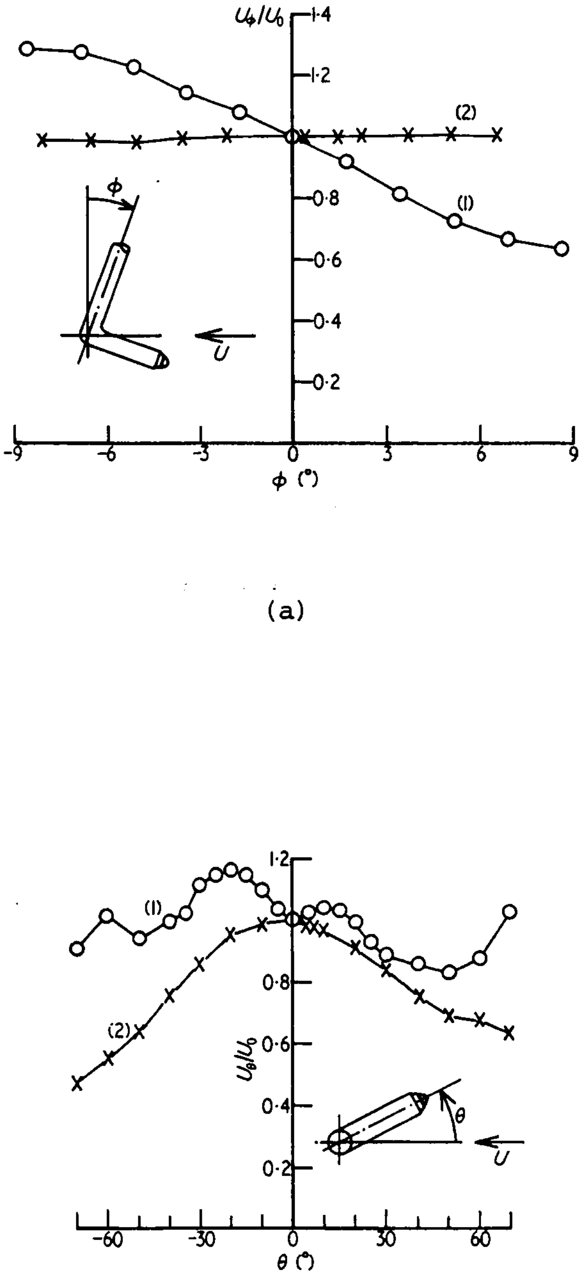

(a)

(b)

Fig.2.3 Probe response to pitch at $\theta=0$ (a) and to yaw (b) at $\phi=0$: (1) cylindrical (2) conical. U_θ is the apparent velocity and U_o is the true velocity i.e. 0.75 m/s. (After Clark,1974)

$$Nu = q / (b . \Delta T . k)$$

$$Pr = \nu / K$$

$$K = k / (\rho \cdot c) \qquad (2.2)$$

where q is the heat transfer rate, b is the gauge length, ΔT is the temperature difference between film and fluid, k is the thermal conductivity of the fluid, ν is the kinematic viscosity, ρ is the density, and c is the specific heat (Clark,1974). Schultz et al.(1969) show that equation (2.1) can be written as:

$$Nu = \frac{V^2}{\Delta T} \quad C + D\,(U)^{1/2} \qquad (2.3)$$

where V is the potential difference across the thin film, U is the the fluid velocity, and C and D are constants. With the temperature difference ΔT held constant, a calibration curve is obtained by plotting the square of the voltage against the square root of the fluid velocity (Woodcock 1975).

The HFA is not sensitive to direction. Fig.2.3(a) and (b) displays the response to pitch and yaw of two types of probe: cylindrical and conical. Note from the figures that the sensitivity of the conical probe is dependent upon θ (best for $\theta=0$) and almost independent upon Φ .

When considering the response of a hot-film probe for conditions of reversed flow, the wall shear over the hot-film becomes an important factor. The heat transfer from the hot-film, and hence the output from the anemometer, is proportional to the one-third power of

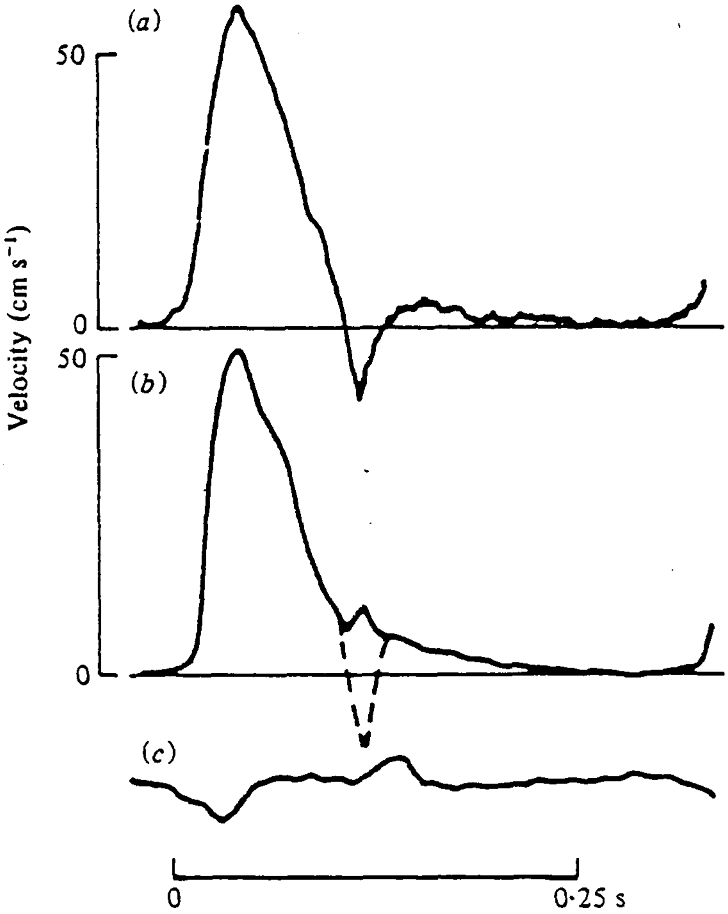

Fig. 2.4 Simultaneous aortic velocity measurements with (a) an electromagnetic flow cuff and (b) a hot-film anemometer located on the vessel centre line. The signal from a second hot-film, (c), indicates when reversal occurs. (After Clark and Schultz, 1973)

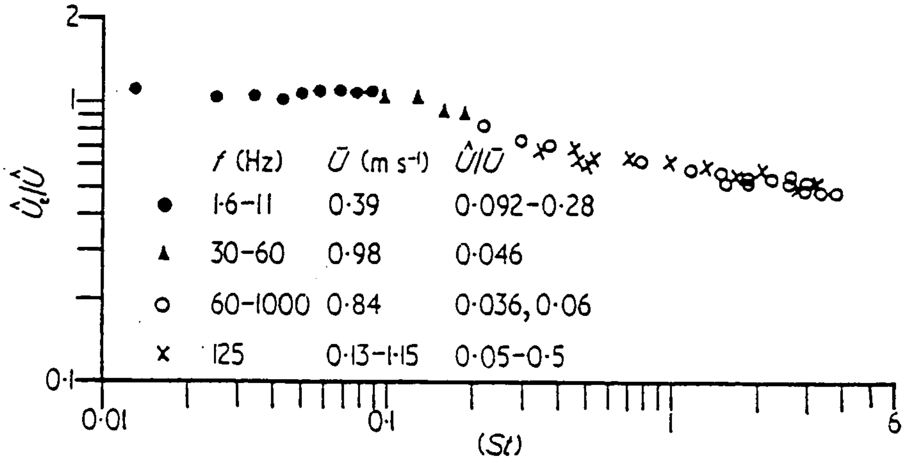

(a)

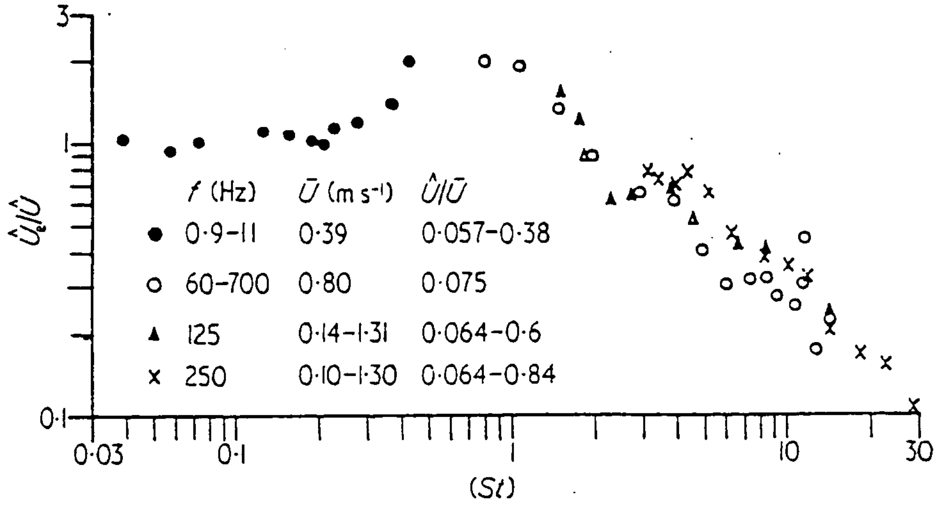

(b)

Fig. 2.5 Amplitude response to oscillatory velocity component as a function of Strouhal number: (a) conical probe (l=0.5 mm); (b) cylindrical probe (l=2.5 mm). $\hat{U}_e$ and $\hat{U}$ are apparent and actual oscillatory velocity components, respectively. (After Clark,1974) the local wall shear (Pedley 1980). Now blood flow in certain large arteries reverses its direction at least twice each beat, and therefore so does the film shear and it is due to this shear reversal - which occurs before the reversal of the centre-line velocity - that the measured velocity signal is subject to rectification before the actual zero crossing of the true signal. Fig. 2.4 shows a cycle of a velocity signal with an apparent 'rectification' effect by a HFA. Notice that: (a) the 'rectified' part of the signal seems to be attenuated, and (b) 'rectification' starts before the velocity goes negative.

Inspite of this disadvantage, hot-film anemometry is still a useful technique in blood velocity analysis because of its good frequency response. Giddens et al.(1976) report good frequency response up to 1 KHz for turbulent flows in rigid tubes. Clark (1974) showed that the amplitude response is a function of Strouhal number ($St=(2 \pi f l)/\bar{u}$ where f is the frequency, l is the length of the film, and $\bar{u}$ is the mean velocity) rather than just of frequency. The amplitude response shown in Fig.2.5 for both conical and cylindrical probes depicts: (a) a gradual decrease in sensitivity with the conical probe for $St > 0.1$,and (b) a region of increased sensitivity and then sharp decline for the cylindrical probe. Although the amplitude response cannot be considered as flat, the behaviour of this device is superior to Doppler ultrasound techniques for measuring turbulent blood velocity signals as we shall see in the next section.

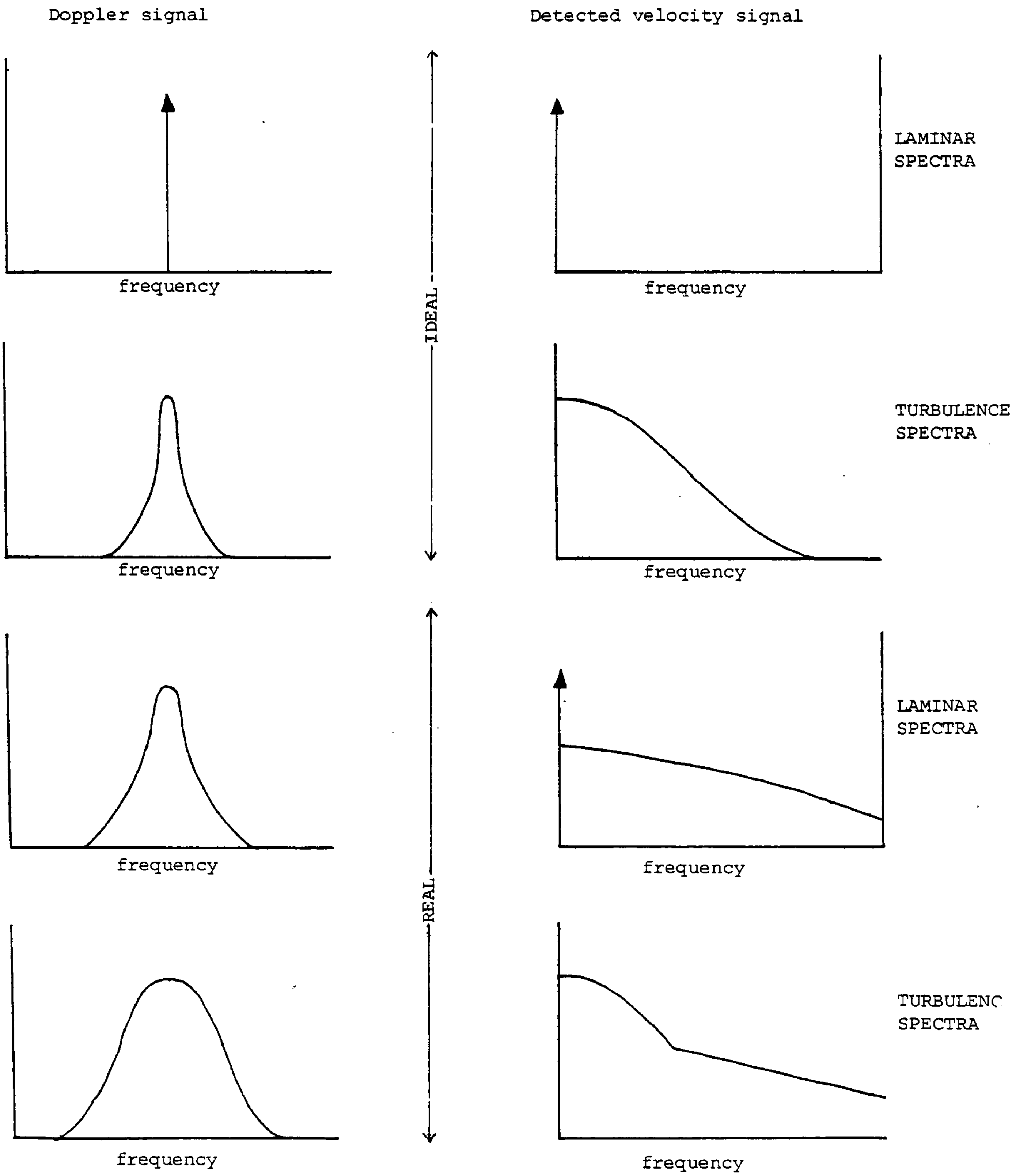

Fig. 2.6 A sketch of ideal and real spectra for laminar and turbulent velocity signals.

2.2.2 Doppler Ultrasound Techniques

Doppler ultrasound velocity meters can be classified into continuous wave (CW) or pulsed devices (PDU). Both types are based on the familiar Doppler principle that moving particles subjected to an incident wave field will create reflected wave frequency shifts. The Doppler shift, Δf, is given by (Woodcock 1975):

$$\Delta f = \frac{v}{c} f_o (\cos \theta + \cos \beta) \qquad (2.4)$$

where f_o is the emitter frequency, v is the blood velocity, c is the the velocity of sound, θ is the angle between the transmitted beam and the direction of the velocity and β is the angle between the received beam and the direction of velocity.

The range ambiguity i.e. the inability to estimate the position of the scattering particles in the CW system is remedied in the pulsed system. In the latter, pulses are transmitted and received using the same transducer. During the interval between emission of successive pulses, the transducer receives the scattered signal. For such a system equation (2.4) becomes:

$$\Delta f = \frac{v}{c} 2 f_o \cos \theta \qquad (2.5)$$

For both laminar and turbulent flow, the output of the PDU velocimeter may be considered in terms of the power spectra of the Doppler and detected velocity signals. The upper four graphs in Fig.2.6 show the ideal spectra for both these signals. One of the main limitations of the Doppler technique is the spectral broadening

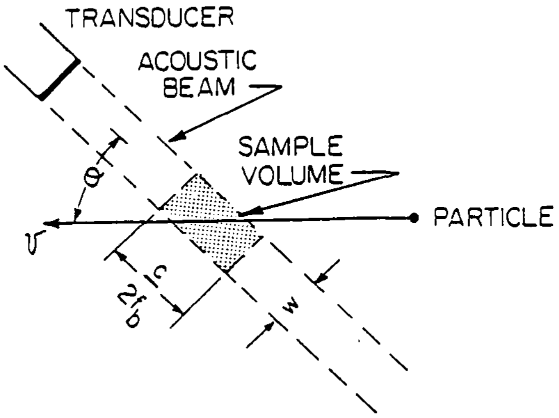
TRANSDUCER
ACOUSTIC BEAM
SAMPLE VOLUME
PARTICLE
θ
v
c/2f_b
w

(a)

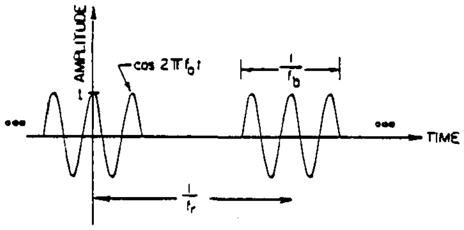
AMPLITUDE
cos 2πf_0 t
1
1/f_0
TIME
1/f_r

(b)

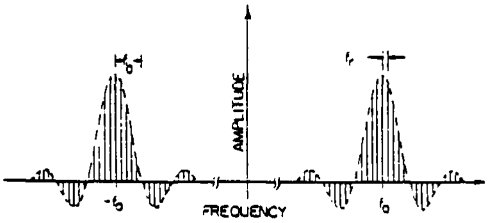
AMPLITUDE
f_b
f_r
-f_0
f_0
FREQUENCY

(c)

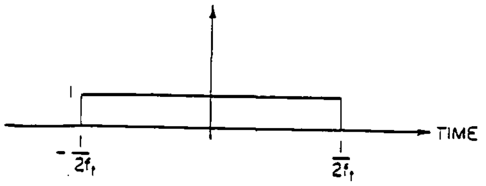
1
TIME
-1/2f_t
1/2f_t

(d)

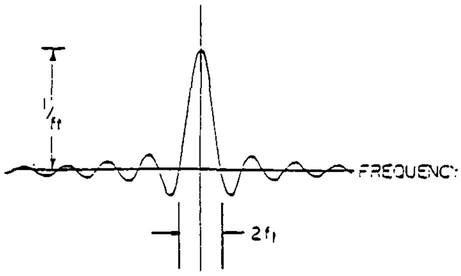
1/f_t
FREQUENCY
2f_t

(e)

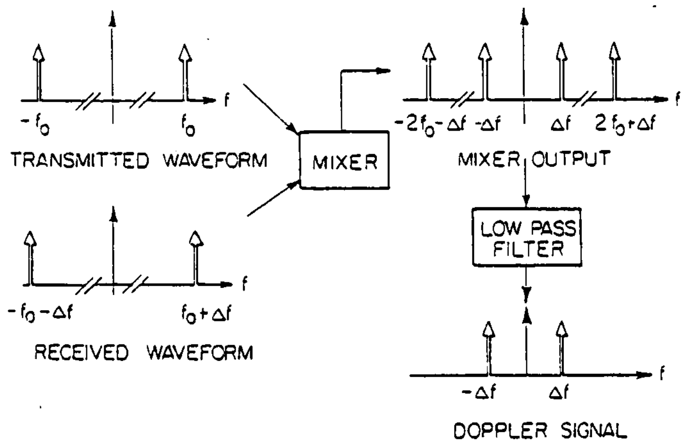

(f)

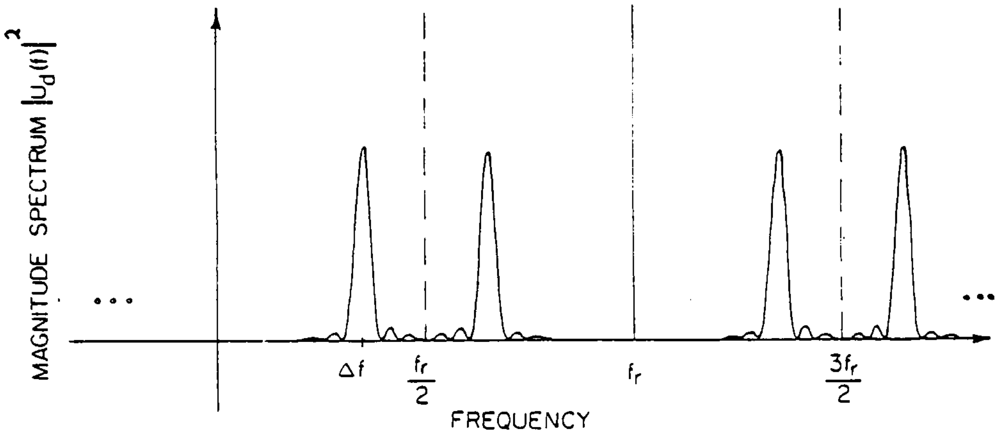

(g)

Fig. 2.7 Idealised operation of the Doppler system for a rectangular sample volume.

(a) The idealised configuration of the acoustic sample volume.

(b) The transmitted signal in the time domain.

(c) The transmitted signal in the frequency domain.

(d) The transit-time window in the time domain.

(e) The transit-time window in the frequency domain.

(f) The ideal mixing process.

(g) The Doppler spectrum for an idealised system.

(After Baker, Forster and Daigle, 1978)

exhibited in the four lower graphs of Fig.2.6. Factors influencing Doppler spectral broadening can be divided into instrument effects and flow-related effects. The instrument effects can be described by considering the movement of a single particle through the acoustic field at constant velocity. The form of the Doppler spectrum is dependent on the sample volume dimensions. For simplicity, consider a single particle intersecting a rectangular sample volume at the centre as shown in Fig.2.7(a). The 'transit time', t_t, is given by:

$$t_t = \frac{1}{f_t} \simeq \frac{w}{v\sin\theta} \qquad (2.6)$$

w, v and θ are defined in Fig.2.7(a). Fig.2.7(b) shows a typical transmitted Doppler signal, $u_t(t)$, and Fig.2.7(c) depicts its representation in the frequency domain, $U_t(f)$. The returning <u>Doppler shifted</u> signal (in the frequency domain), $U_s(f)$ is given by:

$$U_s(f) = C\,U_t(f\,(1+\alpha)) \qquad (2.7)$$

where C=constant, and $\alpha = \Delta f/f_o = 2v\cos\theta$. The returning signal exists only for the time the particle traverses the sound, i.e. during the 'transit time'. This is equivalent to multiplying $u_s(t)$ with the time window, w(t), shown in Fig.2.7(d) or convolving $U_s(f)$ by the transform of w(t), W(f) (see Fig.2.7(e)). Hence the resulting signal, $U_{sw}(f)$, is:

$$U_{sw}(f) = U_s(f) * W(f) \qquad (2.8)$$

where * denotes convolution. The Doppler signal is obtained by mixing (multiplying) $U_{sw}(t)$ with $\cos(2\pi f_o t)$ and sampling. $U_m(f)$, the output of the mixer can be described as:

$$U_m(f) = 0.5U_{sw}(f-f_o) + 0.5U_{sw}(f+f_o) \tag{2.9}$$

Fig.2.7(f) gives a pictorial description of an ideal mixing process. It shows how the contributions centered at $\pm\ 2f_o(1+\alpha)$ are filtered off. The final Doppler signal is obtained by sampling $u_m(t)$. Ideal sampling could be thought of as convolving the filtered $U_m(f)$ or $U_{mf}(f)$ with a sampling function , S(f),i.e.

$$U_d(f) = U_{mf}(f) * S(f) \tag{2.10}$$

where

$$S(f) = \sum_{m=-\infty}^{\infty} \delta(f-mf_r)$$

The resultant power spectrum $|U_d(f)|^2$ of the Doppler signal could be seen in Fig.2.7(g). In practice the signal is low pass filtered at $f_r/2$ to obtain the frequency shift, df. The two factors that affect the general broadening of the spectrum are: (a) the burst duration, $1/f_b$, or the source broadening, and (b) the effect of the acoustic field because of the finite transit time, t_t, or 'transit time broadening'. If we now consider the window function in Fig.2.7(d) and (e), we will find that, by increasing t_t i.e. increasing the sample volume, the width of W(f) decreases and hence the broadening of the Doppler spectrum becomes less. This, however, decreases the spacial resolution of the system.

So far, we have considered the effect of an ideal rectangular sample volume on the Doppler spectrum. In practice however, this sample volume is of a 'tear drop' shape (Saxena 1978) and its contribution to the Doppler spectrum is more difficult to describe. Another complication to the broadening problem is the fact that flow too can worsen this effect. Consider the field in the sample volume as consisting of particles moving with different velocities, we would expect contributions of these particles in the spectrum. The extent of these velocity variations is a function of the velocity gradients across the volume as well as the size of the sample volume(Baker , Forster and Daigle,1978). Arts and Roe vros(1972) assumed that the volume under consideration contains N particles. Every particle is supposed to give the same contribution and hence the definition of an average velocity contribution is as follows(ibid):

$$\Delta w_{av} = 1/N \sum_{i=1}^{N} \Delta w_i \qquad (2.11)$$

where Δw_{av} is defined as the difference between the average angular frequency of the power spectral density of the received signal and the angular frequency of the transmitted signal. However, the distribution of velocities in a sample volume is certainly non-uniform and hence a further study of the velocity distribution (given flow conditions) is necessary.

Although models of the Doppler ambiguity process have been suggested (George and Lumley 1973, Garbini et al. 1982 (a) and (b)), a thorough understanding of Doppler ambiguity remains a challenging task for many researchers. Thus, the choice of the Doppler ultrasound technique for the measurement of disturbed or even turbulent velocity

Table 2.1 Relevant data for in vivo experiment employed as sample study

Percent occlusion (reduction in area)	Constriction diameter	Peak local velocity U_p	Mean volume flow rate Q	Peak Reynolds number $\rho U_p D/\eta_\infty$	Mean Reynolds number $4\rho Q/\pi\eta_\infty D$
	cm	cm/s	ml/s		
0	1.2	59	31	2500	1200
20	1.1	50	29	2100	1100
40	0.9	45	31	1900	1200
58	0.8	41	30	1700	1100
74	0.6	48	29	2000	1100
88	0.4	57	27	2400	1000

Frequency parameter: $\alpha = 13.8 (\omega = 15.0$ rad/s, $\eta_\infty = 0.030$ poise)

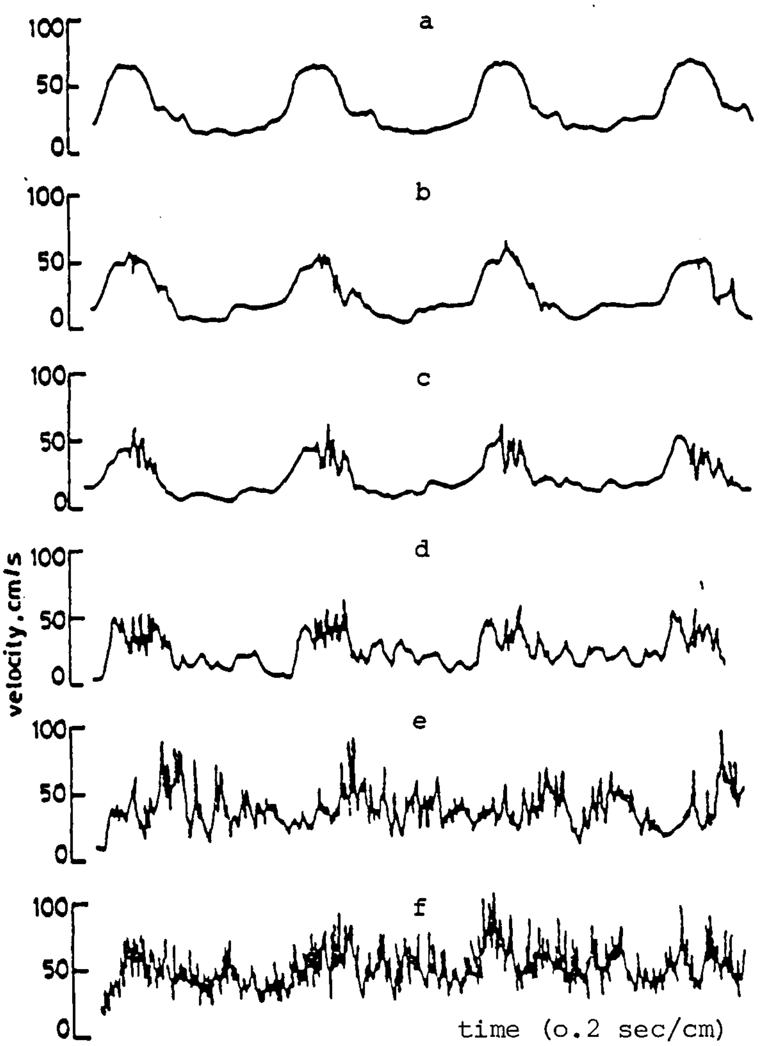

Fig. 2.8 Velocity measurements obtained at the vessel centreline, 2 cm distal to stenoses imposed on the descending thoracic aorta of a dog.

a No occlusion b 20% occlusion
c 40% occlusion d 58% occlusion
e 74% occlusion f 88% occlusion

fields oughtto receive much thought. Another consideration when dealing with a turbulent velocity signal should be the spatial averaging caused by a large sample volume. This tends to obscure small scale fluctuations, particularly at high wavenumbers. Thus, although a larger sample volume tends to reduce ambiguity effects, this improvement is at the expense of spatial resolution. When analyzing a disturbed velocity signal like the signal measured distal to a stenosis, the choice of measurement technique, hot-film or Doppler, is assisted by a clear understanding of what features of the field are important within the context of a particular situation. If it is the overall (or average) behaviour of our physical system which is required, then the Doppler technique could be a useful non-invasive tool. However, if the detailed or fine structure of the velocity field is of interest, then the hot-film anemometer can produce a more accurate signal. Initially, the objective is to use the hot-film technique in order to extract certain features that are not available to us in the Doppler measurements. Eventually, the Doppler technique can be used if and only if we possess an adequate understanding of the system under study.

2.3 Data Preprocessing

2.3.1 Analog to Digital Conversion

The data employed in this study were obtained from the series of in vivo experiments reported in section 2.1. The degree of stenosis ranged from 0 to 88% reduction by area. Table 2.1 summarises the experimental conditions. Fig.2.8 displays the instantaneous velocity measurements for several heart cycles for each degree of constriction. This signal together with the ECG were recorded on an FM tape and then digitized. The sampling rate, f_s, (2560 Hz) was based on the outcome of preliminary experiments conducted by Khalifa and Giddens(1981). These experiments indicated that the turbulence information for this flow system might contain frequencies as high as 500 Hz before being lost in noise. Other factors involved in the choice of f_s were the resolution and appropriate data length for Fourier transform (Kitney, Giddens and Mabon ,1980). In the analog to digital conversion, ADC, procedure the data was stored on digital tape in 1200 sample blocks, each level of occlusion being stored in separate files comprising about 300 blocks. Two channels were recorded, the velocity and the ECG.

2.3.2 Data Sectioning

Respiration, temperature control, and the blood pressure control system, all affect the spatio - temporal nature of the blood velocity waveform. In addition to this underlying physiological variability, there is also noise artefact. To overcome these problems, it is necessary to remove the temporal variation by defining a fiducial point and then selecting the appropriate section of the waveform. The problem due to noise can be solved by either low-pass filtering or ensemble averaging; this will be discussed in the following chapters.

The sectioning procedure consists of defining a timing marker and then choosing a fixed number of samples for given block of data. The timing marker is derived from the R wave of the ECG. The underlying

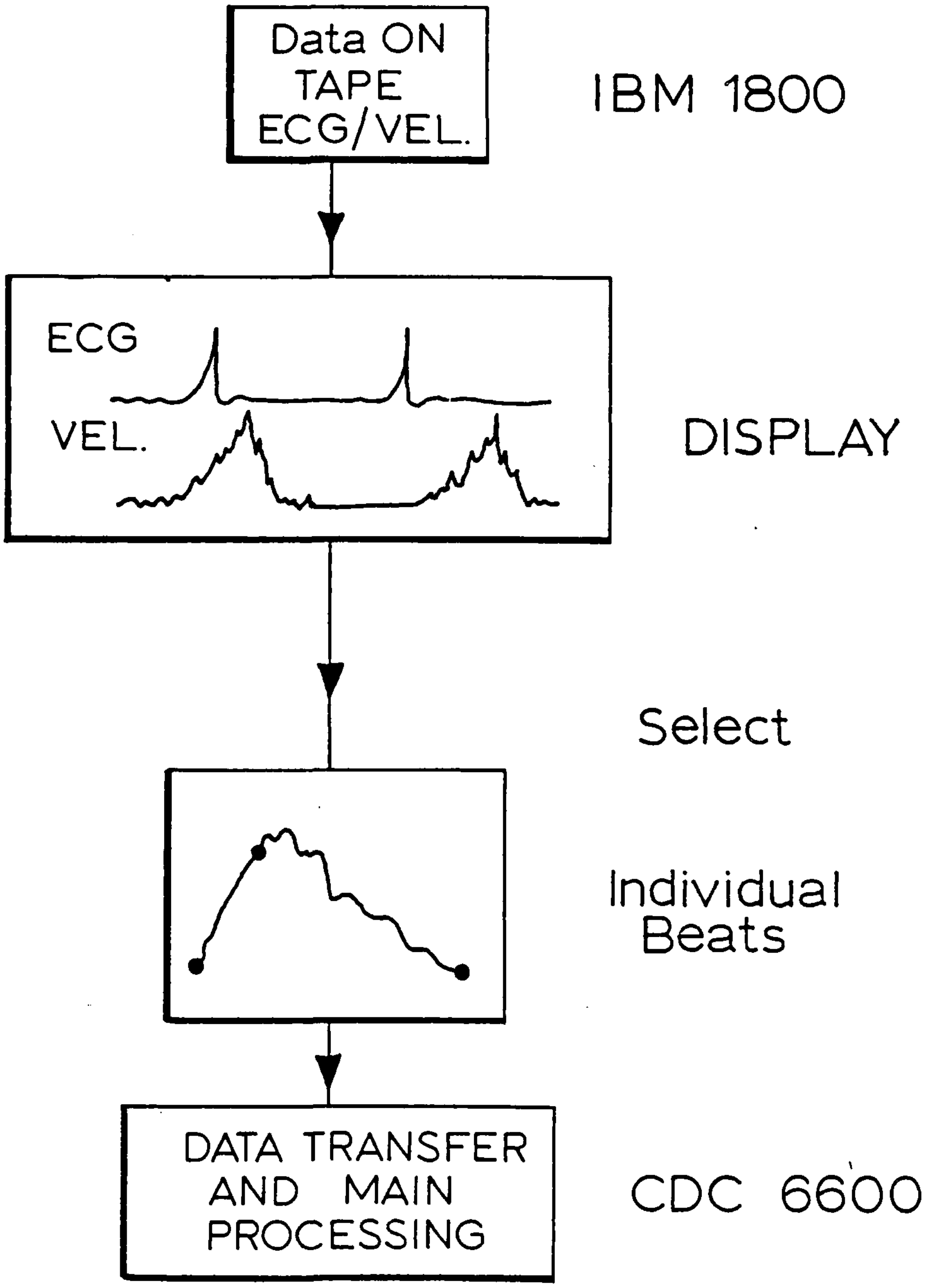

Fig. 2.9 Ensemble selection procedure.

assumption is that even though the RR interval is variable, the interval between the R-wave and the required section is constant. The program which controls the selection process is designed to operate in three modes: manual, semi-automatic and automatic. At the beginning of selection the program is normally run in the manual mode, i.e. the sections of data to be used in the ensemble are selected automatically by the program but the operator can check that each beat to be used is appropriate. Once the operator is satisfied that the detection procedure is working satisfactorally the program can be either run in the semi-automatic mode, where every tenth beat is displayed, or run in the fully automatic mode, where none of the beats detected by the program are displayed. For each level of occlusion, a total of 120 to 125 blocks are chosen automatically with 512 samples for each block. A pictorial description of the sectioning procedure is illustrated in Fig.2.9.

2.3.3 Detection of Unsuitable Beats

With the sectioning program in automatic mode, the unsuitable or mis-triggered beats can amount to 3-5% of the total. Fig.2.10(a) shows 125 beats for a 40% occlusion level. It can be seen that B19, B34, B39, B59 and B79 have been mistriggered (Fig.2.10(b) is a magnification of B19). To deal with this problem, two procedures have been devised. The first procedure relies on our perception of unsuitable beats. These are missed out when the whole 100 ensemble is rewritten to a different file. The second procedure is operator independent and relies on the integral under the velocity section.

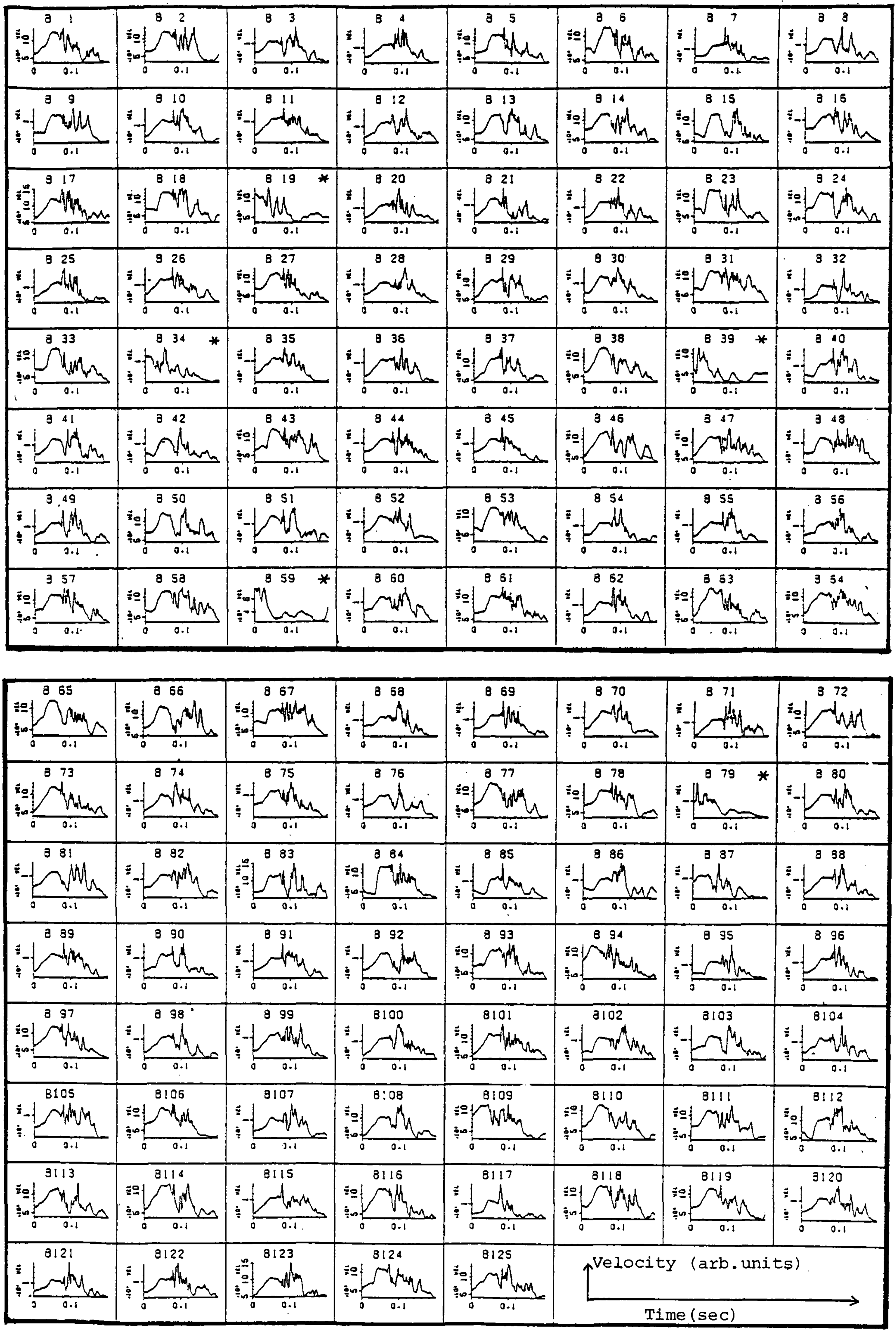

Fig. 2.10(a) An ensemble of 125 sectioned beats showing unsuitable sections (*).

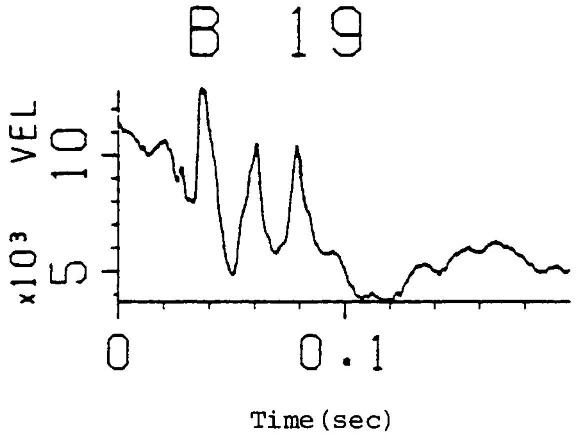

Fig. 2.10(b) A magnification of beat B19 in Fig. 2.10(a).

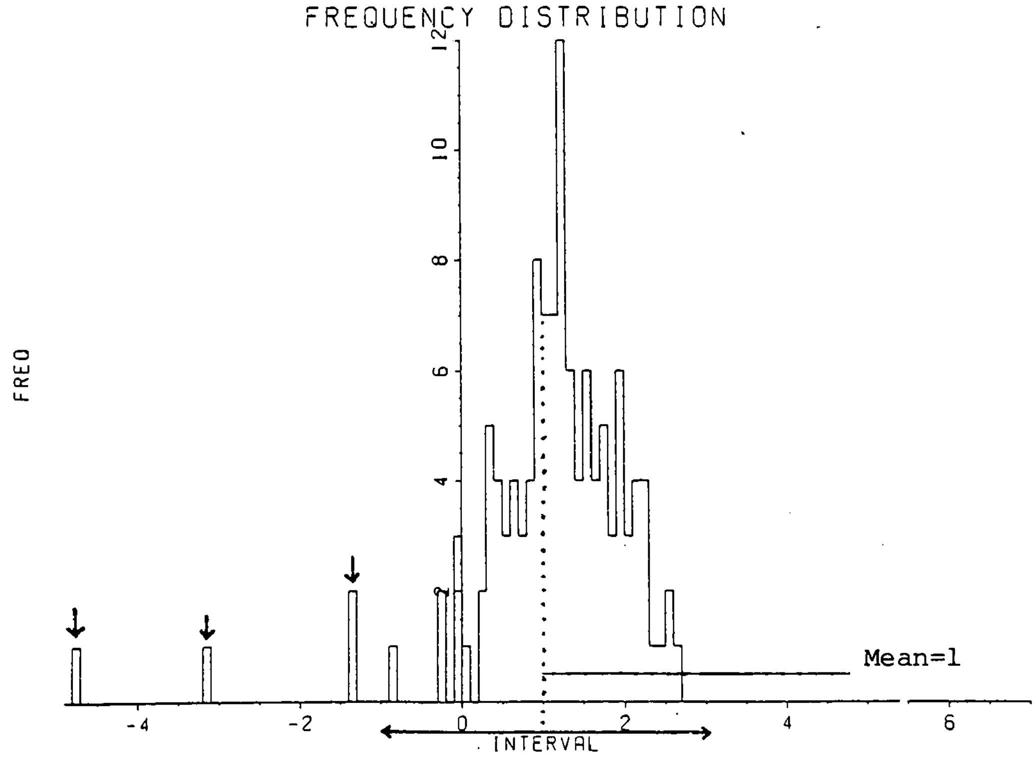

Fig. 2.11 A frequency histogram of the time integral of the velocity waveform for the 125 beats shown in Fig. 2.10(a). The vertical arrows show the beats to be discarded.

The integral is utilized because the signal is positive and because a mistriggering can lead to a considerable reduction in area as seen in Fig.2.10(b). In Fig.2.11 the frequency histogram of the mentioned integrals is plotted. The mean has been normalized and the x-axis has a resolution of 0.1 standard deviation. The beats that are discarded from the 40% occlusion ensemble are those with integrals which are greater than ±2 standard deviations(see arrows in Fig.2.10). This technique has proved to be reliable for occlusion levels of 0,20,40,58,and74%. For the 88% the signal becomes highly disturbed and the histogram of integrals is flattened indicating a large variability. Other techniques have to be used for this level and they will be discussed in the following chapters.

The end result of data preprocessing is to generate 100 blocks of data (each block having 512 samples) for each level of occlusion, namely 0,20,40,58,74 and 88%. In the next two chapters, techniques of analysing these data will be discussed and subsequently an attempt will be made to model the generating velocity field as a stochastic process. The amount of information derived from these measurements is a function of the techniques used. These techniques should be designed or chosen such that they exploit the power of signal processing theory without being detached from the basic physical notions of which the signal is a product.

CHAPTER 3

CHARACTERISATION OF THE VELOCITY WAVEFORM : BASIC METHODS

3.1 The Velocity Waveform as a Time Series

The velocity signal discussed in chapter 2 consists of sampled sections of the continuous signal, each section comprising 512 data points. A section can be considered as a time series i.e. a collection of observations made sequentially in time (Chatfield,1980); and will be denoted by $\{u(t) \; ; \; t=T,2T,3T,...,NT\}$ where T is the sampling interval and N is the total number of observations (i.e. 512). A first step in the analysis of such a time series is to decide whether it can be considered as stationary.

A time series $\{x(t)\}$ is strictly stationary if for any $t_1,t_2,...,t_n$ and any k, the joint probability distribution of $\{x(t_1),x(t_2),..., x(t_n)\}$ is identical with the joint probability distribution of $\{x(t_1+k),x(t_2+k),...,x(t_n+k)\}$ (Priestley,1981). Strict stationarity is, however, a severe requirement and is relaxed by introducing the notion of stationarity up to order m . Under this weaker condition, the probability distribution of, say $x(t_1)$, need not be identical to the probability distribution of $x(t_1+k)$, but the main features of these two distributions should be the same, i.e. their moments, up to a a certain order, m, should be the same. x(t) is called second-order stationary or (weakly stationary) if the following are satisfied:(E[ ] denotes expectation)

(1) $E[\; x(t) \;] = \mu$, i.e. the mean, μ , is a constant

independent of t.

(2) $E[(x(t)-\mu)^2] = \sigma^2$, i.e. the variance is a constant independent of t.

(3) E[x(t) x(s)] = function of (t-s) only, for every t,s; i.e. the covariance between the values at any two points s and t depends on (t-s), the interval between the time points, and not on the location of the points along the time axis.

From the above definitions of stationarity and after inspection of several samples (or blocks) of the same process (i.e. the velocity field), the time series {u(t)} can be considered as non-stationary (i.e. its statistics are a function of time). Consequently, the strategy employed in the analysis of {u(t)} is to break the waveform into its constituent components using an approach adopted by Hussain and Reynolds (1970) and Khalifa and Giddens (1978). The signal can then be described as follows:

VELOCITY SIGNAL = TEMPLATE + RANDOM COMPONENTS

The template of the velocity signal is basically the pulse wave which is to a certain extent, repetitive and reconstructable. The random components on the other hand, seem to be influenced greatly by the degree of constriction. Both of these components will be the object of more rigorous processing and analysis in subsequent sections. Two approaches have been designed to extract these components from the original time series which are:

(1) The time domain method : In this method the template is derived by ensemble averaging several samples (blocks) of the

time series, and the random components are considered to be deviations from the ensemble average and are obtained by subtracting the template from the raw signal. The equation governing this approach is as follows:

$$u(t) = U(t) + u'(t) \tag{3.1}$$

where U(t) is the underlying waveform and u'(t) is the disturbance velocity.

(2) The frequency domain method : In this method the assumption is that the separation of the template and random components can be achieved in the frequency domain assuming the following:

$$F_u(f) = F_T(f) + F_R(f) \tag{3.2}$$

where F_u, F_T and F_R are the Fourier transforms of the velocity time series, the template, and the random components.

As will be explained later, these two approaches are not equivalent and their advantages and disadvantages will also be discussed later especially with regards to the disturbance signal (or random components).

3.2 Ensemble Average Analysis

In this section attention will be focussed on the time domain method suggested by equation (3.1). The template, $\{U(t)\}$, is calculated by ensemble averaging several statistical samples (a sample consists of a series of observations). In our case, ensemble averaging would be used to extract features of the velocity waveform that are consistent from beat to beat, and are characteristic of the ensemble under study. The characteristics of the ensemble may change for each level of occlusion. Before considering in detail the application of the method to the velocity data, it is worth examining certain theoretical aspects of this useful statistical tool.

3.2.1 Ensemble Averaging

(a) General Theory

Mathematically, the ensemble average, $\{\hat{U}(t)\}$, of a time series, $\{u(t)\}$, can be represented by:(^ denotes estimate)

$$\hat{U}(nT) = 1/M \sum_{k=0}^{M-1} u(nT+kT_o) \qquad (3.3)$$

where n denotes the observation number, T is the sampling interval, M is the ensemble size, and T_o is the period of repetition. In the analysis which follows, a more simplified notation will be adopted ; it is based on Bendat(1964) where, for example, $\{u_k(t)\}$ is equivalent to $\{u(nT+kT_o\}$ and $\langle u_k(t)\rangle$ denotes the ensemble average over k, i.e. equation (3.3).

Using the model suggested in equation (3.1), equation (3.3) can be rewritten as follows:

$$\hat{U}(t) = 1/M \sum_{i=1}^{M} [\ U_k(t) + u'_k(t)\ ] \tag{3.4}$$

The ensemble mean and mean square values (size N) of $\{\hat{U}(t)\}$ are given by :

$$< \hat{U}(t) > = 1/N \sum_{i=1}^{N} [\ < U_i > + < u'_i >\ ] \tag{3.5}$$

$$\begin{aligned} < \hat{U}^2(t) > &= 1/N^2 < [\sum_{i=1}^{N} u_i(t)]^2 > \\ &= 1/N^2 [\sum_{i=1}^{N} < u_i^2(t) > + \sum_{\substack{i,j=1 \\ i \neq j}}^{N} < u_i(t)\ u_j(t) >] \end{aligned} \tag{3.6}$$

It will be assumed that the independent nonstationary random process $\{u'(t)\}$ has an ensemble mean value of zero and a variance $\sigma_{u'}^2(t)$. Also, the coherent average U(t) at any time t has an ensemble mean value m(t) and a variance $\sigma_U^2(t)$; i.e.,

$$< U_i(t) > = m(t)$$

$$\sigma_U^2 = < U_i^2(t)> - m^2(t) \tag{3.7}$$

For the velocity signal under consideration, U(t), and u'(t) will be assumed independent, i.e.:

$$< U_i(t)\ u'_j(t) > = 0 \tag{3.8}$$

and $u_i(t)$ and $u_j(t)$ are statistically dependent, i.e.:

$$u_i(t) = U_i(t) + u'_i(t)$$

$$u_j(t) = U_i(t) + u'_j(t) \tag{3.9}$$

where $U_i(t)$ is recurrent in all samples. To obtain $\langle \hat{U}(t) \rangle$ we substitute $\langle U_i(t) \rangle = m(t)$ and $\langle u'_i(t) \rangle = 0$ in (3.5) to get :

$$\langle \hat{U}(t) \rangle = m(t) \tag{3.10}$$

Obtaining $\langle \hat{U}^2(t) \rangle$ is a more difficult task since we need to evaluate $\langle u_i^2(t) \rangle$ and $\langle u_i(t)\, u_j(t) \rangle$. Since U(t) and u′(t) are uncorrelated, we can write $\langle u_i^2(t) \rangle$ as follows :

$$\langle u_i^2(t) \rangle = \langle U_i^2(t) \rangle + \langle u_i'^2(t) \rangle \tag{3.11}$$

Using equation (3.9) for u_i and u_j dependent we get :

$$\begin{aligned} \langle u_i u_j \rangle &= \langle (U_i(t)+u'_i(t))(U_i(t)+u'_j(t)) \rangle \\ &= \langle U_i^2(t) \rangle \qquad \text{for } i \# j \end{aligned} \tag{3.12}$$

Replacing (3.11) and (3.12) in (3.6) we get :

$$\begin{aligned} \langle \hat{U}^2(t) \rangle &= 1/N^2 [N(\langle U_i^2(t) \rangle + \langle u_i'^2(t) \rangle) + N(N-1) \langle U_i^2(t) \rangle] \\ &= \langle U_i^2(t) \rangle + 1/N \langle u_i'^2(t) \rangle \end{aligned}$$

or

$$\sigma^2_{\hat{U}}(t) = \sigma^2_{U}(t) + \frac{1}{N} \sigma^2_{u'}(t) \tag{3.13}$$

Equation (3.13) shows that ensemble averaging filters out random components present in the original signal by reducing their variance by 1/N. If N is large $\hat{U}(t)$ becomes a better estimate of the recurrent underlying process U(t).

(b) Ensemble Averaging - a Filter Approach

Another interesting approach to the theoretical analysis of ensemble averaging is to consider it as a filter and to study its transfer function. The basic idea behind the ensemble average filter is that the present value in time is a weighted average of M past values separated by a period T_o, i.e. :

$$\hat{U}(t) = 1/M \sum_{k=0}^{M-1} u(nT-kT_o)\ w(nT-kT_o) \tag{3.14}$$

In our case, the window, {w(nT)}, is rectangular but it is possible to use a different window shape in order to achieve a better frequency response. To find the transfer function in the frequency domain, we will firstly consider the Z-transform of equation (3.14) which is given by :

$$\hat{U}(z) = \sum_{n=0}^{N-1} \{1/M \sum_{k=0}^{M-1} u(nT-k(T_o/T)\ T)\ w(nT-k(T_o/T)\ T\}z^{-n} \tag{3.15}$$

where N is the number of points in the transform. Given that a rectangular window has {w(nT)=1} and interchanging the order of the summations in equation (3.16) we have :

$$\hat{U}(z) = \frac{1}{M} \sum_{k=o}^{M-1} U(z)\, z^{-k(T_o/T)}$$

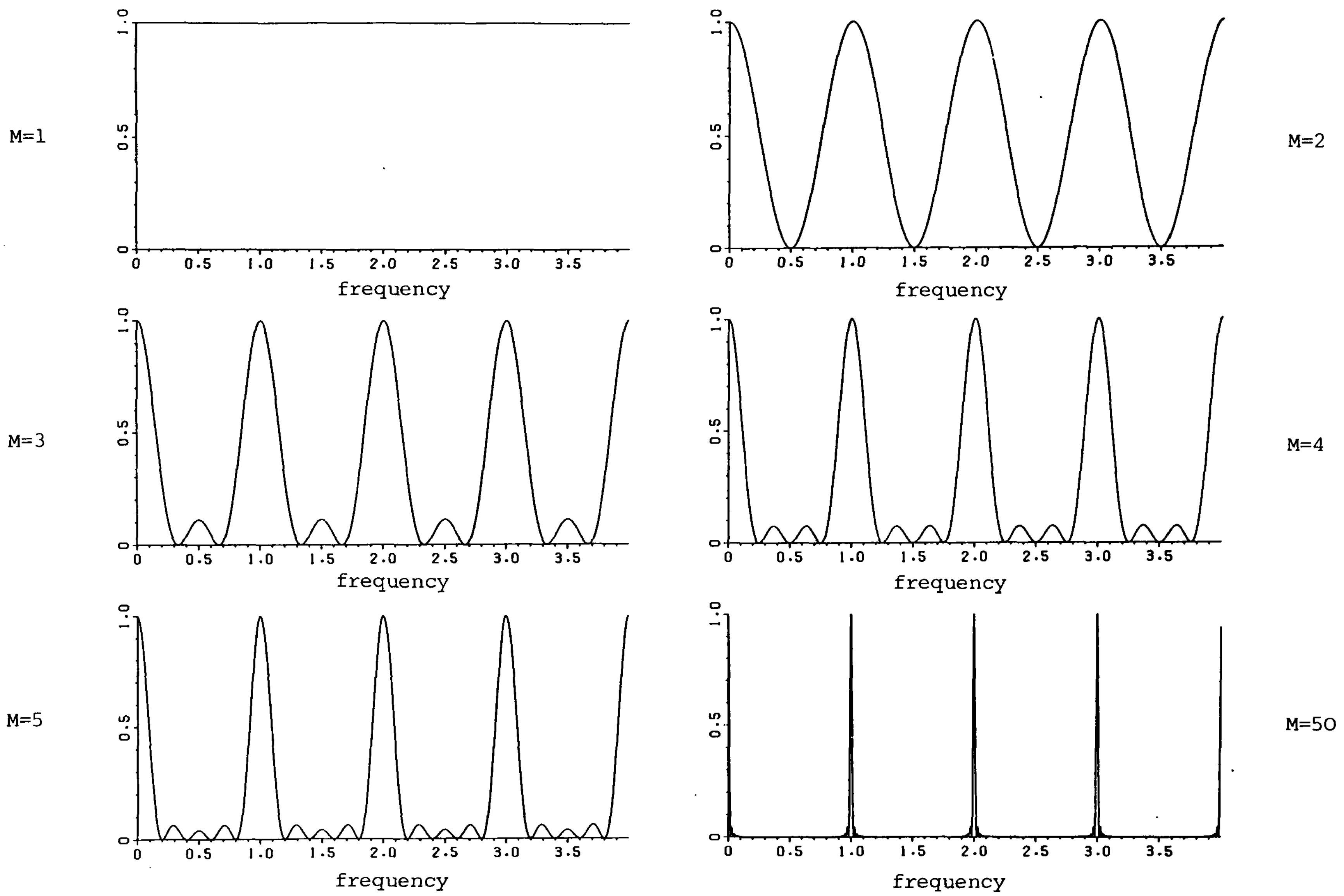

Fig. 3.1 The comb filtering action of the ensemble average filter for different values of M i.e. the ensemble size. The frequency axis has been normalized.

$$\hat{U}(z) = U(z)\,\frac{1}{M}\sum_{k=o}^{M-1} z^{-k(T_o/T)}$$

$$= U(z)\left(\frac{1}{M}\;\frac{1-z^{-M(T_o/T)}}{1-z^{-(T_o/T)}}\right) \tag{3.16}$$

This gives the desired transfer function H(z) which is :

$$H(z) = \frac{1}{M}\;\frac{1-z^{-M(T_o/T)}}{1-z^{-(T_o/T)}} \tag{3.17}$$

In the frequency domain i.e. for $z=\exp(j2\pi\, m/N)$ this becomes :

$$H(mf) = \frac{1}{M}\;\frac{1-\exp(-j\frac{2\pi mM}{N}\frac{T_o}{T})}{1-\exp(-j\frac{2\pi m}{N}\frac{T_o}{T})}$$

or

$$H(mf) = \left(\exp(-j\frac{2\pi mT_o}{2NT}(M-1)\right)\left(\frac{1}{M}\;\frac{\sin(\pi mMT_o/NT)}{\sin(\pi mT_o/NT)}\right) \tag{3.18}$$

which is a form of a comb filter as seen in Fig.3.1 for various values of M. This filter seems to enhance frequency components that are multiples of $1/T_o$ which is an accepted fact intuitively. Also, the choice of M i.e. the size of the ensemble is important: not only does a large M improve the signal to noise ratio (SNR) but it also improves the frequency resolution of the filtered signal (i.e. the sinc function (sinx/x) at $1/T_o, 2/T_o, \ldots$etc. has reduced width and reduced sidelobes as M increases).

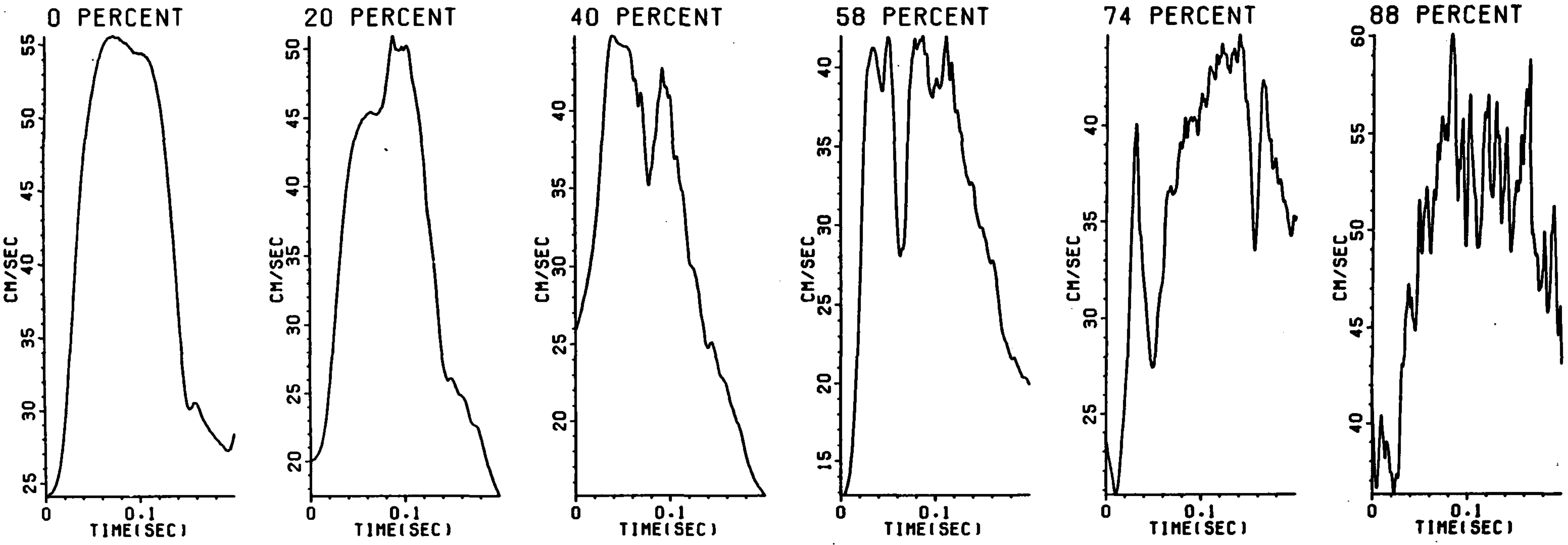

Fig. 3.2 Ensemble averages of the velocity data (ensemble size=100).

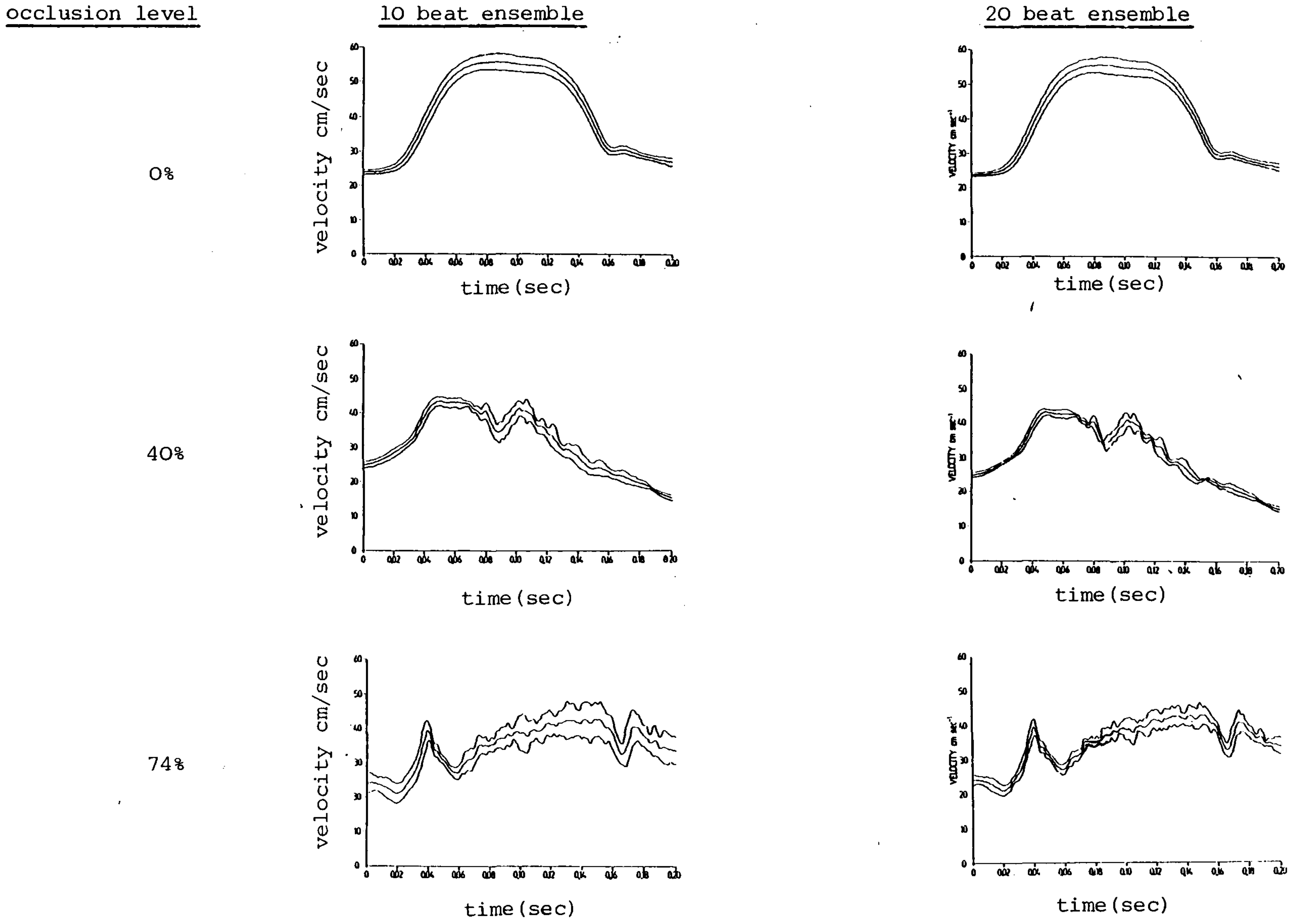

Fig.3.3 Ensemble average velocity waveforms for 0,40 and 74% occlusion data. Central curve is the mean of the ensemble averages and upper and lower curves are ±1 standard deviation.

(c) Application

In the analysis of {u(t)} i.e. the blood velocity signal, 100 blocks of data (512 data points each) are ensemble averaged for each level of occlusion. The template U(t) is assumed to consist of the basic cardiac pulse, some periodic oscillations and other repetitive features. The random components in u′(t) are expected to be due to random velocity components like for example turbulence,and noise. Fig.3.2 shows ensemble averages of six levels of occlusion namely 0, 20, 40, 58, 74 and 88%. The 20% to 74% ensemble averages show an increase in activity with increasing occlusion especially in the deceleration phase of the cardiac cycle. This activity is 'quasi' periodic and its frequency is low as we shall see when applying spectral analysis to the ensemble averaged data.

Because of the difficulty of obtaining 100 beats for the ensemble average under clinical conditions, it would be advantageous to work with ensembles of 10 or 20 beats. To study the feasibility of using a small ensemble size, 100 set were divided into smaller sets of 10 or 20. The mean and standard deviation of the resulting 10 or 5 ensemble averages are displayed in Fig.3.3 for the 0, 40 and 74% data. Although the standard deviation seems to increase with increasing constriction, ensemble averages of size 10 or 20 can produce a reasonable estimate of the underlying process.

One serious disadvantage of this method (seen for example in the 88% data) is the fact that it is very sensitive to phase jitter. In other words, the beats to be averaged have to be properly aligned before averaging can be performed.

3.2.2 Phase Shift Averaging (PSA)

The ensemble of 100 beats obtained earlier on can be represented either as :

$$u(t) = U(t) + u'(t) \tag{3.19}$$

or:

$$u_s(t) = U(t+D) + u'(t) \tag{3.20}$$

where $\{u_s(t)\}$ is the shifted version of $\{u(t)\}$ and D is a variable time delay. In order to obtain an accurate ensemble average, the delay D has to be estimated for each beat and then the beat has to be shifted by an amount $-D$. The method used to determine this time delay is to compute the cross correlation function given by:

$$\begin{aligned} r_{uu_s}(\tau) &= E[\, u(t)\; u_s(t+\tau)\,] \\ &= \frac{1}{T} \sum_{\tau=o}^{T-1} u(t)\, u_s(t+\tau) \end{aligned} \tag{3.21}$$

where T represents the observation interval. The argument that maximizes equa.(3.21) provides an estimate of the delay. In the frequency domain equa.(3.21) becomes (Bracewell,1978) :

$$R(f) = U(f)\; U_s^*(f) \tag{3.22}$$

where $U_s^*(f)$ denotes the complex conjugate of $U_s(f)$. Hence one way of estimating D is to take the Fourier transform of both the reference

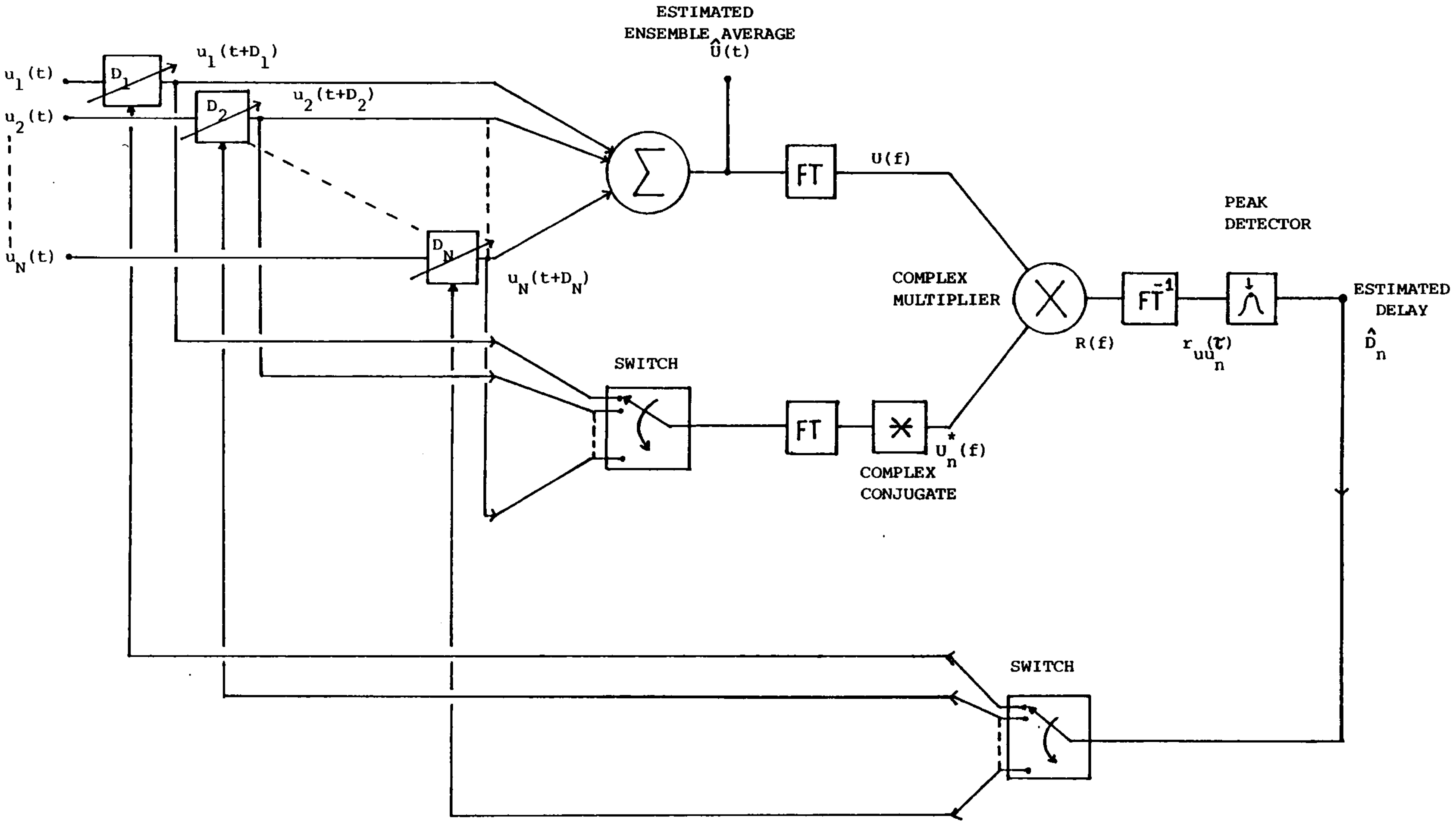

Fig. 3.4 The Phase Shift Averager

signal $\{u(t)\}$ and the shifted signal $\{u_s(t)\}$ and then apply the relation given by (3.22) to obtain R(f), from which $r_{uu_s}(\tau)$ can be obtained. The cross correlation function $r_{uu_s}(\tau)$ is then searched for its maximum and where that occurs (in time) gives an estimate of D.

The phase shift averager, based on a similar technique by Woody(1967), utilizes cross correlation with a template to align the individual beats $\{u_1(t)\}$, $\{u_2(t)\}$, ..., $\{u_N(t)\}$. Its operation is described schematically in Fig.3.4 and can be summarized as follows:

(1) An ensemble average,$\{\hat{U}(t)\}$, is obtained for $\{u_1(t)\}$, $\{u_2(t)\}$, ..., $\{u_N(t)\}$

(2) Its Fourier transform, U(f), is calculated.

(3) Beat 1 to N are transformed; for each $U_n(f)$, the complex conjugate is obtained and multiplied with U(f) to obain R(f). The inverse Fourier transform is then calculated and the resulting cross correlation function is searched for a maximum. D_n is obtained and used to shift the corresponding beat.

(4) Once all the beats have been shifted, a new ensemble average is obtained which replaces the old template.

(5) Steps 1-4 are repeated until a convergence criteria is satisfied. We used the average delay which is defined as:

$$D_{av} = 1/N \sum_{n=1}^{N} \hat{D}_n \tag{3.23}$$

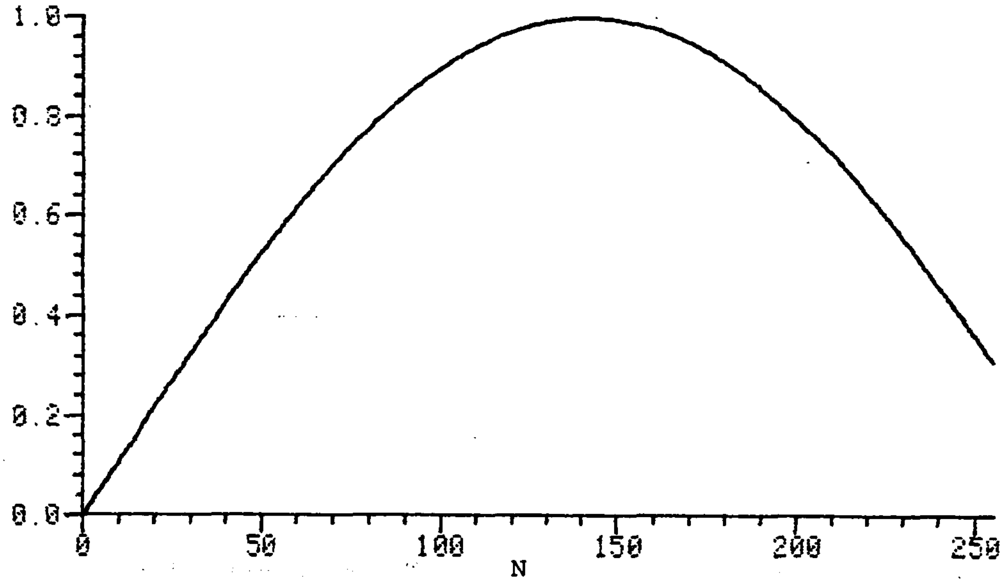

Fig. 3.5 The original truncated sinewave used in the simulation study of the phase shift averager.

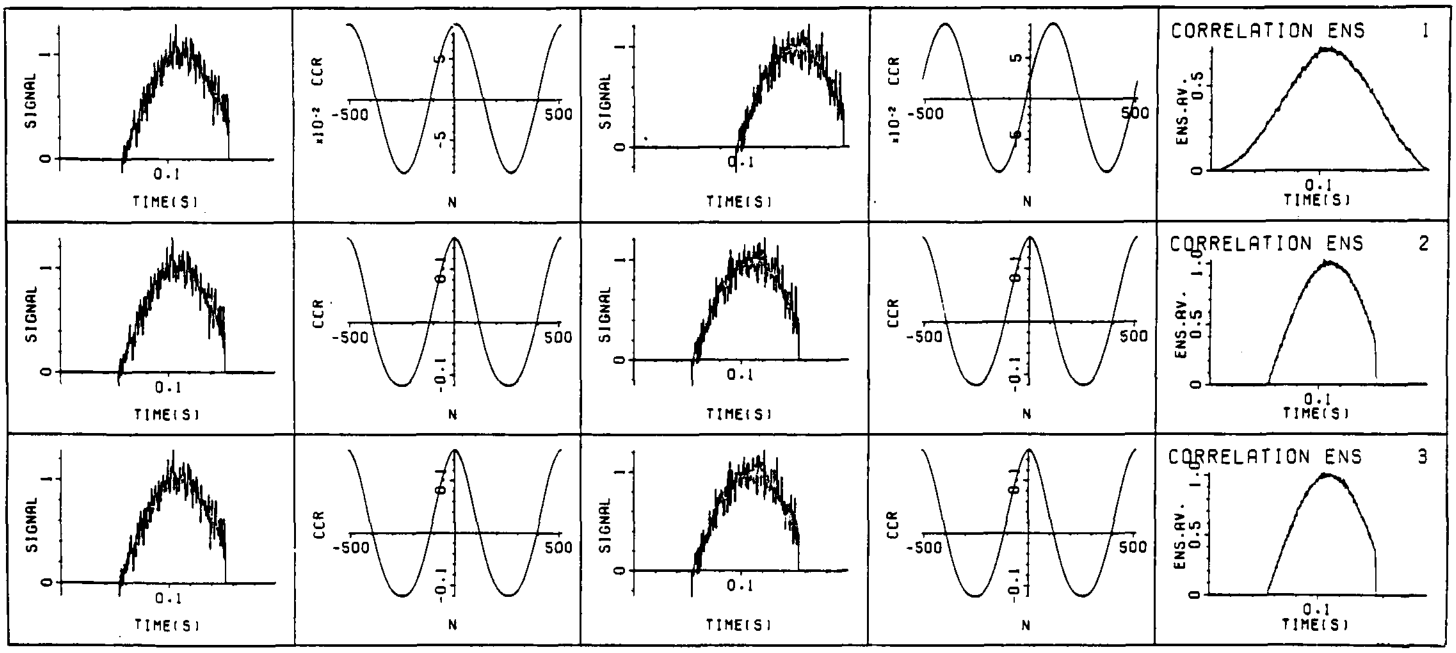

Fig. 3.6 The effect of phase shift averaging on a '100 beat' ensemble of truncated sinewaves randomly distributed in time with random noise added.

where N is the total number of beats.

Before application to velocity waveform data, the effectiveness of the PSA technique was demonstrated on a test signal which consisted of a truncated sinewave (Fig.3.5) to which has been added wideband random noise. The test data comprised one hundred truncated sinewaves randomly shifted in time to which random noise had been added. Fig.3.6 shows the effect of three iterations on the ensemble average. In addition to the noise being reduced, the hundred truncated sinewave signals which form the ensemble have also been accurately realigned in time.

The PSA method has proved to be very useful for the analysis of the 88% occlusion data. In Fig.3.7 an individual beat, its cross-correlation function with the ensemble average, and the ensemble average itself are each shown for the first, fifth and ninth iterations. Most of the evolution of the ensemble average waveform occurs within the first few iterations. For milder degrees of stenosis, convergence was much more rapid, usually no more than three iterations. A comparison of the first and ninth ensemble average waveforms in Fig.3.7 demonstrates that the coherent flow features are identified much better after phase shift averaging.

3.2.3 Fourier Spectral Analysis of the Ensemble Average Waveform

The discrete Fourier transform (DFT) for a time series, {x(t)}, is given by : (w is normalized frequency)

$$X(w) = 1/N \sum_{t=o}^{N-1} x(t) \exp(-jwt) \qquad (3.23)$$

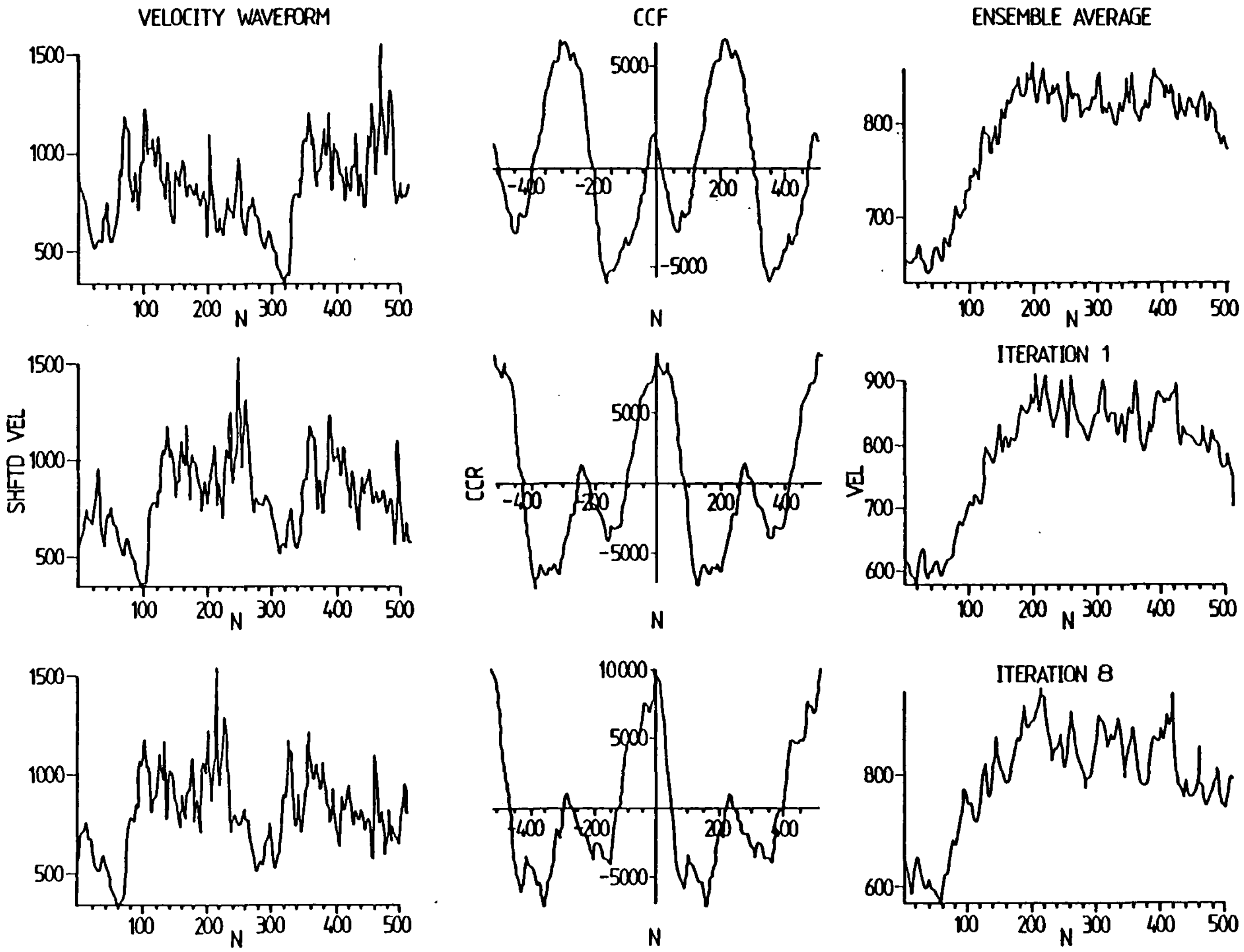

Fig.3.7 Effects of applying the phase shift averaging technique to the 88% occlusion data.

where $w=2\pi f$, and f is the frequency. We will consider the ideal situation where the ensemble average waveform {U(t)} is a truncated cosine and will derive its theoretical transform. Let

$$U(t) = \cos(w_o t + \phi)$$

$$=1/2[\exp(j(w_o t + \phi)) + \exp(-j(w_o t + \phi))] \qquad (3.24)$$

where w_o is the angular frequency of the pulse. Ignoring the negative frequency part, we can represent the DFT of U(t) by (Bloomfield,1976):

$$U(w) = 1/N \sum_{t=o}^{N-1} U(t)\exp(-jwt)$$

$$= 1/N\{1/2\exp(j\phi)\sum_{t=o}^{N-1}\exp(j(w_o-w)t)\}$$

$$= 1/N\{1/2\exp(j\phi)\exp(j\frac{(N-1)(w_o-w)}{2})\frac{\sin\{N(w_o-w)/2\}}{N\sin\{(w_o-w)/2\}}\}$$

(3.25)

The magnitude squared is given by:

$$\left|U(w)\right|^2 = \left[\frac{1}{2N}\frac{\sin N(w_o-w)/2}{N\sin(w_o-w)/2}\right]^2 \qquad (3.26)$$

and for N large and w small,

$$\left|U(w)\right|^2 \cong \left[\frac{1}{2N}\frac{\sin N(w_o-w)/2}{N(w_o-w)/2}\right]^2 \qquad (3.27)$$

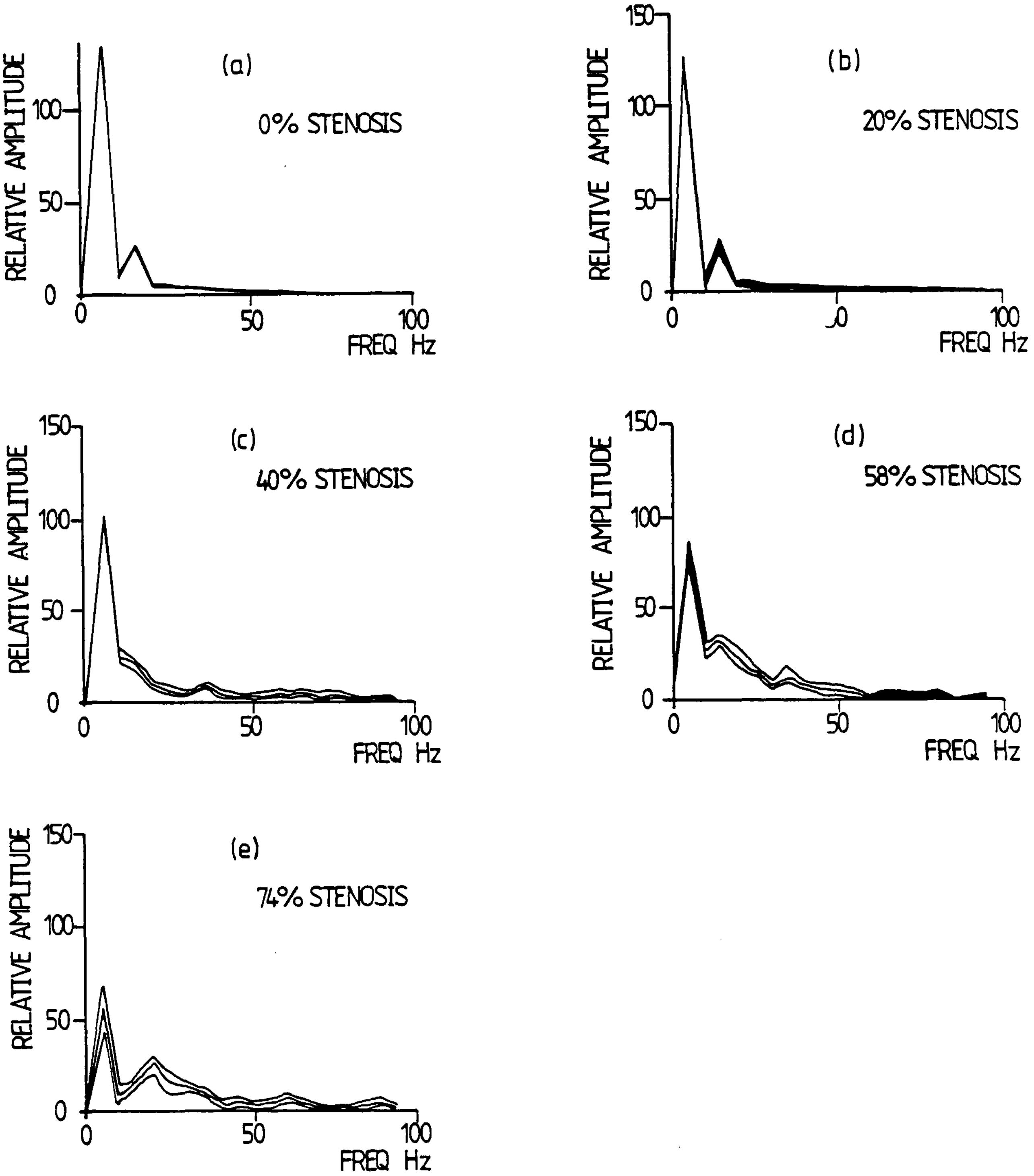

Fig. 3.8 Amplitude spectra graphed for 20-beat ensembles and for occlusions varying from 0 to 74%.

In each Figure the central curve represents the mean value, while the upper and lower curves correspond to ±1 standard deviation.

a No occlusion
b 20% occlusion
c 40% occlusion
d 58% occlusion
e 74% occlusion

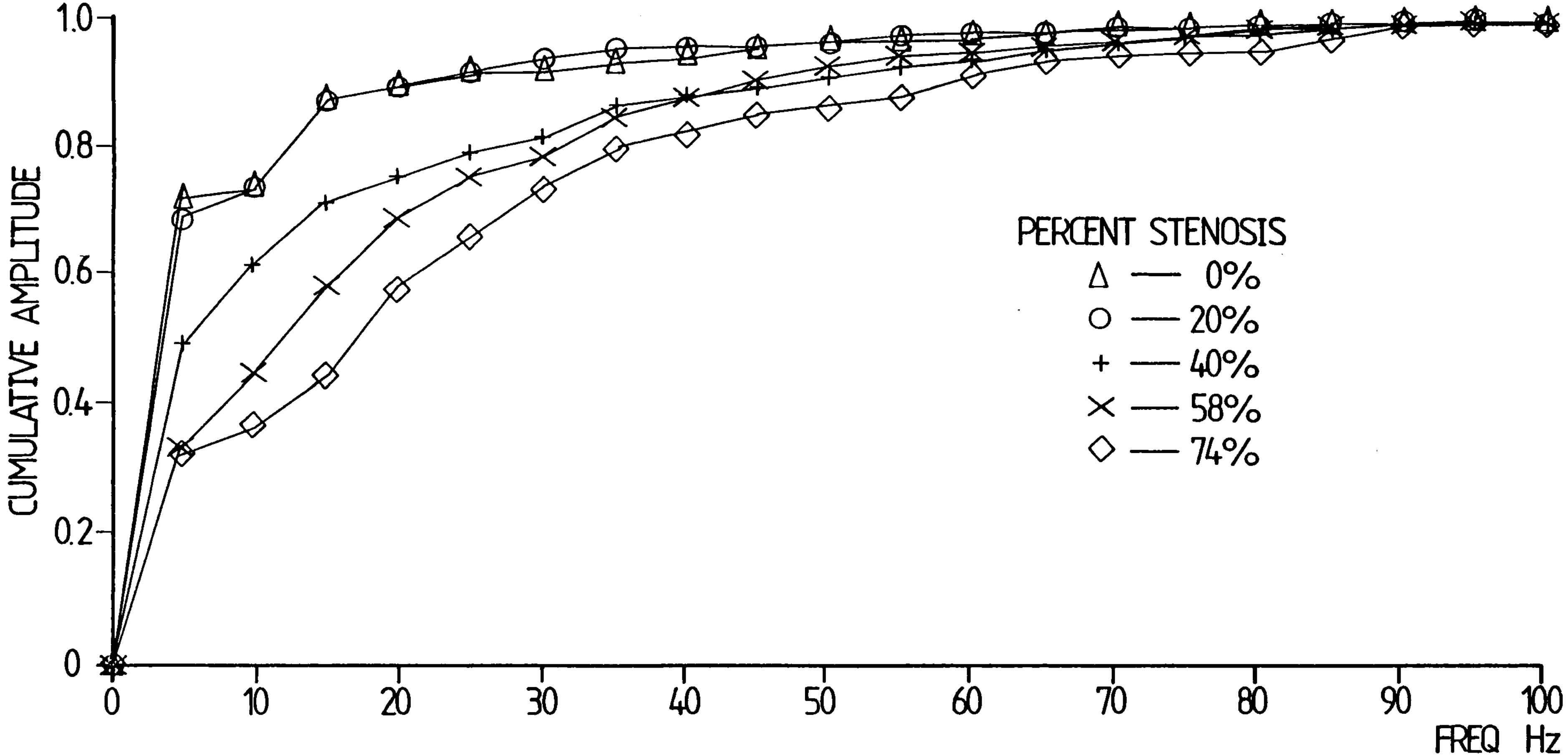

Fig. 3.9 Cumulative amplitude curves for occlusion levels from 0 to 74% illustrate shift to higher frequencies as degree of occlusion increases.

which has a peak at $w = w_o$ and a first zero at $w_o - w = 2\pi/N$. The implication of this result for our data can be shown using a numerical example: given a cardiac pulse of 0.33 seconds duration (dog), then the peak of the function in (3.27) would be at approximately 3 Hz and the first zero crossing would be at 8 Hz. However, with a sampling frequency of 2560 Hz and a 512 point transform (DFT), the peak would appear to be at 5 Hz and we would not be able to observe the zero crossing because of 'leakage' effects from the higher harmonics. Leakage is introduced because each harmonic in the spectrum (i.e. delta function) is convolved with a sinc function, found in eqaution (3.27).

An important aspect of the analysis of ensemble average data is the determination of its frequency content for different degrees of occlusion. Figs 3.8 a-e illustrate the amplitude spectra obtained (using the fast Fourier transform,FFT) from 20-beat ensemble averages for the various degrees of occlusion. Each spectrum consists of a mean characteristic and two other characteristics which correspond to ± standard deviation. Two interesting features of the spectra are:

(1) The absolute, as well as the relative amplitude of the fundamental peak decreases as the degree of occlusion increases.

(2) The variability of the spectra, especially the high frequency content , seems to increase with an increase in occlusion level. This can be seen more clearly in the cumulative amplitude spectra shown in Fig.3.9.

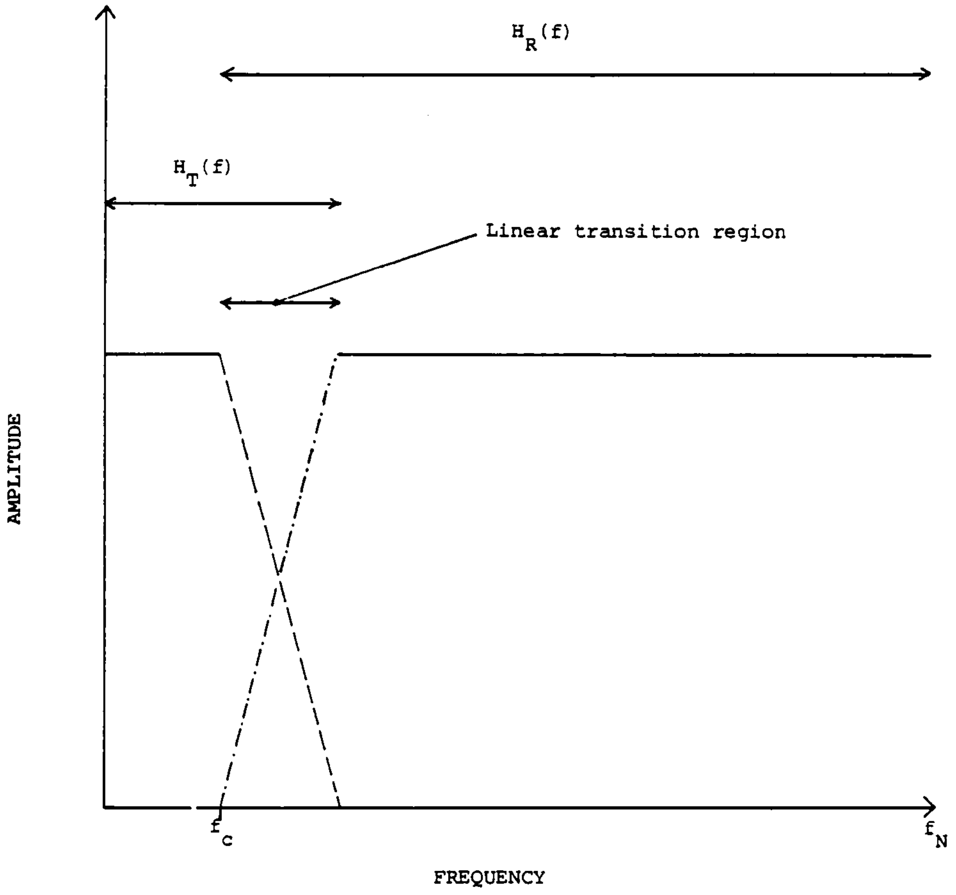

Fig. 3.10 The ideal transfer functions $H_T(f)$ and $H_R(f)$ for extracting $F_T(f)$ and $F_R(f)$ in the model:

$$F_u(f) = F_T(f) + F_R(f)$$

described in the text.

3.3 Disturbance Velocity Analysis

So far, we have discussed ensemble averaging as a method of extracting coherent structures in the velocity waveform. It is also necessary to study random components derived using either the time domain model (equa.(3.1)) or the frequency domain method (equa.(3.2)). Although there are strong similarities between the disturbance velocity waveforms extracted by these two methods, there are also subtle differences which make both techniques useful depending on what is being sought in the data.

In the first method , the disturbance velocity waveform , $\{u_1'(t)\}$, is derived from the velocity signal, $\{u(t)\}$, by subtracting the estimate of the ensemble average, $\{\hat{U}(t)\}$, from it ,i.e.:

$$u_1'(t) = u(t) - \hat{U}(t) \qquad (3.28)$$

for each block of data. The end result is 100 beats of $\{u_1'(t)\}$ which are then processed to obtain the time-varying root mean square function (RMS) given by :

$$\sqrt{\langle u_1'(t)^2 \rangle} = [\ 1/M \sum_{k=o}^{M-1} u_1'(t+kT_o)^2\ ]^{1/2} \qquad (3.29)$$

where M is the ensemble size, and T_o is the period of repetition.

In the second method , the disturbance velocity waveform, $\{u_2'(t)\}$, is obtained by high-pass filtering the raw velocity signal, $\{u(t)\}$, according to the model proposed in equation (3.2). The ideal frequency response of the filter is depicted in Fig.3.10 and is denoted by $H_R(f)$. An estimate of the random signal can be obtained using the following relation:

$$\hat{u}_2'(t) \overset{FT}{\Longleftrightarrow} \hat{F}_R(f) = H_R(f)\ H_u(f) \tag{3.30}$$

The linear transition function shown in Fig.3.10 is only for illustration purposes; the function used is the Kaiser-Bessel function chosen to provide a smooth transition in the frequency domain and hence reduced leakage in the time domain. The Kaiser-Bessel function is defined by (Harris,1978) :

$$w(n) = \frac{I_0\left(\pi\alpha\sqrt{1.0-\left(\frac{n}{N/2}\right)^2}\right)}{I_0(\pi\alpha)} \qquad 0 \leqslant |n| \leqslant N/2$$

where

$$I_0(x) = \sum_{k=0}^{\infty}\left[\frac{\left(\frac{x}{2}\right)^k}{k!}\right]^2 \tag{3.31}$$

where N is the total number of points, and $\pi\alpha$ is half of the time-bandwidth product. From the generalized uncertainty principle, the product of the mean-square time duration , Δt, and the mean-square bandwidth ,Δf, (i.e. the time-bandwidth product) should satisfy,for all functions, the following inequality (Bracewell, 1978) :

$$\Delta t\ \Delta f \geqslant 1/4\pi \tag{3.32}$$

The Kaiser function has the property that, for a restricted energy,

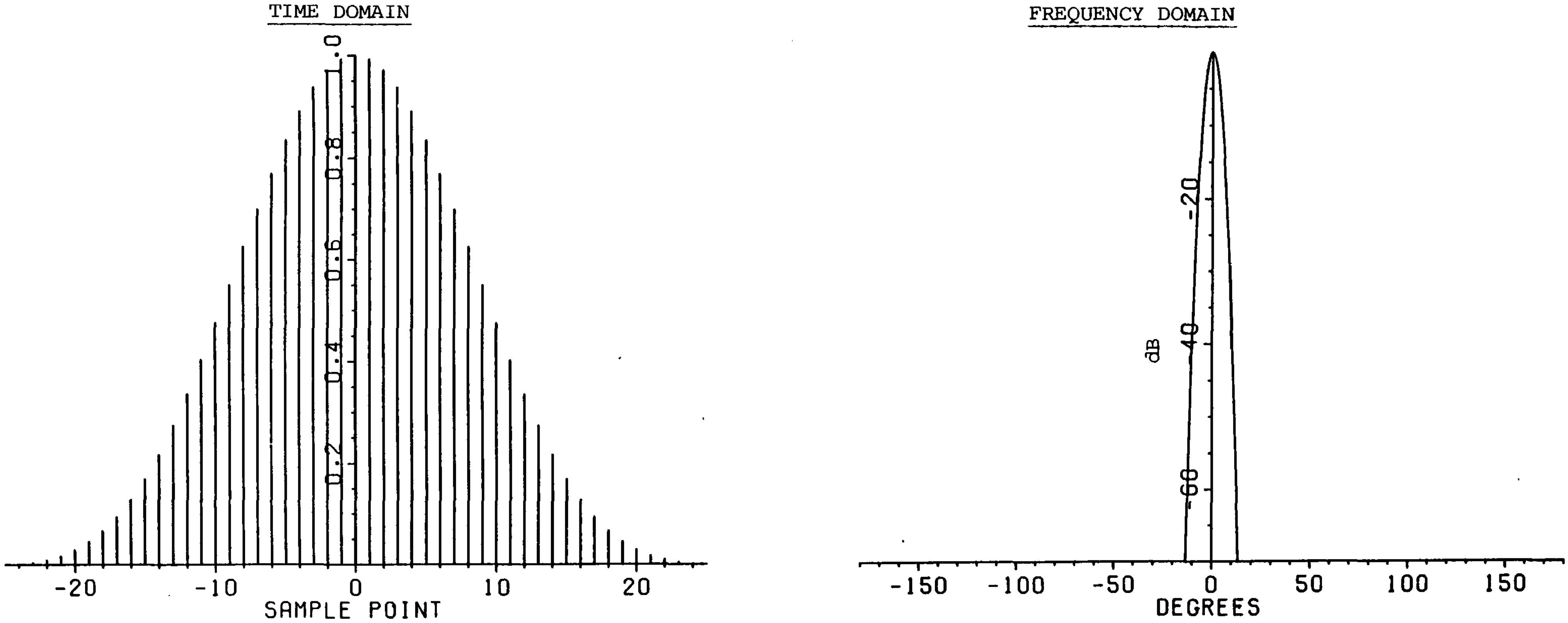

Fig. 3.11 The Kaiser-Bessel window and its transform.

and a restricted time duration this function maximizes the energy in the frequency band Δf. In other words, this function tries to concentrate the energy in the main lobe of its frequency transform given by :

$$W(\theta) \doteq \frac{N}{I_0(\pi\alpha)} \frac{\sinh\left[\sqrt{\alpha^2\pi^2-(N\theta/2)^2}\right]}{\sqrt{\alpha^2\pi^2-(N\theta/2)^2}} \tag{3.33}$$

where $\theta = wT$, T being the sampling interval. Fig.3.11 shows the Kaiser-Bessel function (a) and its transform (b) for $\alpha=3.0$. Notice that the sidelobes are suppressed to a level which is less than -60 dB.

In order to obtain the disturbance velocity according to the scheme depicted in Fig.3.10, the Kaiser-Bessel function is chosen to give a -60 dB cutoff and f_c was in the region of 5Hz, assuming that, below that threshold velocity disturbances are non-existent. A hundred beats are filtered in this way and then the RMS time-variant function is obtained for each degree of stenosis.

To compare results from both models (i.e. equa.(3.1) and equa.(3.2)), a typical example of $\{u_1'(t)\}$ and $\{u_2'(t)\}$ and their respective RMS functions for three degrees of stenosis namely: 20,40, and 74% stenosis (Fig.3.12) have been plotted. Some general remarks can be made about these figures :

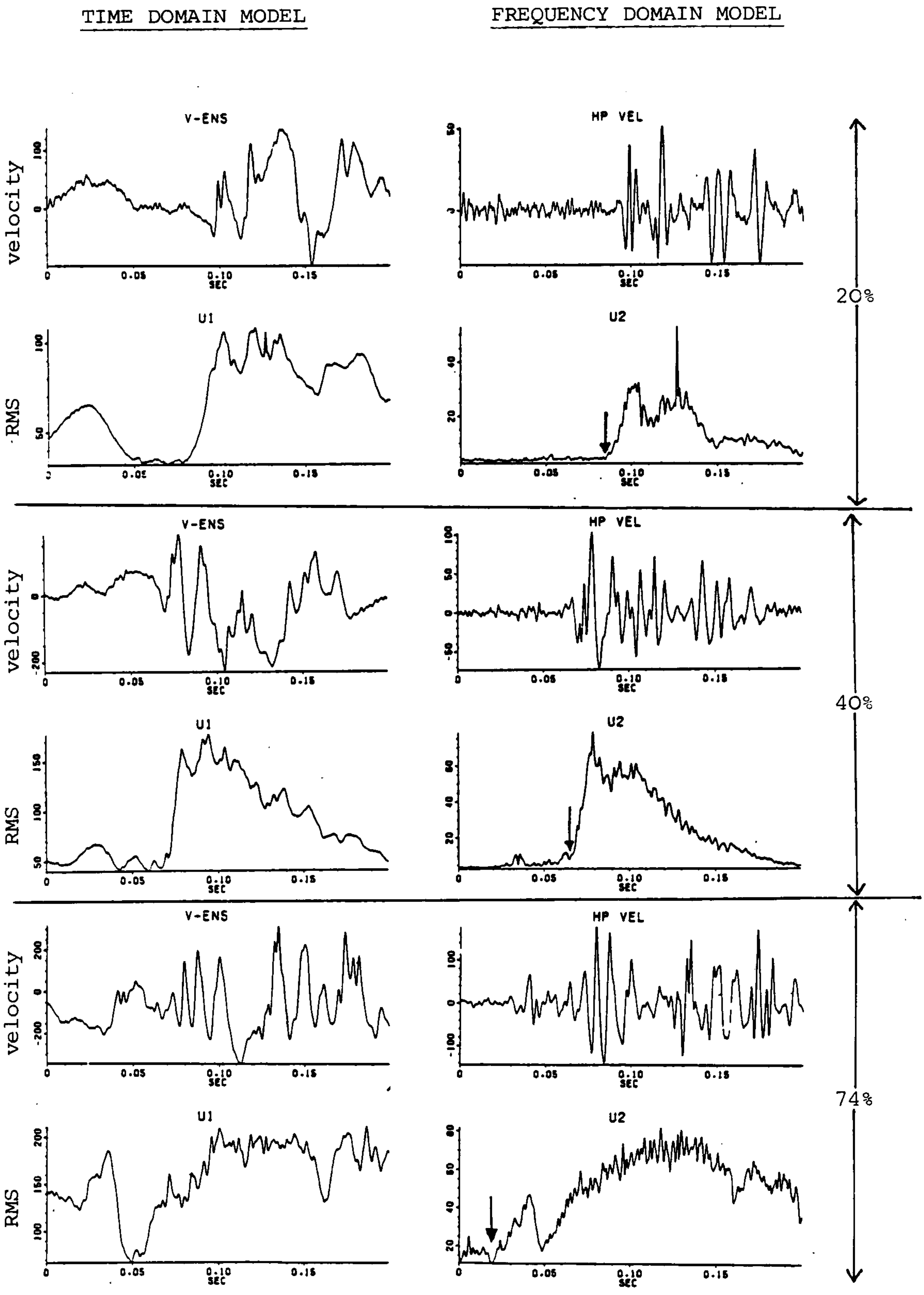

Fig. 3.12 Examples of disturbance velocity waveforms and their respective RMS functions for 20,40 and 74% occlusion for both time and frequency domain models.

(1) The major difference between $\{u_1'(t)\}$ and $\{u_2'(t)\}$ is the fact that $\{u_1'(t)\}$ has an additional low frequency trend which overshadows the high frequency components.

(2) This low frequency trend is also apparent in the RMS function of $\{u_1'(t)\}$.

(3) The initiation and spread of disturbances are more clearly seen in the RMS function of $\{u_2'(t)\}$ than in that of $\{u_1'(t)\}$ where the trend is the dominant feature.

(4) The time lag between the upstroke of the cardiac pulse and the onset of the high frequency signal, which we will call onset delay and denote by T_o, decreases considerably with increasing stenosis (see arrows in Fig.3.12) which is expected since the convection velocity increases with a higher constriction and the disturbances take a lesser time to reach the measurement site.

(5) For the lower degrees of stenosis the disturbances seem to occur in the deceleration phase of the cycle; while for the higher degrees (e.g. 88%) the disturbances are also apparent in the acceleration phase.

The results manifest the complexity of the velocity field and emphasize the importance of using both techniques for the description of this field. The overall statistical behaviour of the signal can be characterized using ensemble and/or phase shift averaging while a more detailed study of the high frequency activity of the signal requires the high-pass filtering technique already described. This high frequency activity is of a stochastic nature and its analysis requires more sophisticated signal processing techniques which are the focus of the coming chapters.

CHAPTER 4

CHARACTERISATION OF THE VELOCITY WAVEFORM : AUTOREGRESSIVE METHODS

In attempting to comprehend the blood velocity waveform with all its complexity, we have come to appreciate the attractiveness and usefulness of autoregressive modelling as a stochastic tool. Its rapidly developing theory and the interest of a wide spectrum of researchers in its application have facilitated its adaptation to our requirements. Its importance to our work lies mainly in its spectral estimation ability i.e. the Maximum Entropy Method which poses a strong challenge to the conventional Fourier methods. Nevertheless, its use should be coupled with a deep theoretical understanding otherwise little knowledge could prove to be a dangerous thing.

4.1 Autoregressive (AR) Modelling

The stochastic model used in the anlysis is based on the idea, (Yule ,1927), that a correlated time series, {y(t)}, can be regarded as generated from an uncorrelated series, {e(t)}, drawn from a fixed distribution usually Normal and having mean zero and variance σ_e^2. Such a sequence, i.e. {e(t)}, is usually termed as a white noise process . This white noise process is transformed into the process {y(t)} by means of linear filter as shown in Figure 4.1.

The output of the filter is a weighted sum of previous observations of {e(t)} i.e. a moving average process (MA) written as (Box and Jenkins ,1976):

$$\hat{y}_n = e_n + b_1 e_{n-1} + b_2 e_{n-2} + \dots$$

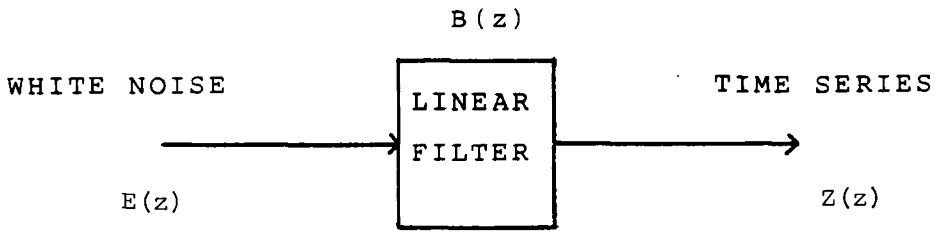

Fig.4.1 Representation of a time series as the output from a linear filter.

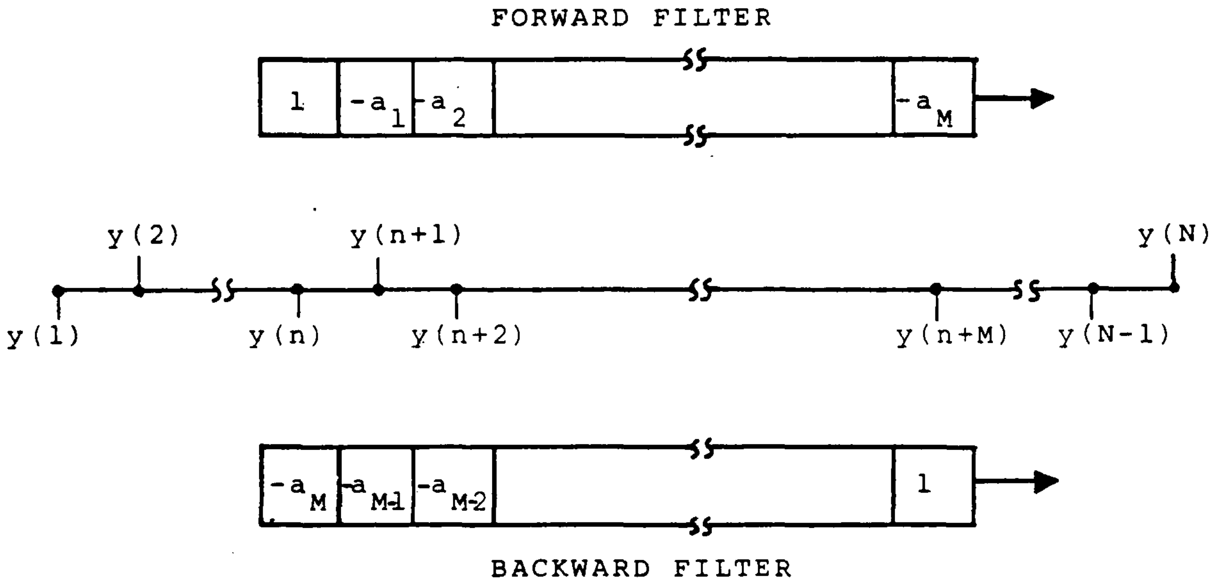

Fig.4.2 The operation of the forward and backward prediction filter.

$$= e_n + \sum_{m=1}^{\infty} b_m e_{n-m} \tag{4.1}$$

where $b_1, b_2, b_3, \ldots$ are the weights or the MA parameters. Using $b_0 = 1$, we can rewrite equation (4.1) as follows :

$$\hat{y}_n = \sum_{m=o}^{\infty} b_m e_{n-m} \tag{4.2}$$

Taking the Z-transform of (4.2) we obtain :

$$Y(z) = B(z)\ E(z) \tag{4.3}$$

Equation (4.1) can, under suitable conditions, be written as a weighted sum of past values of $\{\hat{y}(t)\}$ plus an added noise, $\{e(t)\}$, i.e. an autoregressive (AR) process as follows:

$$\begin{aligned} \hat{y}_n &= - a_1\hat{y}_{n-1} - a_2\hat{y}_{n-2} - \ldots + e_n \\ &= -\sum_{m=1}^{\infty} a_m\hat{y}_{n-m} + e_n \end{aligned} \tag{4.4}$$

Rearranging (4.4) and setting $a_o = 1$ we get

$$\sum_{m=o}^{\infty} a_m\hat{y}_{n-m} = e_n \tag{4.5}$$

Its Z-transform is then

$$Y(z) = E(z) / A(z) \tag{4.6}$$

The condition for (4.4) to be equivalent to (4.1) is that the poles of B(z) should lie inside the unit circle of the Z-plane (see Dorf(1980),p.439) which implies that the series $b_1, b_2, \ldots$ is covergent. If they are equivalent, then we can write A(z) in terms of B(z) as follows:

$$A(z) = 1 / B(z) \qquad (4.7)$$

In practice, the parameters of the AR model are finite and the number of parameters is a very important factor in fitting the model.

Returning to equation (4.4), assumimg a finite model order M, multiplying by y_{n-k}, and taking the expected value we obtain

$$E[\, y_{n-k}y_k \,] = a_1E[\, y_{n-k}y_{n-1} \,] + a_2E[\, y_{n-k}y_{n-2} \,] + \dots$$
$$+a_ME[\, y_{n-k}y_{n-M} \,] + E[\, y_{n-k}e_n \,]$$

$$\gamma_k = a_1\gamma_{k-1} + a_2\gamma_{k-2} + \dots + a_M\gamma_{k-M} \qquad (4.8)$$

where γ is the covariance. Dividing by γ_0 the autocorrelation form is then

$$\rho_k = a_1\rho_{k-1} + a_2\rho_{k-2} + \dots + a_M\rho_{k-M} \qquad (4.9)$$

Subtituting k=1,2,...,M in (4.9) gives

$$\rho_1 = a_1 + a_2\rho_1 + \dots + a_M\rho_{M-1}$$
$$\rho_2 = a_1\rho_1 + a_2\rho_2 + \dots + a_M\rho_{M-2}$$

$$\rho_M = a_1\rho_{M-1} + a_2\rho_{M-2} + \dots + a_M$$

These equations are known as the Yule-Walker equations which, rewritten in matrix form, are

$$\begin{bmatrix} \rho_1 \\ \rho_2 \\ \vdots \\ \rho_M \end{bmatrix} = \begin{bmatrix} 1 & \rho_1 & \cdots & \rho_{M-1} \\ \rho_1 & 1 & \cdots & \rho_{M-2} \\ & & & \vdots \\ \rho_M & \rho_{M-1} & \cdots & 1 \end{bmatrix} \begin{bmatrix} a_1 \\ a_2 \\ \vdots \\ a_M \end{bmatrix} \tag{4.10}$$

A different representation of the Yule-Walker equations can be obtained if we consider the case where k=0. For k>0 we assumed that $E[\, y_{n-k} e_n \,] = 0$, but with k=0 $E[\, y_n e_n \,] = \sigma_e^2$ i.e. the variance of the innovation noise, and equation (4.9) becomes :

$$\rho_0 = a_1\rho_1 + a_2\rho_2 + \ldots + a_M\rho_M + \sigma_e^2 \tag{4.11}$$

This allows us to augment equation (4.10) which then becomes

$$\begin{bmatrix} \rho_0 & \rho_1 & \cdot\cdot & \rho_M \\ \rho_1 & \rho_0 & \cdot\cdot & \rho_{M-1} \\ & & & \\ \rho_M & \rho_{M-1} & \cdot\cdot & \rho_0 \end{bmatrix} \begin{bmatrix} 1 \\ -a_1 \\ \vdots \\ -a_M \end{bmatrix} = \begin{bmatrix} \sigma_e^2 \\ 0 \\ \vdots \\ 0 \end{bmatrix} = \begin{bmatrix} P_{M+1} \\ 0 \\ \vdots \\ 0 \end{bmatrix} \tag{4.12}$$

Solving these equations for the AR parameters, is one of the methods commonly used to obtain a reasonable estimate of AR coefficients. Another method, the Burg technique (Burg ,1967) , is the one used here. Its main advantage is that it does not require prior estimate of the autocovariance function. In this scheme, estimates of the AR parameters are obtained by minimizing the average of the sum of the forward and backward prediction energies i.e. :

$$E_M = \frac{1}{2}\,\frac{1}{N-M} \sum_{n=1}^{N-M} |\, f_M(n)\,|^2 + |\, b_M(n)\,|^2 \tag{4.13}$$

where N is the number of points, and $f_M(n)$ and $b_M(n)$ are the forward and backward errors respectively and are defined as follows:

$$f_M(n) = y_n - \hat{y}_n = y_n - \sum_{m=1}^{M} a_{Mm}\hat{y}_{n+m}$$

$$b_M(n) = y_{n+M} - \hat{y}_{n+M} = y_{n+M} - \sum_{m=1}^{M} a_{Mm}\hat{y}_{n+M-m} \qquad (4.14)$$

where a_{Mm} denotes the m^{th} coefficient for a given order M. Figure 4.2 gives a pictorial description of the filtering process that results in obtaining estimates $\hat{y}_n$ and $\hat{y}_{n+M}$ from which $f_M(n)$ and $b_M(n)$ can be derived.

Vital to the Burg algorithm is the Levinson (1947) and Durbin (1960) recursive procedure which takes advantage of the Toeplitz (equidiagonal) form of the covariance or correlation matrix in (4.10). The recursion will be illustrated by considering a simple example:

Given a set of coefficients [a_{21}, a_{22}], and a_{33} (a_{33} is obtained by solving $\frac{\partial E_3(a_{33})}{\partial a_{33}} = 0$ as will be shown later on), we will obtain a_{31} and a_{32}. Using equation (4.10) and setting M=3, we get

$$\begin{bmatrix} \rho_0 & \rho_1 & \rho_2 \\ \rho_1 & \rho_0 & \rho_1 \\ \rho_2 & \rho_1 & \rho_0 \end{bmatrix} \begin{bmatrix} a_{31} \\ a_{32} \\ a_{33} \end{bmatrix} = \begin{bmatrix} \rho_1 \\ \rho_2 \\ \rho_3 \end{bmatrix}$$

If we now consider the first two equations, i.e.

$$\rho_0 a_{31} + \rho_1 a_{32} + \rho_2 a_{33} = \rho_1$$

$$\rho_1 a_{31} + \rho_0 a_{32} + \rho_1 a_{33} = \rho_2$$

we can now represent a_{31} and a_{32} in terms of a_{33} as follows :

$$\rho_0 a_{31} + \rho_1 a_{32} = \rho_1 - a_{33}\rho_2$$

$$\rho_1 a_{31} + \rho_0 a_{32} = \rho_2 - a_{33}\rho_1$$

or in matrix form

$$\begin{bmatrix} \rho_0 & \rho_1 \\ \rho_1 & \rho_0 \end{bmatrix} \begin{bmatrix} a_{31} \\ a_{32} \end{bmatrix} = \begin{bmatrix} \rho_1 \\ \rho_2 \end{bmatrix} - a_{33} \begin{bmatrix} \rho_2 \\ \rho_1 \end{bmatrix}$$

letting

$$R(1) = \begin{bmatrix} \rho_0 & \rho_1 \\ \rho_1 & \rho_0 \end{bmatrix}$$

we can write the above equation as

$$\begin{bmatrix} a_{31} \\ a_{32} \end{bmatrix} = R(1)^{-1} \begin{bmatrix} \rho_1 \\ \rho_2 \end{bmatrix} - R(1)^{-1} a_{33} \begin{bmatrix} \rho_2 \\ \rho_1 \end{bmatrix} \tag{4.15}$$

Going back to equation (4.10) and setting M=2 we get

$$\begin{bmatrix} \rho_0 & \rho_1 \\ \rho_1 & \rho_0 \end{bmatrix} \begin{bmatrix} a_{21} \\ a_{22} \end{bmatrix} = \begin{bmatrix} \rho_1 \\ \rho_2 \end{bmatrix}$$

or

$$\begin{bmatrix} a_{21} \\ a_{22} \end{bmatrix} = R(1)^{-1} \begin{bmatrix} \rho_1 \\ \rho_2 \end{bmatrix}$$

Replacing this relation into equation (4.15) we get

$$\begin{bmatrix} a_{31} \\ a_{32} \end{bmatrix} = \begin{bmatrix} a_{21} \\ a_{22} \end{bmatrix} - a_{33} \begin{bmatrix} a_{22} \\ a_{21} \end{bmatrix} \tag{4.16}$$

which is the required recursion.

The next step is to derive the recursion for the prediction error variance, P_4, in terms of P_3. For this we need equation (4.12) with M=3 i.e.

$$\begin{bmatrix} \rho_0 & \rho_1 & \rho_2 & \rho_3 \\ \rho_1 & \rho_0 & \rho_1 & \rho_2 \\ \rho_2 & \rho_1 & \rho_0 & \rho_1 \\ \rho_3 & \rho_2 & \rho_1 & \rho_0 \end{bmatrix} \begin{bmatrix} 1 \\ -a_{31} \\ -a_{32} \\ -a_{33} \end{bmatrix} = \begin{bmatrix} P_4 \\ 0 \\ 0 \\ 0 \end{bmatrix}$$

This can be rewritten using (4.16) as follows :

$$\begin{bmatrix} \rho_0 & \rho_1 & \rho_2 & \rho_3 \\ \rho_1 & \rho_0 & \rho_1 & \rho_2 \\ \rho_2 & \rho_1 & \rho_0 & \rho_1 \\ \rho_3 & \rho_2 & \rho_1 & \rho_0 \end{bmatrix} \left\{ \begin{bmatrix} 1 \\ -a_{21} \\ -a_{22} \\ 0 \end{bmatrix} - a_{33} \begin{bmatrix} 0 \\ -a_{22} \\ -a_{21} \\ 1 \end{bmatrix} \right\} = \begin{bmatrix} P_4 \\ 0 \\ 0 \\ 0 \end{bmatrix}$$

and then decomposed giving

$$\left[\begin{bmatrix} 0 & \rho_0 & \rho_1 & \rho_2 \\ 0 & \rho_1 & \rho_0 & \rho_1 \\ 0 & \rho_2 & \rho_1 & \rho_0 \\ 0 & 0 & 0 & 0 \end{bmatrix}\begin{bmatrix} 1 \\ -a_{21} \\ -a_{22} \\ 0 \end{bmatrix} + \begin{bmatrix} 0 & 0 & 0 & 0 \\ 0 & 0 & 0 & 0 \\ 0 & 0 & 0 & 0 \\ \rho_3 & \rho_2 & \rho_1 & 0 \end{bmatrix}\begin{bmatrix} 1 \\ -a_{21} \\ -a_{22} \\ 0 \end{bmatrix}\right]$$

$$-a_{33}\cdot\left[\begin{bmatrix} 0 & 0 & 0 & 0 \\ 0 & \rho_0 & \rho_1 & \rho_2 \\ 0 & \rho_1 & \rho_0 & \rho_1 \\ 0 & \rho_2 & \rho_1 & \rho_0 \end{bmatrix}\begin{bmatrix} 0 \\ -a_{22} \\ -a_{21} \\ 1 \end{bmatrix} + \begin{bmatrix} 0 & \rho_1 & \rho_2 & \rho_3 \\ 0 & 0 & 0 & 0 \\ 0 & 0 & 0 & 0 \\ 0 & 0 & 0 & 0 \end{bmatrix}\begin{bmatrix} 0 \\ -a_{22} \\ -a_{21} \\ 1 \end{bmatrix}\right] = \begin{bmatrix} P_4 \\ 0 \\ 0 \\ 0 \end{bmatrix}$$

Letting $x = \rho_3 - \rho_2 a_{21} - \rho_1 a_{22}$, we get

$$\begin{bmatrix} P_3 \\ 0 \\ 0 \\ x \end{bmatrix} - a_{33}\begin{bmatrix} x \\ 0 \\ 0 \\ P_3 \end{bmatrix} = \begin{bmatrix} P_4 \\ 0 \\ 0 \\ 0 \end{bmatrix}$$

or

$$P_3 - a_{33}x = P_4$$

$$x - a_{33}P_3 = 0$$

which gives

$$P_4 = P_3 \left(1 - |a_{33}|^2 \right) \tag{4.17}$$

Equations (4.16) and (4.17) form the crux of the Levinson algorithm, which generalized can be written as follows (Andersen ,1974) :

$$\begin{aligned} a_{Mm} &= -1 && \text{for } m=0 \\ a_{Mm} &= a_{M-1\,m} - a_{MM}a_{M-1\;M-m} && \text{for } m=1,2,\ldots,M-1 \\ a_{Mm} &= 0 && \text{for } m\geqslant M \end{aligned} \tag{4.18}$$

and

$$P_M = P_{M-1}\ (\ 1 - |a_{MM}|^2\ ) \qquad (4.19)$$

Hence, if we are given the coefficients and variance for order M-1 and using a_{MM} which is derived by the Burg algorithm, we can estimate the rest of the coefficients for order M.

To get a_{MM}, it is necessary to minimize the average forward and backward power given by equation (4.13) which is rewritten as follows:

$$E_M = \frac{1}{2}\,\frac{1}{N-M}\sum_{n=1}^{N-M}\left[\left(\sum_{m=o}^{M} a_{Mm}y_{n+m}\right)^2 + \left(\sum_{m=o}^{M} a_{Mm}y_{n+M-m}\right)^2\right]$$

Representing a_{MM} as in equation (4.18), we get

$$E_M = \frac{1}{2}\,\frac{1}{N-M}\sum_{n=1}^{N-M}\left[\left(\sum_{m=o}^{M} a_{M-1m}y_{n+m} - a_{MM}\sum_{m=o}^{M} a_{M-1M-m}y_{n+m}\right)^2 + \left(\sum_{m=o}^{M} a_{M-1m}y_{n+M-m} - a_{MM}\sum_{m=o}^{M} a_{M-1M-m}y_{n+M-m}\right)^2\right]$$

Letting

$$b_{Mn} = \sum_{m=o}^{M} a_{M-1m}y_{n+m} = \sum_{m=o}^{M} a_{M-1M-m}y_{n+M-m} \qquad (4.20)$$

$$b'_{Mn} = \sum_{m=o}^{M} a_{M-1m}y_{n+M-m} = \sum_{m=o}^{M} a_{M-1M-m}y_{n+m} \qquad (4.21)$$

we obtain

$$E_M = \frac{1}{2}\,\frac{1}{N-M}\sum_{n=1}^{N-M}\left[(b_{Mn}-a_{MM}b'_{Mn})^2 + (b'_{Mn}-a_{MM}b_{Mn})^2\right] \qquad (4.22)$$

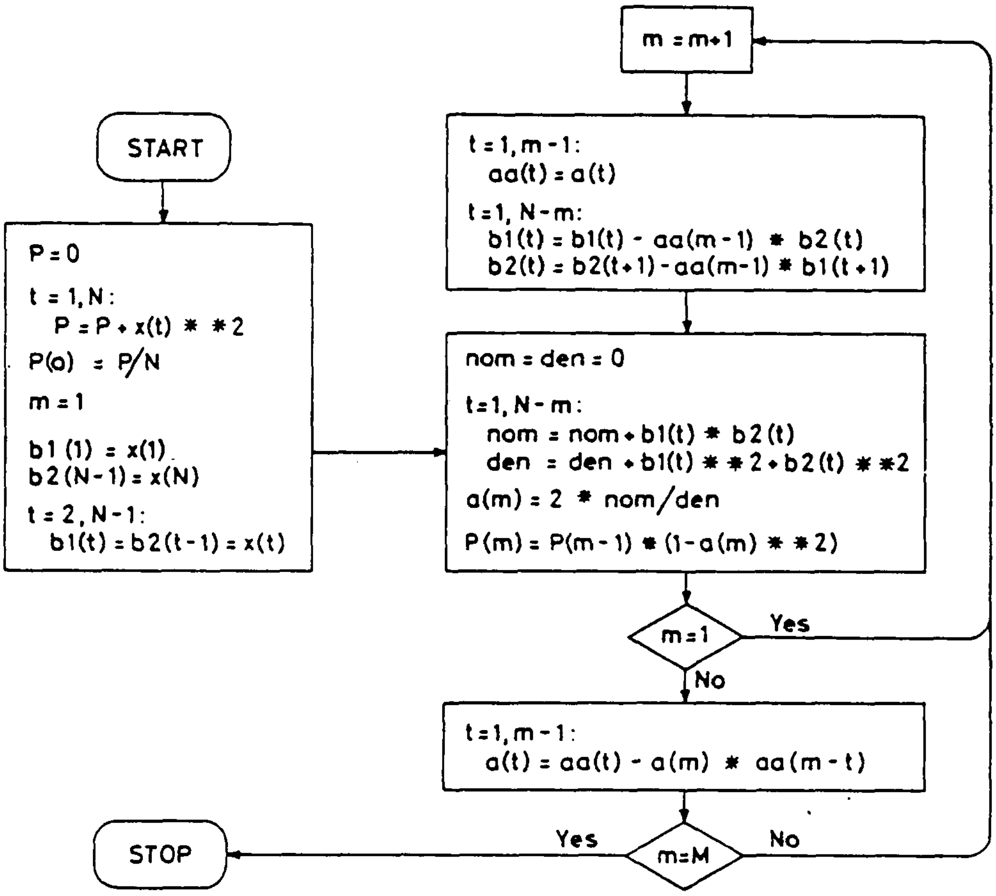

Fig.4.3 Flow diagram of the Burg algorithm.

Differentiating (4.22) with respect to a_{MM} gives:

$$\frac{\partial E_M}{\partial a_{MM}} = 0$$

$$= \frac{1}{N-M} \sum_{n=1}^{N-M} \left[-(b_{Mn} - a_{MM} b'_{Mn}) b'_{Mn} - (b'_{Mn} - a_{MM} b_{Mn}) b_{Mn} \right] = 0$$

this gives

$$a_{MM} = 2 \sum_{n=1}^{N-M} b_{Mn} b'_{Mn} \Big/ \sum_{n=1}^{N-M} (b_{Mn}^2 + b'^2_{Mn}) \tag{4.23}$$

Useful recursion formulas for b_{Mn} and b'_{Mn} can be shown to be (using equation (4.18) and equation (4.21)):

$$b_{Mn} = b_{M-1n} - a_{M-1M-1} b'_{M-1n} \tag{4.24}$$

$$b'_{Mn} = b'_{M-1n+1} - a_{M-1M-1} b_{M-1n+1} \tag{4.25}$$

Starting values are

$$b_{1n} = y_n$$
$$b'_{1n} = y_{n+1} \tag{4.26}$$

Finally, a schematic representation of the Burg algorithm could be seen in the flow diagram of Figure 4.3 where b_1 and b_2 denote b_{Mn} and b'_{Mn} respectively and P(0) is the initial variance of the prediction error.

4.2 The Maximum Entropy Method (MEM) of Spectral Estimation

Having estimated the AR parameters using the methods described, the next step in the analysis procedure is normally the calculation of a spectral estimate of the underlying process which can be derived from these coefficients. The resulting power spectral density (PSD) has certain advantages in relation to conventional spectral estimates like the periodogram and the Fourier transform of the autocorrelation function.

In the periodogram method , it is assumed that outside the data interval the record is periodic with period equal to the length of the data inerval. The data in the interval is transformed and the power spectrum is estimated as the square of the resultant Fourier coefficients. A window function is frequently used in an attempt to reduce the effect of discontinuities at the two ends of the data.

In the traditional autocorrelation method , the autocorrelation function is estimated from the data and an estimate of the power spectrum is obtained as the Fourier transform of the estimated autocorrelation function. The assumption here is that the autocorrelation estimates are zero outside the data interval hence it is customary to taper the known autocorrelation estimates smoothly into the assumed zero values.

Unlike conventional methods, the Maximum Entropy Method does not make assumptions about the data which lie outside the interval of interest. These assumptions that constrain the data to be either periodic or zero outside the known interval are usually incorrect and often result in a poor spectral estimate. The MEM is a spectral estimation method which is consistent with the prior knowledge i.e. the known data and is maximally non-committal with regard to unavailable data. It can be interpreted as predicting the autocorrelation function of the available time series by maximizing the entropy, where entropy here is a measure of our ignorance about the actual structure of the system (Brillouni,1956). The aim is to make sure that no information is added (i.e. no assumptions made) as a result of the prediction process. The relationship between entropy and uncertainty or ignorance is formulated in the Jaynes Principle (Jaynes,1963;1968) as follows:

The prior probability assignment (i.e. the probability distribution to be estimated) that describes the available information but is maximally noncommital with regard to the unavailable information is the one with maximum entropy.

The relationship between entropy rate, H, and the spectral density,S(f), of a stationary Gaussian process is given by (Smylie et al.,1973):

$$H = \frac{1}{4f_N} \int_{-f_N}^{+f_N} \log(S(f)) \, df \tag{4.27}$$

where f_N is the Nyquist frequency. From the Wiener-Khinchin theorem, the power spectrum, S(f), is related to the autocorrelation function $R(\tau)$ of the process by :

$$S(f) = \int_{-\infty}^{+\infty} R(\tau) \exp(-j2\pi\tau f) \, d\tau \tag{4.28}$$

Following the principle of maximum entropy, H is now maximized with respect to the unknown autocorrelation coefficients subject to the constraint that S(f) is consistent with the known , or at least assumed known autocorrelation values. In equation form the constraint can be written as follows:

$$r(\tau) = \int_{-f_N}^{+f_N} S(f)\exp(j2\pi f\tau)\,df \qquad -M \leqslant \tau \leqslant M \tag{4.29}$$

Using the method of Lagrange multipliers (Srinath and Rajasekaran,1979), we can define an augmented function $H'(R(\tau),\lambda_\tau)$ where $\{\lambda_\tau\}$ are the Lagrange multipliers and maximize H′ and set to zero as follows :

$$\frac{\partial H'}{\partial R(\tau)} = \frac{\partial H}{\partial R(\tau)} - \sum_{\tau=-M}^{\tau=M} \lambda_\tau \frac{\partial r(\tau)}{\partial R(\tau)} = 0 \qquad \text{for } |\tau| \geqslant M+1 \tag{4.30}$$

where $\{\lambda_\tau\}$ are positive and symmetric,i.e.

$$\lambda_\tau = \lambda_{-\tau} \tag{4.31}$$

Using (4.27) and (4.29) in (4.30) , we obtain:

$$\int_{-f_N}^{+f_N} \frac{\partial S(f)}{\partial R(\tau)}\left(\frac{1}{4f_N}\,\frac{1}{S(f)} - \sum_{\tau=-M}^{M} \lambda_\tau \cdot \exp(j2\pi f\tau)\right)df = 0 \tag{4.32}$$

The solution is

$$S(f) = \frac{1}{4f_N}\,\frac{1}{\sum_{\tau=-M}^{M} \lambda_\tau \exp(j2\pi f\tau)}$$

$$= \frac{1}{\sum_{\tau=-M}^{M} c_\tau \cdot \exp(j2\pi f\tau)} \tag{4.33}$$

where $c_\tau = 4f_N\lambda_\tau$. Now for $\tau = n\Delta t$ and replacing (4.33) into (4.29), we get

$$r(n\Delta t) = \int_{-f_N}^{+f_N} \frac{\exp(j2\pi fn\Delta t)}{\sum_{m=-M}^{M} c_m \exp(j2\pi fm\Delta t)} \qquad 0 \leqslant n \leqslant M \tag{4.34}$$

If we take the Z-transform of equation (4.34) where $z=\exp(j2\pi f\Delta t)$ and $df = \frac{f_N}{j\pi}(\frac{dz}{z})$ we get

$$\begin{aligned} r(n) &= \frac{f_N}{j\pi} \oint \frac{z^n}{\sum_{m=-M}^{M} c_m z^m} \frac{dz}{z} \\ &= \frac{f_N}{j\pi} \oint \frac{z^{n-1}}{\sum_{m=-M}^{M} c_m z^m} dz \end{aligned} \tag{4.35}$$

where the contour integral is applied to the unit circle in the Z-plane. Since the coefficients $\{c_m\}$ are positive and symmetric , they can be decomposed as follows (Robinson ,1967):

$$\begin{aligned} \sum_{m=-M}^{M} c_m z^m &= \sum_{m=o}^{M} g_m z^m \sum_{m=o}^{M} g_m z^{-m} \\ &= G_M(z) \cdot G_M(1/z) \end{aligned} \tag{4.36}$$

with

$$c_m = \sum_{k=o}^{M-m} g_k g_{k+m}$$

Hence equation (4.35) can be written as follows:

$$r(n) = \frac{f_N}{j\pi} \oint \frac{z^{n-1}}{G_M(z)\,G_M(1/z)}\, dz$$

$$\sum_{m=o}^{M} g_m r(n-m) = \frac{f_N}{j\pi} \oint \frac{z^{n-1}}{G_M(1/z)}\, dz$$

$$= \begin{cases} \dfrac{2f_N}{g_o} & \text{for } n=o \\ o & \text{for } n=1,2,\ldots,M \end{cases} \qquad (4.37)$$

i.e. since the polnomial $G_M(1/z)$ has no zeros inside the unit circle for $n \geqslant 1$, the integrand in (4.37) is equal to zero (Cauchy's residue theorem). However, for n=0 the integrand has a simple pole at z=0 with the residue equal to $1/g_o$.

Comparing our result with equations (4.12) we find that (4.37) has a similar form with

$$g_m = \frac{2f_N}{P_{M+1}} a_m \qquad (4.38)$$

Equation (4.36) becomes

$$\sum_{m=-M}^{M} c_m z^m = \frac{2f_N}{P_{M+1}} A_M(z) A_M(1/z) \qquad (4.39)$$

where $A_m(z)$ is the transfer function of the prediction-error filter. Finally, in order to obtain the maximum entropy spectral estimate, we substitute (4.39), with $z=\exp(j2\pi f\Delta t)$, in (4.33) and obtain

$$S(f) = \frac{P_{M+1}}{2f_N \left|1 + \sum_{m=1}^{M} a_m \exp(-j2\pi m f \Delta t)\right|^2} \tag{4.40}$$

P_{M+1} in (4.40) signifies that if we were to convolve the M+1 coefficients $a_0, a_1, \ldots, a_M$ with the time series $y_1, y_2, \ldots, y_N$ the resultant variance (or power) of the error would be equal to P_{M+1}.

The maximum entropy spectral estimate (MESE), S(f), has a number of important potential advantages, the principal ones being improved resolution over conventional estimators and the continuity or smoothness of the AR spectral estimator. The resolution, or the ability to resolve two frequency components, of conventional techniques is dependent on the record length and on the number of cycles of the fundamental frequency, f_1. As a general rule Fourier spectral analysis requires a minimum of approximately five cycles of f_1 for reasonable resolution (Bergland,1969). On the other hand, the MESE is convenient for short records since this estimate is based on an infinitely long autocovariance function and can be obtained with as little as one cycle of the fundamental frequency (Ulrych, 1972). The MESE has also the property that, given a correct determination of the AR order, it is optimally smooth in a least-squares sense (Ulrych and Ooe,1979). This makes the spectrum continuous unlike Fourier estimators where the spectra can only be defined in terms of the power at harmonics of the fundamental frequency, so that if a true component lies between two harmonics, its power will be divided.

4.3 The Statistical Identification of Model Order

A crucial point in estimating maximum entropy spectra is the determination of the order of the AR process, M. This order determines not only the resolution of the estimate , but also the smoothness. In the present study some statistical methods of determining an optimal model order, M_{opt}, using the available data record(s) have been considered. These are:

(1) The Final Prediction Error

(2) The Autoregressive Transfer Function Criterion

(3) The Akaike Information Criterion

(4) The Modified Akaike Information Criterion

The application of these criteria to time series will be discussed in a later section.

General Definitions

(1) The Final Prediction Error (FPE)

The final prediction error is defined by Akaike (1969) as the expected variance of the prediction error when an autoregressive model fitted to the present series of {x(n)} is applied to another independent realization of {x(n)}. Hence, considering the time series {x(n),n=1,2,...,N} then

$$\text{FPE of } \hat{x}(n) = E[\ \ (x(n)-\hat{x}(n))\ \ ]$$

where $\hat{x}(n)$ is the value estimated from the AR model. Akaike (1969) has shown that the FPE consists of two components : the first corresponding to the error of the best linear predictor for a given model order, and the second due to statistical deviation of $\hat{a}_M(m)$ from $a_M(m)$ where $\hat{a}_M(m)$ is the m^{th} estimated model coefficient for order M and $a_M(m)$ is the true coefficient. As the model order increases the first term in the FPE decreases. The second increases for a given length N of $\{x(n)\}$. The result of Akaike's derivation can be stated as :

$$\mathrm{FPE}(M) = \frac{N + M + 1}{N - M - 1} P_M \tag{4.41}$$

where P_M is the output error power of the filter. P_M decreases with M while the other term which is due to the fluctuations of $\hat{a}_M(m)$ increases with M. The FPE function has a minimum, M_{min}, for which M will be optimal, i.e. the optimal model order. This is only true if the stochastic process under observation is an AR process generated from a strictly stationary and mutually independent innovation. The relative FPE (RFPE) defined as :

$$(\mathrm{RFPE})_M = \frac{(\mathrm{FPE})_M}{(\mathrm{FPE})_o} \tag{4.42}$$

where

$$(\mathrm{FPE})_o = \frac{N + 1}{N - 1} P_M$$

is the one implemented in practice.

(2) The Autoregressive Transfer Function Criterion (CAT)

This method was developed by Parzen(1974) for determining the order of an AR model. The optimal filter order is obtained when the estimate of the difference in the mean-square errors between the true filter, A(z), and the estimated filter, $\hat{A}(z)$, is minimum i.e. when the following quantity is minimized (Sawaragi, Soeda and Nakamizo,1981):

$$J = E\left[\int_{-1/2}^{+1/2} \left| \frac{\hat{A}(\exp(j2\pi f)) - A(\exp(j2\pi f))}{A(\exp(j2\pi f))} \right|^2 df\right] . \tag{4.43}$$

Parzen showed that this difference can be calculated without explicitly knowing the exact filter (Haykin and Kesler,1979) i.e.:

$$CAT(M) = \frac{1}{N} \sum_{m=1}^{M} \frac{N-m}{NP_m} - \frac{N-M}{NP_M} \tag{4.44}$$

where in this case the knowledge of P_1, P_2,...,P_M is necessary for the estimation of CAT(M).

(3) The Akaike Information Criterion (AIC)

This criterion, due to Akaike (1973), is based on the minimization of the logarithm of the likelihood function of the prediction-error variance as a function of the filter order M. Assuming the process has Gaussian statistics, the AIC to be minimized is :

$$AIC(M) = \ln(P_M) + 2M/N \qquad (4.45)$$

It is interesting to note that the FPE and the AIC are asymptotically related as follows :

$$\lim_{N\to\infty} [\ln(FPE(M))] = AIC(M) \qquad (4.46)$$

Also, the term 2M/N in equation (4.45) introduces a penalty on choosing too high a model order i.e. the AIC increases for increasing M.

(4) The Modified AIC or BIC

Critical evaluation of the statistical behaviour of AIC shows that the minimum AIC does not produce a consistent estimate of the order even when the system has a clearly defined finite order (Akaike,1970 ; Shibata,1976). Akaike (1977) suggested a modified criterion whose minimum produces a consistent estimate of the true order when this does exist. This new criterion, termed BIC by Akaike, is defined as follows (Akaike,1978) :

$$BIC(M) = (N-M)\ln(\frac{S(M)}{N-M}) + M \ln(\frac{S(o)-S(M)}{M}) \qquad (4.47)$$

where S(M) is N times the maximum likelihood estimate, assuming Gaussian statistics , of the variance of the prediction error. The usefulness of the BIC becomes apparent when it is applied to different records derived from the same stochastic AR model. Since in these records the AR model is the same yet there is some variability caused by either noise or outliers (e.g. spikes,steps etc...) in the data, a criterion that provides a consistent estimate of model order is indispensable.

4.4 AR Analysis of Ensemble Average Waveforms

In terms of signal analysis the velocity ensemble average waveform is a time series of a relatively short duration. As discussed before, the resolution of FFT methods (in this case it is 5Hz) is not good enough for detecting the main harmonic. Furthermore, with the Fourier methods the spectral content of a waveform can only be defined in terms of the power at harmonics of the fundamental frequency, so that if a true component lies between two harmonics, its power will be divided. Provided the correct model order is chosen, the MESE provides a better resolution and is continuous; thus in a way it is an 'interpolated' version of the FFT estimate.

4.4.1 Model Order

The ensemble average velocity waveform consists mainly of coherent structures which are not removed during the averaging process and hence constitutes a weakly stationary process. For a weakly stationary time series of length N, low values of model order give insufficient resolution due to a smoothing effect of the true spectrum. Conversely, large values of M produce a peaky spectrum with

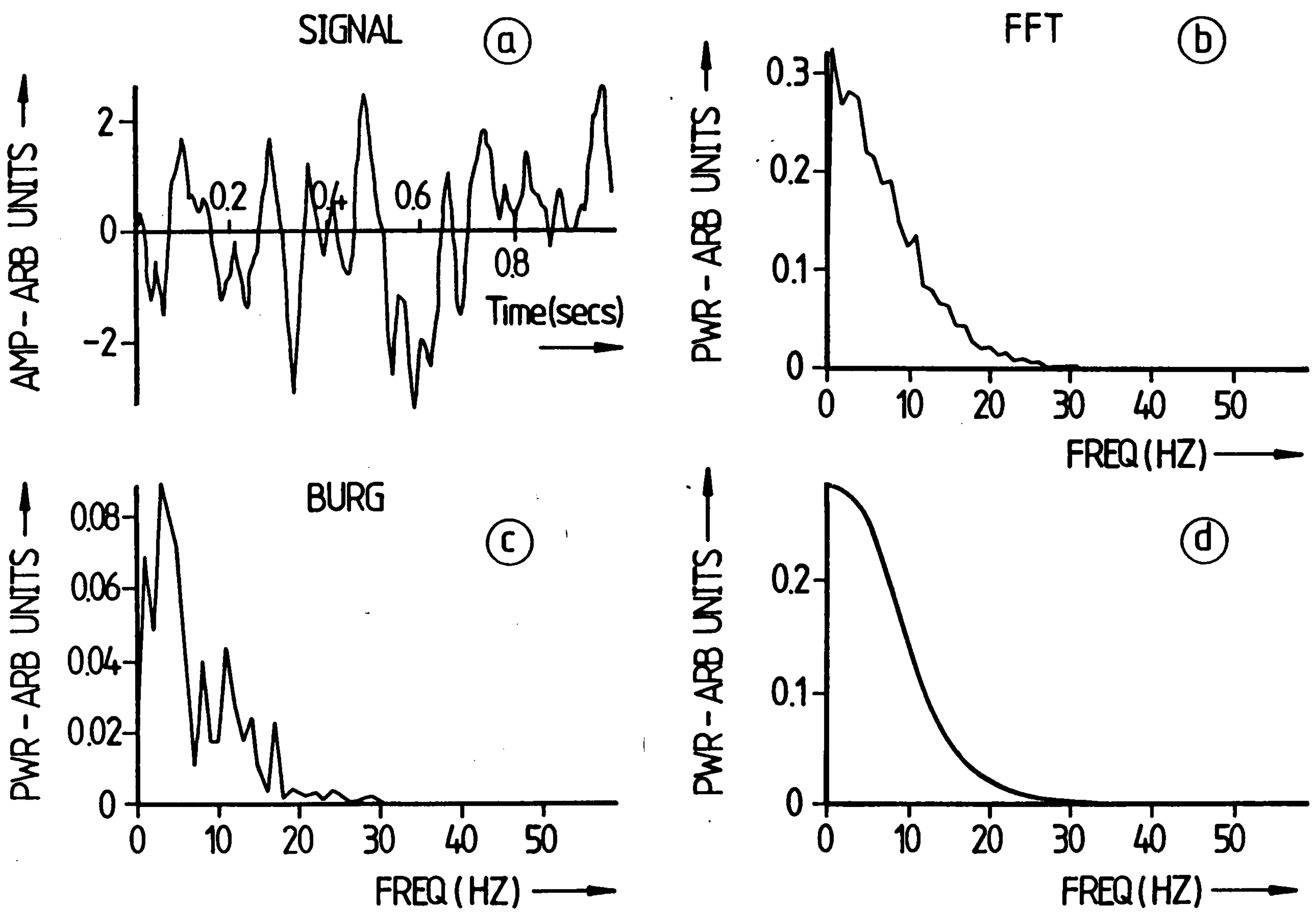
SIGNAL
ⓐ
AMP-ARB UNITS
2
0
-2
0.2
0.4
0.6
0.8
Time(secs)
FFT
ⓑ
PWR-ARB UNITS
0.3
0.2
0.1
0
0
10
20
30
40
50
FREQ(HZ)
BURG
ⓒ
PWR-ARB UNITS
0.08
0.06
0.04
0.02
0
0
10
20
30
40
50
FREQ(HZ)
ⓓ
PWR-ARB UNITS
0.2
0.1
0
0
10
20
30
40
50
FREQ(HZ)

(Fig.4.4)

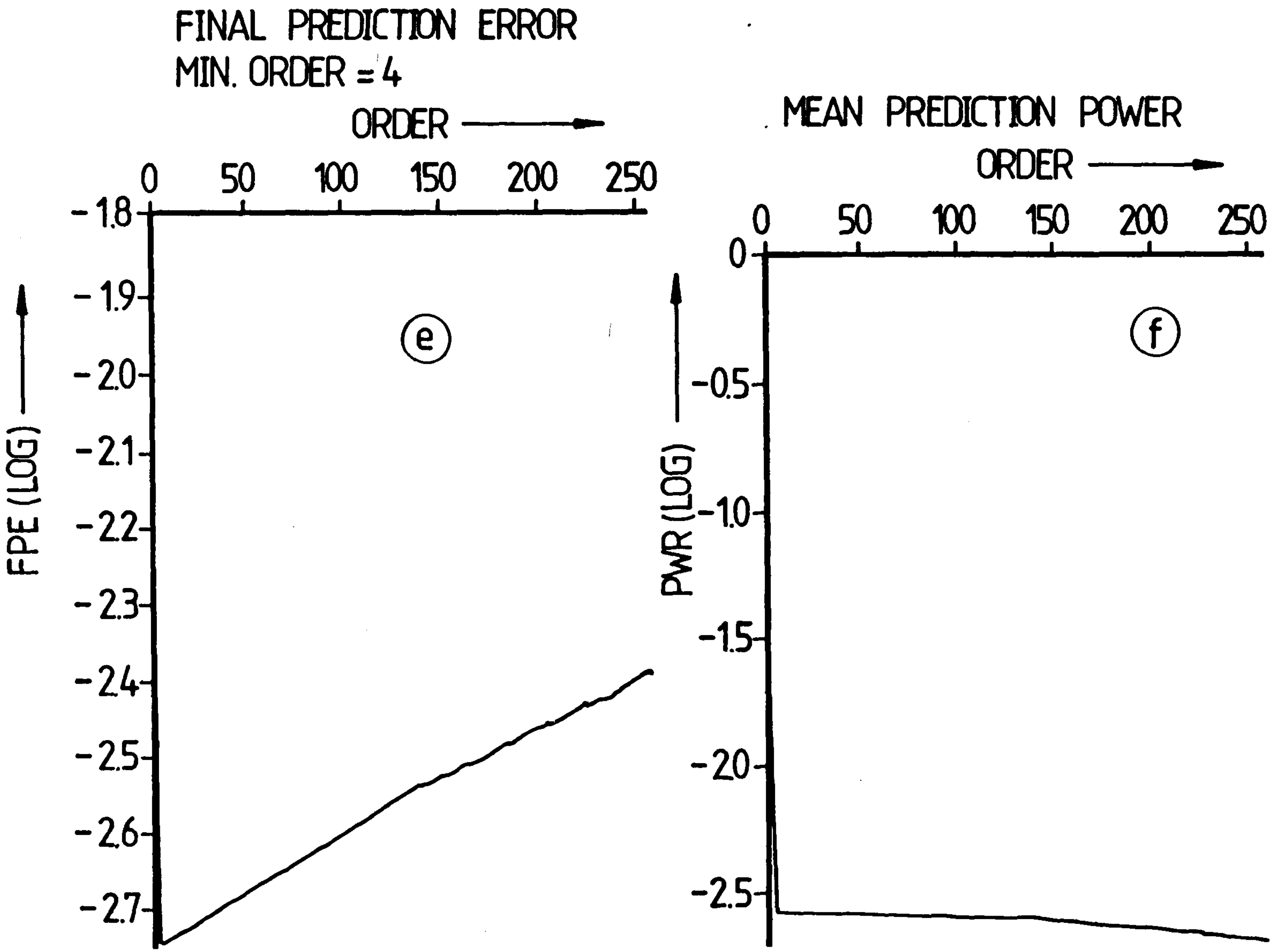

Fig.4.4 A realization of a 4th order autoregressive model. Model order 256, from a 512 point data set. (a) The time series.(b) FFT power spectrum. (c) Burg-AR spectrum calculated from the time series. (d) AR spectrum calculated from the filter characteristics. (e) Final prediction error as a function of model order. (f)Mean prediction power as a function of model order.

statistically erroneous estimates (Haykin, 1979). We have studied the effect of model order on the spectrum of the ensemble average velocity waveform and other simulated signals. Two model order criteria were used : The Final Prediction Error (FPE) and the First Zero Crossing (FZC) of the autocorrelation function.

By way of an example we applied the FPE criterion to a simulated 4^{th} order stationary AR process. Figure 4.4(a) shows a realization of the 4^{th} order AR series:

$$x(n) = -a_1 x(n-1) - a_2 x(n-2) - a_3 x(n-3) - a_4 x(n-4) + e(n) \tag{4.48}$$

where

$a_1 = -0.2373$

$a_2 = +0.1940$

$a_3 = -0.6312$

$a_4 = +0.7293$

and e(n) is a Gaussian bandlimited white noise source of variance σ_e^2. Comparing the power spectrum obtained using the FFT, Figure 4.4(b), with the theoretical MEM spectrum, Figure 4.4(d), calculated from the coefficients by applying equation (4.40), it is clear that the FFT spectrum has some random fluctuations. The Burg MEM, Figure 4.4(c), for M=256, N=512, overspecifies the model order resulting in a spurious spectrum with peaks not representative of the true frequency content of the time series. The FPE gives a minimum at 4 (Figure 4.4(e)) which is the correct model order for the process. Note that the FPE in this case is characterised by sharp fall and then rise

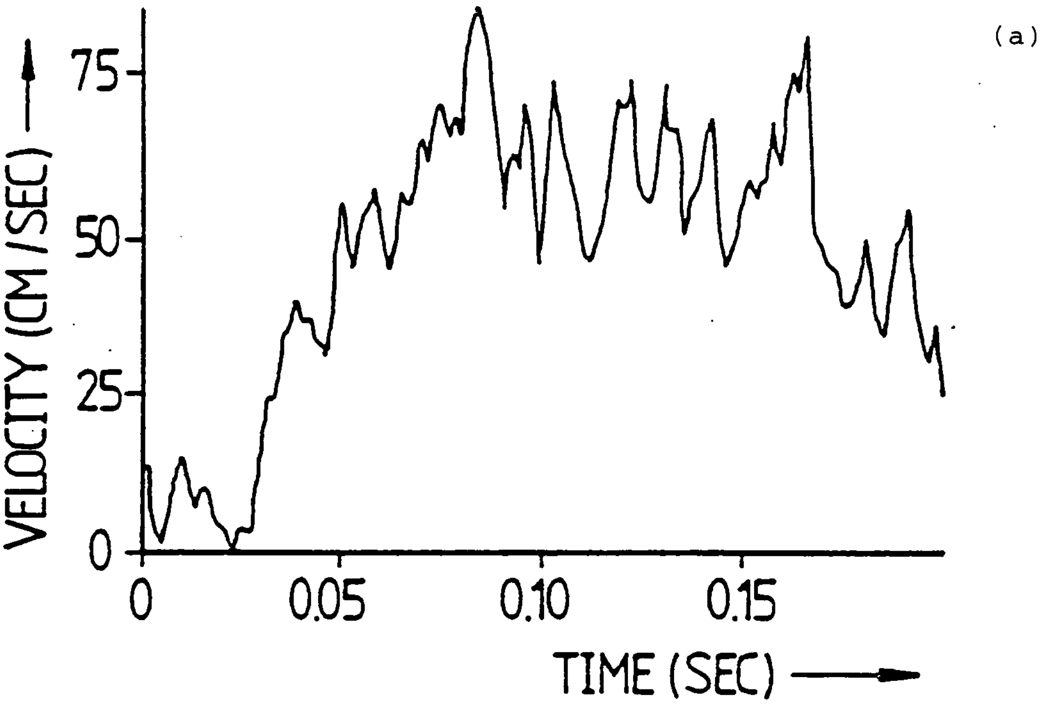

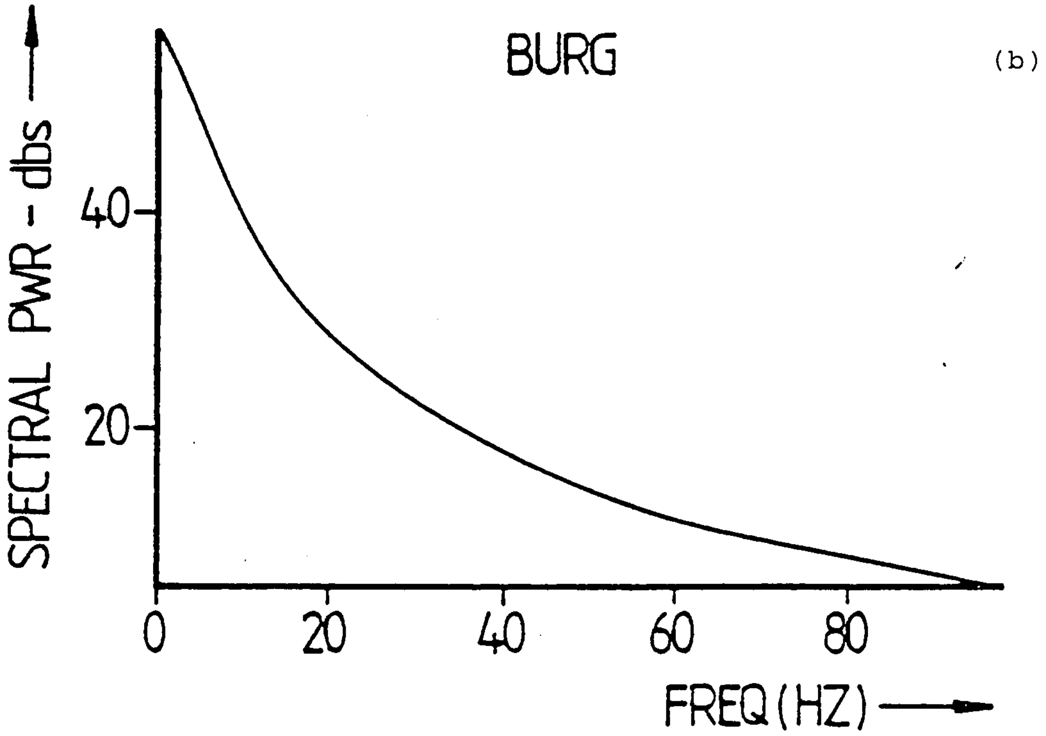

Fig.4.5 Low model order applied to the 88% occlusion ensemble average waveform. (a) The time series. (b) AR spectrum, model order 3 using 512 data points.

(Figure 4.4(e)) and therefore is of a form consistent with the Akaike's criterion. The mean output power of the filter , Figure 4.4(f), drops sharply for M<4 and continues decreasing with higher model orders but at a slower rate. For M=4 the spectrum is consistent with that predicted theoretically.

The FPE for the 88% velocity ensemble average waveform (Figure 4.5(a)) gives a minimum at M=3. The corresponding spectrum is illustrated in Figure 4.5(b). Note the overall smoothing of the spectrum and the large component at zero frequency. It is clear that the optimal order chosen by the FPE criterion has resulted in a bad estimate with very poor resolution. This result is typical for the application of the FPE criterion to ensemble averaged blood velocity waveform data.

An alternative criterion based on the <u>first zero crossing of the autocorrelation function (the FZC criterion)</u> gives a much improved estimate. As shown in section 4.1, the model coefficients are related to the autocorrelation coefficients by the Yule-Walker equations (Equations (4.10)), the size of the autocorrelation matrix being equal to the model or filter order. It will be shown that the resolution of a harmonic in the MESE is a function of how well the extension of the ACF based on the Burg estimte matches the true ACF, which lies in the range $\pm\infty$. The accuracy of the prediction of the ACF depends on the model order and there is a minimum requirement for model order M, the FZC of the ACF.

For a typical signal of N sample values, the ACF can be calculated directly in the time domain over a maximum shift range of $\pm$ (N-1) lags

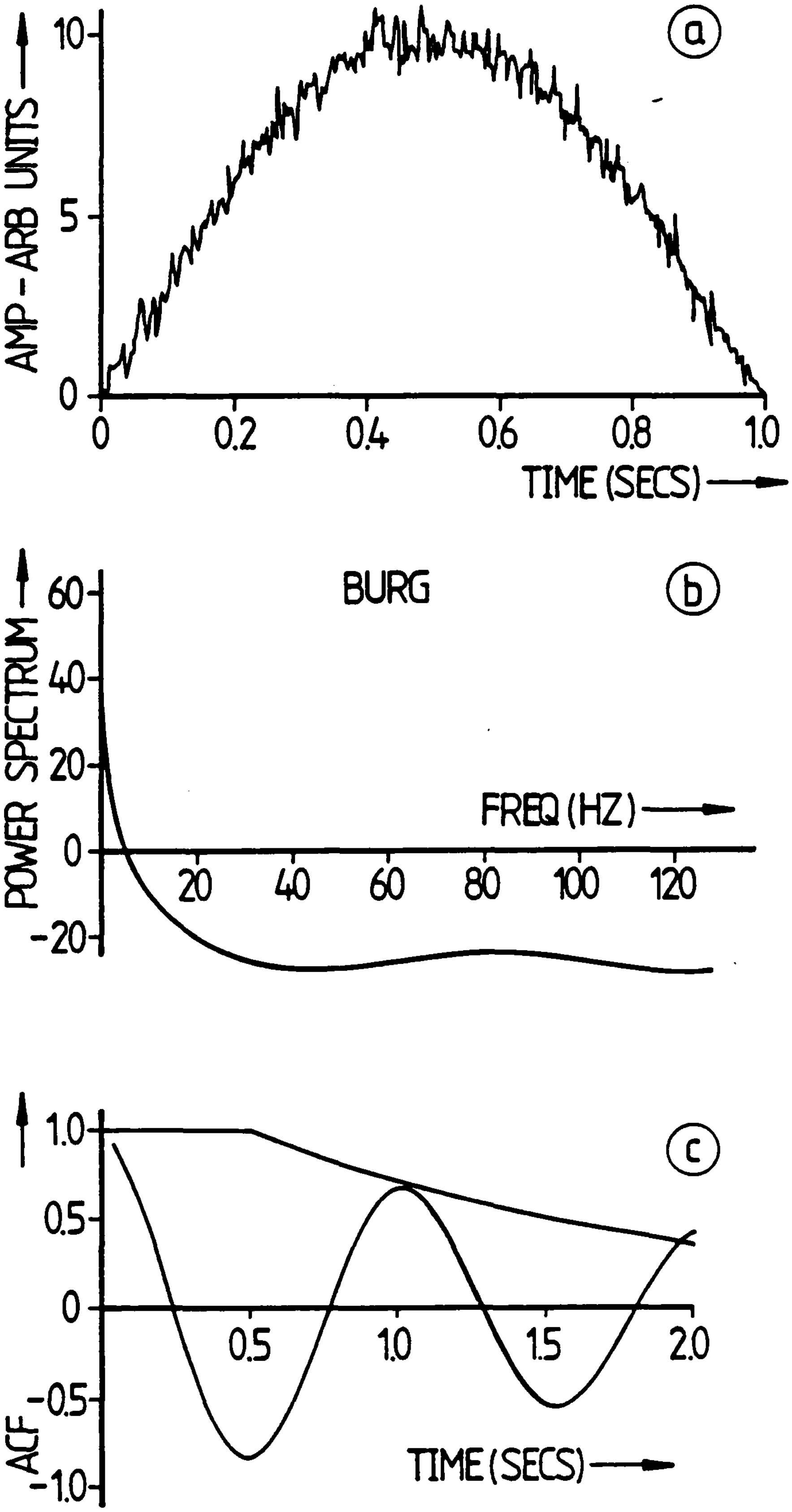

Fig.4.6 Half sinewave test signal with bandlimited random noise added. (a) The time series. (b) Burg AR spectrum - model order 128, 256 points. (c) Autocorrelation function of waveform 'a' together with the 'exponential' AR extrapolation.

or ± (N-1) T seconds, where T is the sample interval. Given M AR coefficients, the ACF can be extended recursively beyond this point. Hence the ACF can be represented by :

$$r_{xx}(n) = \begin{cases} R_{xx}(n) & \text{for } |n| \leqslant M \\ -\sum_{m=1}^{M} a_M r_{xx}(n-m) & \text{for } |n| > M \end{cases} \qquad (4.49)$$

where R_{xx} = true ACF and r_{xx} = calculated ACF. For a sinusoid of frequency f_0 the ACF is a cosine with the same frequency and the expression in (4.49) is equivalent to multiplying the true ACF with a window which can be defined as :

$$w(n) = \begin{cases} 1.0 & \text{for } |n| \leqslant M \\ f(n) & \text{for } |n| > M \end{cases} \qquad (4.50)$$

where the shape of f(n) is dependent on M and on the noise level in the original time series.

A simulated single beat was used to investigate the effect of a window on the spectral estimate. The simulated beat is illustrated in Figure 4.6(a) and consists of a 1Hz sine wave to which Gaussian white noise- standard deviation 1 - has been added. The section of the beat used in the calculations is 0.45 of a cycle (sampling rate 64Hz), the point of primary interest being how effectively the AR method can resolve the fundamental frequency for this fraction of a cycle. For the FPE minimum model order (M=4), the Burg spectrum (Figure 4.6(b)) has a primary peak at f=0. The true peak at 1Hz is not resolved. The ACF of the signal (Figure 4.6(c)) shows an exponential decay in the theoretical function as the number of lags is increased beyond 4. Referring to equation (4.49), this corresponds to the condition $|n|>M$ where the observed ACF, $r_{xx}(n)$, can be described by the product of the true ACF, R_{xx}, and a window function w(n). Here,

$$r_{xx}(\tau) = \exp(-a\tau)\cos(w\tau) \qquad (4.51)$$

where $\exp(-a\tau)$ is the window function and τ the time variable of the ACF (Figure 4.6(c)). In the frequency domain the window is convolved with the 1Hz spectral component and produces resultant power in the zero frequency region (see Figure 4.6(b)). As the model order is increased the unity range of the window expands (Equation (4.50)), i.e., $r_{xx} = R_{xx}$, for n<M, and the low frequency resolution improves. Figure 4.7(a) shows the Burg spectral estimate for M=16 from which it can be seen that the 1Hz component has been resolved.

In the <u>Z-plane</u> the interpretation of the ACF window is as follows: A sinusoid, i.e. $\sin(w_0t)$ has the following Z-transform :

$$F(z) = \frac{(\sin w_oT)z}{z^2 - (2\cos w_oT)z + 1} \qquad (4.52)$$

Equation (4.52) corresponds to two poles on the unit circle

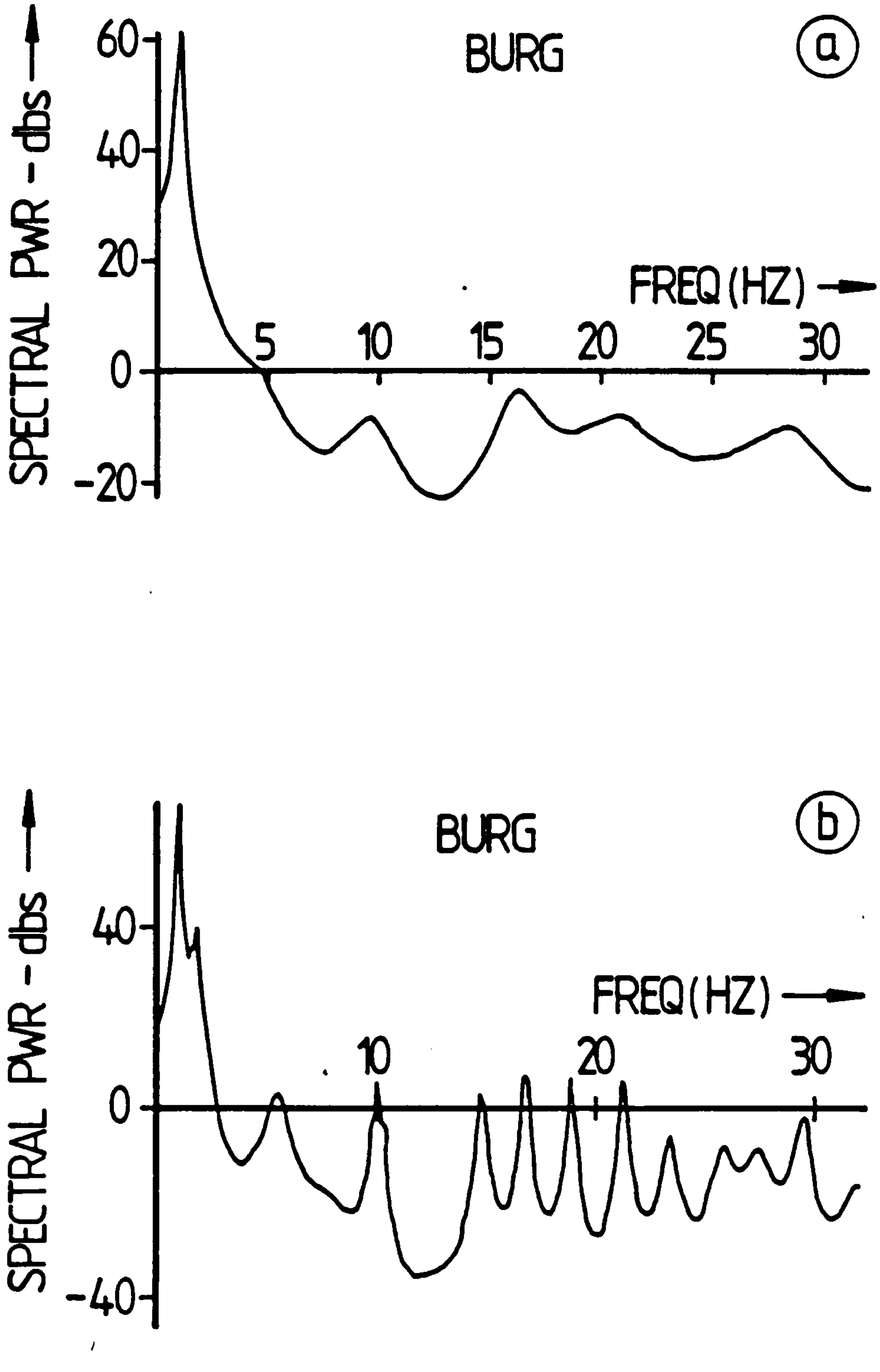

Fig.4.7 AR spectrum of the test signal (Fig.4.6(a)) decimated to 64 data points. (a) Model order 16. (b) Model order 32.

$z_1 = \exp(+jw_0T)$ and $z_1^* = \exp(-jw_0T)$. The quality of the AR model representation of the sinusoid depends on how close the poles are to the unit circle. The Burg MESE restricts the poles to within the unit circle (Claerbout,1976), which happens to be a sufficient condition for an AR process to be stationary (Pagano,1973). However, the further away from the unit circle the poles are, the more severely convergent is the prediction of the ACF. If the decay of the ACF is assumed to be exponential, which is consistent with what is observed in practice, than it can be represented by $\exp(-t/T_c)$ where T_c is the time constant. T_c in this case controls the width of the transform of the window which is inversely proportional to T_c and hence to the resolution of the ME spectrum.

The basis of the FZC is that M=16 corresponds to the point where the ACF crosses the time axis, i.e. n=16, and is also a function of sampling rate. Hence, the FZC criterion provides a reliable means of obtaining the minimum model order consistent with adequate low frequency resolution. Figure 4.7(a) shows the AR power spectrum calculated for a model order of 16. Referring to the figure the fundamental frequency is now clearly resolved in spite of the fact that the original time series is only 0.45 of a cycle. With M=32 (Figure 4.7(b)) there is peak splitting due to a noise component close to f=1Hz, indicating that the model order is too large.

The need to compromise between good low frequency resolution and modelling of noise components is of importance in AR spectral estimation. The previous example illustrates that increasing model order moves the 'harmonic' poles towards the unit circle. However, the noise poles will also move closer to the unit circle (Kay,1979) ; and if the model order is too high, this will cause the appearance of 'false' peaks, or peak splitting, in the spectrum. Hence an optimum model order to produce good low frequency resolution should be high enough to achieve this objective while at the same time not be too high in order that problems with noise poles are avoided. This can be achieved by using the FZC criterion.

4.4.2 Decimation and Spectra

Choosing an optimal model order is only one factor in improving the resolution of the MESE of the process consisting of one harmonic or more. Another important factor is decimation, whereby reducing the sampling rate while still using the same model order would produce a vaste improvement to resolution. A heuristic explanation of this phenomen can be given as follows :

A fundamental aspect of AR modelling is that the model (order M) will attempt to describe the entire frequency range , [$0,f_s$] where f_s is the sampling frequency. In the Z domain this means spreading M/2 poles over the upper half of the cicle - [$0,f_N$] where f_N is the Nyquist frequency. Therefore, if the sampling frequency is significantly in excess of twice the highest frequency of interest in the signal, the AR model will include an estimate of at best irrelevant signal information and, at worst, noise. It is therefore often important to decimate the original signal (i.e. the oversampled signal) prior to modelling.

To illustrate this point, we will consider an example based on the

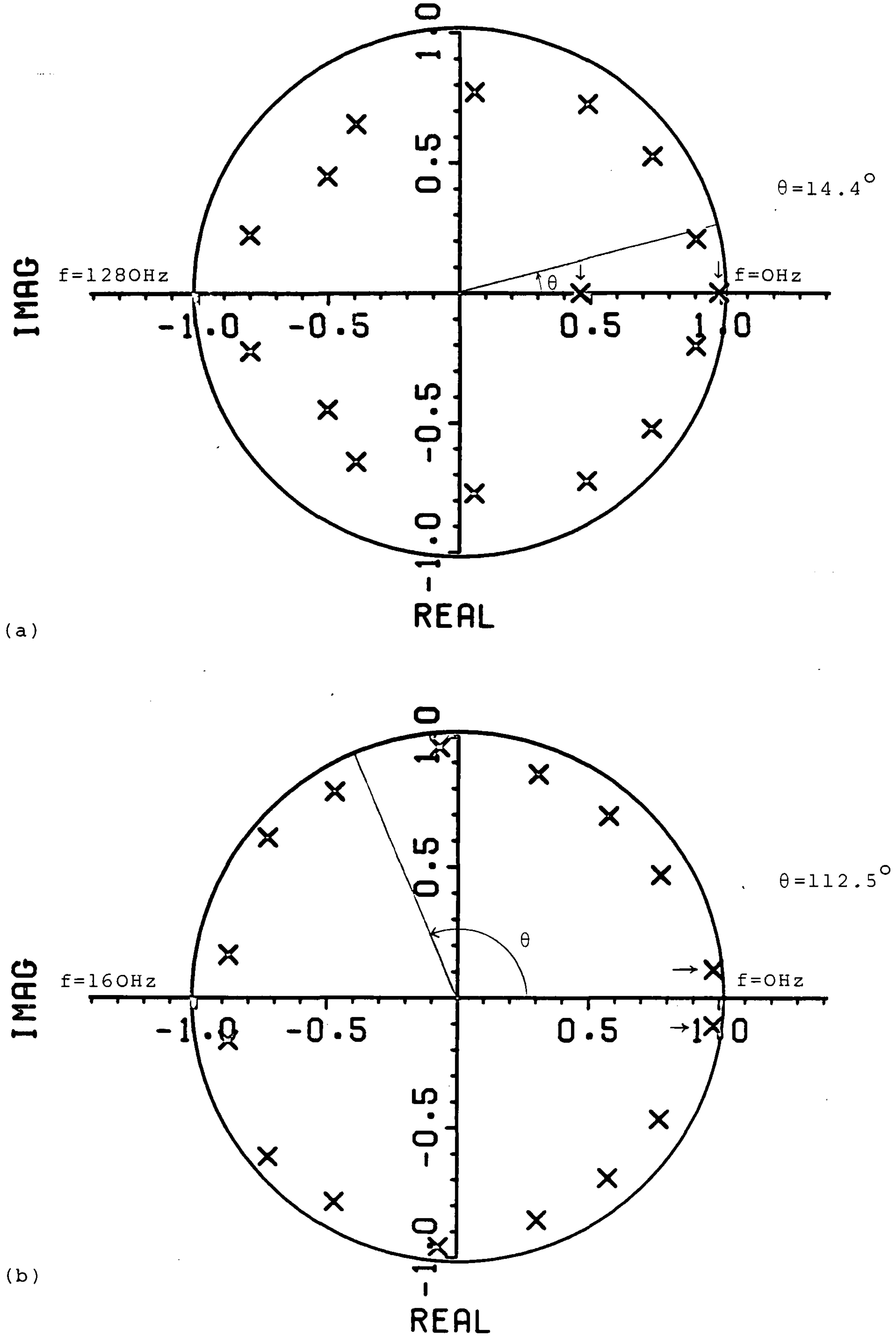

Fig.4.8 Poles of the autoregressive model: (a) explains the smoothing effect observed in the AR spectrum of Fig.4.5(b), (b) demonstrates the effect of decimation on the spectrum as seen in Fig.4.9(c).

ensemble average data. The FFT spectral analysis has shown that this signal , sampled at 2560Hz, does not have any significant power components above 100Hz. In terms of the Z-plane representation the 100Hz band would be the sector of the circle defined by $\theta = 14.4^{\circ}$ (see Figure 4.8(a)). Within that sector three poles can be seen , two of them sitting on the real axis (see arrows). The poles on the real axis correspond to the high magnitude D.C. component seen in the spectrum. By decimating the time series to a sampling frequency of 320Hz we can see from Figure 4.8(b) that the 100Hz sector has been extended to $\theta = 112.5^{\circ}$ and that the spectrum has a much better resolution. Notice too that the conjugate poles of the main harmonic (see arrows) are now close to the unit circle. Hence, by decimating from N=512 to N=64 while still retaining the same model order M=16, we have improved considerably the resolution of the MESE.

The application of decimation and the FZC to ensemble average waveforms for 0,20,40,58,74 and 88% ooclusion levels produced spectra with better resolution than the FFT spectra especially when the duration of the time series is less than one cycle. Figures 4.9(a)-(c) illustrate the use of the FZC criterion in defining model order for velocity data for three different levels of occlusion 0,40 and 88% respectively. The original sampling rate was 2560Hz but because the ensemble average velocity waveform comprises low frequencies only, the signal was decimated by a factor of 8, i.e. to a new sampling rate of 320Hz. In all three cases, it was clear from the ACF's that the FZC occurred at n=16. Consequently, applying the FZC criterion , we set the model order to 16. Referring to Figures

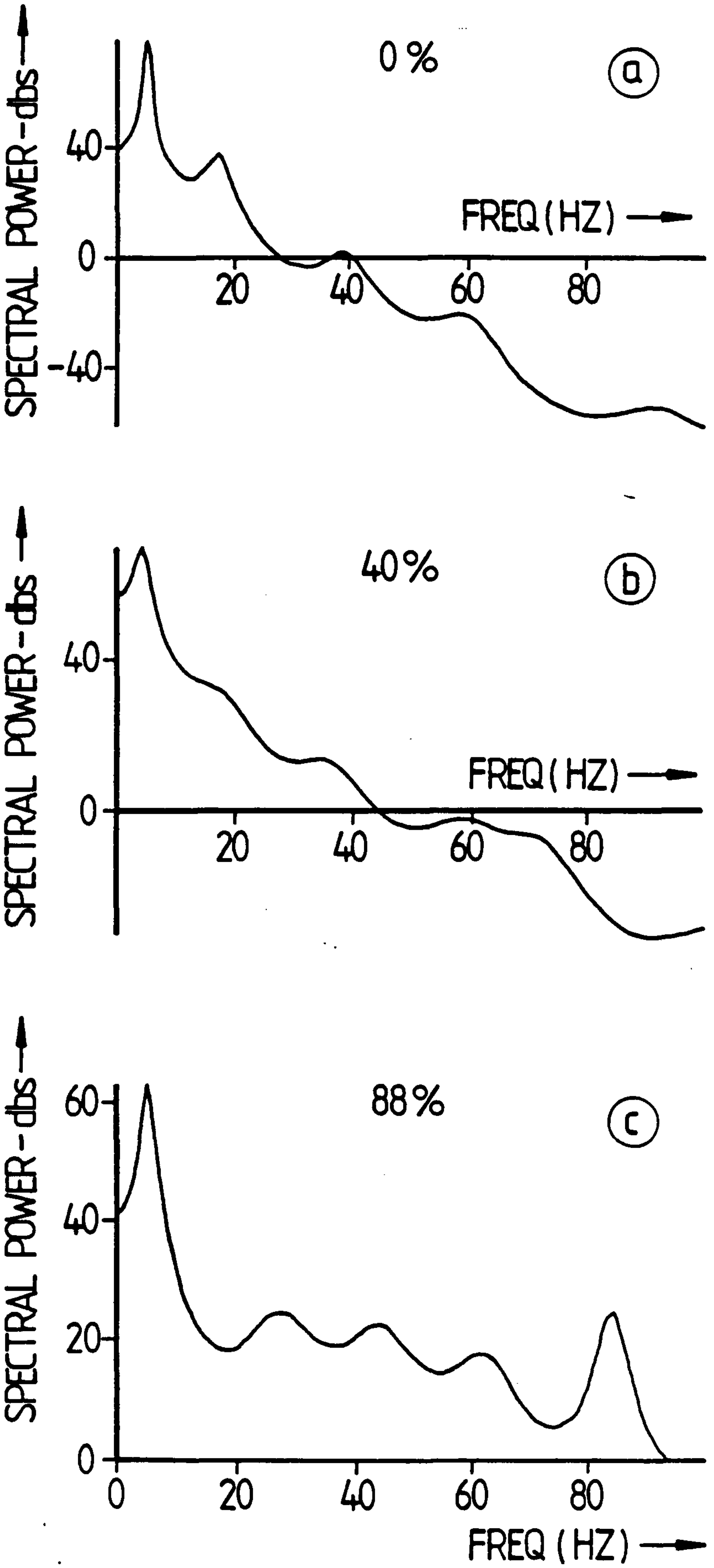

Fig.4.9 AR spectra of ensemble average velocity waveforms, 512 decimated to 64 points. (a) 0% occlusion. (b) 40% occlusion. (c) 88% occlusion.

4.9(a)-(c), there is a primary peak in all three at $f<5$Hz. It should be noted that at the decimated sampling frequency the number of data points per cycle is 64, hence, as in the previous example, the FZC occurs after a quarter of a cycle. Also, an important feature of the spectra in Figures 4.9(a)-(c) is the increase in high frequency activity with increasing percentage of stenosis. This is consistent with the results discussed in chapter 3.

4.5 AR Analysis of the Disturbance Velocity Waveforms

The AR anlysis considered sofar has focused on the ensemble average waveforms for different levels of occlusion ; equally important is the anlysis of individual disturbance velocity records. These will be derived using the frequency domain method suggested by equation (3.2), i.e. high-pass filtering. The reason for this choice as opposed to subtraction of the ensemble average from the individual velocity beat is that both the simple and phase shift average techniques optimize the accurate representation of the low frequency content of the signal at the expense of the high frequency content. Hence, when studying the high frequency content of individual beats, high pass filtering is likely to be a more appropriate alternative.

4.5.1 Model Order

In attempting to define an order for the disturbance velocity waveform ,$\{u_2'(t)\}$, we have to start with a certain notion or assumption about the system under study i.e. the flow field with a varying parameter which is the occlusion level. The assumption here

Fig.4.10 Plots of FPE, AIC, BIC and CAT against model order M.

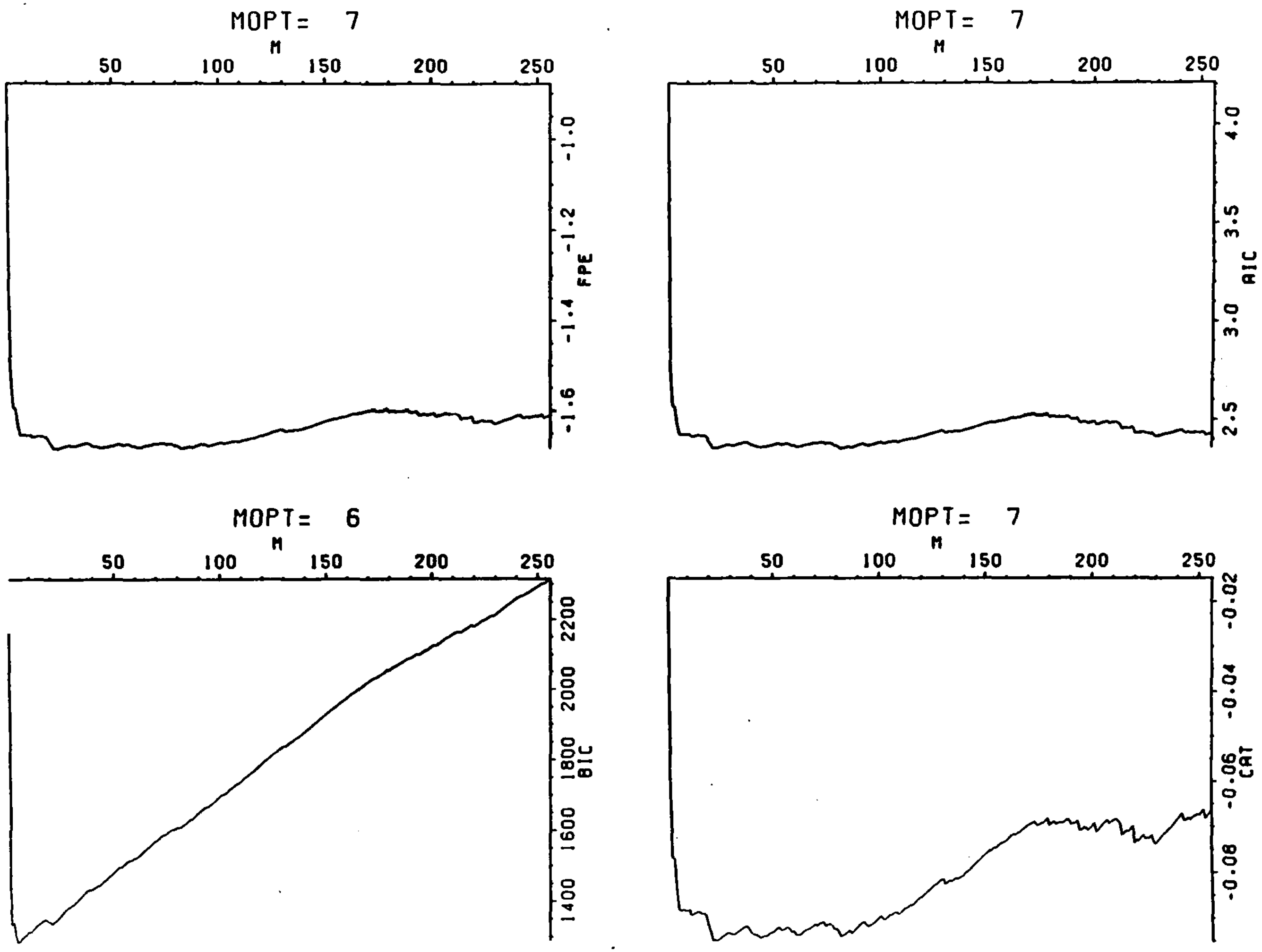

is that the model order, M, is fixed for all levels ,yet what is changing are the values of these M AR coefficients $\{a_1,a_2,\ldots,a_M\}$. By fixing the model order we hope to be able to reduce the variability obtained by having a different M for each level and hence we would be able to observe the variability of the AR transfer function, A(z), itself.

Using the statistical methods described in section 4.3, we investigated the choice of model order for a set of ten disturbance velocity waveforms for 40% occlusion. Figure 4.10 shows an example of the behaviour of FPE, AIC, BIC and CAT for M=256 and N=512. The result of the study can be summed as follows :

(1) The behaviours of the FPE, AIC and CAT were similar in that they dropped sharply and then fluctuated about a mean which is almost horizontal (see Figure 4.10) . Therefore, the absolute minimum was not well defined and consequently the optimal orders chosen were not consistent.

(2) The BIC, on the other hand, though showing a steep fall , it also had also a large-slope ($=45^o$) rise. The absolute minimum was well defined and the order chosen was relatively more consistent as predicted by Akaike (1977).

The results for all four criteria can be seen in Table 4.1. From these results we concluded that the model order to be used was M=6 (based on the BIC criterion).

4.5.2 Spectra

With the order selected by the BIC criterion, we studied two types

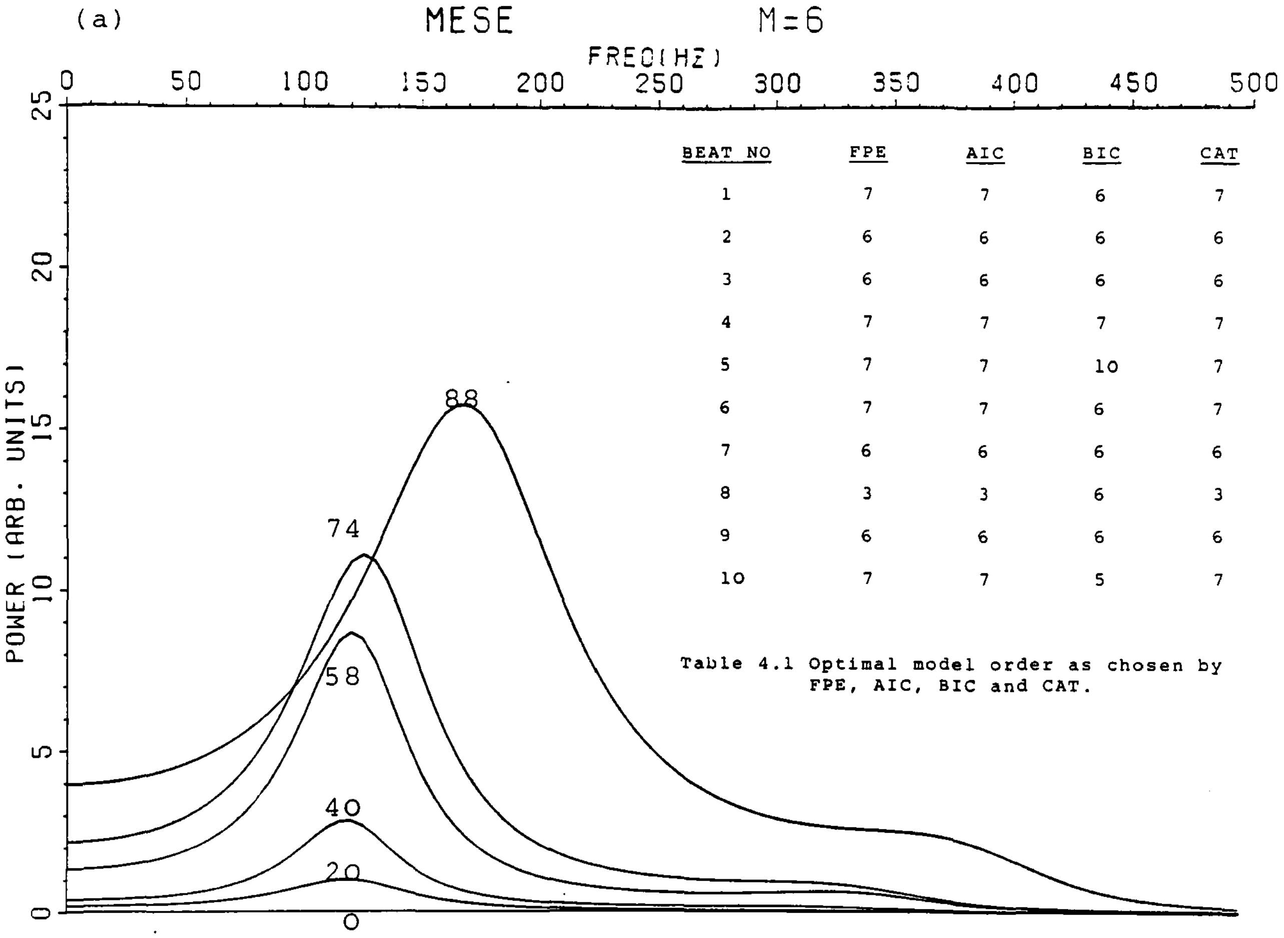

BEAT NO	FPE	AIC	BIC	CAT
1	7	7	6	7
2	6	6	6	6
3	6	6	6	6
4	7	7	7	7
5	7	7	10	7
6	7	7	6	7
7	6	6	6	6
8	3	3	6	3
9	6	6	6	6
10	7	7	5	7

Table 4.1 Optimal model order as chosen by FPE, AIC, BIC and CAT.

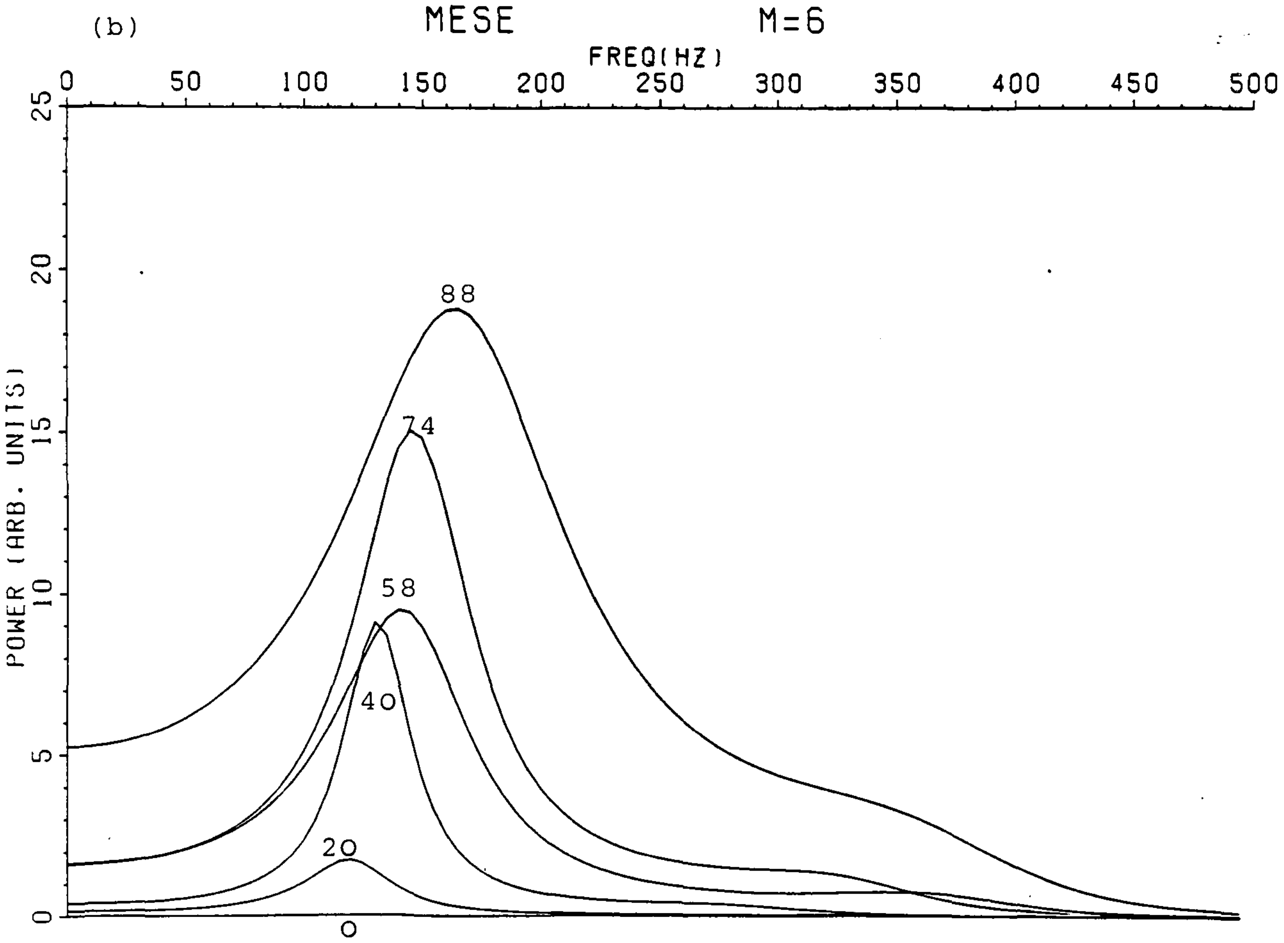

Fig.4.11 Two typical examples (a&b) of spectra of the individual disturbance velocity waveforms for 0, 20, 40, 58, 74 an 88% occlusion.

of ME spectra representing the disturbance velocity data: (1) stationary spectra i.e. spectra based on the whole observation time window ; and (2) evolutionary spectra i.e. spectra based on sections of the whole time window and evolving in time (Priestley,1965;1981).

Two typical examples of stationary ME spectra for the occlusion data can be seen in Figures 4.11 (a) and (b). The following features are of interest in these diagrams :

(1) The MESE shows a narrowband process for all occlusion data (only half of the frequency scale is shown in the figures).

(2) The magnitude of the main peak tends to increase with increasing occlusion level.

(3) There is an increase of spectral broadening with an increase in occlusion level.

The previous examples were based on a time interval of 0.2 seconds (512 points sampled at 2560Hz). In order to study the evolution of spectra in the mentioned interval, segments of 0.05 seconds (128 points) each were considered. It was found that a large overlap (i.e. 0.0375 seconds or 96 points) in the moving window is more sensitive to small data variations. Figures 4.12 (a) , (b) and (c) show a typical disturbance velocity record for 0,40 and 74% occlusion respectively with 13 segments and their respective spectra (the MESE is the smooth curve). We noted the following:

(1) The spectra of the 0% occlusion level were consistently (i.e. for all 13 segments) broadband and of low magnitude compared to the rest.

(2) The 40% level showed a different behaviour: the first three segments showed broadband spectra similar to those of the 0% level ;

the rest of the segments had narrow band spectra with a well defined peak, the magnitude of which dropped slowly as the moving window reached the end of the record.

(3) In the 74% record, the initiation of the narrow band process could be seen in the first segment. The spectra became more broadband in segments 8,9,10,11 and 12. In segment 13 the spectrum showed again narrow band activity which was still of considerable magnitude. In general, the disturbances either narrow band or broadband were spread over most of the record.

From these examples we can see that evolutionary MESE are of importance in trying to follow up time variations in the disturbance record. The fact that the MESE has a reasonably good resolution even for short records makes it useful in detecting fine structures in the velocity field that might not be detected if the whole record is considered. Its smoothness makes it very attractive in characterising noisy or broadband random processes which have rugged spectra when the FFT is employed. Yet, for a signal as variable as that of the disturbance velocity, the wish is to obtain , if possible, information about every single new data point based on its recent past. The information desired is the spectral content and obtaining time-variable ME spectra with a resolution of even a sampling interval, though overambitious , can still be realized if the AR process is considered as adaptive i.e. the AR coefficients are adapted to the new information acquired by the inclusion of a new data point. The adaptive AR technique used, its implementation and the difficulties encountered is the subject matter of the next chapter.

In Fig.4.12 (pp.132-140) the velocity signal is in arbitrary units, the FFT spectrum is the dotted curve and the AR spectrum is the smooth curve.

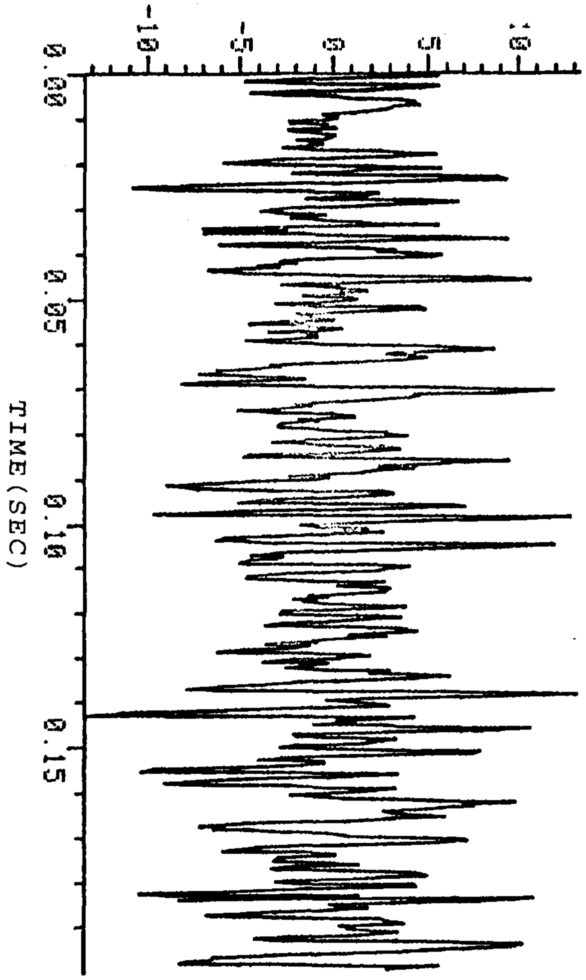

The disturbance velocity record(0%)

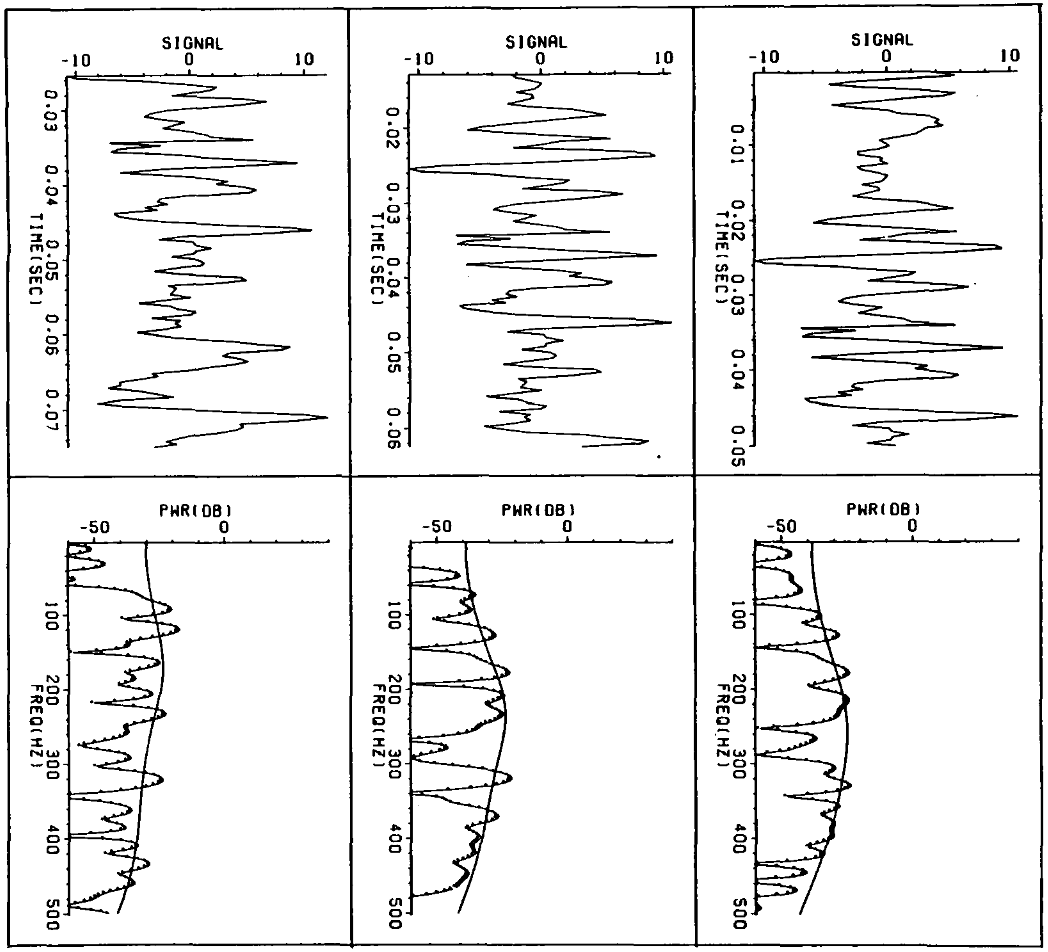

(Fig.4.12(a))

(Fig.4.12(a))

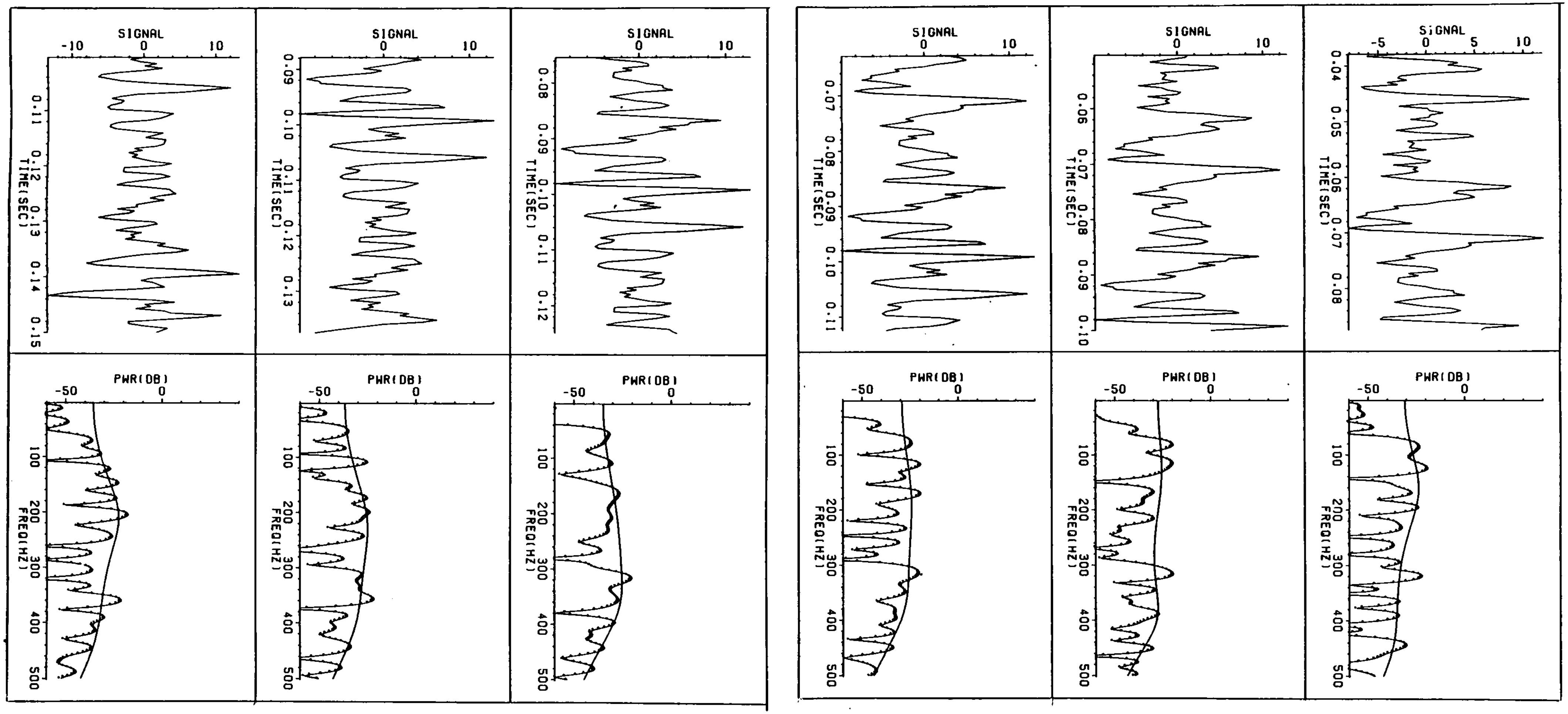
SIGNAL
TIME(SEC)
PWR(DB)
FREQ(HZ)
-10
-5
0
5
10
-50
0.04
0.05
0.06
0.07
0.08
0.09
0.10
0.11
0.12
0.13
0.14
0.15
100
200
300
400
500

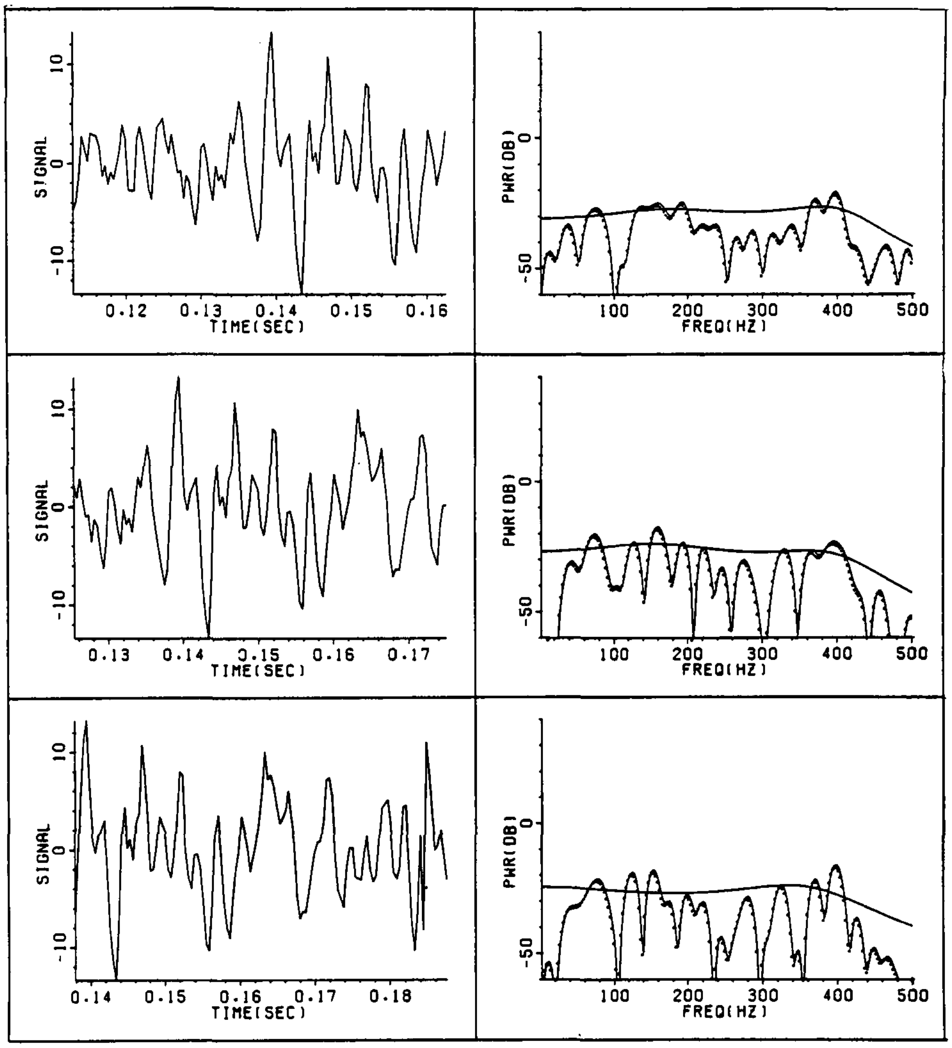
SIGNAL
10
0
-10
0.12
0.13
0.14
0.15
0.16
TIME(SEC)
PWR(DB)
0
-50
100
200
300
400
500
FREQ(HZ)
SIGNAL
10
0
-10
0.13
0.14
0.15
0.16
0.17
TIME(SEC)
PWR(DB)
0
-50
100
200
300
400
500
FREQ(HZ)
SIGNAL
10
0
-10
0.14
0.15
0.16
0.17
0.18
TIME(SEC)
PWR(DB)
0
-50
100
200
300
400
500
FREQ(HZ)

(Fig.4.12(a))

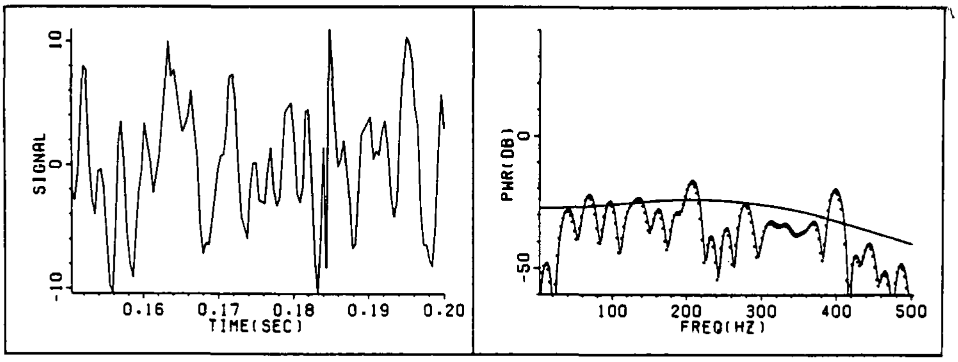
SIGNAL
10
0
-10
0.16
0.17
0.18
0.19
0.20
TIME(SEC)
PWR(DB)
0
-50
100
200
300
400
500
FREQ(HZ)

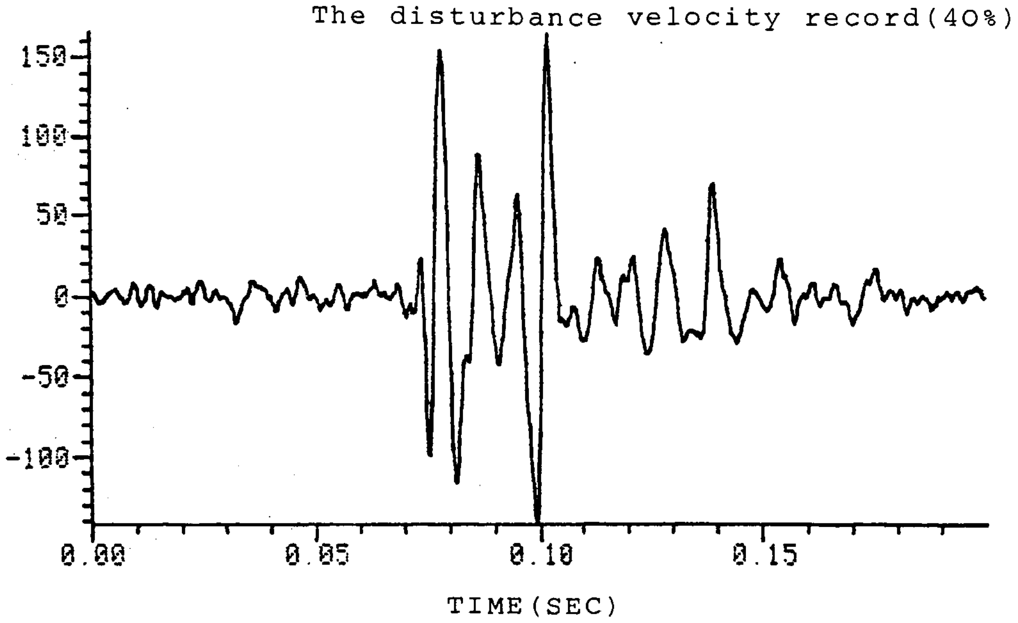
The disturbance velocity record(40%)
150
100
50
0
-50
-100
0.00
0.05
0.10
0.15
TIME(SEC)

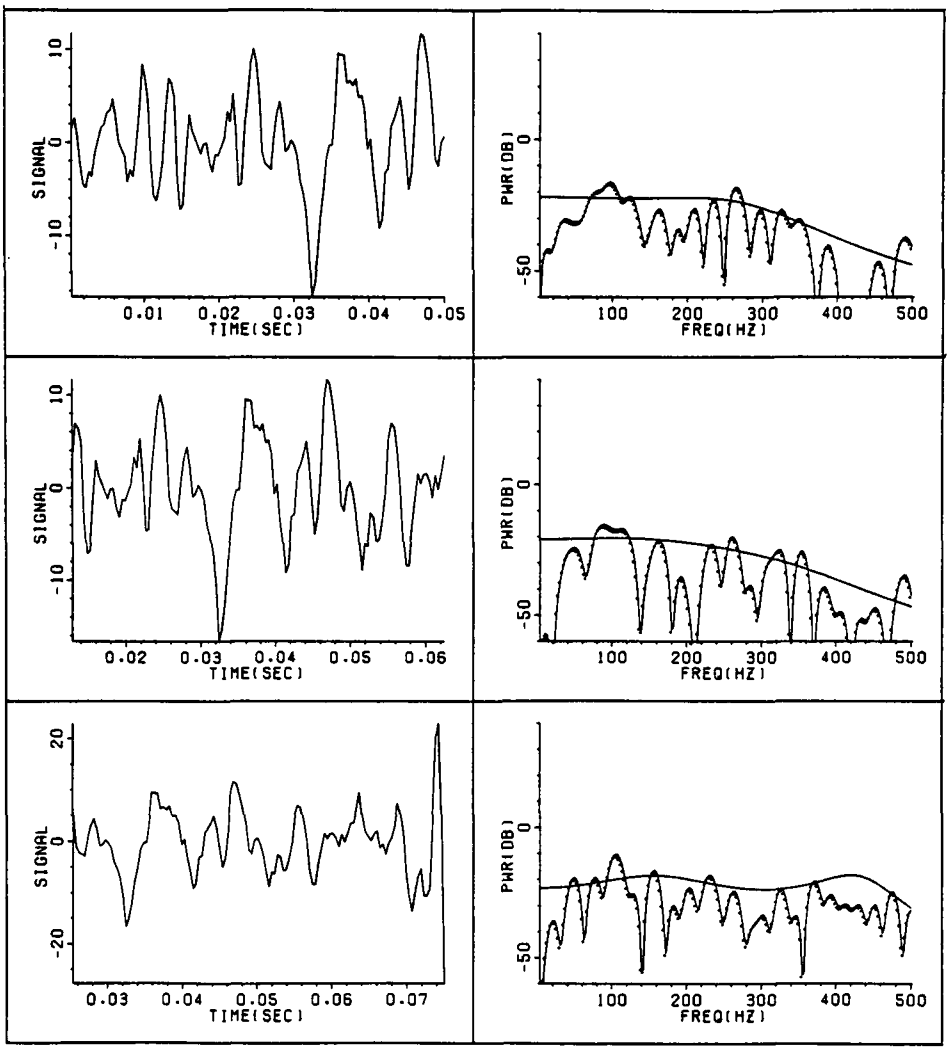
SIGNAL
10
0
-10
0.01
0.02
0.03
0.04
0.05
TIME(SEC)
PWR(DB)
0
-50
100
200
300
400
500
FREQ(HZ)
SIGNAL
10
0
-10
0.02
0.03
0.04
0.05
0.06
TIME(SEC)
PWR(DB)
0
-50
100
200
300
400
500
FREQ(HZ)
SIGNAL
20
0
-20
0.03
0.04
0.05
0.06
0.07
TIME(SEC)
PWR(DB)
0
-50
100
200
300
400
500
FREQ(HZ)

(Fig.4.12(b))

(Fig.4.12(b))

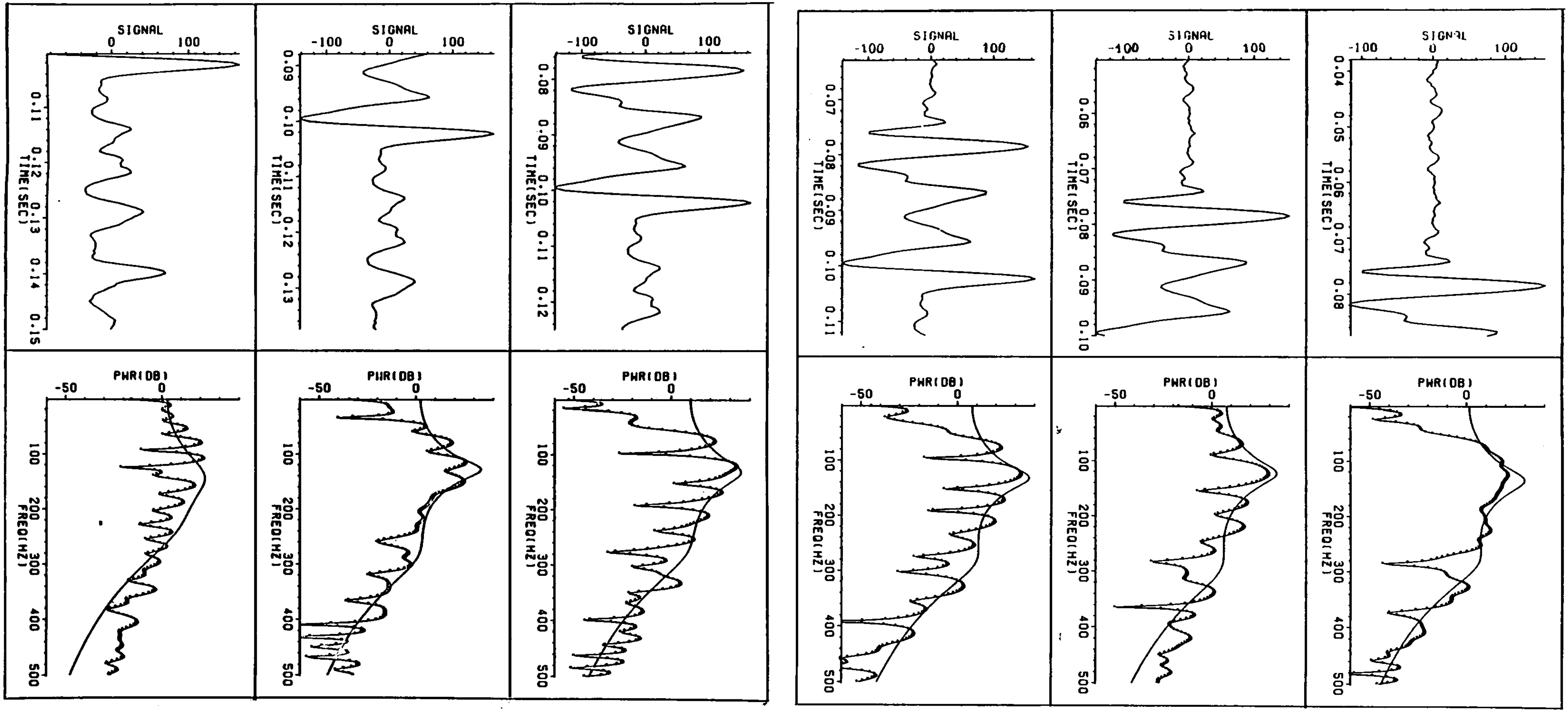

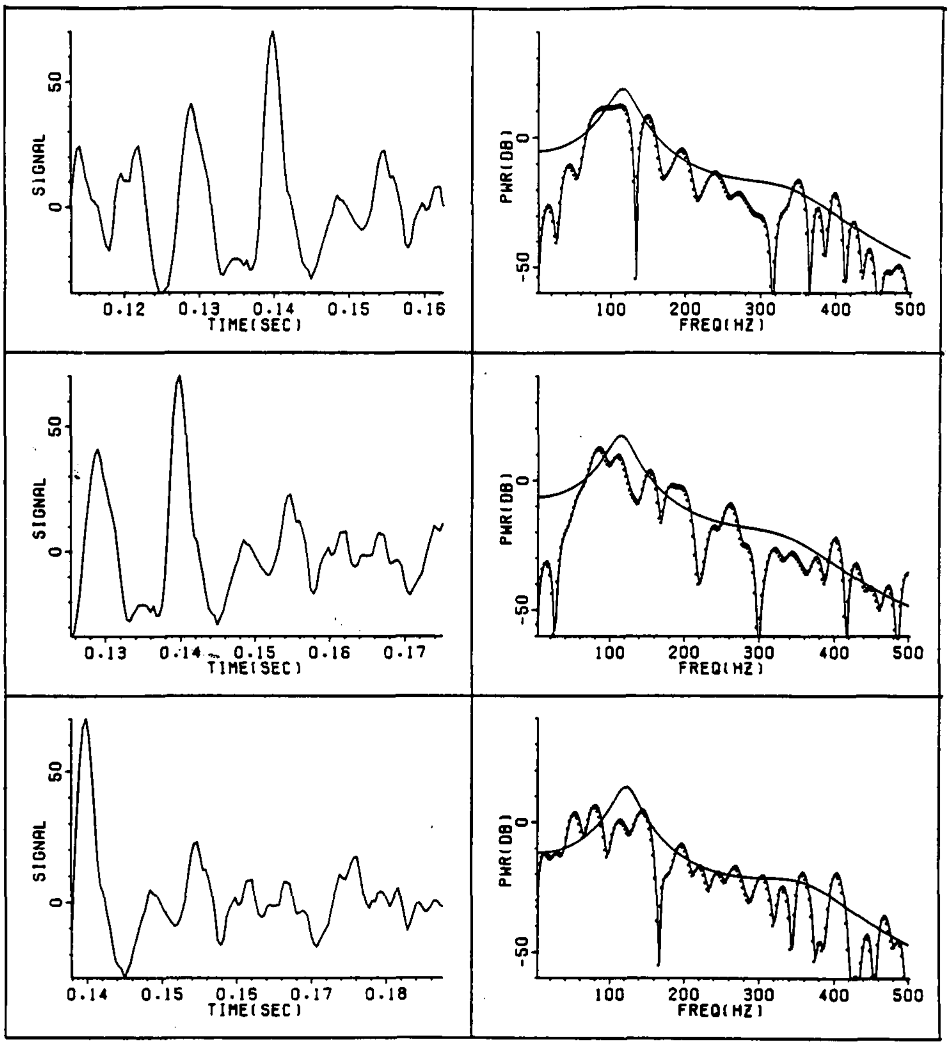
SIGNAL
50
0
0.12
0.13
0.14
0.15
0.16
TIME(SEC)
PWR(DB)
0
-50
100
200
300
400
500
FREQ(HZ)
SIGNAL
50
0
0.13
0.14
0.15
0.16
0.17
TIME(SEC)
PWR(DB)
0
-50
100
200
300
400
500
FREQ(HZ)
SIGNAL
50
0
0.14
0.15
0.16
0.17
0.18
TIME(SEC)
PWR(DB)
0
-50
100
200
300
400
500
FREQ(HZ)

(Fig.4.12(b))

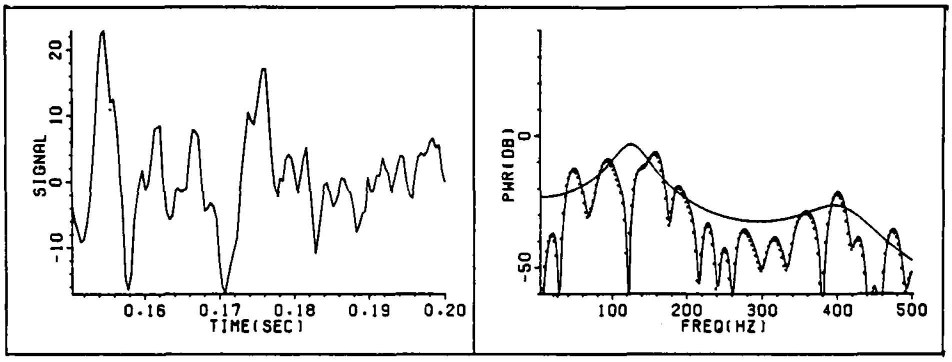
SIGNAL
20
10
0
-10
0.16
0.17
0.18
0.19
0.20
TIME(SEC)
PWR(DB)
0
-50
100
200
300
400
500
FREQ(HZ)

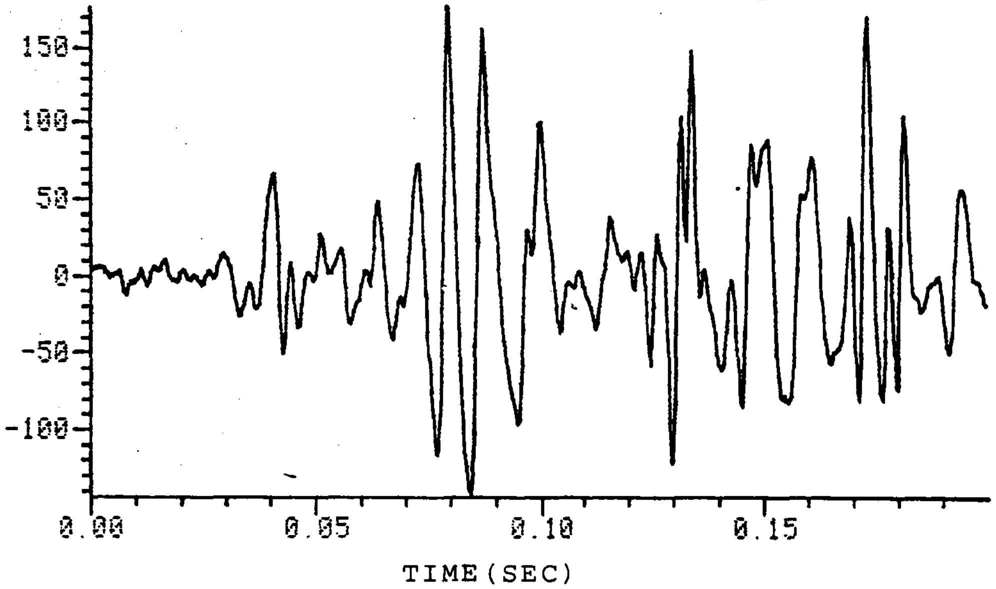

The disturbance velocity record(74%)

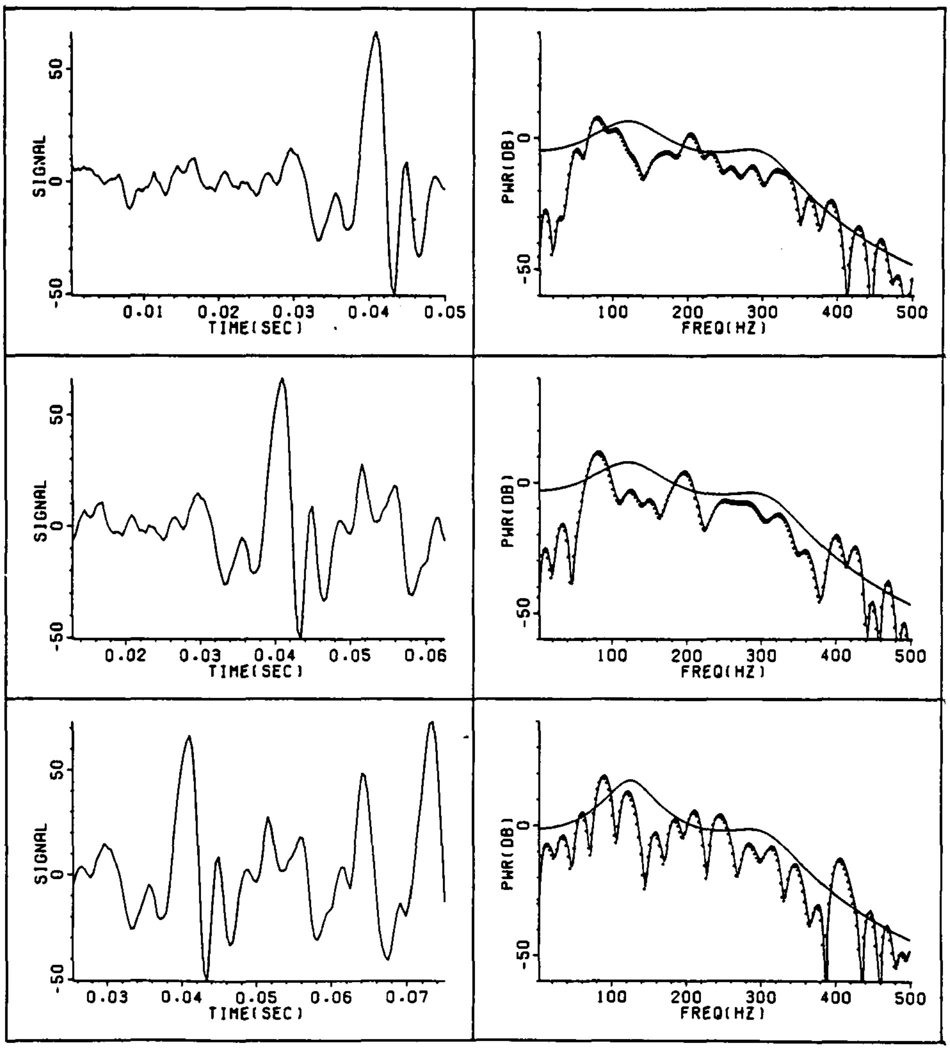

(Fig.4.12(c))

(Fig.4.12(c))

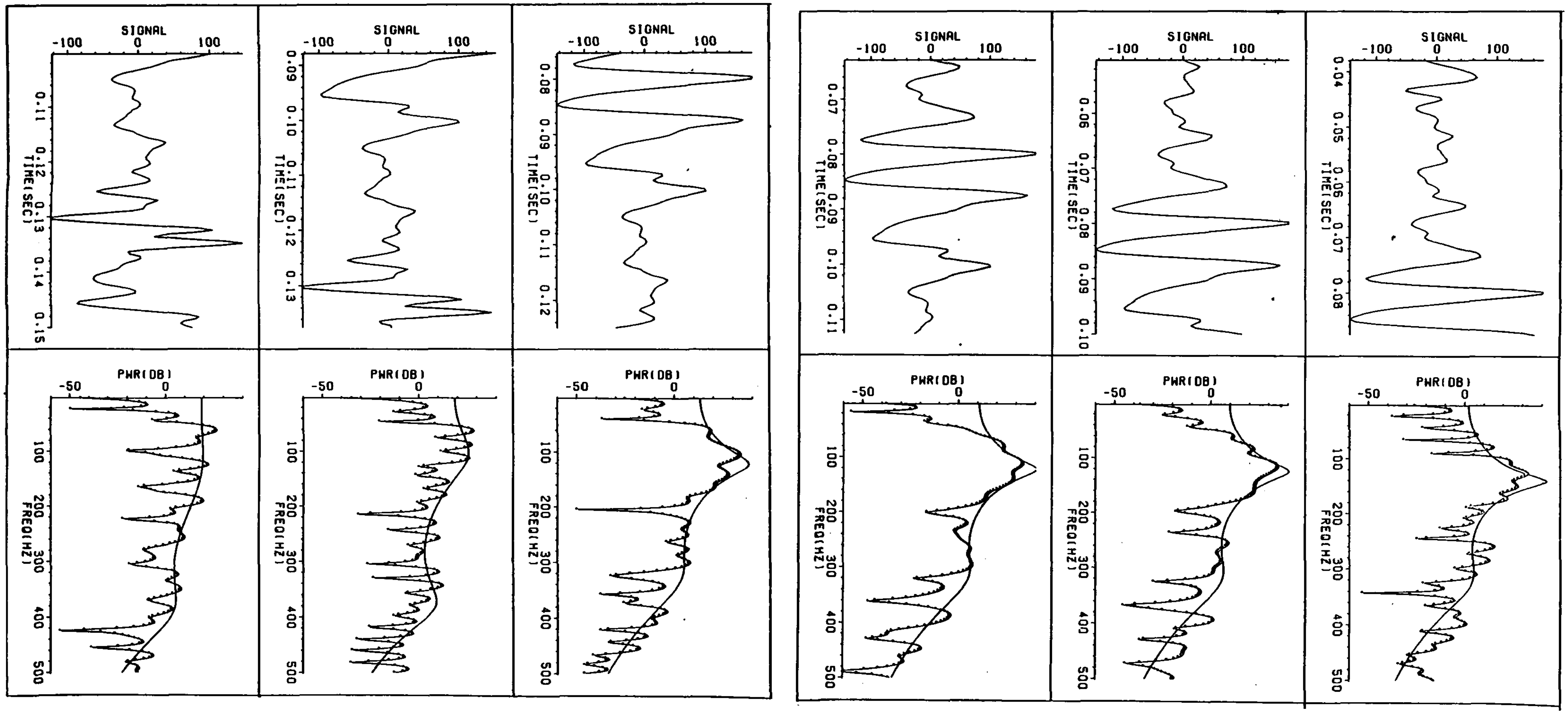

(Fig.4.12(c))

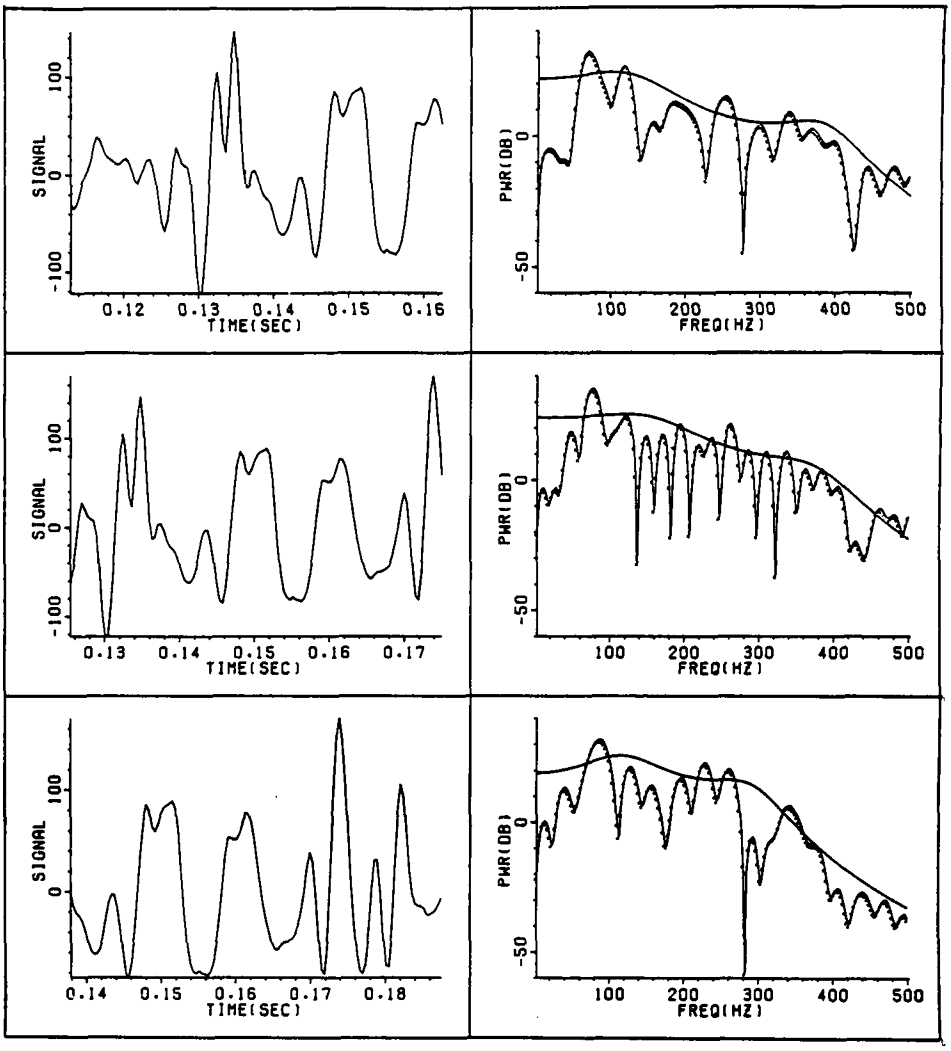

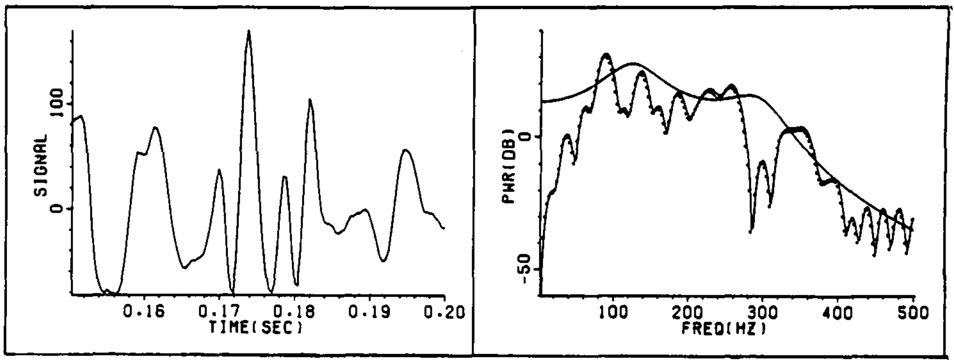

Fig.4.12 Evolutionary Maximum Entropy spectra for 0% (a), 40% (b) and 88% (c) stenosis disturbance velocity waveforms.

CHAPTER 5

NONSTATIONARY MODELLING OF THE DISTURBANCE VELOCITY WAVEFORMS
THE ADAPTIVE AUTOREGRESSIVE METHOD

The analysis of the disturbance velocity waveform is crucial in the overall understanding of the flow field downstream of a stenosis. Yet the non-stationary character of this signal is a matter that cannot be disregarded and presents some difficulties for techniques which are based on stationarity. The usual way of dealing with such a signal is to divide its time interval into smaller 'stationary' segments from which information can be derived. Sectioning in this way has been illustrated in the previous chapter in connection with the Maximum Entropy Spectral Estimate. Here an adaptive autoregressive technique will be explored allowing us to adapt the AR coefficients to data non-stationarity. Time-variant spectra will be estimated and will be used to describe fine-scale flow structures that conventional techniques might fail to detect.

5.1 The Adaptive AR Method

The stationary representation of an AR process of order M is given by(4.4):

$$\hat{y}_n = -\sum_{m=1}^{M} a_m \hat{y}_{n-m} + e_n \tag{5.1}$$

The main assumptions underlying equation (5.1) are that: (i) a_1, $a_2, \dots, a_M$ are invariant over the record length N; and (ii) that $\{e(n)\}$ is a Gaussian white noise source with zero mean and a

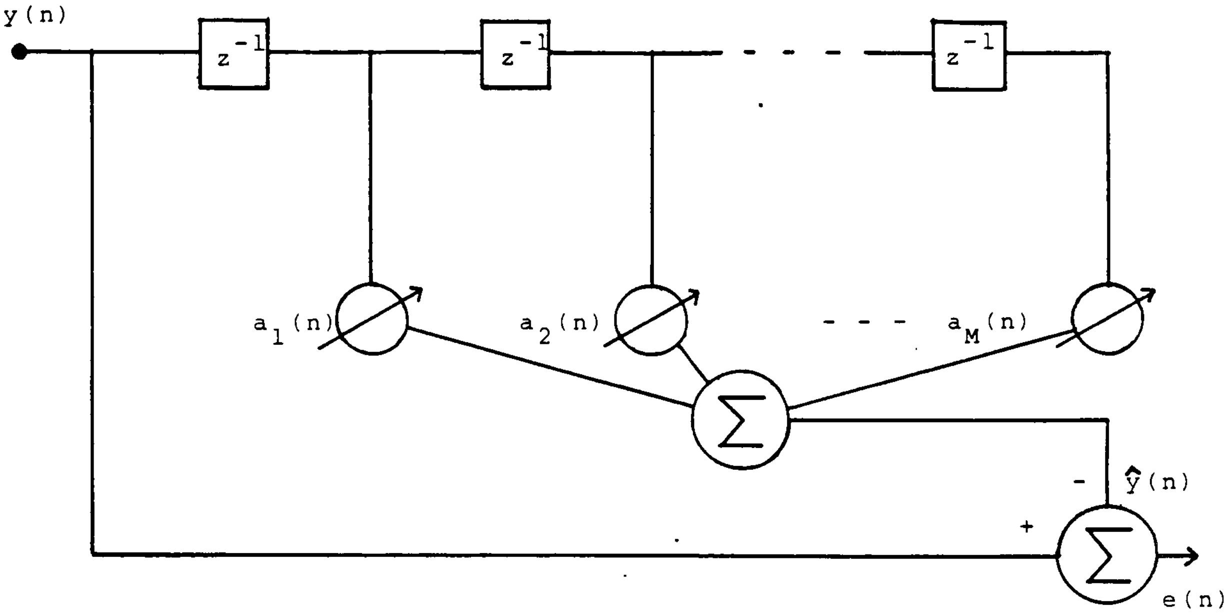

Fig.5.1 Schematic representation of an M^{th} order adaptive autoregressive process.

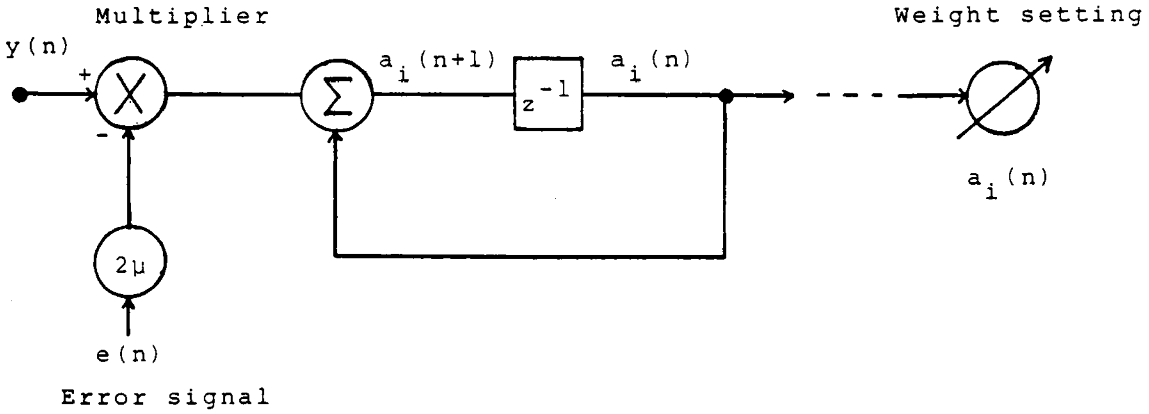

Fig.5.2 The Least Mean Square (LMS) algorithm.

time-invariant variance σ_e^2.

In the nonstationary case, the AR coefficients are time-variant and the process can be represented as follows :

$$\hat{y}(n) = - \sum_{m=1}^{M} a_m(n)\ \hat{y}(n-m) + e(n) \tag{5.2}$$

The noise time series ,{e(n)}, is nonstationary with zero mean but with a time dependent variance $\sigma_e^2(n)$.

In modelling the time series , {y(n)}, as a time-variant AR process, we can regard the series, {e(n)}, as the nonstationary prediction error given by:

$$e(n) = y(n) - \hat{y}(n) \tag{5.3}$$

where $\hat{y}(n)$ satisfies equation (5.2). A pictorial description of this process is given in Figure 5.1 where the weights $a_1(n)$, $a_2(n)$, ..., $a_M(n)$ are adjusted according to the nature of the data's nonstationary properties. The adjustment of the weights can be achieved using an adaptive filter. Adaptation begins with an initial estimate of the AR parameters, these are then changed such that an error function is minimized. The function considered here is the mean square error defined by:

$$e_{ms} = E[\ e^2(n)\ ] = E[\ (\ y(n) - \sum_{m=1}^{M} a_m(n)\ \hat{y}(n-m)\ )^2\ ]$$

In vector form this becomes:

$$e_{ms} = E[\ (\ y(n) - A_M^T(n)\ \hat{Y}(n-1)\ )^2\ ] \tag{5.4}$$

where $A_M^T(n) = [\ a_1(n)\ a_2(n)\ \dots\ a_M(n)\ ]$ and $\hat{Y}^T(n-1) = [\ y(n-1)\ y(n-2)\ \dots\ y(n-M)\ ]$. Expanding equation (5.4) and taking expectations gives

$$\begin{aligned} e_{ms} &= E[\ y^2(n)\ ] - 2E[\ y(n)\ \hat{Y}(n-1)\ ]\ A_M(n) \\ &\quad + A^T(n)\ E[\ \hat{Y}(n-1)\ \hat{Y}^T(n-1)\ ]\ A_M(n) \\ &= \overline{y^2}(n) - 2\ \Phi_{y\hat{y}}\ A_M(n) + A_M^T(n)\ \Phi_{\hat{y}\hat{y}}\ A_M(n) \qquad (5.5) \end{aligned}$$

where $\Phi_{y\hat{y}}$ is the vector of crosscorrelations between the desired signal, $\{y(n)\}$, and the estimated signal, $\{\hat{y}(n)\}$, and $\Phi_{\hat{y}\hat{y}}$ is the correlation matrix $\{\hat{y}(n)\}$. From equation (5.5) it can be seen that, for stationary input signals, the mean square error is a second-order function of the filter coefficients i.e. a 'bowl shaped' surface (Widrow , 1970). The adaptive process continuously adjusts the weights, while seeking the minimum value of the surface i.e. the 'bottom of the bowl'. For the nonstationary case, the adaptive process attempts to track the surface minimum, which may be moving.

5.2 The Adaptive Least Mean Square (LMS) Algorithm

The adaptive LMS algorithm was first proposed by Widrow and Hoff (1960) and was applied to AR modelling of nonstationary data by Griffiths (1975) and Griffiths and Prieto-Diaz (1977). The basis of the algorithm is the method of steepest descent; this uses gradients of the performance surface (i.e. the bowl) to seek its minimum vector (i.e. $A_M^T(n)$) which is proportional to the negative of the gradient vector (Widrow, McCool, Larimore and Johnson 1976), as follows :

$$A_M(n+1) = A_M(n) + \mu(-\nabla_n) \tag{5.6}$$

where ∇_n is the gradient at the n^{th} iteration and μ is a covergence factor which controls stability and rate of adaptation. Differentiating equation (5.5) with respect to the filter weights, $A_M(n)$, gives:

$$\nabla_n = \frac{\partial e_{ms}}{\partial A_M(n)} = -2\Phi_{y\hat{y}} + 2\Phi_{\hat{y}\hat{y}} A_M(n) \tag{5.7}$$

Now, equation (5.7) can be written as follows :

$$\nabla_n = -2E[\ y(n)\hat{Y}(n-1)\ ] + 2E[\ \hat{Y}(n-1)\ \hat{Y}^T(n-1)\ ]\ A_M(n)$$

and if the gradient of a single time sample of the squared error is required the gradient becomes :

$$\begin{aligned} \nabla_n &= -2[\ y(n) - A_M^T(n)\ \hat{Y}(n-1)\ ]\ \hat{Y}(n-1) \\ &= -2\ e(n)\ \hat{Y}(n-1) \end{aligned} \tag{5.8}$$

Substituting (5.8) in (5.6), gives the LMS algorithm i.e.

$$A_M(n+1) = A_M(n) + 2\mu\, e(n)\ \hat{Y}(n-1) \tag{5.9}$$

The algorithm is primed with estimates of the AR parameters and requires as inputs: the error signal ,{e(n)}, and the input time series , {y(n)}, as seen in Fig.5.2. The output is a new set of coefficients to be used to obtain a new error signal as in Fig.5.1.

The choice of the proportionality constant, μ, determines the rate of convergence of the processor and the steady state mean square-error. Griffiths (1975) showed that convergence is assured if:

$$\mu = \frac{\alpha}{M\rho_y(o)} \tag{5.10}$$

where $0 < \alpha < 2$ and $\rho_y(0)$ is the zero lag autocorrelation, or power level. For a nonstationary time series the power level is time-variant and hence $\rho_y(0)$ and μ both become functions of time.

The choice of the initial coefficient vector, $A_M(0)$, affects only the preliminary portion of time output. The length of time required for the transient to decay is called the adaptive time constant, τ_a, and is bounded as follows (Griffiths 1975):

$$\frac{-1}{\ln(1-\mu\lambda_{max})} \leqslant \tau_a \leqslant \frac{-1}{\ln(1-\mu\lambda_{min})} \tag{5.11}$$

where λ_{min} and λ_{max} are the minimum and maximum eigenvalues respectively of the autocorrelation matrix Φ_{yy}.

5.3 The LMS Forward and Backward Filtered Error (FBFE) Algorithm

The LMS algorithm considered sofar is based on the forward prediction error, $e_f(n)$, given by :

$$e_f(n) = y(n) - \sum_{m=1}^{M} a_m(n)\, y(n-m)$$

or in vector form

$$e_f(n) = y(n) - A^T(n)\ Y(n-1) \tag{5.12}$$

where $Y^T(n-1) = [\ y(n-1)\ \ y(n-2)\ \ \ldots\ \ y(n-M)\ ]$. This algorithm has been modified (Jurkevics and Ulrych, 1978) to include both forward and backward errors as follows :

$$\begin{aligned} A(n+1) &= A(n) - \mu\ \nabla\{\ E[\ e_f^2(n) + e_b^2(n)\ ]\ \} \\ &= A(n) - \mu\ \nabla\{\ E[\ e_f^2(n)\ ] + E[\ e_b^2(n)\ ]\ \} \end{aligned} \tag{5.13}$$

where $e_b(n)$ is the backward error defined as :

$$e_b(n) = y(n-M) - \sum_{m=1}^{M} a_m(n)\ y(n-M+m)$$

or

$$e_b(n) = y(n-M) - A^T(n)\ Y(n-M+1) \tag{5.14}$$

where $Y(n-M+1) = [\ y(n-M+1)\ \ y(n-M+2)\ \ \ldots\ \ y(n)\ ]$. The gradient of the mean squared error can be obtained by taking the gradients of single time samples of the squared errors :

$$\begin{aligned} \nabla\{\ E[\ e_f^2(n)\ ] + E[\ e_b^2(n)\ ]\ \} &= \nabla\{\ e_f^2(n) + e_b^2(n)\ \} \\ &= 2\ e_f(n)\cdot\nabla\{\ e_f(n)\ \} + 2\ e_b(n)\cdot\nabla\{\ e_b(n)\ \} \end{aligned} \tag{5.15}$$

From (5.12) and (5.14) the gradients $\{\ e_f(n)\ \}$ and $\{\ e_b(n)\ \}$

become

$$\nabla\{\ e_f(n)\ \} = -\ Y(n-1) \qquad (5.16)$$

$$\nabla\{\ e_b(n)\ \} = -\ Y(n-M+1) \qquad (5.17)$$

Thus equation (5.13) becomes

$$A(n+1) = A(n) + \beta\{\ e_f(n)\ Y(n-1) + e_b(n)\ Y(n-M+1)\ \} \qquad (5.18)$$

Since the iteration can be performed for each coefficient , the algorithm becomes:

$$a_m(n+1) = a_m(n) + \beta\ \{\ e_f(n)\ y(n-m) + e_b(n-M+m)\ \} \qquad (5.19)$$

where β is the new proportionality constant given by (Jurekevics and Ulrych,1978) :

$$\beta = \frac{\gamma}{M\rho_y(o)} \qquad (5.20)$$

where $0<\gamma<1$.

Because the gradient of a single time sample of the squared errors is noisy, there is a need to filter that gradient in order to have faster convergence and to reduce the fluctuations caused by noise. The gradient under consideration , g(n), appears in equation (5.19) as follows :

$$a_m(n+1) = a_m(n) + \beta g(n) \tag{5.21}$$

where

$$g(n) = e_f(n)\, y(n-m) + e_b(n)\, y(n-M+m)$$

The filter suggested here is the low-pass RC filter given by :

$$g_{out}(n) = q\, g_{out}(n-1) + (1-q)\, g_{in}(n) \tag{5.22}$$

where $g_{in}(n)$ is the noisy input and $g_{out}(n)$ is the smoothed output of the filter and q is a positive constant which is less than one. The idea behind the new algorithm is to replace g(n) in (5.21) by the filtered gradient , $g_{out}(n)$, in (5.22) as follows :

$$\begin{aligned} a_m(n+1) &= a_m(n) + \beta g_{out}(n) \\ &= a_m(n) + \beta\, [\, q\, g_{out}(n-1) + (1-q)\, g_{in}(n)\,] \end{aligned} \tag{5.23}$$

Substituting for $g_{out}(n-1)$ using

$$g_{out}(n-1) = (\, a_m(n) - a_m(n-1)\,) \,/\, \beta \tag{5.24}$$

we can write (5.23) as folows :

$$a_m(n+1) = a_m(n) + q\, (\, a_m(n) - a_m(n-1)\,) + \beta\, (1-q)\, g_{in}(n) \tag{5.25}$$

where

$$g_{in}(n) = e_f(n)\ y(n-m) + e_b(n)\ y(n-M+m)$$

Equation (5.25) is the forward and backward filtered error (FBFE) algorithm used in this study to estimate the time varying spectra of the nonstationary signal under consideration.

5.4 Spectra and Disturbance Velocity Simulations

The MEM of spectral estimation can be used in conjunction with the FBFE algorithm using a modified form of equation (4.40) which relates power spectral density and AR coefficients given by:

$$S_n(f) = \frac{P_{M+1}(n)}{2f_N \left| 1 + \sum_{m=1}^{M} a_m(n) \exp(-j2\pi m f \Delta t) \right|^2} \qquad (5.26)$$

where now the PSD , $S_n(f)$, the prediction error variance ,$P_{M+1}(n)$, and the coefficients ,$\{ a_m(n) \}$, are functions of n - the position of the sample point in the record. With the coefficients given by (5.25) the only parameter that remains undetermined in equation (5.26) is the prediction error power $P_{M+1}(n)$ for each sample point. This can be derived from the coefficients themselves if the initial power level for each sample point i.e. $P_0(n)$ is known. The prediction error power can be determined by using the Levinson algorithm with a backward recursion to estimate M reflection coefficients, k_i or a_{ii}, for i = M,M-1,...,1. The recursion is as follows (Makhoul,1975) :

$$k_i = a_{ii}$$

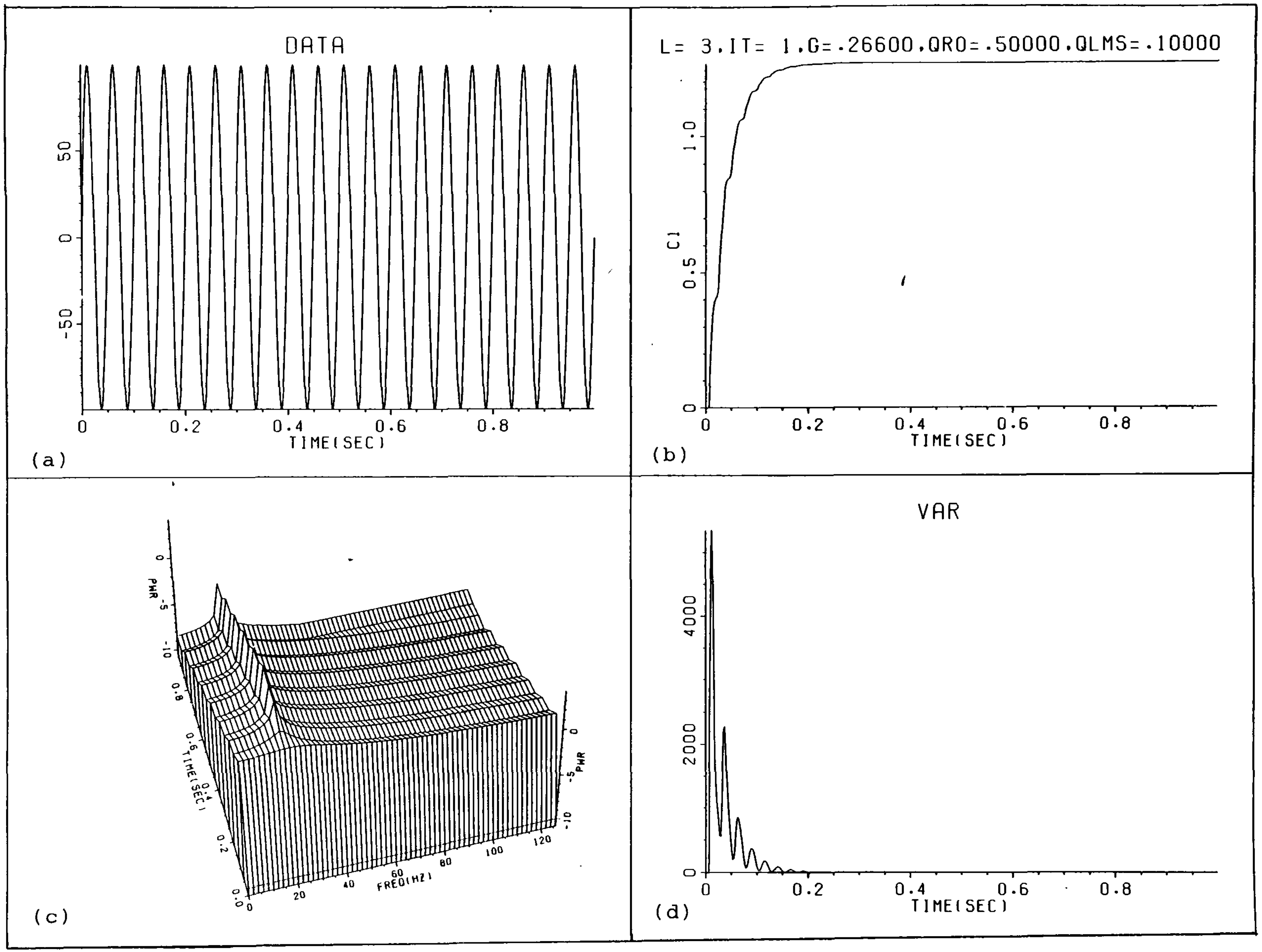

Fig.5.3 Convergence study of the adaptive algorithm: (a) the test signal, (b) plot of first coefficient against time, (c) AR spectra and (d) variance of the prediction error.

$$a_{ji-1} = \frac{a_{ji} - a_{ii}a_{i-ji}}{1 - k_i^2} \qquad 1 \leqslant j \leqslant i-1 \tag{5.27}$$

$P_M(n)$ is then computed from these reflection coefficients, $\{ a_{11}, a_{22}, \ldots, a_{MM} \}$, using the Levinson equation for the error variance propagation given in equations (4.19) as follows :

$$P_i(n) = P_{i-1}(n) \; (\; 1 - a_{ii}^2(n) \;) \tag{5.28}$$

for $i=1,2,\ldots,M$.

The importance of this algorithm lies in its frequency tracking ability i.e. the ability of the derived MESE to follow up frequency changes in the data. However, it is also interesting to study its start-up process. A simulated sinewave (Fig.5.3(a)) having a frequency of 20Hz (sampling rate is 2560 Hz) was used for this purpose. The model order chosen was three i.e. M=3 and initially the AR parameters were set to zero. In Fig. 5.3(b) the evolution of the first coefficient was plotted against time. Fig. 5.3(d) shows the variance of the prediction error filter, $P_2(n)$, which approaches zero as the first coefficient reaches its steady state value. The resulting maximum entropy spectra are displayed in Fig. 5.3(c) where a sharp peak at f=20Hz can easily be seen especially towards the end of the adaptation. These figures display the fast and almost smooth convergence of the adaptive FBFE algorithm , since as seen from Fig. 5.3(b), the first coefficient rose quickly and smoothly from zero to a steady state value of approximately 1.2 while $P_2(n)$ dropped sharply to a value which is almost zero.

In applying the algorithm to the nonstationary disturbance velocity signals we are faced with two significant problems: (a) estimating the time-varying power level of the signal i.e. $\rho_y(0)$ in equation (5.20); and (b) instability in the algorithm itself.

(a) Estimation of the time-varying power level

The time-varying power level, $\rho_{y(k)}(0)$, was first computed using L data points surrounding the time location of the adaptive filter, k, as follows :

$$\rho_{y(k)}(0) = \sum_{m=k-L}^{k+L} y^2(n) \tag{5.29}$$

but this approach gave a noisy estimate. In the final version of the algorithm, a filtered version of this estimate based on the recursive low-pass filter described in equation (5.22), was used i.e.

$$\bar{\rho}_{y(k)}(0) = q\ \bar{\rho}_{y(k-1)}(0) + (1-q)\ \rho_{y(k)}(0) \tag{5.30}$$

where $\bar{\rho}_{y(k)}(0)$ denotes the smoothed estimate of $\rho_{y(k)}(0)$ and q is a positive constant which is less than unity and controls the smoothness of the estimate, such that q=0 and q→1 are equivalent to no smoothing and severe smoothing respecively.

(b) Instability of the algorithm

Instability took place when the filter poles i.e. the poles of A(z) attempted to go outside the unit circle. The criterion used to monitor the stability of A(z) is as follows (Markel and Gray,1973;

Makhoul,1975):

$$|k_i(n)| < 1 \qquad 1 \leqslant i \leqslant M \tag{5.31}$$

where $k_i(n)$ is the i^{th} reflection coefficient i.e. $a_{ii}(n)$, M is the chosen model order and n is the position of the data point in the record. The condition given by equation (5.31) insures that the output power of the filter i.e. $P_i(n)$ in equation (5.28) stays positive and hence the filter remains stable. The stability of the filter was maintained by reducing the value of γ in (5.20) whenever instability was detected according to the criterion described above.

Having achieved dynamic filter stability, the <u>frequency tracking</u> ability of the FBFE algorithm was next investigated. Hence a waveform with a time-varying instantaneous frequency was used as a test signal. The approach adopted was based on the work of Griffiths(1975) who derived a phase function for a digital FM signal given by:

$$y(t) = A\cos[\ \theta(t)\ ] \tag{5.32}$$

where $\theta(t)$ is the time-variant phase. The instantaneous frequency, $\Omega(t)$, can be derived by differentiating $\theta(t)$ in discrete form as follows:

$$\begin{aligned} \Omega(t) &= \theta(t) - \theta(t-1) \\ \theta(t) &= \sum_{n=-\infty}^{\infty} \Omega(n) \end{aligned} \tag{5.33}$$

The signal's instantaneous frequency can be considered to comprise a

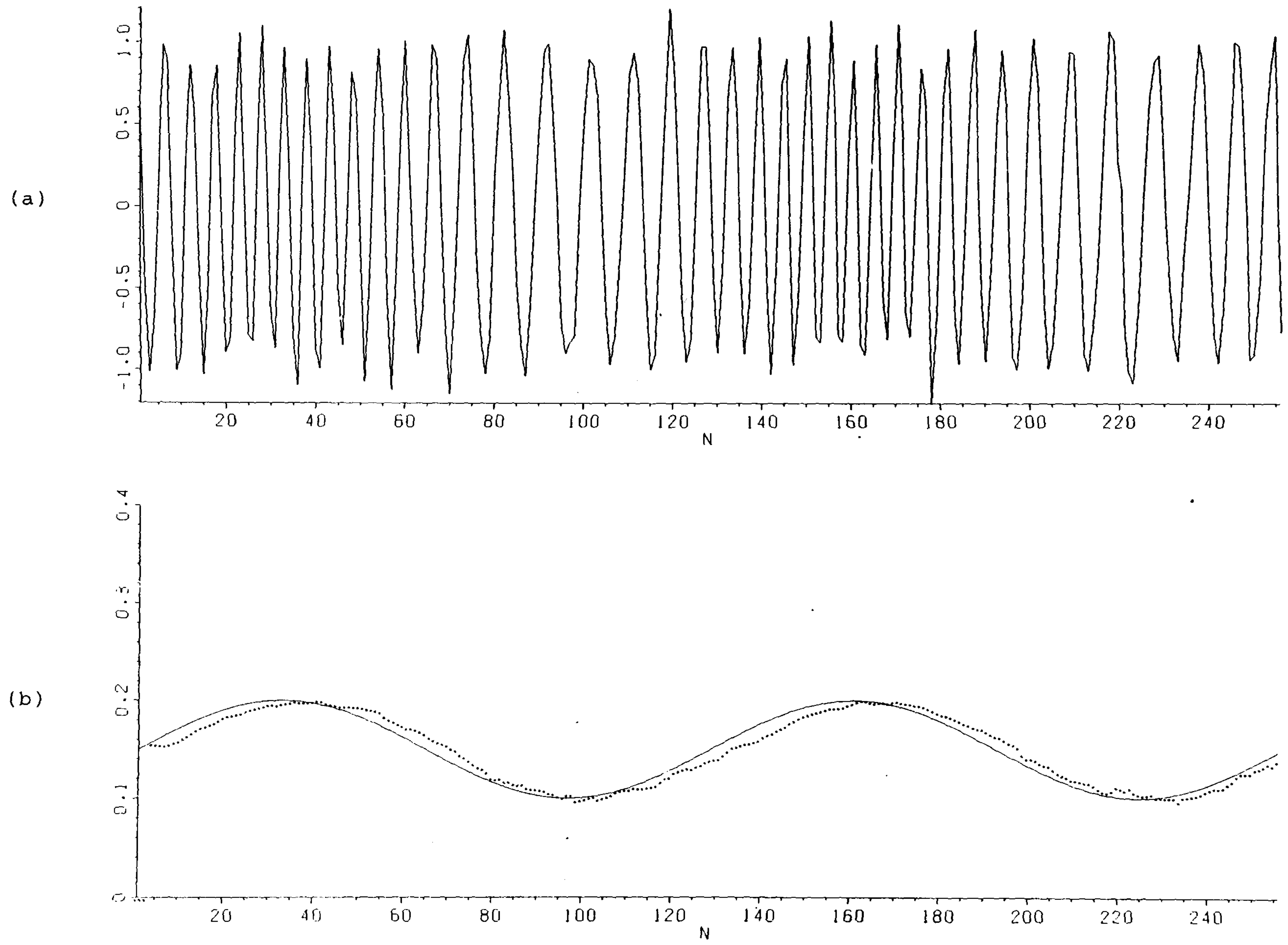

Fig.5.4 Simulation study of the frequency tracking ability of the adaptive algorithm: (a) The simulated FM signal, (b) The message signal (smooth line) and the estimated message (dotted line).

constant, w_0, and a message signal (i.e. the signal that carries information in a frequency modulated signal), $\{m(t)\}$, follows :

$$\Omega(t) = w_0 + m(t) \tag{5.34}$$

Combining (5.34) with (5.33) results in

$$\theta(t) = \theta(t-1) + w_0 + m(t) \tag{5.35}$$

which is a recursive equation for generating the phase, given the time-varying function m(t).

For the purposes of the test, the signal $\{m(t)\}$ was chosen to be a sinusoid i.e.

$$m(t) = A \sin(w_s t) \tag{5.36}$$

where $w_s = 2\pi f_s$ and f_s=2Hz (sampling rate is 2560 Hz). In normalized frequency, A had a value of 0.05 and $w_0=2\pi f_0$ where $f_0=0.15$ (normalized). The FM signal generated using (5.35) and the function in (5.36) were then analysed using the FBFE algorithm with a model order M=2. The MESE was calculated for each data point in the record where N=256. The frequency location of the spectral peak as a function of time was then compared with the function given by (5.35) i.e. the real phase. Fig. 5.4(a) shows the simulated FM signal in the time domain and in Fig. 5.4(b) two frequency domain signals are displayed: (1) the true phase of the FM signal (continuous line) ; and (2) the estimated phase using the FBFE algorithm (broken line). The close agreement between the two curves suggests that the algorithm is

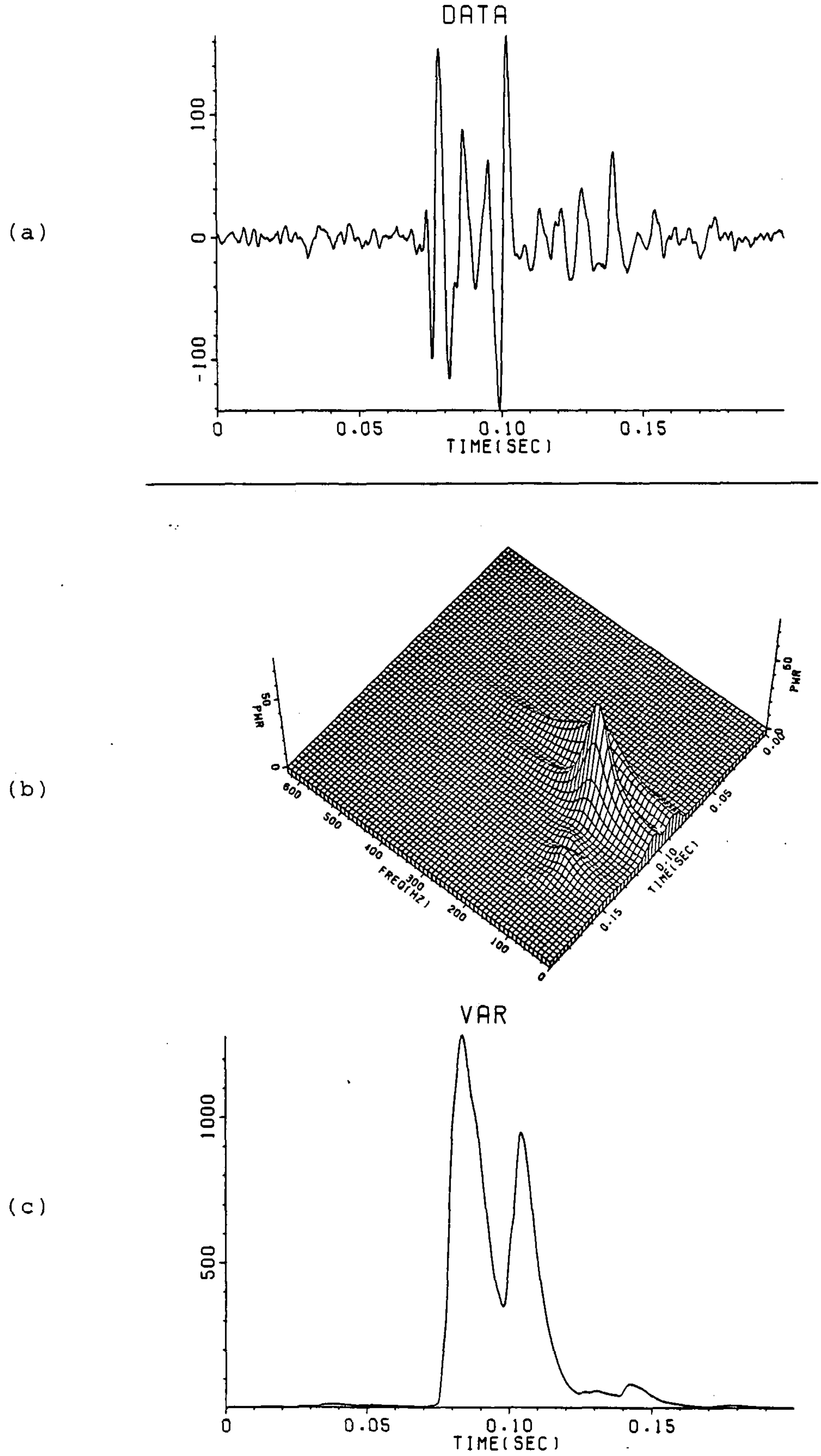

Fig.5.5 Application of the adaptive algorithm to the 40% occlusion data: (a) the time series (b) AR spectra and (c) variance of the prediction error.

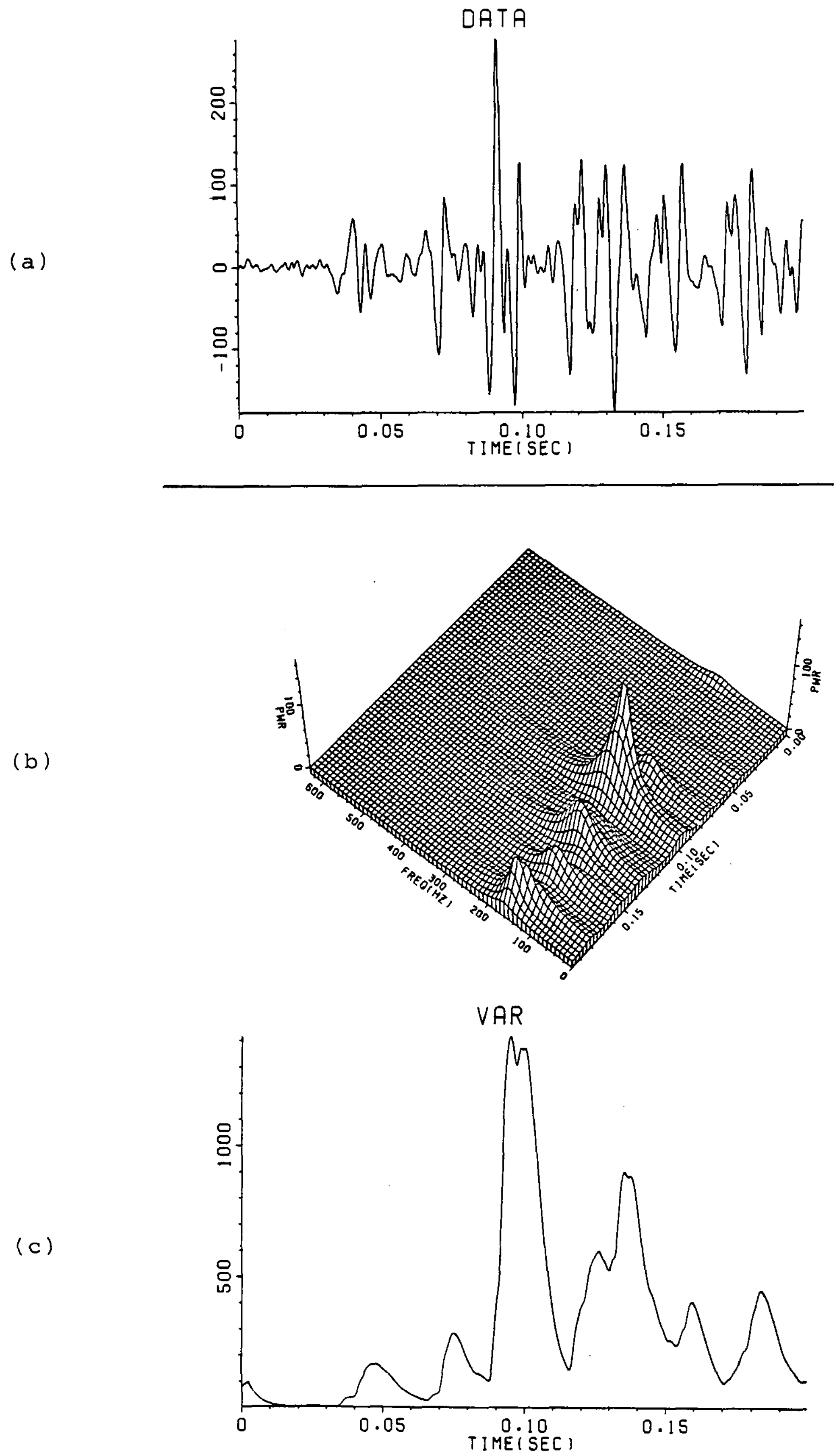

Fig.5.6 Application of the adaptive algorithm to the 74% occlusion data: (a) the time series (b) AR spectra and (c) variance of the prediction error.

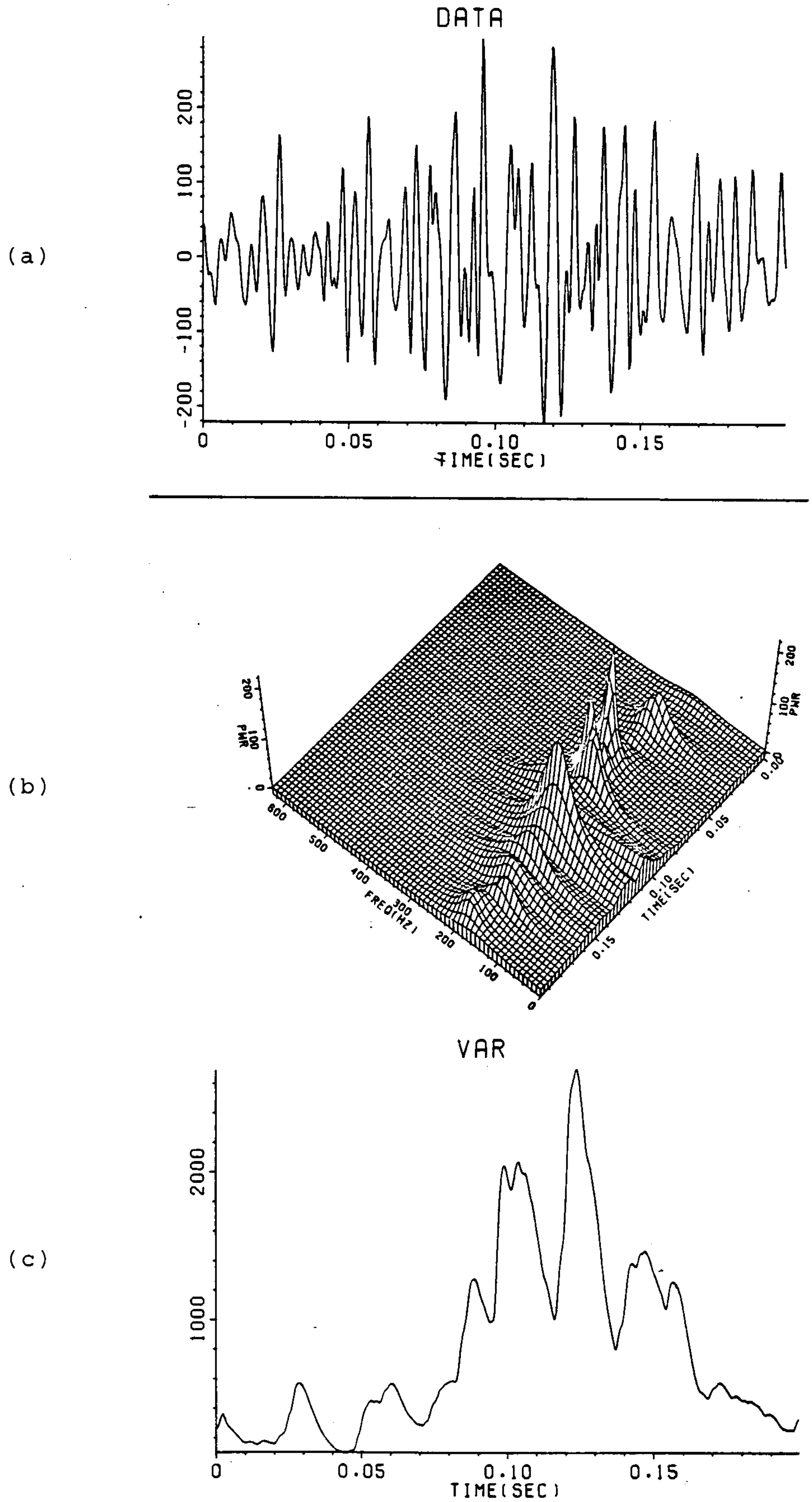

Fig.5.7 Application of the adaptive algorithm to the 88% occlusion data: (a) the time series (b) AR spectra and (c) variance of the prediction error.

capable of tracking, with a small amount of error, high frequency fluctuations in the data.

The algorithm proved extremely effective when it was applied to the disturbance velocity signal because of the insight it gave into the frequency and time composition of this highly variable, yet not completely random, signal. Waveforms for the stated occlusion levels were analysed and spectra were plotted against time. However, it was found that the 40,74 and 88% waveforms were illustrative of the evolution and intensification of disturbances as the constriction is tightened . Because of this it was decided to choose a typical example from each of the stated levels in order to demonstrate the remarks we have made concerning the nature of the disturbance velocity data. Three beats of 40,74 and 88% occlusion levels are shown in Figures 5.5(a), 5.6(a) and 5.7(a) respectively. The relevant spectra are illustrated in Figures 5.5(b), 5.6(b) and 5.7(b) in the form of two-dimensional perspective plots. In Figures 5.5(c), 5.6(c) and 5.7(c) the respective prediction error variances are plotted against time. The following points were noted:

(i) In all three cases the spectra showed narrowband activity that occured with a stenosis-dependent time delay (the delay decreased with increasing percent stenosis).

(ii) The main peak shifted slightly to the left, i.e. the main harmonic had a higher frequency for a higher level of occlusion.

(iii) The spectra showed orderly and fairly resolved structures that appeared and disappeared during the 0.2 second interval. The superimposed envelopes of these structures could be seen more clearly

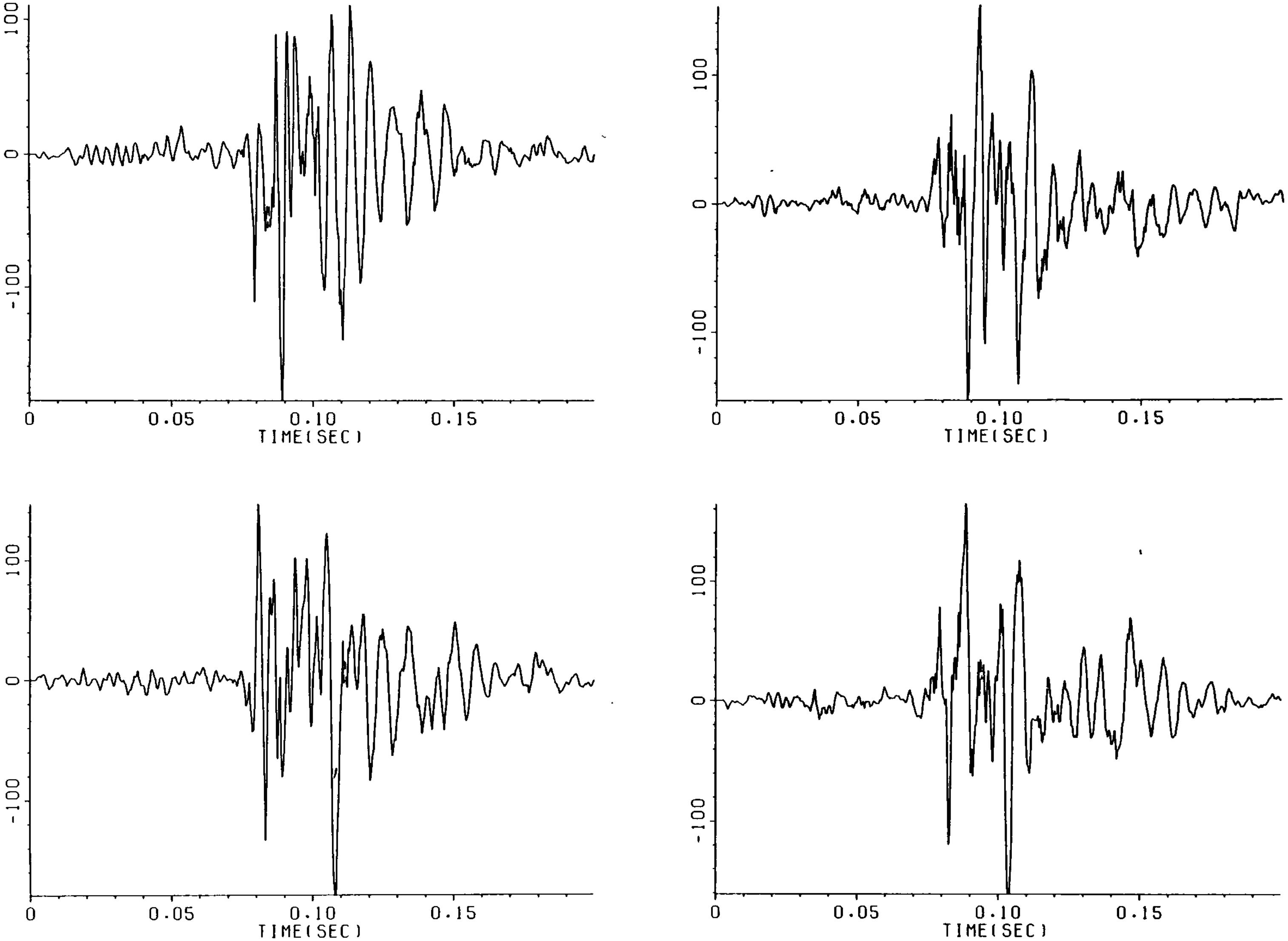

Fig.5.8(a) Simulations of 40% occlusion data.

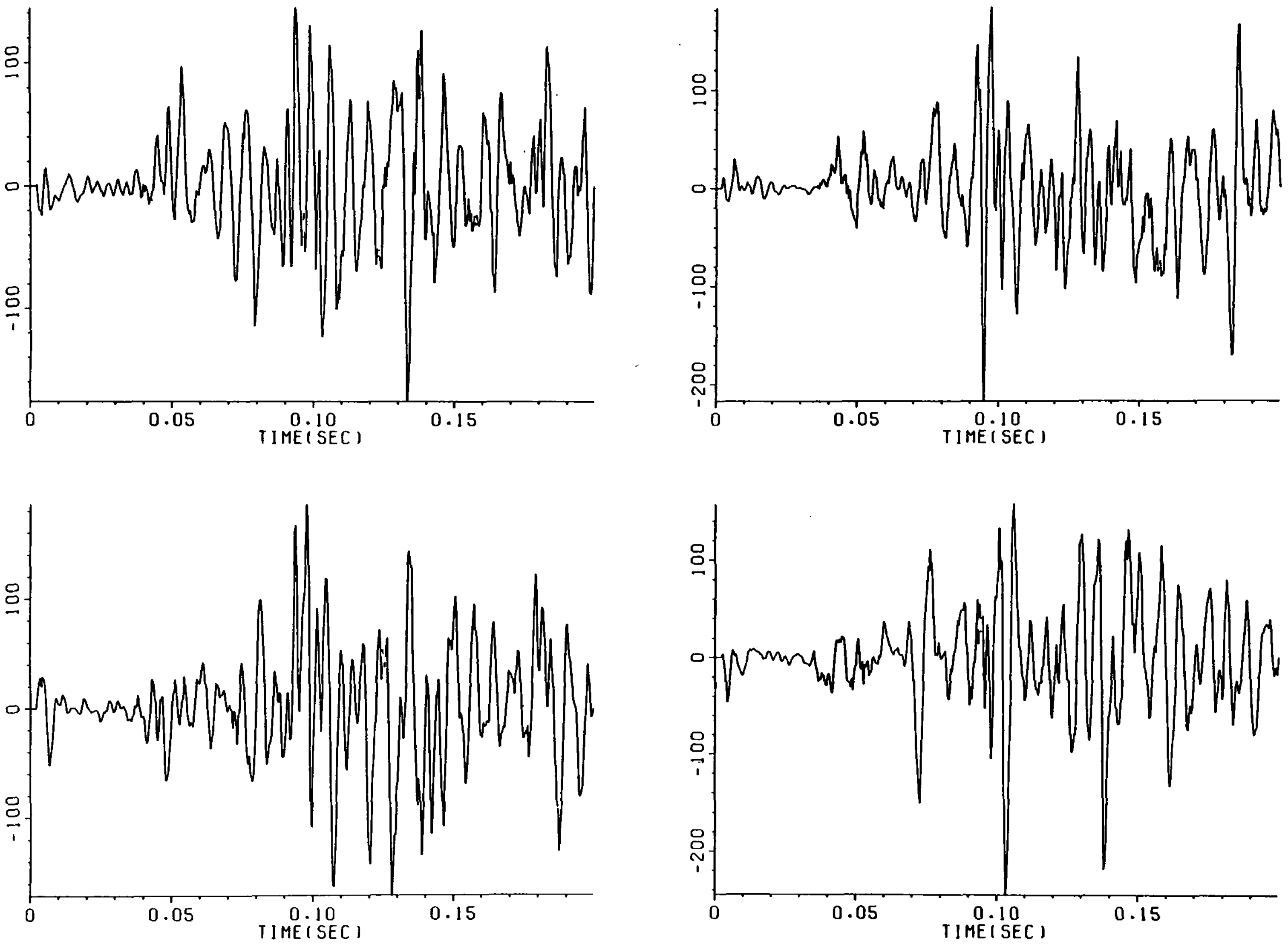

Fig.5.8(b) Simulations of 74% occlusion data.

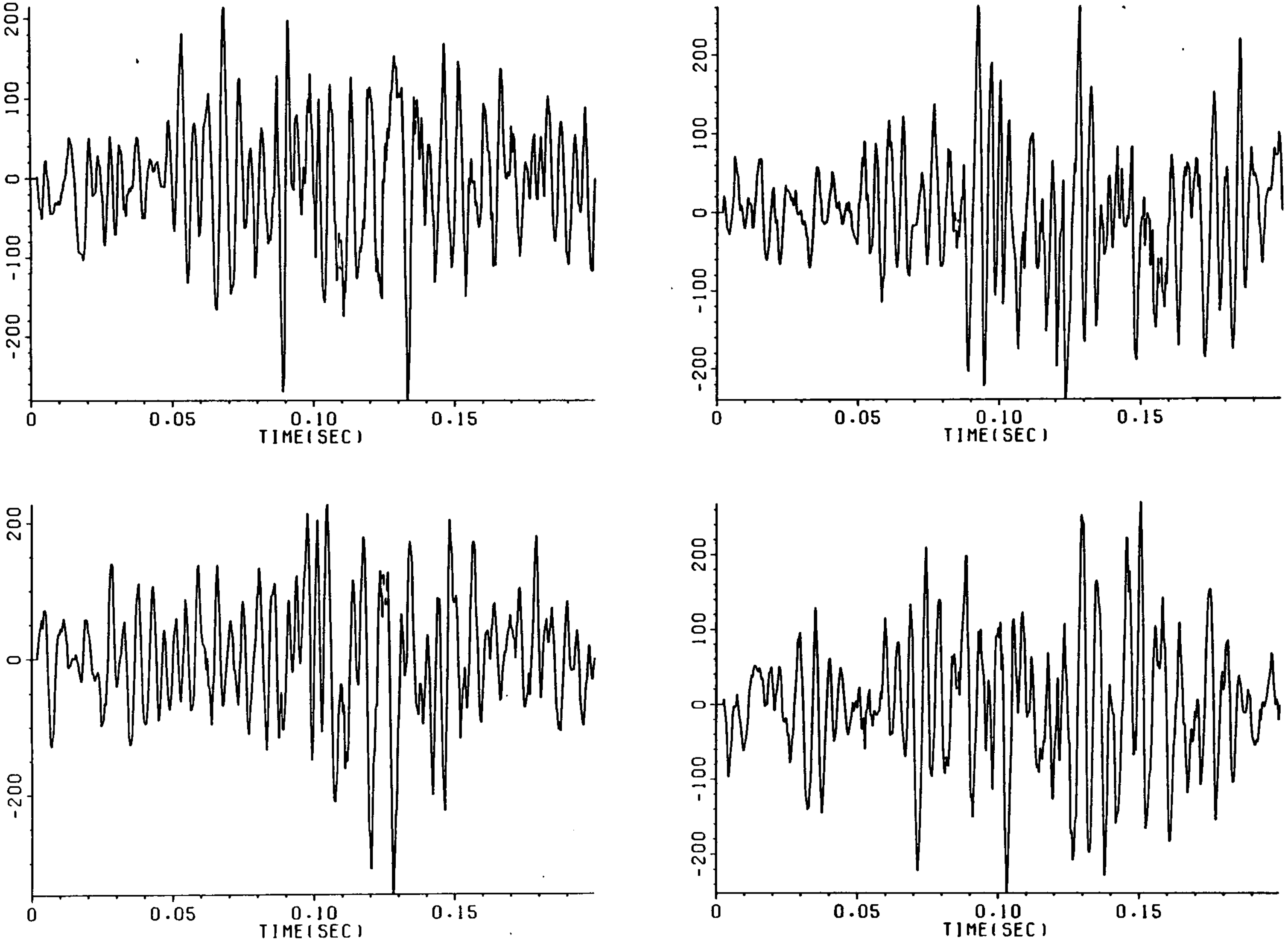

Fig.5.8(c) Simulations of 88% occlusion data.

in plots of $P_M(n)$ i.e. Figures 5.5(c), 5.6(c) and 5.7(c).

In order to establish the effectiveness of the adaptive stochastic AR model in representing the original data or physical process, it was decided to carry out a series of simulation studies. These were based on a slightly modified version of equation (5.2) which was adapted to include a Gaussian random number generator. This new equation is:

$$\hat{y}(n) = - \sum_{m=1}^{M} a_m(n)\ \hat{y}(n-m) + N(\ 0, P_M(n)\ ) \tag{5.37}$$

where $N(\ 0,P_M(n)\ )$ denotes a random number derived from a Gaussian distribution with zero mean and variance ,$P_M(n)$, which is a time varying function. Figures 5.8 (a),(b) and (c) are plots of 4 simulated beats of the 40,74 and 88% waveforms shown in Figures 5.5(a), 5.6(a) and 5.7(a) respectively. The striking similarity between the simulated and original data suggests that this adaptive method is a very effective technique for the analysis of disturbance velocity data.

Because of its good amplitude and frequency tracking ability, the forward and backward filtered-error LMS algorithm has provided us with an insight into the intricate and stimulating nature of the disturbance velocity signal. Its has unveiled orderly structures in time which the velocity probe seems to pick up as the fluid flows past. These structures can be described by their time-variant narrow-band spectra which are derived from the AR coefficients of the adaptive filter. Also, their intensity (or multitude) in the defined time interval increases with an increase in occlusion level as seen in the perspective plots (Figures 5.5(b), 5.6(b) and 5.7(b)). These results, though not yet conclusive, are a demostration of the power and potentiality of this technique in comprehending the complex flow field. Its ease of implementation makes it one of the few rosy paths that could lead to that long desired objective.

CHAPTER 6

NONSTATIONARY MODELLING OF THE DISTURBANCE VELOCITY WAVEFORMS

THE IMPULSIVE NOISE MODEL

The hot-film probe positioned at a fixed location downstream of the constrictions appears to be pulling out flow structures that might be characteristic of occlusion data. An attempt will be made at identifying these time-dependent structures and observing their behaviour in a fixed and already defined time interval. Previous analysis has suggested that these flow patterns have a narrow-band frequency content and the idea here is to use this property for the suggested model. Having defined the type of model to be used and knowing the model output (i.e. the disturbance velocity waveform), we need to describe the type of input series which if applied to the model reproduces the output. Since little is known beforehand about the input, it can be best described as noise; however, the usual assumption of Gaussianity we have found to be inappropriate and instead, we have characterised it as impulsive in nature (or point process). In what follows we seek to demonstrate the viability of representing the disturbance velocity as a narrow-band stochastic process driven by impulsive noise.

6.1 The Impulsive Noise Model

There are numerous physical phenomena which can be modelled as a process driven by impulsive noise as is shown in Fig. 6.1. Some examples taken from electrical engineering, physics , astronomy and

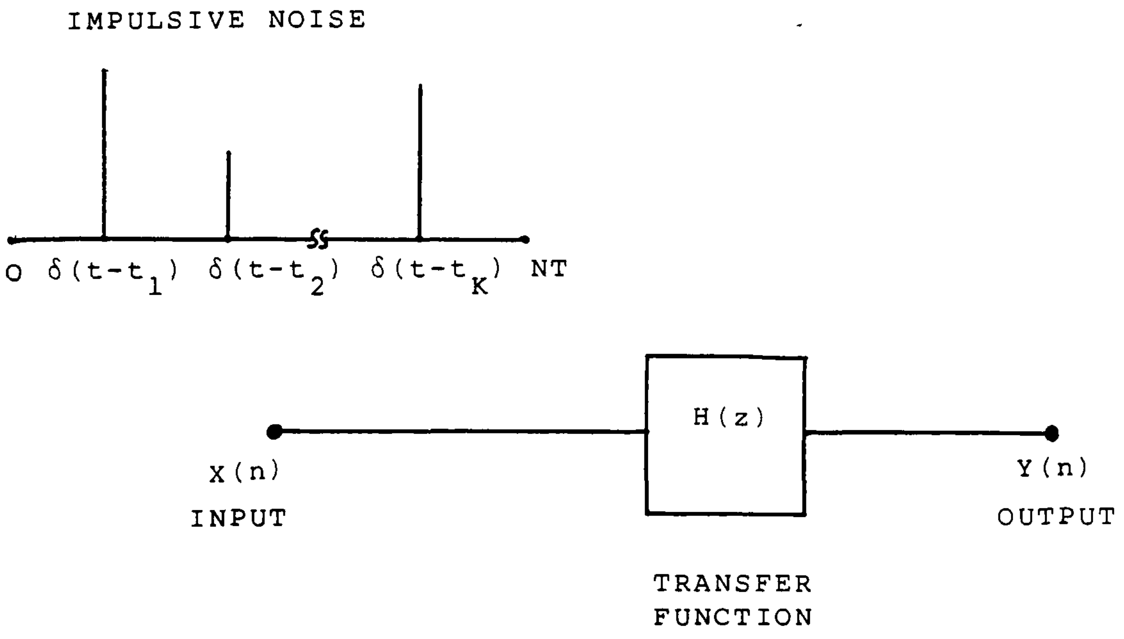

Fig.6.1 System driven by an impulsive noise.

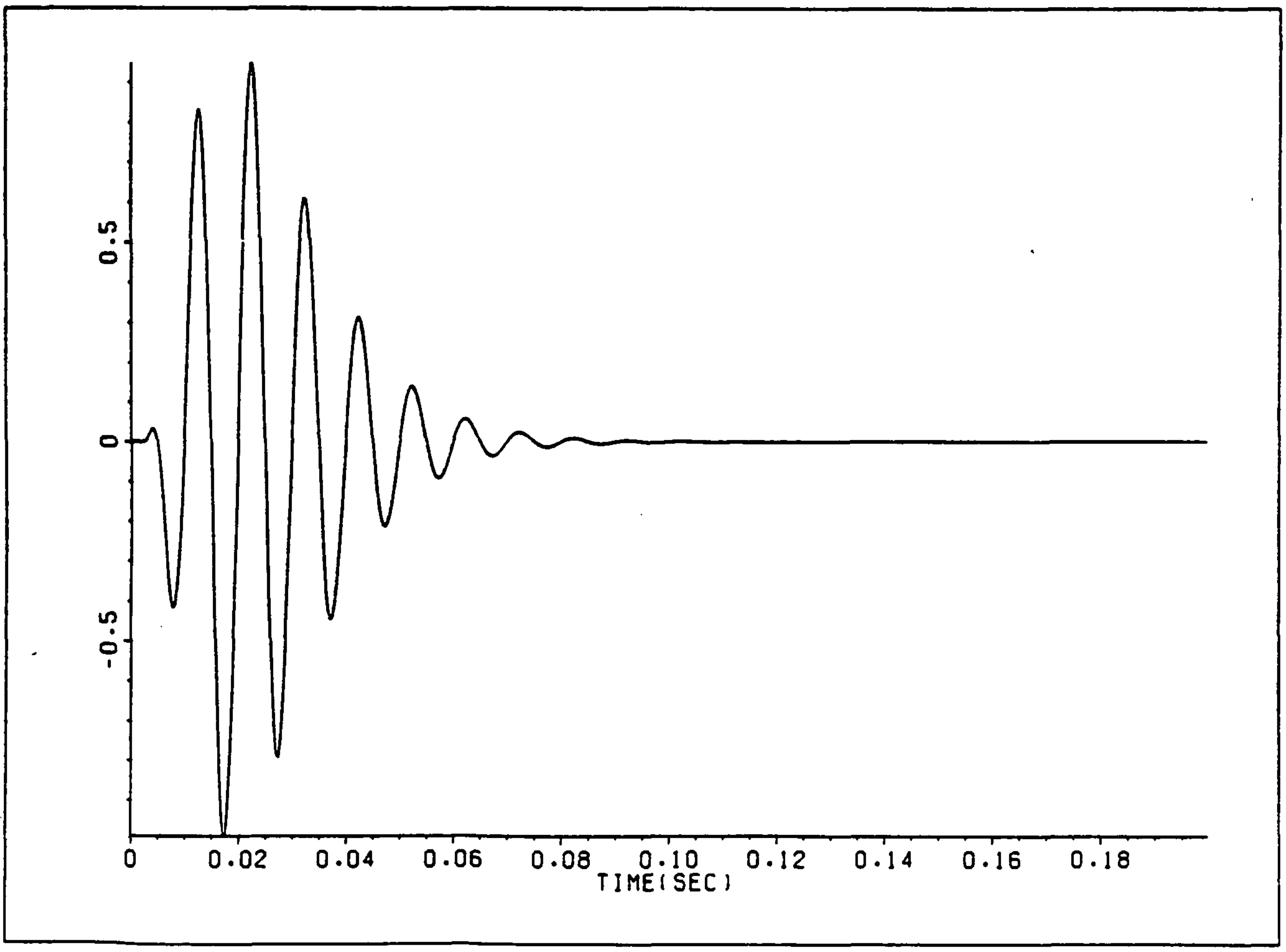

Fig.6.2 The wave packet

medicine are given by Snyder (1975) who described the output of such a system as a filtered point process . Mathematically the discrete output, { y(t) }, can be written in terms of the discrete input, { x(t) }, as follows :

$$y(t) = \sum_{j=o}^{N} h(t-j)\ x(j) + e(t) \qquad (6.1)$$

where N is the number of data points , { h(t) } is the impulse response and { e(t) } is Gaussian white noise with zero mean and variance σ^2. The input series is given by :

$$x(t) = \sum_{k=1}^{K} A_k\ \delta(t-t_k) \qquad (6.2)$$

where A_k and t_k are the respective amplitude and time delay of the k^{th} pulse and K is the total number of pulses. The Delta function , $\delta(t-t_k)$, can be defined as :

$$\delta(t-t_k) = \begin{cases} 1 & \text{for } t=t_k \\ 0 & \text{for } t\neq t_k \end{cases} \qquad (6.3)$$

for k=1,2,...,K. Assuming that the impulse response is known and time-invariant , then the problem remains estimating the input series i.e. the pulse heights and time delays from the available noisy output data. This deconvolution problem has been the subject of recent research (Clayton and Ulrych,1977; Haddad,1978; Taylor, Banks and McCoy,1979; Kwarkernaak, 1980; Kormylo and Mendel,1982; Arya and

Aggarwal ,1982 and Mendel,1983). It has proved to be of a difficult nature mainly because of the numerical instabilities associated with discrete deconvolution of a noisy sequence but also because the input series is sparse i.e. it has only a few elements with values greater than zero.

Modelling the velocity disturbance waveform as a process driven by impulsive noise, requires the estimation of the impulse response as well as the input series, solely from the available output. Attempting to do so would be extremely difficult, if not impossible, unless the problem is tackled in stages. Consequently, the modelling process has been divided into three distinct stages :

(1) Frequency domain system identification : whereby a kernel i.e. an analytical impulse response, is chosen for the system impulse response and the parameters are estimated from the data by minimizing the error between the analytical and virtual frequency responses.

(2) Estimation of pulse heights and arrival times using homomorphic filtering : The idea here is that the envelope of the disturbance velocity waveform can be used to estimate the pulse heights and arrival times. A stochastic homomorphic filter based on the Wiener filter has been designed to obtain a good estimate of the signal envelope.

(3) Modelling of the non-stationary velocity waveform using nonlinear regression : This is the final stage of the modelling procedure and is dependent on the first two. The impulse response is assumed to be time-variant and it is fitted to sections of the data by a nonlinear regression method developed by Marquardt (1963).

These stages will be discussed in detail in subsequent sections. However, it is important to bear in mind that the objective of this exercise is the demonstrate the validity of the model suggested in (6.1) i.e. to show that the disturbance velocity can be considered as a system driven by impulsive noise. The choice of kernel is in a sense immaterial i.e. the importance given to the model itself should overweigh the importance given to the kernel itself, yet a good choice is an advantage. Another consideration is that higher levels of occlusion i.e. 74 and 88% show a high degree of complexity and variability while the 40% occlusion data, for example, exhibits a relatively organized behaviour though it is also subject to physiological variation. Thus for the rest of the chapter the 40% signal will form the database for modelling and analysis.

6.2 Frequency Domain System Identification

Before describing the identification technique used, we ought to begin by defining the kernel used in the analysis and state reasons for its choice. Also, an easy method of implementing equation (6.1) based on the defined kernel ought to be discussed. The kernel will be called 'wave packet' partly because of a similar structure that has been observed by Gaster(1981) in boundary layer flows and partly because the name carries a description of the shape of the kernel.

6.2.1 The Wave Packet

The form of the suggested impulse response or wave packet can be described by the following equation :

$$w(t) = h\, t^n \exp(-t/t_c) \cos(w_o t) \qquad (6.4)$$

where h is an arbitrary height , n is an arbitrary integer, t_c is the time constant and w_o is the characteristic frequency. The simplicity of of this function has made it very attractive to statistical modelling and analysis (see, for example, Hasan (1982,1983)).

One of the important features of this kernel (shown in Fig.6.2) is that n controls the asymmetry or skewness of the resulting waveform . In order to obtain the time location of the absolute maximum of w(t), we will assume that (6.4) is obtained by multiplying $f(t) = t^n \exp(-t/t_c)$ with a constant amplitude sine waveform. Hence the maximum can be obtained by differentiating f(t) and equating to zero. The result can easily be shown to be :

$$t_{max} = n\, t_c \qquad (6.5)$$

and

$$f_{max} = (n t_c)^n \exp(-n) \qquad (6.6)$$

where t_{max} and f_{max} are the location and amplitude of the maximum. To normalize w(t) in equation (6.4) , one could choose h as equal to $1/f_{max}$.

Another interesting observation about w(t) is that its implementation as a model can be simplified if its Z-transform is considered. To simplify the derivation further, we have considered the case where n=2 and a good starting point was the well-known

Z-transform of $\exp(-t/t_c)\cos(w_o t)$ given by :

$$F(z) = \frac{z^2 - \exp(-aT)\cos(w_o T)\,.\,z}{z^2 - 2\exp(-aT)\cos(w_o T)\,.z + \exp(-2aT)} \tag{6.7}$$

where $a=1/t_c$ and T is the sampling interval. The Z-transform of w(t) i.e. W(z) can be derived by noting the following Z-domain rule (Jury,1973):

$$tf(t) \Longleftrightarrow - Tz\,\frac{dF(z)}{dz} \tag{6.8}$$

i.e. multiplying a time function ,f(t), by t is equivalent to -Tz times the differential of its Z-transform. Using relation (6.8), we can derive a similar relation for the case $t^2f(t)$ as follows:

$$t^2f(t)=t(tf(t)) \Longleftrightarrow -Tz\,\{\frac{d}{dz}(-Tz\frac{dF(z)}{dz})\}$$

$$\Longleftrightarrow T^2\{z^2\,\frac{d^2F(z)}{dz^2} + z\frac{dF(z)}{dz}\} \tag{6.9}$$

With F(z) being given by (6.7), W(z) comes out to be

$$W(z) = \frac{z(b_1z^4 + b_2z^3 + b_4z + b_5)}{z^6+a_1z^5+a_2z^4+a_3z^3+a_4z^2+a_5z+a_6} \tag{6.10}$$

where

$a_1 = - 6 \exp(-T/t_c) \cos(w_oT)$

$a_2 = + 3 \exp(-2T/t_c) [1 + 4 \cos^2(w_oT)]$

$a_3 = - 4 \exp(-3T/t_c) \cos(w_oT) [3 + 2 \cos^2(w_oT)]$

$a_4 = - 3 \exp(-4T/t_c) [4 \cos^2(w_oT) - 1]$

$a_5 = - 6 \exp(-5T/t_c) \cos(w_oT)$

$a_6 = + \exp(-6T/t_c)$

and

$b_1 = h T^2 \exp(-T/t_c) \cos(w_oT)$

$b_2 = 2 h T^2 \exp(-2T/t_c) [\cos^2(w_oT) - 2]$

$b_4 = 2 h T^2 \exp(-4T/t_c) [2 - \cos^2(w_oT)]$

$b_5 = - h T^2 \exp(-5T/t_c) \cos(w_oT)$

To obtain $W(z^{-1})$, we divide both numerator and denominator in (6.10) by z^6 which gives :

$$W(z) = \frac{b_1z^{-1} + b_2z^{-2} + b_4z^{-4} + b_5z^{-5}}{1+a_1z^{-1}+a_2z^{-2}+a_3z^{-3}+a_4z^{-4}+a_5z^{-5}+a_6z^{-6}} \tag{6.11}$$

W(z) can be considered to be the transfer function described in Fig. 6.1 and hence it can be written in terms of the input, X(z), and the output, Y(z), as follows :

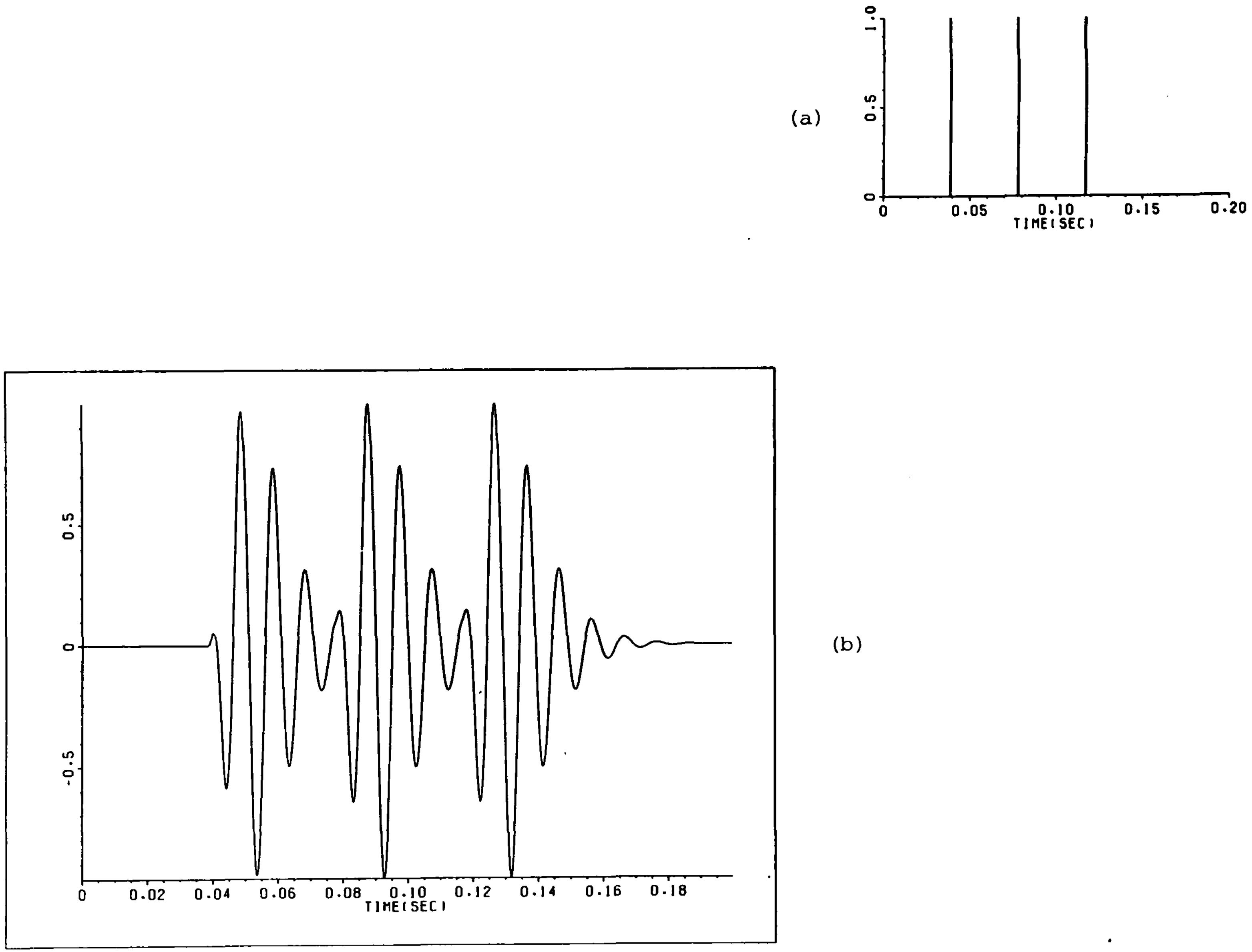

Fig.6.3 Wavepacket model driven by impulsive noise: (a) the impulsive input and (b) the output.

$$W(z) = Y(z) \;/\; X(z) \tag{6.12}$$

Substituting for W(z) in (6.11) by (6.12) and knowing that $z^{-1}F(z)$, $z^{-2}F(z),\ldots$ for an arbitrary function F(z) are equivalent to f(n-1), f(n-2),... in the time domain, we get a recursive equation for implementing (6.10) given by :

$$\begin{aligned} y(n) = &- a_1\, y(n-1) - a_2\, y(n-2) - a_3\, y(n-3) \\ &- a_4\, y(n-4) - a_5\, y(n-5) - a_6\, y(n-6) \\ &+ b_1\, x(n-1) + b_2\, x(n-2) + b_4\, x(n-4) \\ &+ b_5\, x(n-5) \end{aligned} \tag{6.13}$$

Fig. 6.3 (b) shows a record of 512 data points generated using (6.13) and with an input , {x(n)}, which consists of three impulses of equal height (Fig. 6.3(a)) and is given by :

$$x(n) = \delta(n-100) + \delta(n-200) + \delta(n-300) \tag{6.14}$$

The system given by equation (6.13) is an autoregressive moving average (ARMA) system which can be driven by impulsive noise and the aim of the rest of this chapter is to show that the disturbance velocity waveforms can be modelled by such a system.

6.2.2 System Identification

The disturbance velocity can be considered as composed of the output of the model in equation (6.13) plus a Guassian white noise component , {e(n)} , as follows :

$$y(n) = \sum_{m=1}^{6} a_m y(n-m) + \sum_{\ell=1}^{5} b_\ell x(n-\ell) + e(n) \qquad (6.15)$$

where the ARMA coefficients can be computed as in equation (6.10) solely from the characteristic frequency, f_o, and the time constant, t_c. Hence, it is required that the values of f_o and t_c be estimated from the data. This is a nonlinear problem that can be solved by minimizing the following cost function in the frequency domain :

$$E(f_o,t_c) = \sum_{k=o}^{N_f} [\ S(f_k) - \hat{S}(f_k)\ ]^2 \qquad (6.16)$$

where $S(f_k)$ is the parametric spectrum i.e. a spectrum derived analytically and is dependent on f_o and t_c , $\hat{S}(f_k)$ is the estimated spectrum and should also be the frequency response of the system and N_f is the total number of harmonics. The minimization of this cost function can be achieved using a numerical optimization technique that does not require derivatives.

The usual way of obtaining $\hat{S}(f)$ is by sectioning the data record and then averaging the resulting spectra to obtain an estimate of the system frequency transfer function (Rabiner and Allen,1980). In this case, however, we found it more convenient to use the MESE since it gives a smoother estimate of the system response. The chosen model order was M=6 based on the already mentioned BIC criterion.

As for the parametric spectrum, S(f), it was obtained by considering the Fourier transform of the function in (6.4) with n=2 i.e.

$$w(t) = t^2 \exp(-at)\cos(bt) \qquad (6.17)$$

where $a=1/t_c$ and $b=w_o$ (previous notation). An easy method of deriving the transform of (6.17) is to consider the general relation

$$f(t)\cos(bt) \Longleftrightarrow 1/2\ [\ F(w-b) + F(w+b)\ ] \tag{6.18}$$

where F(w) is the transform of f(t) and F(w-b) and F(w+b) signify replacing the variable w in F(w) by (w-b) and (w+b) respectively. Hence, what is required now is the transform of $t^2\exp(-at)$ which can be derived from the well-known transform of exp(-at) using the following relation :

$$t^n f(t) \Longleftrightarrow j^n \frac{d^n F(w)}{dw^n} \tag{6.19}$$

Therefore the transform of $t^2\exp(-at)$ is

$$\begin{aligned} F(w) &= j^2 \frac{d^2}{dw^2} FT\{\exp(-at)\} \\ &= -\frac{d^2}{dw^2} \{\frac{1}{a+jw}\} \\ &= \frac{1}{(a+jw)^3} \end{aligned} \tag{6.20}$$

where FT denotes the Fourier transform and j is $\sqrt{-1}$. Using (6.20) and applying the relation (6.18) we get

$$W(w) = \frac{1}{(a+j(w-b))^3} + \frac{1}{(a+j(w+b))^3} \tag{6.21}$$

which is the required transform. S(f) can now be computed by taking

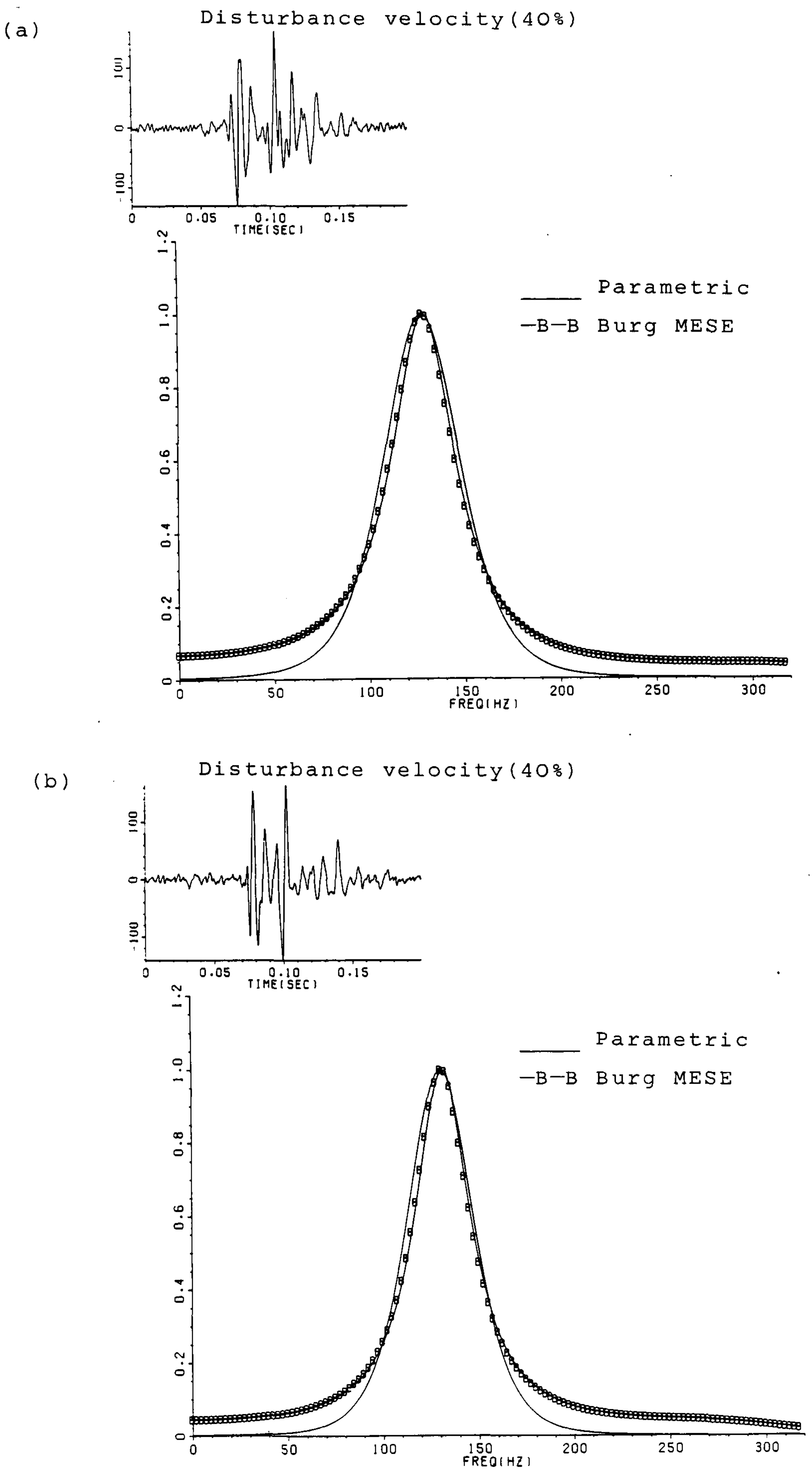

Fig.6.4 System identification in the frequency domain: Two 40% stenosis records (a&b) and their respective spectra.

the modulus squared of (6.21) i.e.

$$S(f) = |W(f)|^2 \qquad (6.22)$$

where the shape of S(f) is dependent on t_c (t_c=1/a) and f_o (f_o=w_o/2π =b/2π) .

In the actual optimization procedure the cost function was minimized with respect to t_c only since f_o can be estimated from the MESE (its peak). Typical results for two 40% occlusion data are shown in Figures 6.4 (a) and (b). Each set of figures shows the waveform analysed (top left hand side), the parametric spectrum (bottom smooth line) and the estimated spectrum (bottom broken line).

The identification procedure was repeated for ten beats and average values of f_o and t_c were 130Hz and 0.03 seconds respectively.

These values together with the initial estimates of pulse heights and arrival times (obtained by homomorphic filtering) will be used in the final stage of this analysis to obtain nonstationary estimates of some disturbance velocity waveforms.

6.3 Estimation of Pulse Heights and Arrival Times using Homomorphic Filtering

Homomorphic filtering allows us to derive the envelope of a signal and in our case the envelope carries information about the input of the system. This point will be demonstrated in the following argument:

Let the output of the system be (equations (6.1) and (6.2)):

$$\begin{aligned} y(t) &= \sum_{k=1}^{K} A_k (t-t_k)^2 \exp(-(t-t_k)/t_c)\ \cos(w_o(t-t_k)\ ) \\ &= \sum_{k=1}^{K} A_k (t-t_k)^2 \exp(-(t-t_k)/t_c)\ \cos(w_o t + \phi_k\ ) \end{aligned} \tag{6.23}$$

Now, going back to the wave packet itself, let us consider the case where the frequency , w_o, is high compared with the frequency of the envelope itself. If that is the case then we can ignore the initial phase ϕ_k and hence (6.23) can be written as follows :

$$\begin{aligned} y(t) &= \sum_{k=1}^{K} A_k (t-t_k)^2 \exp(-(t-t_k)/t_c)\ \cos(w_o t) \\ &= e(t)\ \cos(w_o t) \end{aligned} \tag{6.24}$$

where this is clearly an amplitude modulated waveform with the overall envelope, $\{e(t)\}$, given by :

$$e(t) = \sum_{k=1}^{K} A_k (t-t_k)^2 \exp(-(t-t_k)/t_c) \tag{6.25}$$

from which we can derive amplitude and arrival time information about the impulsive input as we shall see later.

6.3.1 Homomorphic Filtering

When considering the problem of filtering signals that have been added , we often use a linear system. In contrast, when determining a filtering procedure to separate signals that have been nonadditively combined, such as through multiplication or convolution, it is usually more difficult, and in many cases less meaningful to use a linear system. Oppenheim, Schafer and Stockham (1968) generalized the notion

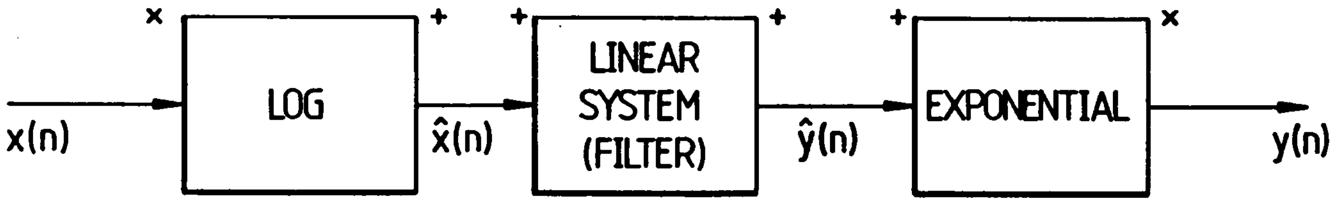

Fig.6.5(a) Generalised homomorphic filtering for a multiplicative system.

of linear filtering in such a way that it encompasses this broader class of problems. This new type of filtering has been called homomorphic filtering and the aim of this section is to describe its application to a certain class of multiplied signals.

A homomorphic multiplicative system represented by

$$y(t) = e(t)\ v(t) \tag{6.26}$$

should satisfy the following properties:

$$P\ [\ e(t)\ v(t)\ ] = P\ [\ e(t)\ ] + P\ [\ v(t)\ ] \tag{6.27}$$

$$P\ [\ (\ y(t)\ )^{c}\ ] = c\ P\ [\ y(t)\ ] \tag{6.28}$$

and

$$P^{-1}\ \{\ P\ [\ y(t)\ ]\ \} = y(t) \tag{6.29}$$

where P is a transformation that changes the nonlinear problem into a linear problem where the components are added. If the signal {y(t)} is positive and greater than zero, then P is the natural logarithm and P^{-1} is the exponential function. This class of homomorphic systems can be represented pictorially as in Figure 6.5(a).

When the signal is bipolar i.e.positive and negative the treatment of the problem under homomorphic systems is possible only if one of the components is positive. With reference to equation (6.26) this means that the envelope ,{e(t)}, should be positive if the carrier , {v(t)}, is bipolar. In this case the signal , {y(t)}, can be treated

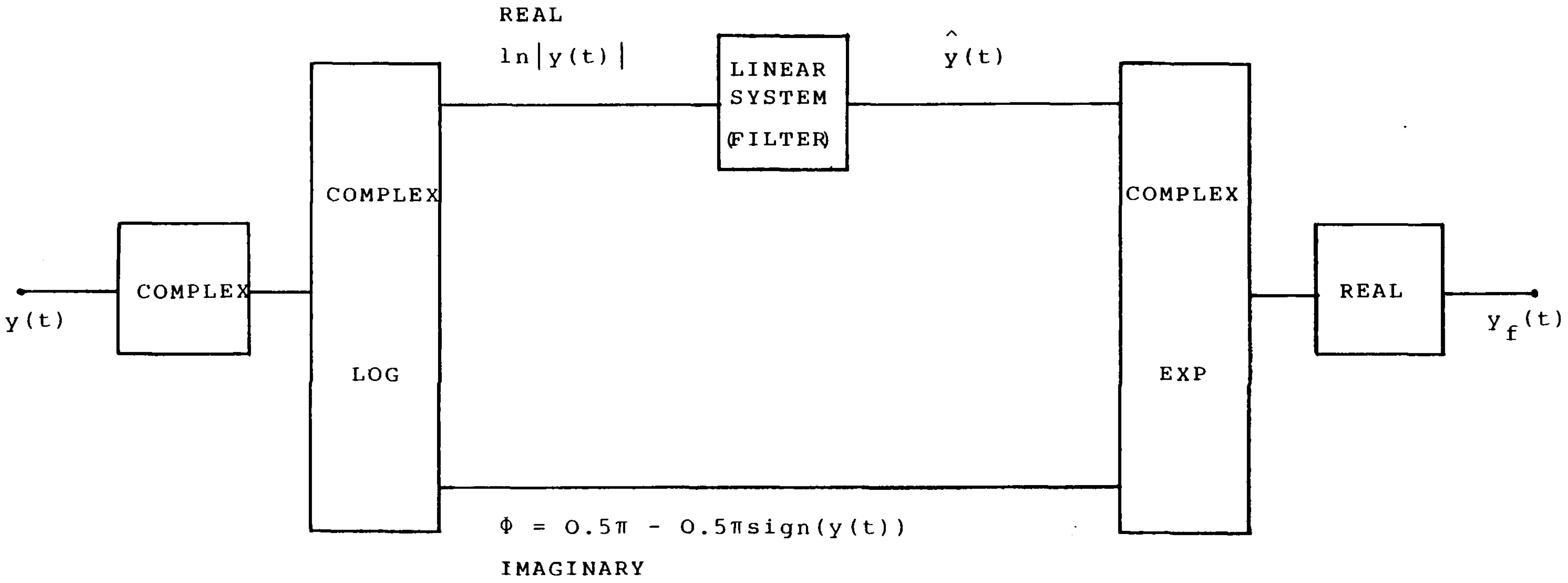

Fig.6.5(b) Homomorphic filter for a bipolar signal y(t).

as a complex signal as follows:

$$y_c(t) = |y(t)| \exp(j\ \phi) \tag{6.30}$$

where

$$\phi = \begin{cases} \pi & \text{if } y(t)<0 \\ 0 & \text{if } y(t)>0 \end{cases} \tag{6.31}$$

Taking the complex logarithm of both sides gives:

$$\ln(\ y_c(t)\ ) = \ln(\ |\ y(t)\ |\ ) + j\ \phi \tag{6.32}$$

The inverse transform is the complex exponential and if $\{\hat{y}(t)\}$ is the filtered version of $\{\ln(\ |\ y(t)\ |\ )\}$ then the inverse can be written as follows :

$$y_f(t) = \exp(\ \hat{y}(t)\ )\ \cos(\ \phi\ ) \tag{6.33}$$

where $\{y_f(t)\}$ is the filtered version of $\{y(t)\}$ (see Fig. 6.5(b)).

The multiplicative homomorphic system studied here is that system where the product consists of a slowly varying but always positive component, and a rapidly varying bipolar component with constant amplitude as in equation (6.24). To be able to separate these two components using a linear filter as in Figures 6.5(a) and (b), the frequency content of the logarithm of the signal should be understood.

The logarithm of the signal in equation (6.24) can be written as :

$$\ln[\ y(t)\ ] = \ln[\ e(t)\ ] + \ln[\ |\cos(w_o t)|\ ] \qquad (6.34)$$

We are interested in the envelope {e(t)} and hence the component $\ln[\ |\cos(w_o t)|\ ]$ in (6.34) has to filtered out. The Laplace transform of the logarithm of a cosine function is given as (Roberts, Kaufman and Saunders,1966) :

$$\ln|2\cos(w_o t)| \Longleftrightarrow \sum_{k=1}^{\infty} \frac{(-1)^{k-1} s}{k(s^2+4k^2w_o^2)} \qquad (6.35)$$

From the Laplace transform of a cosine function i.e.

$$C(s) = \frac{s}{s^2 + \Omega^2} \qquad (6.36)$$

we see that (6.35) can be written as

$$\ln[\ 2\cos(w_o t)\ ] \Longleftrightarrow \sum_{k=1}^{\infty} \frac{(-1)^{k-1}}{k} \cdot C(s, \Omega(k)) \qquad (6.36)$$

where

$$\Omega(k) = 2\ k\ w_o \qquad (6.37)$$

In the frequency domain this signifies that, if we represent the spectrum of a cosine function as $A\delta(w-\Omega)$ we can write (6.36) as follows :

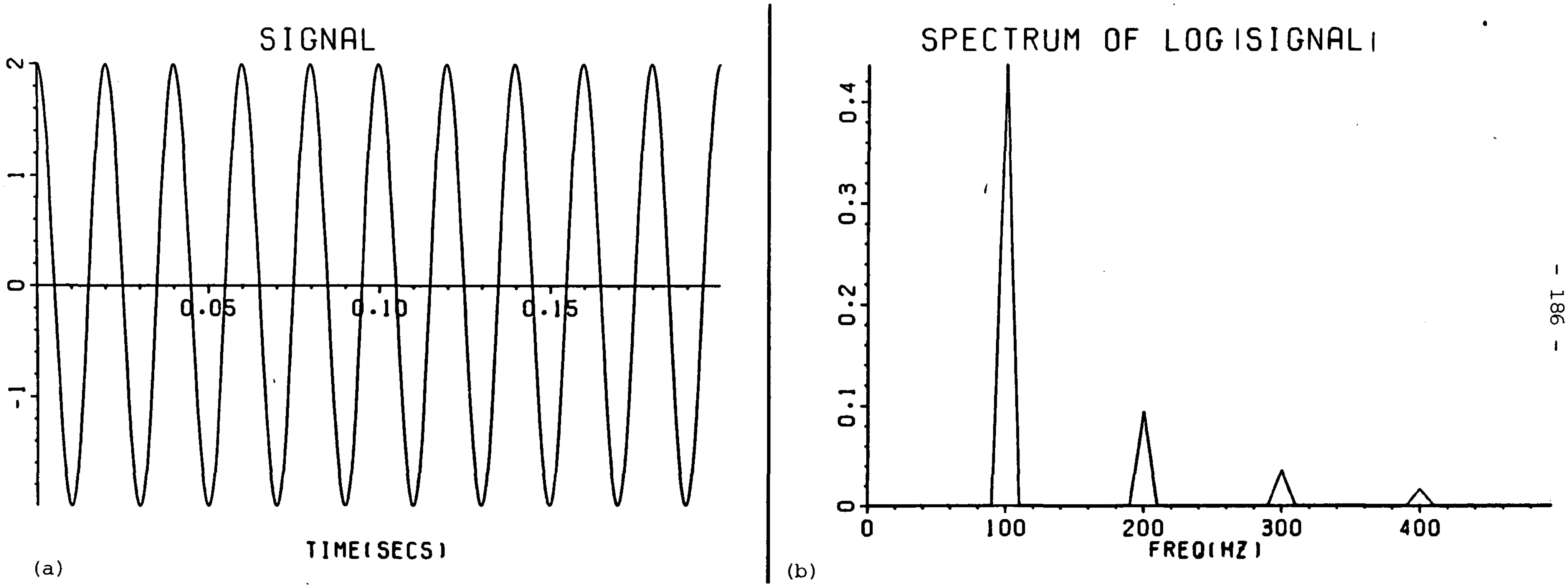

(a)

(b)

Fig.6.6 The spectrum of the logarithm of a cosine function: (a) the function and (b) its FFT spectrum.

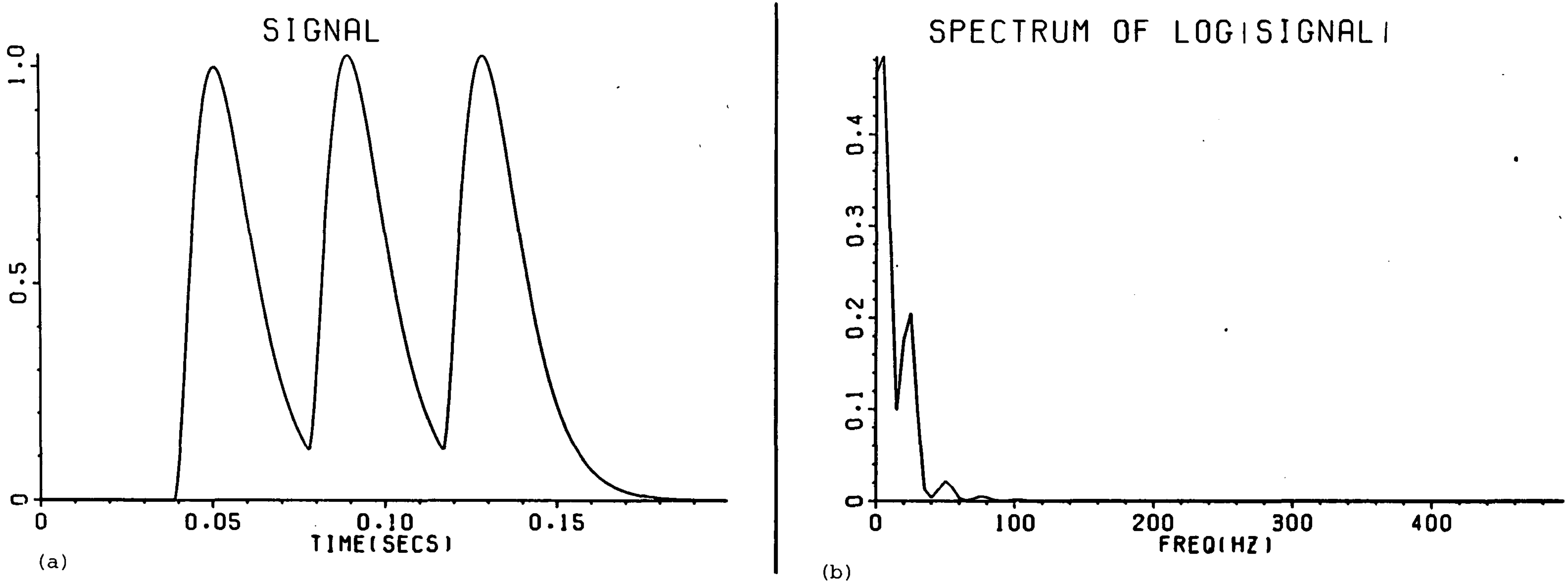

Fig.6.7 The spectrum of the logarithm of a slowly varying function: (a) the function and (b) its FFT spectrum.

$$\ln[\ 2\ \cos(\ w_0 t)\ ] \Longleftrightarrow \sum_{k=1}^{\infty} \frac{(-1)^{k-1}}{k} \quad A \cdot \delta(w - \Omega(k)) \qquad (6.38)$$

i.e. the sum of delta functions occurring at $w=2w_0, 4w_0, 6w_0, \ldots$ and decreasing in amplitude i.e. A,A/2,A/3,... (the sign is ignored here because the spectrum is always positive). Fig. 6.6(a) shows 512 data points of a cosine function (f_0=50Hz) sampled at 2560 Hz and Fig. 6.6(b) is an example of the type of spectrum onbtained when the Fourier transform of the logarithm of that function is computed. Notice that in the region 0-500Hz of Fig. 6.6(b) there are four peaks at f=100Hz ($2w_0$), f=200Hz ($4w_0$) , f=300Hz ($6w_0$) and f=400Hz ($8w_0$) , and that the power decreases by $1/k^2$ which is expected in theory. However, unlike what is predicted in theory, k in equation (6.38) cannot increase indefinitely because of the finite sampling rate.

With this known about the logarithm of the rapidly varying component in equation (6.34) what remains is to try to study the frequency content of the low frequency component. Fig. 6.7(a) shows the envelope of the signal in Fig. 6.3 and the transform of its logarithm can be seen in Fig. 6.7(b) where most of the power is concentrated in the lower end of the spectrum. This facilitates the separation of the two components in equation (6.34) since they occupy separate frequency bands. As a general rule we found that if we are to filter a signal such as (6.24), then we should make sure that the highest frequency in {e(t)} should not exceed $0.25f_0$ and a good setting for the linear filter in the homomorphic filtering process would be in the region of $1.5f_0$. This criterion will be used in the next section to separate the two components in the disturbance velocity signal (i.e. envelope and carrier) using a stochastic homomorphic filter.

6.3.2 The Stochastic Homomorphic Filter

Stochastic homomorphic filters have been used in image processing for the removal of multiplicative noise or blur (see, for example, Fries and Modestino(1979) and Peli and Quatieri (1984)). These are based on a knowledge of the process and the noise statistics and are usually implemented using the well-known Wiener filter.

The stochastic homomorphic filter used here is based on the model:

$$y(t) = e(t) \,.\, v(t) \,.\, n(t) \qquad (6.40)$$

where {y(t)}, {e(t)} and {v(t)} are as described before and {n(t)} is Gaussian white noise with zero mean and a variance σ_n^2. Now let the Fourier transforms of ln[y(t)], ln[e(t)], ln[v(t)] and ln[n(t)] be $G_y(w)$, $G_e(w)$, $G_v(w)$ and $G_n(w)$ then the required Wiener filter has the following frequency response :

$$W(w) = \frac{G_e(w)}{G_e(w)+G_v(w)+G_n(w)} \qquad (6.41)$$

and applying it to the data gives an estimate of $G_e(w)$ i.e.

$$\hat{G}_e(w) = W(w)\ Y(w) \qquad (6.42)$$

Equation (6.41) assumes knowledge of the theoretical response of $G_e(w)$, $G_v(w)$ and $G_n(w)$ which is only true in the case of $G_n(w)$ which

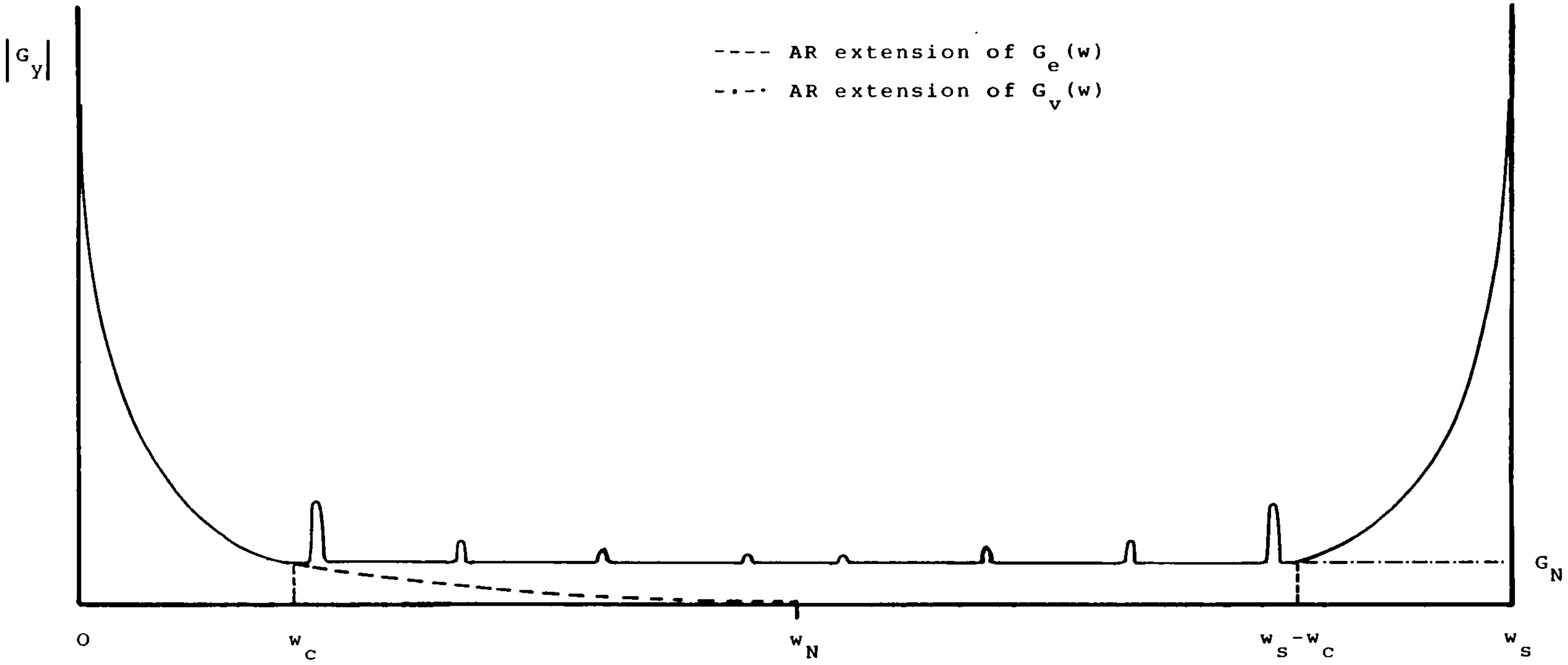

Fig.6.8 Frequency domain analysis of the ideal stochastic homomorphic filter.

can be chosen to be equal to a constant i.e. a horizontal line of height σ_n^2 (see Fig. 6.8). As for $G_e(w)$ and $G_v(w)$ these can be estimated from $G_y(w)$ by AR modelling as follows :

$$G'_e(w) = \begin{cases} G_y(w) & w<w_c \\ \sum_{m=1}^{M_e} a_m G_y(w-m) & w \geqslant w_c \\ & 0 \leqslant w \leqslant w_N \end{cases} \tag{6.43}$$

and

$$G'_v(w) = \begin{cases} G_y(w) & w<(w_s-w_c) \\ \sum_{m=1}^{M_v} a_m G_y(w-m) & w \geqslant (w_s-w_c) \\ & w_N < w \leqslant w_s \end{cases} \tag{6.44}$$

where w_c is the cutoff frequency (see Fig.6.8) , w_s is the sampling rate and M_e and M_v are two different model orders found empirically using the BIC criterion.

A complex version of the Burg algorithm is used for modelling and the linear phase component of the signal is conserved by considering only the moduli of $G'_e(w)$ and $G'_v(w)$ as follows :

$$G_e(w) = \frac{|G'_e(w)|}{|G'_e(w)|+|G'_v(w)|+ G_N} \tag{6.45}$$

where G_N here is a constant independent of frequency. An estimate of the envelope $\{e(t)\}$ can be obtained by transforming $\hat{G}_e(w)$ back to the time domain then taking the exponential.

Pulse information can be derived from the envelope by locating the local maxima. The resulting record of sparse impulses is then used as input to the model of equation (6.13) whose coefficients have already been estimated. The output is then correlated with the original signal to find the optimal shift. The end result is a set of impulses with given time locations and heights. These will be the input to the nonlinear regression scheme that models the velocity waveform as a nonstationary process.

6.4 Modelling of the Nonstationary Velocity Waveform using Nonlinear Regression

The model to be fitted to the data is of the form

$$y(t) = \sum_{k=1}^{K} h_k\,(t-t_k)\,\exp(-(t-t_k)/\tau_k)\,\cos[\,2\pi\,\Omega_k(t-t_k)\,] \tag{6.46}$$

where K is the total number of impulses, h_k, t_k, τ_k and Ω_k are the height, arrival time, time constant and frequency of the k^{th} pulse respectively. Let us define the vector $\underline{b}_k$ as follows :

$$\underline{b}_k^T = [\; t_k \quad h_k \quad \tau_k \quad \Omega_k \;] \tag{6.47}$$

Then the problem is to compute the parameters $\{\, \underline{b}_1, \underline{b}_2, \ldots, \underline{b}_K \,\}$ which will minimize

$$\Phi = \sum_{t=1}^{N} [\; y(t) - \hat{y}(t) \;]^2 \tag{6.48}$$

where y(t) is the t^{th} data value and $\hat{y}(t)$ is the value predicted by equation (6.46). To reduce storage requirements, we have divided the overall optimization scheme involving 4K parameters into K smaller optimization schemes of 4 parameters each. This has been achieved through the use of the function

$$f(t,\underline{b}_k) = h_k\,(t-t_k)\,\exp(-(t-t_k)/\tau_k)\,\cos[\,2\pi\,\Omega_k\,(t-t_k)\,] \tag{6.49}$$

in equation (6.48) which gives

$$\Phi = \sum_{t=1}^{N}[\,y(t) - \sum_{k=1}^{K} f(t,\underline{b}_k)\,]^2 \tag{6.50}$$

The algorithm used is based on a procedure by Marquardt (1963,1970) and it minimizes Φ with respect to an arbitrary $\underline{\delta}_j$ given by:

$$\underline{\delta}_j^T = \begin{cases} \begin{bmatrix} \Delta t_j & \Delta h_j & \Delta \tau_j & \Delta \Omega_j \end{bmatrix} & \text{for } k=j \\ \underline{0} & \text{for } k \neq j \end{cases} \tag{6.51}$$

Replacing $f(t,\underline{b}_k)$ in (6.50) by $f(t,\underline{b}_k + \underline{\delta}_j)$ and differentiating we get

$$\frac{\partial \Phi}{\partial \underline{\delta}_j} = \sum_{t=1}^{N} 2(y(t) - \sum_{k=1}^{K} f(t,\underline{b}_k+\underline{\delta}_j)\,)\,\frac{\partial f(t,\underline{b}_k+\underline{\delta}_j)}{\partial \underline{\delta}_j} \tag{6.52}$$

Using a Taylor series expansion of $f(t,\underline{b}_k + \underline{\delta}_j)$ we have

$$f(t,\underline{b}_k+\underline{\delta}_j)=f(t,\underline{b}_k)+\Delta t_j\frac{\partial f}{\partial t_j}+\Delta h_j\frac{\partial f}{\partial h_j}+\Delta\tau_j\frac{\partial f}{\partial \tau_j}+\Delta\Omega_j\frac{\partial f}{\partial \Omega_j}$$

or in matrix form

$$\underline{F} = \underline{F}_0 + P_j\,\underline{\delta}_j \tag{6.53}$$

where $\underline{F}^T = [\ f(1,\underline{b}_j+\underline{\delta}_j),f(2,\underline{b}_j+\underline{\delta}_j),\quad \ldots,f(N,\underline{b}_j+\underline{\delta}_j)\ ]$,
$\underline{F}_0^T = [\ f(1,\underline{b}_j),\ f(2,\underline{b}_j),\ldots,f(N,\underline{b}_j)\ ]$ and

$$P_j = \begin{bmatrix} \frac{\partial f_1}{\partial t_j} & \frac{\partial f_1}{\partial h_j} & \frac{\partial f_1}{\partial \tau_j} & \frac{\partial f_1}{\partial \Omega_j} \\ \frac{\partial f_2}{\partial t_j} & \frac{\partial f_2}{\partial h_j} & \frac{\partial f_2}{\partial \tau_j} & \frac{\partial f_2}{\partial \Omega_j} \\ \vdots & \vdots & \vdots & \vdots \\ \frac{\partial f_N}{\partial t_j} & \frac{\partial f_N}{\partial h_j} & \frac{\partial f_N}{\partial \tau_j} & \frac{\partial f_N}{\partial \Omega_j} \end{bmatrix}$$

Using (6.53) in (6.52) and setting $\frac{\partial \Phi}{\partial \underline{\delta}_j} = 0$ we obtain

$$P_j^T\,P_j\,\underline{\delta}_j = P_j^T\,[\ \underline{Y} - \hat{\underline{Y}}_0\ ] \tag{6.54}$$

where

$$\hat{\underline{Y}}_0 = \sum_{k=1}^{K} F_0(\underline{b}_k)$$

and

$$\underline{Y}^T = [\ y(1),y(2),\ldots,y(N)\ ]$$

Because the initial guesses might be far away from the true values of the parameters , Marquardt introduced the constant Lambda , λ , to accelerate the convergence, and the new set of equations to be solved are

$$(P_j^T P_j + \lambda I) \ \underline{\delta}_j = P_j^T [\underline{Y} - \hat{\underline{Y}}_0] \tag{6.55}$$

where I is the identity matrix. These equations are solved for $\underline{\delta}_j$ and then the vector $\underline{b}_j$ is updated i.e.

$$\underline{b}_j^{(n)} = \underline{b}_j^{(n-1)} + \underline{\delta}_j^{(n-1)} \tag{6.56}$$

where n denotes the n^{th} iteration. This process is repeated until Φ reaches a minimum.

At this point , it is worthwhile to clarify the overall operation of our optimization procedure. The Marquardt algorithm is used to estimate an optimal vector for a certain pulse (in this case it is $\underline{b}_j$). Once $\underline{b}_j$ has been estimated we can move either sequentially or randomly to the $(j+p)^{th}$ pulse and find $\underline{b}_{j+p}$ and so on until K pulse vectors [$\underline{b}_1, \underline{b}_2, \ldots, \underline{b}_K$] have been computed. The initial values of arrival times, $\{t_k\}$, and pulse heights , $\{h_k\}$, are obtained from the output of the stochastic homomorphic filter. As for the initial time constants, $\{ \tau_k\}$, and frequencies, $\{\Omega_k\}$, these are all set to the two values obtained by the frequency domain system identification procedure.

The application of this modelling procedure to the disturbance velocity waveforms of the 40% occlusion case has shown promising results. Fig. 6.9 shows three examples of these waveforms with their envelopes, reconstructed signals and estimated impulse trains. The striking similarity between true and modelled signals demonstrates the

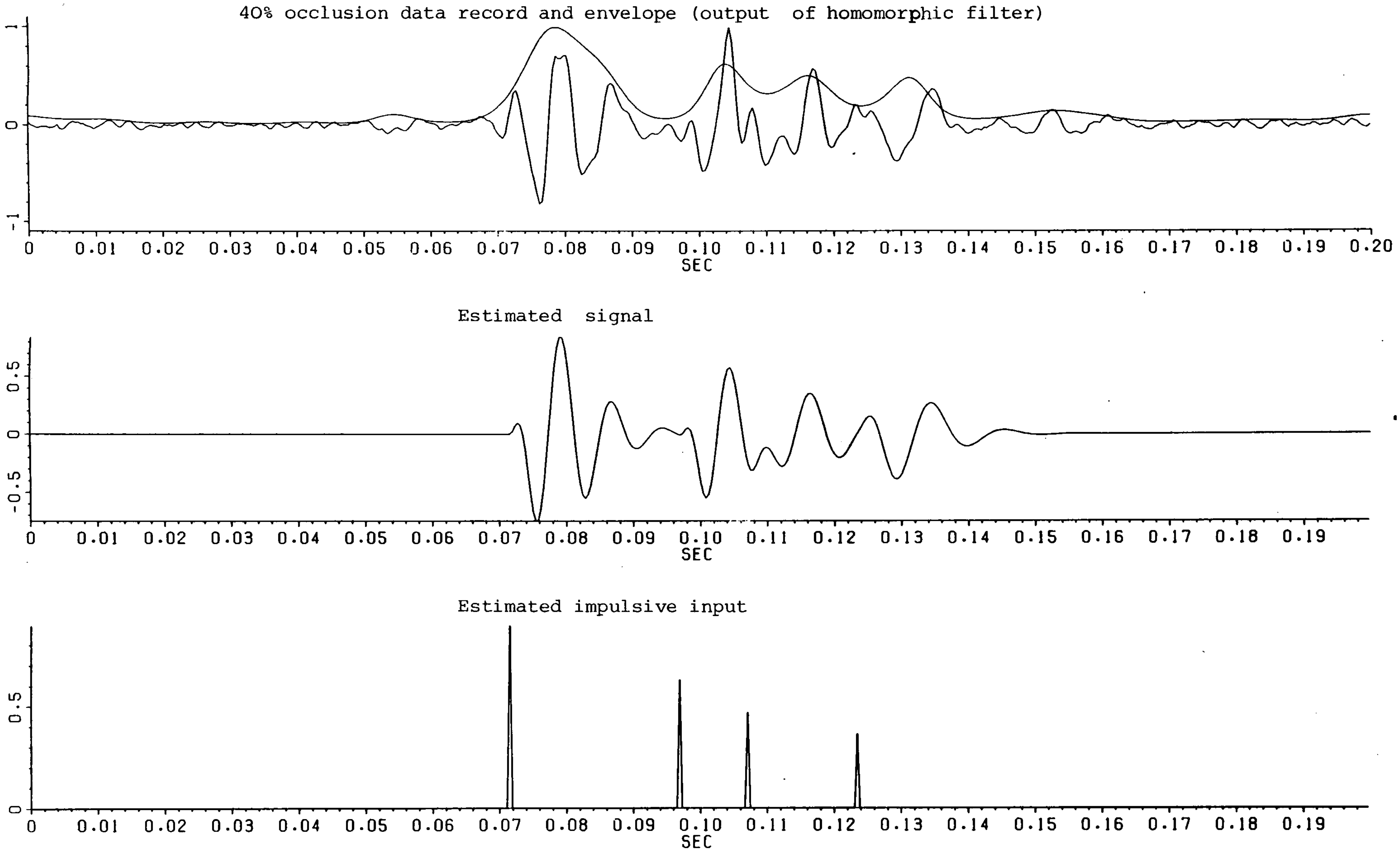

40% occlusion data record and envelope (output of homomorphic filter)

Estimated signal

Estimated impulsive input

(Fig.6.9)

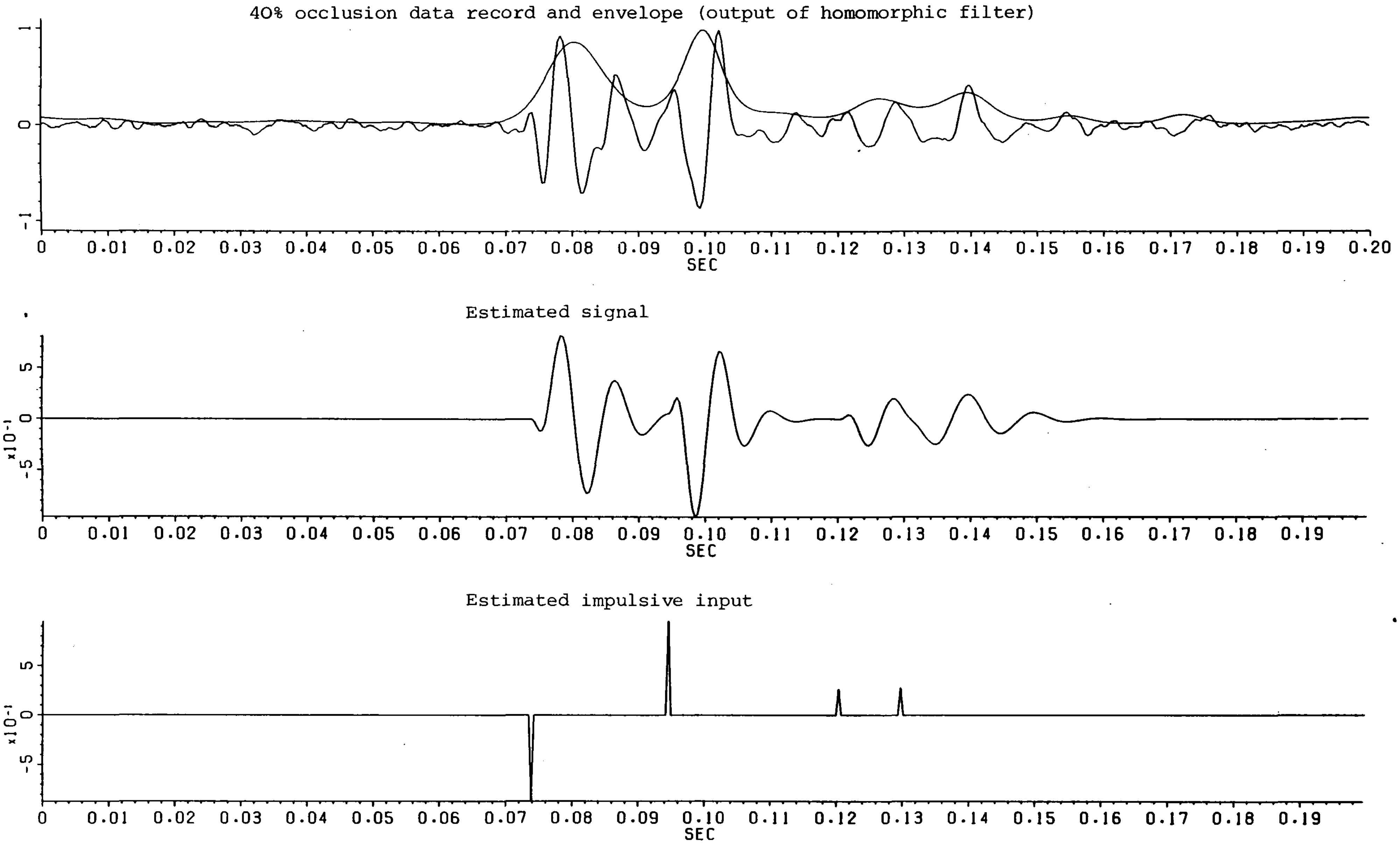
40% occlusion data record and envelope (output of homomorphic filter)

Estimated signal

Estimated impulsive input

(Fig.6.9)

40% occlusion data record and envelope (output of homomorphic filter)

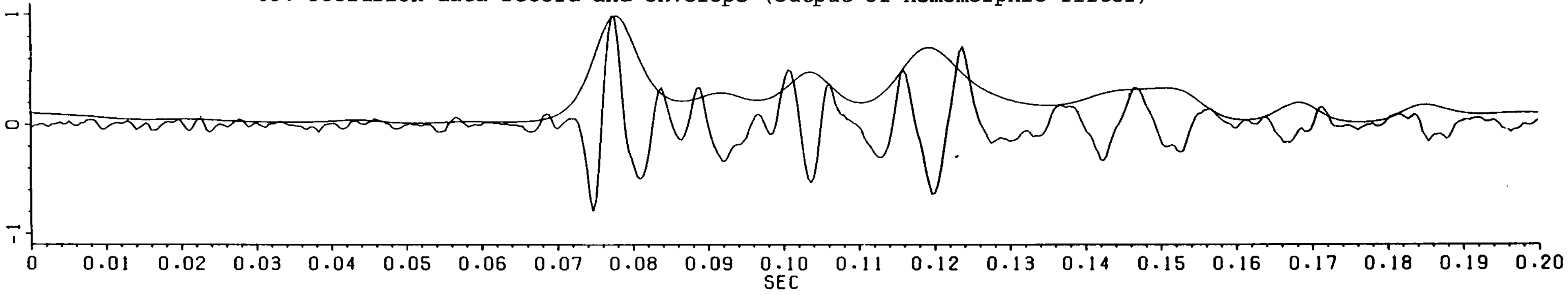

Estimated signal

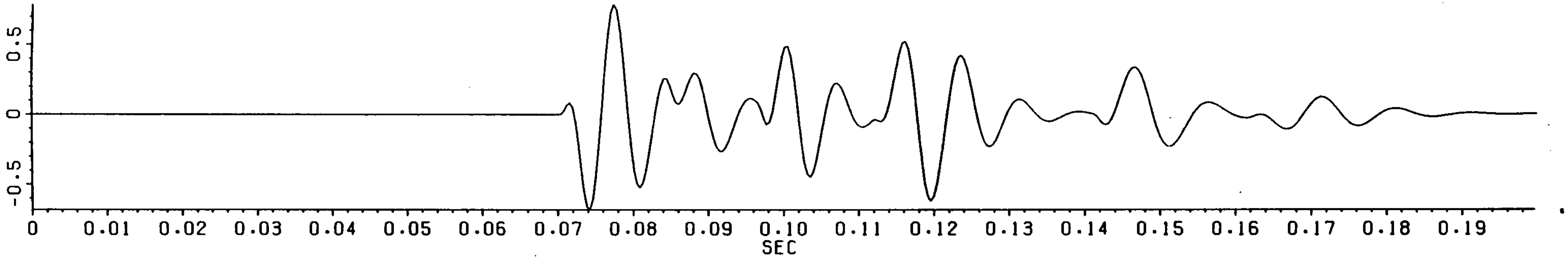

Estimated impulsive input

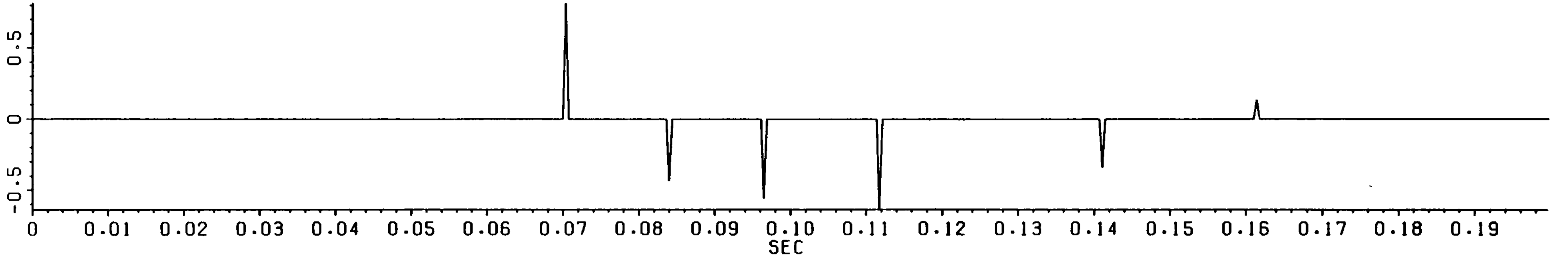

(Fig.6.9)

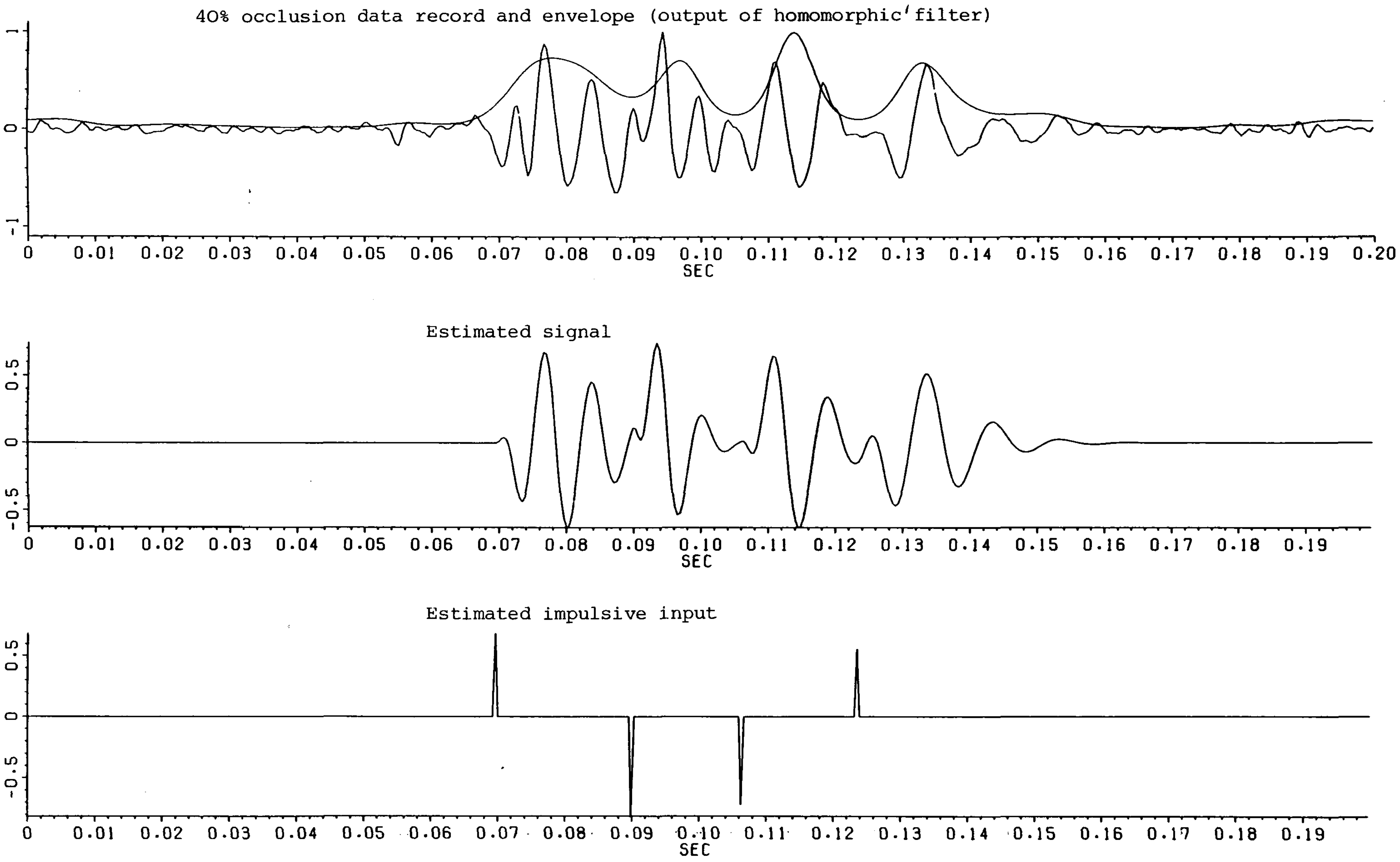

40% occlusion data record and envelope (output of homomorphic filter)

Estimated signal

Estimated impulsive input

Fig.6.9 Modelling of the disturbance velocity as a wave packet model driven by impulsive noise.

feasibility of the suggested model i.e. a narrowband process driven by impulsive noise (equation (6.1)). This could prove to be a useful tool in the comprehensive understanding of the generating flow field and hence the unravelling of the discrete relationship between flow disturbances and degree of stenosis.

CHAPTER 7

DISCUSSION

7.1 Summary of Analysis

If the material presented sofar has managed to raise more questions than provide answers concerning the nature of poststenotic flow, then this work has achieved its objective. For, the chief aim has been to provide techniques of analysis that might shed some light on the solution of the problem and hence provide a basis for further investigation.

A description of the complexity of this physical system (i.e. the poststenotic velocity field) was given at the beginning of this thesis, as well as its clinical significance with regards to the early detection of atherosclerosis. Practical methods of dealing with experimental data i.e. velocity waveforms have been discussed together with types of perspective velocity measuring devices in order to assess the usefulness and quality of the data set at hand. Some basic methods of analysing the sectioned velocity waveforms have been presented, for example: ensemble averaging and/or phase shift averaging (the time domain model), high-pass filtering (the frequency domain model) and a comparison of the two approaches has been made.

Autoregressive modelling has proved to be a useful technique in studying the frequency content of both the ensemble average and disturbance velocity waveforms. The maximum entropy spectral estimate provides smooth spectra with good resolution that are a much better improvement on the conventional FFT spectra. Also, the AR spectrum

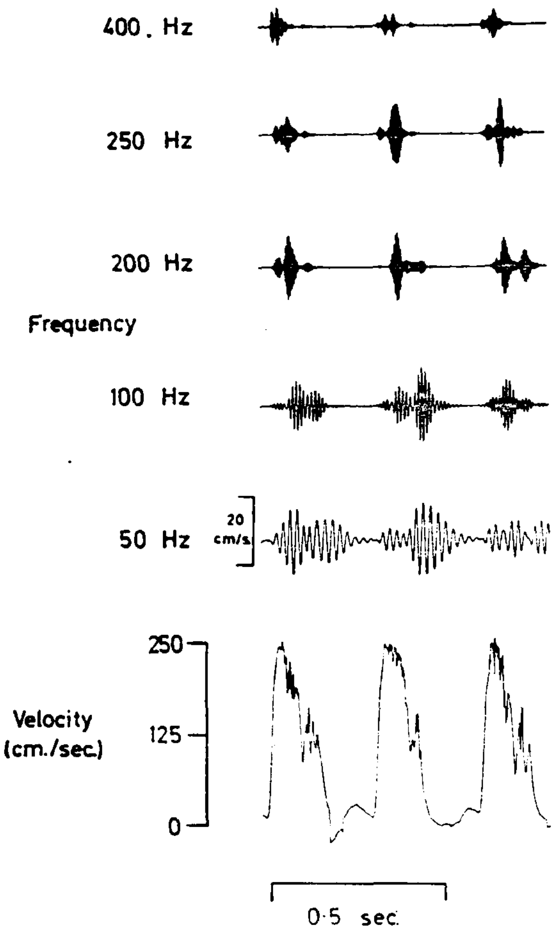

Fig.7.1 Frequency analyser output for highly disturbed flow in descending aorta. The input waveform is shown at the bottom. The velocity scale opposite the 50 Hz signal applies to all frequencies. (After Nerem and Seed,1972)

has been treated as the frequency response of a system driven by white noise. The adaptive AR algorithm- the LMS forward and backward filtered error algorithm - has proved to be useful in detecting hidden structures in the disturbance velocity records. These structures have been termed wave packets because of their shape i.e. they look like sinusoidal beats or bursts of short duration. Not only is this new algorithm capable of following amplitude changes in the data but it is also very useful and accurate in tracking frequency fluctuations and hence it is also applicable to the Doppler blood velocity signal.

Based on these observations and similar observations by other authors e.g. Nerem and Seed (1972) and Gaster(1981), a wave packet model driven by impulsive noise has been presented. In a relevant flow system i.e. a highly disturbed flow, Nerem and Seed (ibid) observed these wave packets when the disturbed velocity signal was passed through a frequency analyser. They observed with different frequencies when the signal was band-pass filtered as seen in Fig. 7.1. Notice also that the dominant amplitude is that of the lowest frequency component i.e. the 50Hz component. No interpretation of these wave packets were given but they seemed to behave in a similar fashion to the wavepackets observed in this study i.e. they were associated with peak systole and the subsequent deceleration, were damped out during diastole and were generated anew in each beat. Nerem and Seed also hinted about a possible relationship between these disturbances and sound generation in the aorta.

These disturbances have also been described as modulated simple waves in a theoretical study of unsteady flow in flexible tubes

(Seymour,1975) and Lou (1975), yet a fully comprehensive interpretation of these wavepackets is not readily available. Hence, there is need for more experimental work to be done by fluid dynamicists to investigate the generation, propagation and decay of such structures in flexible tube models of the artery. The primary question is whether these structures are a feature of turbulence or whether they are wall effects. Recently, there has been more interest in the role of coherent structures in turbulence (Jimenez,1980 and Hussain,1983) and the stress is now shifting from the overall statistical behaviour of turbulence to its more detailed structure. Hence, it is hoped that in the near future the results of more rigorous experimental and analytical work on disturbed flow in flexible tubes will be available.

7.2 Clinical Considerations

The detection and quantification of arterial stenosis might become a reality if more is known about the statistical behaviour of the proposed model i.e. the statistical fluctuations of the model parameters for a given level of occlusion. Another probably more important source of information is the impulsive noise which needs to be characterised. We noted that the arrival time of the first disturbance seems to decrease with increasing stenosis . Also, the pulse intensity appears to be directly proportional to the occlusion level though this is also subject to physiological variability. Hence its quantification requires the use of some more sophisticated statistical methods.

It might also be possible to derive the realtionship between flow disturbances and sound generation in the artery. This could prove to be very useful for phonoangiography which, though noninvasive is still in its infancy as a technique because little is known about the generating process. Some correlation might be found between sound spectra and disturbance velocity spectra which might also lead to a better understanding of the transmission of sound waves through the human body.

The application of the technique developed in this study to Doppler ultrasound measurements of blood velocity in humans is the subject of future research because of the fact that the disturbance could have a narrow-band frequency content could help in isolating effects in the signal that might be due to ambiguity and noise. Again autoregressive techniques can be applied to this signal to extract a good estimate of the process spectral density. In addition, since directional components can be detected using Doppler ultrasound techniques , a study of the mentioned process in more than one dimension could prove to be useful in the better understanding of the three dimensional velocity field.This could make an important contribution to medical imaging by Doppler ultrasound and could trigger the development of the relevant image processing techniques and hence the localization of arterial obstructions.

Although some clinicians might find it hard to accept that there is indeed a relationship between stenosis and blood velocity disturbances, the understanding of this process makes possible the interpretation of clinical techniques that, though widely used in practice are still theoretically vague like sonography , for example. Also, clinical decisions should not only be based on the presence or absence of flow disturbances but also on the nature or detailed structure of these disturbances.

7.3 Future Reflections

As mentioned before, experiments with simple laboratory models of pulsatile flow in a constricted artery are essential in clarifying the generation , propagation and decay of flow disturbances. In addition, more sophisticated signal processing techniques should be developed to extract more precise information about the fine structure of this velocity field.

7.3.1 Experimental Data Requirements

The techniques chosen are highly dependent on the ability to acquire good measurements of velocity components at prescribed locations in the model. Since the velocity field is a three dimensional field which is varying in time, the ideal situation would be to try to describe it in that context. Unfortunately, this can only be a long term objective; consequently, in the short term we can only regard the disturbance field as a function of both time and distance away from the constriction.

Of interest in this space time analysis is the location of the disturbance source. In the present study a time delay has been observed between the start of the cycle and the onset of the first disturbance. This could signify that the observed disturbances have been generated in the vicinity of the constriction (downstream) and have travelled from that location to the site of measurement. In locating that source, it is considered important to find the point of maximum disturbance intensity as this is considered to be a favourable site for meaningful measurements.

With the source located, it would be equally interesting to follow up the propagation of the disturbances downstream while still keeping the same distances away from the wall. Two dimensional spectra i.e. spectra of time and axial distance can then be obtained to analyse the frequency content of the propagating signal.

Equally important would be the monitoring of the wall motion and its effects on the velocity signal and vice versa. Flow induced vibrations could also be investigated and measurement of the velocity signal at resonance could produce an understanding of the coupling between flow and wall motion.

Although all these data requirements might not be satisfied because of the limitations of the measuring devices and other experimental difficulties, the few that are satisfied could provide many clues to the complex nature of the disturbance velocity field and would eventually lead to the development of a more general stochastic model of the process.

7.3.2 Theoretical Modelling and Analysis

The next step in modelling would be to consider the disturbance velocity as a state space model driven by a point process noise. This means that the system transfer function

$$H(z) = \frac{b_1 z^{M-1} + b_2 z^{M-2} + \; \ldots \; + b_{M-1} z + b_M}{z^M + a_1 z^{M-1} + \; \ldots \; + a_{M-1} z + a_M} \tag{7.1}$$

can be represented in state space form where the state equation is given by:

$$\underline{X}(k+1) = \Phi \underline{X}(k) + \underline{\gamma}\, u(k) \tag{7.2}$$

where $\underline{X}(k)$ is an Mx1 state vector , u(k) is the point process input sequence and Φ the transition MxM matrix and $\underline{\gamma}$ the Mx1 input distribution vector are defined as follows :

$$\Phi = \begin{bmatrix} 0 & 1 & 0 & \cdots & 0 \\ 0 & 0 & 1 & \cdots & 0 \\ \vdots & \vdots & \vdots & & \vdots \\ -a_M & -a_{M-1} & -a_{M-2} & \cdots & -a_1 \end{bmatrix} \tag{7.3}$$

and

$$\underline{\gamma}^T = [\; 0 \quad 0 \ldots \quad 1 \;] \tag{7.4}$$

On the other hand the measurement equation can be written as follows :

$$\underline{Z}(k) = \underline{h}^T \underline{X}(k) + n(k) \tag{7.5}$$

where $\underline{Z}(k)$ is the observation vector, n(k) is an additive noise source and $\underline{h}^T$, the measurement vector, is given as :

$$\underline{h}^T = [\ b_M \quad b_{M-1} \quad \dots \quad b_1\ ] \tag{7.6}$$

The state space representation of a discrete ARMA process can be solved using a <u>Kalman filter</u> and can be used to estimate the transfer function parameters as well as the statistical parameters of the noise input sequence (for references on state-space filtering see Meditch (1969), Gelb(1974) and Srinath and Rajasekaran (1979))

For the optimal operation of the Kalman filter, the noise statistics of the input noise should be known apriori. Hence, one of the objectives of the future analysis is to try to determine the statistical nature of the point process noise (for example its distribution). This would require the analysis of a vast amount of experimental data which would be acquired from carefully controlled experiments on pulsatile flow in models of stenosed arteries. Human data would also be considered at a later stage for comparison.

Once the statistics of the noise are obtained the filter would be applied to study the variations of the statistical parameters (for example, the parameters that define a distribution) with changing occlusion level. Also, the transfer function parameters can be estimated accurately and hence waveforms for a given level can be quantified in an optimal statistical fashion. This might provide a more accurate estimate of the degree of stenosis be it in the low or high range.

The long desired objective might still be far away but we now have a clearer vision of the path. Some of the difficulties we have overcome but many more are still to come. The battle is not yet over and since the challenges remain, the interest will never fade away. The hope is that the future will carry an abundance of work by those who believe that progress is not a relic of the past.

REFERENCES

Ahmed,S.A.(1981)

An experimental investigation of steady and pulsatile flow through a constricted tube.

PhD Thesis, Georgia Institute of Technology, Atlanta Georgia.

Akaike,H.A.(1969)

Fitting autoregressive models for prediction.

Ann.Inst.Stat.Math.,Vol.21,pp.243-247.

Akaike,H.A.(1970)

Statistical predictor identification.

Ann.Inst.Stat.Math.,Vol.22,pp.203-217.

Akaike,H.A.(1973)

Information theory and an extension of the maximum likelihood principle.

Second International Symposium on Information Theory, edited by B.N.Petrov and F.Csaki, Akademiai Kiado, Budapest,pp.267-281.

Akaike,H.A.(1977)

On entropy maximization principle.

Applications of Statistics, edited by P.R.Krishnaiah,North-Holland,Amsterdam, pp.27-41.

Akaike,H.A.(1978)

Time series analysis and control through parametric models, in Applied Time Series Analysis, edited by D.F.Findley,Academic

Press,New York, pp.1-23.

Arts,M.G.J. and Roevros,J.M.J.G.(1972)
On the instantaneous measurement of bloodflow by ultrasonic means.
Med.Biol.Engng.,Vol.10,pp.23-34.

Arya,V.K., and Aggarwal,J.K.(1982)
Deconvolution of Seismic Data.
Hutchinson Ross, Stroudsburg.

Attinger,E.O.(1981)
Analysis of Pulsatile Blood Flow, in Advances in Fluid Mechanics, edited by E.Krause, Springer Verlag,Berlin, pp.1-59.

Baker,D.W.,Forster,F.K.,andDaigle,R.E.(1978)
Doppler Principles and Techniques,
in Ultrasound: its Applications in Medicine and Biology, edited by S.P.Wolsky and A.W.Czanderna, Elsevier,Amsterdam.

Bendat,J.S.(1964)
Mathematical Analysis of Average Response Values for Nonstationary Data.
IEEE Trans. on Biomedical Engng.,Vol.11, pp.73-81.

Bergland,G.D.(1969)
A guided tour of the fast Fourier transform.
IEEE Spectrum July 6,pp.41-52.

Bloomfield,P.(1976)
Fourier Analysis of Time Series: An Introduction.

John Wiley and Sons, New York.

Box,G.E.P., and Jenkins,G.M.(1976)
Time Series Analysis:Forecasting and Conrol.
Holden-Day, San Francisco.

Bracewell,R.N.(1978)
The Fourier Transform and its Applications.
McGraw-Hill,Tokyo.

Breslau,P.J., and Strandness,D.E.,Jr(1983)
Noninvasive Assessment of Carotid Artery Disease,
in Blood Flow:Theory and Practice,edited by D.E.M.Taylor and A.L.Stevens,Academic Press,London,pp.175-190.

Burg,J.P.(1967)
Maximum entropy spectral analysis,
paper presented at the 37th Annual International Meeting,Soc.of Explor. Geophys., Oklahoma City,Okla.

Caro,C.G.,Pedley,T.J.,Schroter,R.C.,and Seed,W.A.(1978)
The Mechanics of the Circulation.
Oxford University Press, Oxford.

Cassanova,R.A.and Giddens,D.P.(1978)
Disorder distal to modeled stenoses in steady and pulsatile flow.
Journal of Biomechanics,Vol.11,pp.441-453.

Chatfield,C.(1980)
The Analysis of Time Series:Theory and Practice.

Chapman and Hall,London.

Claerbout,J.F.(1976)
Fundamentals of Geophysical Data Processing.
McGraw-Hill,New York.

Clark,C. and Schultz,D.L.(1973)
Velocity distribution in aortic flow.
Cardiovascular Research,Vol.7,pp.601-613.

Clark,C.(1974)
Thin film gauges for fluctuating velocity measurements in blood.
Journal of Physics,Ser.E,Sci.Instrum., Vol.7,pp.548-556.

Clark,C.(1976)
The fluid mechanics of aortic stenosis- II- Unsteady flow experiments.
Journal of Biomechanics,Vol.9,567-573.

Clark,C.(1980)
The propagation of turbulence produced by a stenosis.
J.Biomechanics,Vol.13,pp.591-604.

Clayton,R.W.,and Ulrych,T.J.(1977)
A Restoration Method for Impulsive Functions.
IEEE Trans. on Information Theory,Vol.23,pp.262-264.

Dorf,R.C.(1980)
Modern Control Systems.
Addison-Wesley,Reading-Massachusetts.

Duncan,G.W.,Gruber,J.O.,Dewey,C.F.,Jr.,Myers,G.S., and Lees,R.S.(1975)
Evaluation of Carotid stenosis by Phonoangiography.
New England Journal of Medicine,Vol.293,pp.1124-1128.

Durbin,J.(1960)
The fitting of time series models.
Rev.Int.Inst.Statist.,Vol.28,pp.233-244.

Fries,R.W.,and Modestino,J.W.(1979)
Image Enhancement by Stochastic Homomorphic Filtering.
IEEE Trans. on Acoustics,Speech,and Signal Processing,
Vol.ASSP-27,pp.625-637.

Gabrini,J.L.,Forster,F.K.and Jorgensen,J.E.(1982a)
Measurement of fluid turbulence based on pulsed ultrasound techniques,
Part 1:Analysis.
J.Fluid Mech.,Vol.118,pp.445-470.

Gabrini,J.L.,Forster,F.K.and Jorgensen,J.E.(1982b)
Measurement of fluid turbulence based on pulsed ultrasound techniques,
Part 2:Experimental investigation.
J.Fluid Mech.,Vol.118,pp.471-505.

Gaster,M.(1981)
On Transition to Turbulence in Boundary Layers,
in Transition and Turbulence, edited by R.E.Meyer, Academic,New York,pp.95-112.

Gelb,A.(1974)

Applied Optimal Estimation.
The M.I.T. Press,Cambridge,Massachusetts.

George,W.K.and Lumley,J.L.(1973)
The laser-Doppler velocimeter and its application to the measurement of turbulence.
J.Fluid Mech.,Vol.60,pp.321-363.

Giddens,D.P.,Mabon,R.F.and Cassanova,R.A.(1976)
Measurements of disordered flows distal to subtotal vascular stenoses in the thoracic aortas of dogs.
Circulation Research,Vol.39,pp.112-119.

Griffiths,L.J.(1975)
Rapid Measurement of Digital Instantaneous Frequency
IEEE Trans.Acoustics,Speech,and Signal Processing,
Vol.ASSP-23,pp.207-222.

Griffiths,L.J.,and Prieto-Diaz,R.(1977)
Spectral analysis of natural seismic events using autoregressive techniques.
IEEE Trans. on Geoscience Electronics, GE-15,pp.13-25.

Haddad,A.H.(1978)
Suboptimal Sequential Estimation-Detection Scheme for Poisson Driven Linear Systems.
Information Sciences,Vol.16,pp.95-113.

Harris,F.J.(1978)

On the Use of Windows for Harmonic Analysis with the Discrete Fourier Transform.
Proceedings of the IEEE,Vol.66,pp.51-83.

Hasan,T.(1982)
Nonlinear time series regression for a class of amplitude modulated cosinusoids.
J.of Time Series Analysis,Vol.3,pp.109-122.

Hasan,T.(1983)
Complex Demodulation: Some Theory and Applications, in Handbook of Statistics 3,edited by D.R. Brillinger and P.R.Krishnaiah,North-Holland,Amsterdam,pp.125-156.

Haykin,S.(1979)
Nonlinear Methods of Spectral Analysis.
Springer-Verlag,Berlin.

Haykin,S.,and Kesler,S.(1979)
Prediction-Error Filtering and Maximum-Entropy Spectral Estimation, in Nonlinear Methods of Spectral Analysis, edited by S.Haykin, Springer Verlag, Berlin,pp.9-70.

Hussain,A.K.F and Reynolds,W.C.(1970)
The mechanics of an organized wave in turbulent shear flow.
J.Fluid Mech.,Vol.41,pp.241-258.

Hussain,A.K.M.F.(1983)
Coherent structures- reality and myth.

The Physics of Fluids,Vol.26,pp.2816-2850.

Jaynes,E.T.(1963)
New engineering applications of information theory,
in Proceedings of the First Symposium on Engineering Applications of Random Function Theory and Probability, edited by J.L.Bogdanoff and F.Kozin,John Wiley,New York,pp.163-203.

Jaynes,E.T.(1968)
Prior probabilities.
IEEE Trans.Systems Sci.Cybern.,Vol.4, pp.227-241.

Jimenez,J.(1980)
The Role of Coherent Structures in Modelling Turbulence and Mixing.
Springer-Verlag,Berlin.

Jurkevics,A.,and Ulrych,T.J.(1978)
Representing and simulating strong ground motion.
Bulletin of the Seismological Society of America,Vol.68,pp.781-801.

Jury,E.I.(1973)
Theory and Application of the Z-Transform Method.
Robert E.Krieger,New York.

Kay,S.M.(1979)
The effects of noise on the autoregressive spectral estimator.
IEEE Trans.ASSP,Vol.5,pp.478-485.

Kitney,R.I.,Giddens,D.P.,and Mabon,R.F.(1980)
Flow disturbance analysis of aortic velocity waveforms.

Proc.Int.Blood Flow Conf.,London.

Kitney,R.I.,and Giddens,D.P.(1982)
Extraction and characterisation of underlying velocity waveforms in poststenotic flow.
IEE Proceedings,Vol.129,Pt.A,pp.651-662.

Khalifa,A.M.A.,and Giddens,D.P.(1981)
Characterization and evolution of poststenotic flow disturbances.
Journal of Biomechanics,Vol.14,279-296.

Kormylo,J.J.,and Mendel,J.M.(1982)
Maximum Likelihood Detection and Estimation of Bernoulli-Gaussian Processes.
IEEE Trans. on Information Theory,Vol.IT-28, pp.482-488.

Kwarkernaak,H.(1980)
Estimation of Pulse Heights and Arrival Times.
Automatica,Vol.16,pp.367-377.

Langlois,Y.,Roederer,G.O.,Chan,A.,Phillips,D.J.,Beach,K.W.,
Martin,D.,Chikos,P.M.,Strandness,D.E.,Jr(1983)
Evaluating Carotid Artery Disease: The Concordance Between Pulsed Doppler/Spectrum Analysis and Angiography.
Ultrasound in Medicine and Biology,Vol.9,pp.51-63.

Levinson,H.(1947)
The Wiener RMS(root mean square) error criterion in filter design and prediction.

J.Math.Phys.,Vol.25,pp.261-278.

Lou,Y.S.(1975)
Two-dimensional finite amplitude theory of arterial blood flow.
Journal of Biomechanics,Vol.8,pp.57-63.

Makhoul,J.(1975)
Linear Prediction: A Tutorial Review.
Proc.IEEE,Vol.63,pp.561-580.

Markel,J.D.,and Gray,A.H.(1973)
On autocorrelation equations as applied to speech analysis.
IEEE Trans. Audio Electroacoust.,Vol.AU-20,pp.69-79.

Marquardt,D.W.(1963)
An algorithm for least-squares estimation of nonlinear parameters.
J.Soc.Indust.Appl.Math.,Vol.11,pp.431-441.

Marquardt,D.W.(1970)
Generalized Inverses, Ridge Regression, Biased Linear Estimation, and Nonlinear Estimation.
Technometrics,Vol.12,pp.591-612.

McDonald,D.A.(1974)
Blood Flow in Arteries, second edition.
Arnold,London.

Meditch,J.S.(1969)
Stochastic Optimal Linear Estimation and Control.
McGraw-Hill,New York.

Mendel,J.M.(1983)

Optimal Seismic Deconvolution: An Estimation-Based Approach.

Academic,New York.

Mills,C.J.,Gabe,I.T.,Gault,J.H.,Mason,D.T., Ross,J.,Braunwald,E.,and

Shillindford,J.P.(1970)

Pressure-flow relationships and vascular impedance in man.

Cardiovascular Research,Vol.4,pp.405-417.

Mitchell,J.R.A.,and Schwartz,C.J.(1965)

Arterial Disease.

F.A.Davis Co.,Philadelphia,Pa.

Nerem,R.M.,and Seed,W.A.(1972)

An in vivo study of aortic flow disturbances.

Cardiovascular Research,Vol.6,pp.1-14.

Oppenheim,A.V.,Schafer,R.W.and Stockham,T.G.(1968)

Nonlinear Filtering of Multiplied and Convolved Signals.

Proc.IEEE,Vol.56,pp.1264-1291.

Pagano,M.(1973)

When is an autoregressive scheme stationary?

Communications in Statistics,Vol.1,pp.533-544.

Parzen,E.(1974)

Some recent advances in time series analysis.

IEEE Trans.Autom.Control,Vol.19,pp.723-730.

Pedley,T.J.(1976)

Heat transfer from a hot-film in reversing shear flow.
J.Fluid Mech.,Vol.73,pp.513-534.

Pedley,T.J.(1980)
The Fluid Mechanics of Large Blood Vessels.
Cambridge University Press,Cambridge.

Peli,T.,and Quatieri,F.(1984)
Homomorphic restoration of images degraded by light cloud cover.
Proc.IEEE Int.Conf. on Acoustics,Speech and Signal Processing,San Diego,pp.37.8.2-37.8.4.

Priestley,M.B.(1965)
Evolutionary Spectra and Non-stationary Processes.
J.Roy.Statist.Soc.,Ser.B,Vol.27,pp.204-237.

Priestley,M.B.(1981)
Spectral Analysis and Time Series.
Academic Press, London.

Rabiner,L.R., and Allen,J.B.(1980)
On implementation of a short-time spectral analysis method
for system identification.
IEEE Trans. on Acoustics,Speech,and Signal Processing, Vol.ASSP-28, pp.69-78.

Roberto,C.E. and Kaufman,H.(1966)
Table of Laplace Transforms.
W.B.Saunders,London.

Robinson,E.A.(1967)
Statistical Communication and Detection.
Griffin,London.

Sawaragi,Y.,and Soeda,T.,and Nakamizo,T.(1981)
Classical Methods and Time Series Estimation,
in Trends and Progress in System Identification, edited by P.Eykhoff,Pergamon Press,Oxford,pp.67-102.

Saxena,V.(1978)
Turbulence measurements using pulsed Doppler ulrasound.
PhD Thesis,Georgia Institute of Technology.

Schultz,D.L.,Tunstall-Pedoe,D.S.,Lee,G.deJ.,Gunning,A.J.,and Bellhouse,B.J.(1969)
Velocity distribution and transition in the arterial system,
in Circulatory and Respiratory Mass Transport, a CIBA Foundation Symposium,edited by G.E.W.Wolstenholme and J.Knight.Churchill,London.

Seymour,B.R.(1975)
Unsteady Flow in Flexible Tubes: A Modulated Simple Wave.
Int.J.Engng.Sci.,Vol.13,pp.579-594.

Shibata,R.(1976)
Selection of the order of an autoregressive model by Akaike's information criterion.
Biometrika,Vol.63,pp.117-126.

Smylie,D.E.,Clarke,G.K.C.,and Ulrych,T.J.(1973)
Analysis of irregularities in earth's rotation,
in Methods in Computational Physics, Vol.13, Academic,
New York, pp.391-430.

Snyder,D.L.(1975)
Random Point Processes.
John Wiley and Sons, New York.

Srinath,M.D.,and Rajasekaran,P.K.(1979)
An Introduction to Statistical Signal Processing With Applications.
John Wiley and Sons,New York.

Stein,P.D.,Sabbah,H.N.(1976)
Turbulent blood flow in the ascending aorta of humans with normal and diseased aortic valves.
Circulation Research,Vol.39,pp.58-65.

Strandness,D.E.,Jr(1983)
Noninvasive Evaluation of Arteriosclerosis: Comparison of Methods.
Arteriosclerosis,Vol.3,pp.103-116.

Taylor,H.L.,Banks,S.C.,and McCoy,J.F.(1979)
Deconvolution with the l_1 norm.
Geophysics,Vol.44,pp.39-52.

Ulrych,T.F.(1972)
Maximum entropy spectrum of truncated sinusoids.
J.Geophysical Res.,Vol.77,pp.1396-1399.

Ulrych,T.J.,and Ooe,M.(1979)

Autoregressive and Mixed Autoregressive-Moving Average Models and Spectra,

in Nonlinear Methods of Spectral Analysis, edited by S.Haykin,Springer-Verlag,Berlin, pp.73-125.

Widrow,B.,and Hoff,M.E.(1960)

Adaptive switching circuits.

IRE Wescon.Con.Rec., part4,pp.96-104.

Widrow,B.(1970)

Adaptive Filters,

in Aspects of Network and System Theory, edited by R.E.Kalman and N.De Claris, Holt,Rinehart and Winston,New York, pp.563-587.

Widrow,B.,McCool,J.M.,Larimore,M.G., and Johnson,C.R.(1976)

Stationary and Nonstationary Learning Characteristics of the LMS Adaptive Filter.

IEEE Proc.,Vol.64,pp.1151-1162.

Woodcock,J.P.(1975)

Theory and Practice of Blood Flow Measurement.

Butterworths,London.

Woody,C.D.(1967)

Characterization of an adaptive filter for the analysis of variable latency neuroelectric signals.

Med. and Biol.Engng.,Vol.5,pp.539-553.

Young,D.F.(1979)

Fluid Mechanics of Arterial Stenoses.

Journal of Biomechanical Engineering,Vol.101, pp.157-175.

Yule,G.U.(1927)

On a method of investigating periodicities in disturbed series, with special reference to Wolfer's sunspot numbers.

Phil.Trans.Roy.Soc.London,Ser.A,Vol.226, pp.267-298.